CARBON DIOXIDE ABSORPTION IN PIPERAZINE ACTIVATED N-METHYLDIETHANOLAMINE

Samenstelling promotiecommissie:

Prof. dr. ir. J.A.M. Kuipers, voorzitter	Universiteit Twente
Prof. dr. ir. G.F. Versteeg, promotor	Universiteit Twente
Dr. ir. J.A. Hogendoorn, assistent-promotor	Universiteit Twente
Prof. dr. ir. H. van den Berg	Universiteit Twente
Prof. dr. ir. M.M.C.G. Warmoeskerken	Universiteit Twente
Dr. F.H. Geuzebroek	Shell Global Solutions, Nederland
Ir. P.H.M Feron, PhD	TNO Industrie en Techniek, Nederland
Prof. dr. W.C. Turkenburg	Universiteit Utrecht
Prof. dr. ing. H.F. Svendsen	Norwegian University of Science & Technology, Noorwegen

This work was financially supported by Shell Global Solutions International BV. This research is part of the CATO programme, the Dutch national research programme on CO_2 Capture and Storage. CATO is financially supported by the Dutch Ministry of Economic Affairs (EZ) and the consortium partners. (www.co2-cato.nl).

Derks, P.W.J.
Carbon Dioxide Absorption in Piperazine Activated N-Methyldiethanolamine
PhD thesis, University of Twente, The Netherlands
ISBN: 90-365-2439-3

CARBON DIOXIDE ABSORPTION IN PIPERAZINE ACTIVATED N-METHYLDIETHANOLAMINE

PROEFSCHRIFT

ter verkrijging van
de graad van doctor aan de Universiteit Twente,
op gezag van de rector magnificus,
prof. dr. W.H.M. Zijm,
volgens besluit van het College van Promoties
in het openbaar te verdedigen
op donderdag 30 november 2006 om 15.00 uur

door

Peter Wilhelmus Jacques Derks

geboren op 31 december 1976

te Helmond

Dit proefschrift is goedgekeurd door de promotor

Prof. dr. ir. G.F. Versteeg

en de assistent-promotor

Dr. ir. J.A. Hogendoorn

Aan mijn ouders
en mijn broertje

Summary

The removal of carbon dioxide from process gas streams is an important step in many industrial processes for a number of technical, economical or environmental reasons. The conventional technology to capture CO_2 on large scale is the absorption - desorption process, in which (aqueous) solutions of alkanolamines are frequently used as solvents [Kohl and Nielsen, 1997].

Nowadays, the addition of an activator, or more specifically piperazine (PZ) to an aqueous N-methyldiethanolamine (MDEA) solution has found widespread application in the bulk removal of carbon dioxide. The principle of such a blend of a primary or secondary (alkanol)amine and a tertiary alkanolamine is based on the relatively high rate of reaction of CO_2 with the primary or secondary alkanolamine combined with the low heat of reaction of CO_2 with the tertiary alkanolamine, which leads to higher rates of absorption in the absorber column and lower heats of regeneration in the stripper section. Detailed knowledge on mass transfer related issues (including e.g. hydrodynamics and kinetics) on one hand and thermodynamic equilibrium on the other hand is indispensable for an optimal design and operation of both an absorber and a desorber column using the piperazine activated MDEA solvent. As the aforementioned information related to this particular solvent in the literature was still rather limited, it was the incentive of this thesis to provide more insights into the absorption of carbon dioxide into aqueous solutions containing piperazine and MDEA, both with regard to mass transfer issues (e.g. physico-chemical properties and chemical kinetics) and thermodynamic equilibrium (both from an experimental and a theoretical point of view).

Accurate knowledge on the relevant physico-chemical properties of a system is indispensable as it is essential for a correct and accurate interpretation of many (lab scale) absorption rate experiments one one hand, while, on the other hand, they serve as important (input) parameters in (rate based) mass transfer modelling. Therefore, the density, viscosity, surface tension of aqueous piperazine solutions and the physical solubility of N_2O (related to CO_2 via the CO_2:N_2O analogy) in these solutions were experimentally determined over a wide range of conditions. In addition, also the density and viscosity of aqueous solutions containing both piperazine and MDEA were listed for various concentrations and temperatures. Furthermore, the Taylor dispersion method was used to determine the diffusion coefficient of piperazine in aqueous piperazine and the diffusion coefficient of both MDEA and PZ in an aqueous 4.0 kmol m^{-3} MDEA solution activated with 0, 0.5 and 1.0 kmol m^{-3} piperazine. A modified Stokes-Einstein equation was found to be able to estimate the experimental PZ and MDEA diffusivity data from the diffusion coefficient at infinite dilution and the viscosity of the solution. It was also shown that only the estimation method proposed by Othmer and Thakar [1953] was able to predict the diffusion coefficient of piperazine at infinite dilution in water with a reasonable accuracy.

The kinetics of carbon dioxide with piperazine in aqueous solution has been studied in a stirred cell reactor. The experimentally obtained absorption rates were interpreted using the DeCoursey equation [DeCoursey, 1974] to extract the kinetics of the main reaction, $2PZ + CO_2 \rightarrow PZCOO^- + PZH^+$. Under the assumption that the reaction was first order in both CO_2 and PZ, the second order kinetic rate constant was found to be 76 m^3 mol^{-1} s^{-1} at a temperature of 298.15 K, with an activation temperature of 4.1 $\cdot 10^3$ K. Furthermore, the absorption rate of CO_2 into partially protonated piperazine solutions was experimentally investigated to identify the kinetics of the reaction $2PZH^+ + CO_2 \rightarrow H^+PZCOO^- + PZH_2^+$. These results were interpreted using the Hogendoorn approach [Hogendoorn et al., 1997], which uses the explicit DeCoursey equation with an infinite enhancement factor which is

corrected for reversibility. Also, this reaction was assumed to be first order in both reactants and the second order rate constant for this reaction was found to be 0.30 ± 0.10 m^3 mol^{-1} s^{-1} at 298.15 K. The Brønsted plot technique showed that a relation seems to exist between the pKa and the forward kinetic rate constant for amines with a structure resembling piperazine.

The conventional stirred cell setup is not suitable for absorption rate experiments at very low partial pressures, as the accuracy in this quantity rapidly deteriorates when the total reactor pressure approximates the vapor pressure of the solution. To overcome this limitation, a new mode of operation for the stirred cell was proposed to allow for experiments at substantially lower partial pressures (required for fast, pseudo first order kinetic rate, absorption experiments). Hereto, a second cell with a solution identical to the one in the 'reactor cell' was added to the original setup, which served as a reference for the vapor pressure. Consequently, in case a pure, reactive gas was fed to the reactor cell, its partial pressure was, in fact, given by the pressure difference between the two cells. The new mode of operation was experimentally validated with the well-documented CO_2 - OH^- reaction (in aqueous NaOH solutions) at 25 and 40 °C. The obtained forward second order kinetic rate constants, deduced from the experimental data taken at low partial pressures (down to 1.5 mbar), were found to be in good agreement with the values reported in literature.

The rate of absorption of carbon dioxide into aqueous solutions containing a mixture of piperazine and MDEA was also studied experimentally in a stirred cell contactor. CO_2 fluxes have been determined in aqueous solutions containing 4.0 kmol m^{-3} MDEA, activated with either 0.5 or 1.0 kmol m^{-3} PZ (resulting in a total amine concentration of 4.5 or 5.0 kmol m^{-3}), at various carbon dioxide loadings and partial pressures and at ambient temperature. The obtained experimental results were compared to predictions made by a Fick based mass transfer model, which a.o. incorporated the kinetics of the individual components PZ and MDEA with CO_2. The theoretical absorption model was able to describe the experimental results with

reasonable accuracy at low carbon dioxide loadings. Experimental data at higher loadings, however, were increasingly underpredicted by the model. This is likely due to the non-ideality of the liquid phase, which was not taken into account in the model.

The aforementioned study of the absorption rate of CO_2 in mixed and loaded MDEA - PZ solutions showed that the equilibrium composition of the liquid phase forms an important class of input parameters in a mass transfer model. An accurate calculation of the liquid phase speciation requires a sound thermodynamic equilibrium model, and therefore, the development of such a model was the subject of the remainder of this thesis. Firstly, new experimental data were presented on the solubility of carbon dioxide in aqueous piperazine solutions, for concentrations of 0.2 and 0.6 molar piperazine and temperatures of 25, 40 and 70 $^{\circ}$C. Those data, and other data available in literature, were correlated using a model based on the electrolyte equation of state (EoS), as originally proposed by Fürst and Renon [1993]. The final model derived was able to describe the available experimental data with an average deviation of 16 %. Moreover, the model was also able to accurately predict experimental pH and conductivity data. Subsequently, the thermodynamic framework was extended to include MDEA. Also, new experimental equilibrium data were reported on the solubility of carbon dioxide into PZ activated MDEA over a wide range of conditions. These data not only included CO_2 solubilities and their corresponding partial pressures, pH and conductivities, but also a limited number of liquid speciation data obtained using NMR spectroscopy. These new data, and other data reported in the literature, were correlated with the developed thermodynamic model, and it was concluded that the EoS model was generally well suited to describe and predict equilibrium data. However, in its current form the model was not able to also accurately describe the liquid phase equilibrium speciation in the system CO_2 - PZ - MDEA - H_2O. The reason for this probably lies in the uncertainty in some of the physical input parameters, which is a direct consequence of the lack of reliable experimental vapor-liquid equilibrium data of the binary sub-systems. Nevertheless, the electrolyte equation of state model has shown very promising results.

Future research on this system should be directed towards the determination of more and reliable physical equilibrium data to improve the accuracy of the different input parameters as needed in the EoS equilibrium model. Once this has been achieved, the EoS model can provide reliable input for the aforementioned mass transfer model used to describe absorption rates in (partially loaded) piperazine activated MDEA solutions, which might aid in the understanding, design and optimization of PZ activated absorption processes.

Samenvatting

Het verwijderen van kooldioxide uit procesgassen is een belangrijk onderdeel in veel industriële processen, hetzij om technische of ecomische redenen, of omwille van de steeds stringentere milieu-wetgeving. De conventionele manier om op industriële schaalgrootte CO_2 te verwijderen is het absorptie-desorptie proces, waarin vaak (waterige) oplossingen van (alkanol)amines als absorptie vloeistof fungeren [Kohl en Nielsen, 1997].

Bij de bulkverwijdering van CO_2 wordt tegenwoordig vaak een activator toegevoegd aan een waterige oplossing van een langzaamreagerend amine, zoals bijv. piperazine (PZ) aan een waterige N-methyldiethanolamine (MDEA) oplossing. Het principe van een dergelijke mix van een snelreagerend primair of secundair (alkanol)amine - zoals piperazine - met een tertiair alkanolamine - zoals MDEA - is gebaseerd op de relatief hoge reactiesnelheid van CO_2 met het primaire of secundaire amine, in combinatie met de lage reactiewarmte van CO_2 met het tertaire alkanolamine. Dit leidt tot hogere absorptiesnelheden in de absorptiekolom en tot een lagere energiebehoefte en dus tot lagere kosten in de desorptiekolom. Voor een optimaal ontwerp van een dergelijk absorptie-desorptie proces met het piperazine geactiveerd MDEA als oplosmiddel is een gedegen kennis van zowel stofoverdrachtsaspecten (inclusief bijv. hydrodynamica en kinetiek) als thermodynamisch evenwicht noodzakelijk.

De in de literatuur aanwezige kennis van het (absorptie)gedrag van waterige mengsels van MDEA en PZ is relatief beperkt, en het doel van dit proefschrift is dan

ook om meer inzicht te verwerven in de absorptie van CO_2 in waterige oplossingen van MDEA en piperazine. Daarbij is de aandacht zowel gericht op de stofoverdrachtssnelheid (met daarbij o.a. van belang de fysisch-chemische eigenschappen en kinetiek) als op het thermodynamisch evenwicht.

Betrouwbare fysisch-chemische data van een oplosmiddel zijn van groot belang, omdat deze enerzijds nodig zijn voor een correcte interpretatie van absorptie experimenten en anderzijds dienen ze als belangrijke input voor hydrodynamica- en stofoverdrachtsmodellen, zoals die gebruikt worden bij het ontwerp van gas-vloeistof processen. Daarom zijn uitgebreide experimentele studies uitgevoerd naar de dichtheid, viscositeit en oppervlaktespanning van waterige piperazine oplossingen, en is daarnaast ook de fysische oplosbaarheid van CO_2 bepaald (indirect via de CO_2:N_2O analogie). Ook de dichtheid en viscositeit van waterige MDEA-PZ oplossingen zijn gemeten, en daarnaast is de Taylor dispersie methode gebruikt om de diffusiecoëfficiënt van piperazine in verschillende waterige piperazine en MDEA/PZ oplossingen te bepalen. De experimenteel bepaalde diffusiecoëfficiënten bleken goed te beschrijven met een soort van Stokes-Einstein vergelijking, waarmee de diffusiecoëfficiënt afgeschat kan worden op basis van de viscositeit van een oplossing en de diffusiecoëfficiënt bij oneindige verdunning in water. Voor een redelijke schatting van deze laatste grootheid bleek de methode van Othmer en Thakar [1953] het meest geschikt.

De absorptiesnelheid van kooldioxide in waterig piperazine is gemeten in een geroerde cel bij verschillende partiaaldrukken, temperaturen en piperazine concentraties. De experimentele resultaten zijn geïnterpreteerd met de DeCoursey vergelijking [DeCoursey, 1974] om uitspraken te kunnen doen over de reactiesnelheid van de hoofdreactie, $2PZ + CO_2 \rightarrow PZCOO^- + PZH^+$. In de verwerking van de resultaten is aangenomen dat deze reactie tussen piperazine en kooldioxide een eerste orde gedrag vertoont naar zowel CO_2 als piperazine. De overall tweede orde reactiesnelheidsconstante is uiteindelijk vastgesteld op 76 $m^3\ mol^{-1}\ s^{-1}$ bij een temperatuur van 298.15 K, met een activatie temperatuur van $4.1 \cdot 10^3$ K. Ook de absorptie van

CO_2 in waterig piperazine, waaraan een equimolaire hoeveelheid zoutzuur (HCl) was toegevoegd, is gemeten om de reactiviteit van de reactie tussen CO_2 en PZH^+, $2PZH^+ + CO_2 \rightarrow H^+PZCOO^- + PZH_2^+$, te kunnen bepalen. Deze resultaten zijn geïnterpreteerd met de benadering van Hogendoorn et al. [1997]. Deze benadering is gebaseerd op de expliciete DeCoursey vergelijking, met dien verstande dat de oneindige versnellingsfactor gecorrigeerd is voor de reversibiliteit van de reactie. Ook bij deze reactie is aangenomen dat deze eerste orde in beide reactanten is, en de gevonden reactiesnelheidsconstante bleek 0.30 ± 0.10 m^3 mol^{-1} s^{-1} bij 298.15 K. De Brønsted plot techniek toonde aan dat er ook voor amines met een op piperazine gelijkende structuur een relatie blijkt te bestaan tussen de pKa van het amine en de reactiesnelheid met CO_2.

Bij de bepaling van de reactiekinetiek tussen van kooldioxide met piperazine moest een analytische benadering gebruikt worden om de experimentele absorptiesnelheden te interpreteren. De oorzaak hiervan lag in de gekozen meettechniek: in de conventionele geroerde cel bleek het niet mogelijk om te meten bij zo'n lage partiaaldruk dat altijd aan de pseudo eerste orde condities voldaan kon worden. Om absorptiemetingen bij aanzienlijk lagere partiaaldrukken, en dus metingen onder pseudo eerste-orde condities mogelijk te maken, is de conventionele geroerde cel opstelling aangepast. In de nieuwe experimentele opstelling werd een tweede geroerde cel toegevoegd, die gevuld werd met dezelfde oplossing als de originele cel. De tweede cel diende daarbij als referentie voor de dampspanning van de absorptievloeistof. Indien een (reactief) gas boven de oplossing in de originele cel aanwezig was, kon de partiaalspanning van dit gas direct bepaald worden uit de verschildruk tussen de twee cellen, wat de nauwkeurigheid voor lage partiaaldrukken aanzienlijk vergrootte. Dit nieuwe geroerde cel principe is experimenteel gevalideerd met de reactie tussen kooldioxide en NaOH bij 25 en 40 $^\circ$C. In de nieuwe opstelling zijn absorptiesnelheden bepaald bij relatief lage CO_2 partiaaldrukken ($P_{CO2,min} = 1.5$ mbar), en de aldus bepaalde kinetiekconstanten kwamen goed overeen met de waarden zoals gevonden in de literatuur.

Het absorptiegedrag van kooldioxide in waterig MDEA-PZ is onderzocht in een (conventionele) geroerde cel bij CO_2 partiaaldrukken tussen ca. 20 en 400 mbar. Absorptiesnelheden zijn gemeten als functie van de beladingsgraad, in oplossingen van 4.0 kmol m^{-3} MDEA, waaraan 0.5 of 1.0 molair PZ is toegevoegd - zodat de totale amine concentratie dus 4.5 of 5.0 molair bedroeg. De verkregen experimentele data zijn vergeleken met berekeningen, die gemaakt zijn met een stofoverdrachtsmodel. Dit numerieke model gaat uit van een Fick-diffusie model waarin de individuele reacties van de componenten MDEA en PZ met CO_2 geïntegreerd zijn. Bij lage beladingsgraden kwamen experiment en model goed overeen, maar met toenemende CO_2 belading begonnen model en experiment steeds meer van elkaar af te wijken, waarbij het model de experimenteel gevonden flux systematisch onderschatte. Dit is waarschijnlijk vooral te wijten aan de non-idealiteit van het systeem, die niet is meegenomen in het model.

Bovenstaande bevindingen ten aanzien van de absorptie van CO_2 in (beladen) oplossingen met MDEA en piperazine toonden aan dat de uitkomsten van een numeriek stofoverdrachtsmodel sterk beïnvloed worden door de non-idealiteit van de oplossing, en de hiermee samenhangende berekening van de evenwichtssamenstelling van de vloeistof. Een betrouwbare berekening van deze vloeistofspeciatie kan alleen gemaakt worden indien een goed thermodynamisch model voorhanden is, en derhalve is het laatste deel van dit proefschrift gewijd aan de ontwikkeling van een dergelijk thermodynamisch evenwichtsmodel. In een eerste stap is de (chemische) oplosbaarheid van CO_2 gemeten in waterige piperazine oplossingen van 0.2 en 0.6 molair piperazine, bij temperaturen van 25, 40 en 70 $^{\circ}$C. Deze data zijn samen met de beschikbare literatuurdata gecorreleerd met een thermodynamisch model dat gebaseerd is op de 'electrolyte equation of state (EoS)', geïntroduceerd door Fürst en Renon [1993]. Dit model bestaat uit een toestandsvergelijking die uitgebreid is met extra termen om de aanwezigheid van ionen in het systeem te verdisconteren. Het ontwikkelde model kon de beschikbare experimentele oplosbaarheidsdata van CO_2 in waterig piperazine beschrijven met een gemiddelde afwijking van slechts 16 %. Daarnaast bleek het model in staat de experimenteel beschikbare pH en

geleidbaarheidsdata goed te voorspellen. In een tweede stap is het hierboven beschreven model uitgebreid met MDEA. Tevens zijn experimenten uitgevoerd waarin de oplosbaarheid van CO_2 in waterige mengsels van MDEA en piperazine gemeten is. In deze experimenten zijn niet alleen oplosbaarheden met de daarbij behorende CO_2 partiaaldruk gemeten, maar tegelijkertijd zijn ook de pH en geleidbaarheid van de oplossingen bepaald. Daarnaast zijn van een aantal MDEA-PZ oplossingen, beladen met kooldioxide, NMR spectra opgenomen, waaruit de concentratie van verschillende reactieprodukten berekend kon worden. De beschikbare literatuurdata (CO_2 oplosbaarheid in combinatie met partiaal- of totaaldruk) zijn gecorreleerd met het thermodynamisch model. Daarna is bestudeerd in hoeverre het EoS model de eigen experimentele data kon voorspellen. Het bleek dat het model goed in staat was de partiaaldrukken als functie van de belading te voorspellen, maar de theoretisch voorspelde speciatie van de vloeistof bleek daarbij duidelijk af te wijken van de experimentele samenstelling zoals bepaald aan de hand van de NMR data. De oorzaak hiervoor moet waarschijnlijk gezocht worden in het ontbreken van betrouwbare evenwichtsdata van enkele binaire subsystemen - en de daaruit voortvloeiende onzekerheid in enkele fysische input parameters. Desondanks kan gesteld worden, dat de 'electrolyte equation of state' een veelbelovend thermodynamisch model blijkt voor het beschrijven van de oplosbaarheid van CO_2 in waterige oplossingen van MDEA en/of piperazine.

Vervolgonderzoek aan het absorptiegedrag van kooldioxide in waterige PZ-MDEA oplossingen zou zich moeten richten op het verkrijgen van meer, en meer betrouwbare fysische evenwichtsdata, waarmee de betrouwbaarheid van de verschillende input parameters in het EoS model aanzienlijk verhoogd kan worden. Indien na deze verfijning zou blijken dat het EoS model ook de evenwichtssamenstelling van beladen MDEA-PZ oplossingen goed kan voorspellen, kan dit model de input leveren voor het reeds beschikbare numerieke stofoverdrachtsmodel. Op zijn beurt, zou het stofoverdrachtsmodel dan de gemeten absorptiesnelheden in met name beladen oplossingen van MDEA en piperazine beter moeten kunnen beschrijven. Het stofoverdrachtsmodel zou uiteindelijk in combinatie met het verfijnde EoS model

moeten zorgen voor een nog beter begrip van de absorptie van kooldioxide in waterige MDEA-PZ oplossingen, wat nieuwe mogelijkheden biedt bij het ontwerpen en optimalizeren van absorptieprocessen waarin gebruik wordt gemaakt van waterig MDEA met piperazine als activator.

Contents

Chapter 1

General Introduction

1.1 Carbon dioxide capture

The removal of carbon dioxide from process gas streams is an important step in many industrial processes and is required because of process technical, economical or environmental reasons. In the presence of water, CO_2 - being an acid gas - can cause corrosion to process equipment. Besides this, the presence of CO_2 reduces the heating value of a natural gas stream and also wastes valuable pipeline capacity. In LNG (liquefied natural gas) plants, it should be removed to prevent freezing in the low-temperature chillers, moreover, in the manufacture of ammonia, it would poison the catalyst. Finally, CO_2 - which is also the most important greenhouse gas - is also held responsible for the recent climate changes. One technology which is frequently used to capture CO_2 is the absorption - desorption process, which is schematically shown in Figure 1.1.

The untreated, sour gas stream enters the absorber at the bottom of the column where it is contacted with a solvent. The solvent normally flows counter-currently down the column, where it gradually takes up more and more CO_2, until it leaves the absorber at the bottem as the so-called rich solvent. The purified gas leaves the absorber at the top, where it can be further processed. The rich solvent is heated in a heat exchanger prior to entering the desorber column. In the desorber,

the absorbed carbon dioxide is stripped from the solvent due to a higher temperature and lower pressure. Subsequently, the regenerated solvent is fed to the top of the absorber column again, while the stripped CO_2 can be further processed to make it suitable for use in e.g. greenhouses or (underground) storage.

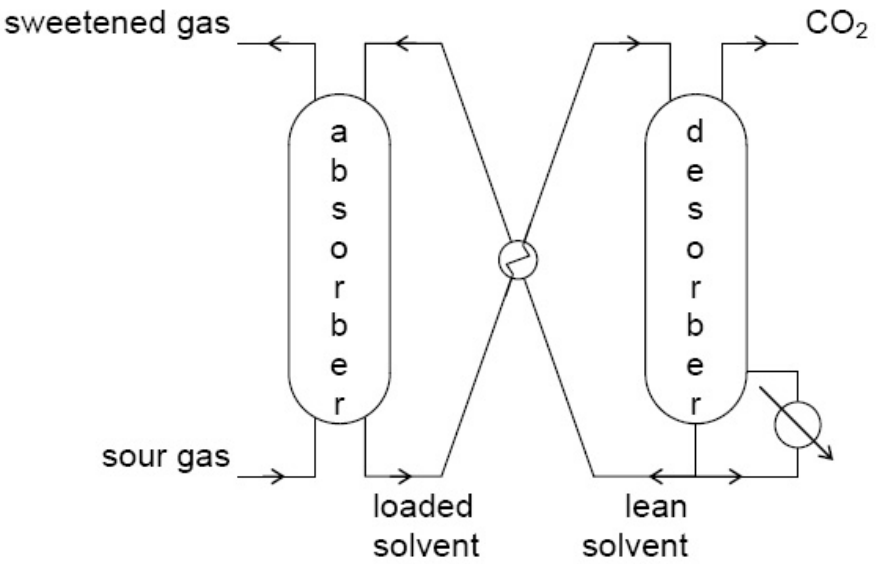

Figure 1.1: Schematic drawing of an absorber-desorber unit.

The majority of the variable costs of the absorber-desorber process are usually determined by the regeneration energy required in the desorber column. Depending on the process requirements, different types and combinations of both physical and chemical solvents can be used to remove CO_2 from gas streams. One frequently used group of chemical absorbents are (aqueous) solutions of alkanolamines.

1.2 Alkanolamines

These ammonia derivatives can be subdivided into three different classes depending on the number of substituent groups on the nitrogen atom:

1. Primary alkanolamines, where one hydrogen atom of the ammonia molecule is replaced by an ethanolgroup. The best-known example is monoethanolamine or MEA:

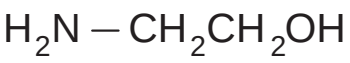

Figure 1.2: Monoethanolamine (MEA).

2. Secondary alkanolamines, where two ethanolgroups are present in the molecular backbone, such as e.g. diethanolamine or DEA:

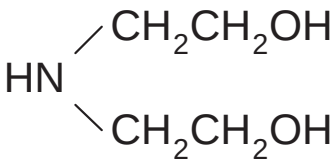

Figure 1.3: Diethanolamine (DEA).

3. Tertiary alkanolamines, where all hydrogen atoms have been replaced by either alkyl or alkanolgroups. The most popular amine in this group is N-methyldiethanolamine or MDEA:

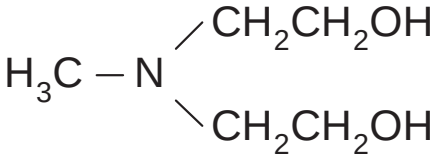

Figure 1.4: N-Methyldiethanolamine (MDEA).

The sterically hindered (alkanol)amines - usually considered to be the fourth class - are not regarded in this introduction as they will not be subject of research in this thesis.

In aqueous solutions, primary, secondary and tertiary alkanolamines exhibit a different behavior towards CO_2 due to their molecular structure. Primary and

secondary alkanolamines react with CO_2 under the formation of a carbamate species according to the following overall reaction:

$$2Am + CO_2 \rightleftarrows AmH^+ + AmCOO^-$$

Tertiary amines cannot form a carbamate (due to their lack to eliminate a hydrogen atom) and hence their reaction with CO_2 is considered to be a hydrolysis catalyzed reaction:

$$Am + CO_2 + H_2O \rightleftarrows AmH^+ + HCO_3^-$$

Further characteristics with respect to the reaction of these alkanolamines with CO_2 in aqueous solution, such as typical kinetic rate constants for the various groups of amines and the heat of solution of CO_2, are listed in Table 1.1 below.

Table 1.1: Characteristics of the reaction between CO_2 and MEA, DEA and MDEA.

Class	alkanolamine	Am : CO_2	k_2[a][b] ($T = 25\ ^\circ$C) [m^3 $kmol^{-1}$ s^{-1}]	Heat of solution of CO_2[c] kJ mol^{-1}
Primary	MEA	2 : 1	6.0	-82
Secondary	DEA	2 : 1	1.3	-69
Tertiary	MDEA	1 : 1	$4 \cdot 10^{-3}$	-49

[a] Assuming the reaction rate is given by $R_{CO2} = -k_2 C_{Am} C_{CO2}$
[b] Taken from Versteeg et al. [1996]
[c] Taken from Carson et al. [2000]

Table 1.1 illustrates that MEA shows the highest rate of reaction of the three amines with carbon dioxide, whereas MDEA has the more advantageous properties with respect to the reaction stoichiometry (capacity) and the heat of solution (heat of regeneration). These different absorption characteristics are one of the reasons that an aqueous MEA solution is a popular solvent in flue gas treating - where the CO_2 content is typically below 15 % - while aqueous MDEA is frequently used in carbon dioxide bulk removal processes, mostly due to its lower heat of regeneration and therewith a lower energy requirements.

1.3 Piperazine activated MDEA

Nowadays, the addition of a primary or secondary (alkanol)amine to an aqueous MDEA solution has found widespread application in the removal and absorption of carbon dioxide. The principle of such an aqueous blend of a so-called 'activator' with a tertiary amine is based on the relatively high rate of reaction of CO_2 with the primary or secondary alkanolamine combined with the low heat of reaction of CO_2 with the tertiary alkanolamine, which leads to higher rates of absorption in the absorber column and lower heats of regeneration in the stripper section. One of the activators presently used in industry is the cyclic diamine piperazine:

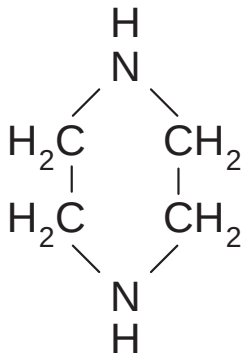

Figure 1.5: Piperazine (PZ).

The piperazine (PZ) activated MDEA process was patented by BASF in the early 80s [Appl et al., 1982], and has been subject of several studies over the past decade as it has proven to be a successfull solvent in the bulk removal of carbon dioxide. Crucial for an optimal design and operation of both an absorber and a desorber column is information concerning mass transfer related issues (including e.g. hydrodynamics and kinetics) on one hand and thermodynamic equilibrium on the other hand. However, the information available in the literature on CO_2 absorption in piperazine activated MDEA is still rather limited:

Xu et al. [1992] used a disk column to investigate the kinetics of absorption of carbon dioxide into piperazine activated MDEA solutions. Further studies within

the same research group included the equilibrium solubility of CO_2 [Xu et al., 1998, Liu et al., 1999] and absorption rates [Zhang et al., 2001, 2003] into PZ activated MDEA solutions. Their (experimental) studies were usually carried out at conditions where the molar ratio between carbon dioxide and piperazine in solution was well over unity.

Bishnoi and Rochelle [2000, 2002b,a] performed a more fundamental study in which they firstly reported the individual kinetics of CO_2 with piperazine and reported CO_2 equilibrium data in aqueous piperazine solutions. Next, they investigated the thermodynamics of the H_2O - CO_2 - MDEA - PZ system, reporting experimental solubility data and using the electrolyte NRTL model [e.g. Austgen et al., 1989] to correlate their results. Finally, they determined experimental absorption rates of CO_2 into PZ activated MDEA solutions and used a rigorous mass transfer model to correlate their results.

Ermatchkov et al. [2002], Pérez-Salado Kamps et al. [2003] performed studies on the thermodynamic equilibrium in systems containing piperazine. Ermatchkov et al. [2002] used ^{1}H NMR spectroscopy to determine the equilibrium constants for the reactions involving piperazine and carbon dioxide, while Pérez-Salado Kamps et al. [2003] reported CO_2 solubilities in both aqueous piperazine solutions and aqueous PZ - MDEA solutions at high total pressures (up to about 95 bar) and they used the Pitzer model [e.g. Li and Mather, 1994] to correlate their results.

Besides the literature mentioned above, several other studies are reported on the kinetics between piperazine and CO_2 [Seo and Hong, 2000, Sun et al., 2005] and on the equilibrium solubility of carbon dioxide in aqueous piperazine solutions [Aroua and Mohd Salleh, 2004] and aqueous PZ - MDEA solutions [Si Ali and Aroua, 2004, Jenab et al., 2005].

1.4 This thesis

Despite the studies mentioned in the previous section, the mechanism of absorption of carbon dioxide into the piperazine activated aqueous MDEA is still not known in detail yet at present. Therefore, it is the incentive of this thesis to provide more insights into the absorption of carbon dioxide into aqueous solutions containing piperazine and MDEA, both from the experimental and the theoretical point of view.

Chapters 2 and 3 contain various physico-chemical properties which are needed in the interpretation and modelling of carbon dioxide absorption in aqueous systems containing piperazine and/or MDEA. Chapter 2 deals with properties concerning aqueous piperazine solutions, such as density, viscosity and surface tension as well as the physical solubility of N_2O which is related to that of CO_2 using the well known CO_2:N_2O analogy (see e.g. Laddha et al. [1981]). Densities and viscosities of piperazine activated aqueous MDEA solutions have been listed in Chapter 3. In this chapter, also the Taylor dispersion technique is described, which was used for the experimental determination of the diffusion coefficient of piperazine in aqueous PZ solutions and the diffusivity of both PZ and MDEA in an activated MDEA solution.

Chapter 4 describes the kinetics of carbon dioxide in aqueous piperazine solutions. Absorption experiments carried out in a stirred cell contactor are used to deduce the kinetic rate constant of this reaction at different temperatures. Also, an attempt is made to derive a Brønsted relation for amines containing a ring structure similar to piperazine.

In Chapter 5, a new mode of operation is proposed for the conventional stirred cell setup which should make it suitable for absorption rate experiments at very low (carbon dioxide) partial pressures. The new configuration is validated with the absorption of CO_2 into aqueous NaOH solutions.

The absorption rate of carbon dioxide into piperazine activated MDEA solutions is the subject of Chapter 6: Experimentally obtained fluxes into aqueous

4.0 kmol m^{-3} MDEA solutions activated with either 0.5 or 1.0 kmol m^{-3} piperazine at different carbon dioxide partial pressures were compared to a 'first principles' numerical model, after which conclusions are drawn regarding the mechanism of absorption.

Chapters 7 and 8, finally, are studies on the thermodynamic equilibrium of the CO_2 - H_2O - PZ system (Chapter 7) on one hand, and the CO_2 - H_2O - MDEA and CO_2 - H_2O - MDEA - PZ system (Chapter 8) on the other hand. Both chapters contain various experimental data on the solubility of carbon dioxide in the respective systems studied, not only equilibrium partial pressure data but also pH, conductivity and liquid composition data.The electrolyte equation of state, as introduced by Fürst and Renon [1993], is used to describe the present data as well as the equilibrium solubility data published in the literature.

Chapter 2

Solubility of N_2O in, and Density, Viscosity, Surface Tension of Aqueous Piperazine Solutions

Abstract

The physical solubility of N_2O in, and the density and viscosity of aqueous piperazine solutions have been measured over a temperature range of 293.15 to 323.15 K for piperazine concentrations ranging from about 0.6 to 1.8 kmol m^{-3}. Furthermore, this chapter contains experimental surface tension data of aqueous piperazine solutions at temperatures of 293 and 313 K and at concentrations of 0.5, 1.0 and 1.5 kmol m^{-3} piperazine in water.

2.1 Introduction

The removal of acid gases, such as CO_2 and H_2S , from industrial gases is frequently carried out by an absorption - desorption technology, using (aqueous) solutions containing alkanolamines as solvents [Kohl and Nielsen, 1997]. One industrially applied solvent is the piperazine (PZ) activated aqueous N-methyldiethanolamine (MDEA) solution [Appl et al., 1982]. Such a blend of an activator (usually a primary or secondary amine) with a tertiary amine combines the relatively high rate of reaction of the former with CO_2 with the lower reaction heat of the latter with CO_2, thereby gaining higher rates of absorption in the absorption column while maintaining a low energy of regeneration in the stripper section.

An optimal design and operation of absorption and desorption columns requires detailed knowledge concerning (among other things) the mass transfer rate of carbon dioxide into the absorption liquid, which in turn is to a large extent determined by the kinetic rates of both the activator (PZ) and the tertiary amine (MDEA) with CO_2. And, while the kinetics of MDEA with CO_2 has been studied extensively in the past [Versteeg et al., 1996], only two publications have dealt with the (independent) measurement of the reaction rate of PZ with CO_2 [Bishnoi and Rochelle, 2000, Sun et al., 2005]. A correct interpretation of these kinetic experiments, as the kinetics have been derived from mass transfer experiments, requires the knowledge of the physical solubility and diffusivity of CO_2 in aqueous piperazine solutions. Unfortunately, it is not possible to determine these properties directly, due to the chemical reaction(s) between CO_2 and (aqueous) piperazine. In the literature [Sada et al., 1977, 1978, Laddha et al., 1981, Versteeg et al., 1996] therefore, it is suggested to apply the 'N_2O analogy' to estimate both of the aforementioned physico-chemical properties. This seems reasonable, since N_2O resembles CO_2 in configuration, molecular volume and electronic structure, moreover, it is a non-reactive gas.

Recently, research [Kumar et al., 2002] has also focused on the application of microporous membranes as a gas-liquid contactor, which (within certain operating conditions) could offer some advantages over conventional contactors, such as ease

of scale-up, higher interfacial area per unit volume and the possibility to vary mass transfer coefficients and interfacial area independently. One major disadvantage when working with organic solvents is the possibility of wetting of the membrane, which means that the absorption liquid penetrates the membrane pores, thereby imposing an additional (very large) mass transfer resistance. The minimum pressure, ΔP_{LY}, required for the liquid to penetrate into the membrane pores (with pore diameter d_{pore}) is, according to the Laplace-Young equation, linearly dependent on its surface tension, γ_{GL}:

$$\Delta P_{LY} = -\frac{4\gamma_L \cos\theta}{d_{pore}} \tag{2.1}$$

Also for conventional gas-liquid contactors like absorption columns, the surface tension of a liquid is a non-trivial property, since it affects important design parameters, such as hydrodynamics, volumetric mass transfer coefficient and gas holdup [Deckwer, 1992].

This chapter contains densities, viscosities and N_2O solubilities at temperatures in the range 293.15 to 323.15 K, and surface tensions at 293 and 313 K. The piperazine concentration range studied was about 0.6 to 1.8 kmol m^{-3} in the density, viscosity and N_2O solubility measurements, while the surface tension was measured at piperazine concentration of 0.5, 1.0 and 1.5 kmol m^{-3}.

2.2 Experimental

Solutions of PZ were prepared by dissolving a known amount of piperazine (purity 99 %, Aldrich) in double distilled water. The actual concentration of the prepared solution was measured (at T = 293 K) by means of a volumetric titration with a 1.0 N solution of HCl. The experimentally determined piperazine concentrations were accurate to within 0.5 %. The nitrous oxide (purity 99.5 %) used in the solubility experiments was obtained from Hoekloos.

2.2.1 Density and viscosity

The density was determined with a commercial density meter (DMA 58, Anton Paar GmbH), in which the temperature could be controlled within ± 0.05 K. The viscosity was measured using a PSL Ubbelohde viscometer (type ASTM-IP, capillary 0C), submerged in a thermostatbath for temperature control (within ± 0.1 K).

2.2.2 N_2O solubility

The physical solubility of N_2O was measured in a thermostatted reactor (volume ≈ 2 L), equipped with a gas inducing impeller, connected to a calibrated gas vessel. Both reactor and gas supply vessel were provided with a temperature and pressure indicator. A known amount of PZ solution was transferred to the reactor vessel and allowed to reach the desired temperature, after which the liquid was degassed by applying vacuum for a short period. Then, the gas supply vessel was filled with pure N_2O and the initial pressure in this vessel was recorded. Next, a sufficient amount of N_2O was fed from the gas supply vessel to the reactor. Subsequently, the valve between the gas supply vessel and the reactor was closed and the final pressure in the gas supply vessel was recorded. After this, the agitator in the reactor was switched on and the contents of the reactor was allowed to reach equilibrium (which was reached when the reactor pressure remained constant) and the equilibrium pressure and the corresponding temperature in the reactor were recorded. Subsequently, the temperature in the reactor was adjusted to a different desired temperature using the thermostat bath, and again the solution was allowed to reach equilibrium. Following this method, a series of experimental solubilities at different temperatures could be obtained using one solution of certain piperazine concentration.

The distribution coefficient, defined in this work as the ratio between the equilibrium concentrations in the liquid and the gas phase, at each temperature was calculated using the difference between the initial and final pressure in the gas supply vessel, the equilibrium pressure and the vapor pressure of the lean solution

at the corresponding temperature, according to Eqs. 2.2, 2.3 and 2.4:

$$\Delta n_{N_2O} = \frac{\Delta P_{GV} V_{GV}}{R T_{GV}} \tag{2.2}$$

$$P_0(T) = \frac{\Delta n_{N_2O} R T}{V_{gas}} + P_{vap}(T) \tag{2.3}$$

$$m(T) = \left(\frac{C^{liq}_{N_2O}(T)}{C^{gas}_{N_2O}(T)} \right)_{eq} = \frac{P_0(T) - P_{eq}(T)}{P_{eq}(T) - P_{vap}(T)} \frac{V_{gas}}{V_{liq}} \tag{2.4}$$

The vapor pressure in the reactor was calculated from the vapor pressure of pure water thereby assuming Raoult's law to correct for the piperazine content:

$$P_{vap}(T) = x_{H_2O} \cdot P^{pure}_{H_2O}(T) \tag{2.5}$$

The error introduced with this assumption is expected to be minimal, considering the concentration range studied ($x_{H_2O} > 0.96$). The experimental procedure and accuracy were verified by measuring the solubility of N_2O in water. Results are shown in Table 2.1 and Figure 2.1.

Table 2.1: The distribution coefficient of N_2O in water at various temperatures.

T [K]	m [-]
293.15	0.674
298.15	0.592
303.15	0.524
313.15	0.428
323.15	0.366

From Figure 2.1 it is clearly shown, that the measured solubilities are well in line with experimental data taken from various literature sources [Duda and Vrentas, 1968, Versteeg and Van Swaaij, 1988b, Xu et al., 1991a, Sun et al., 2005].

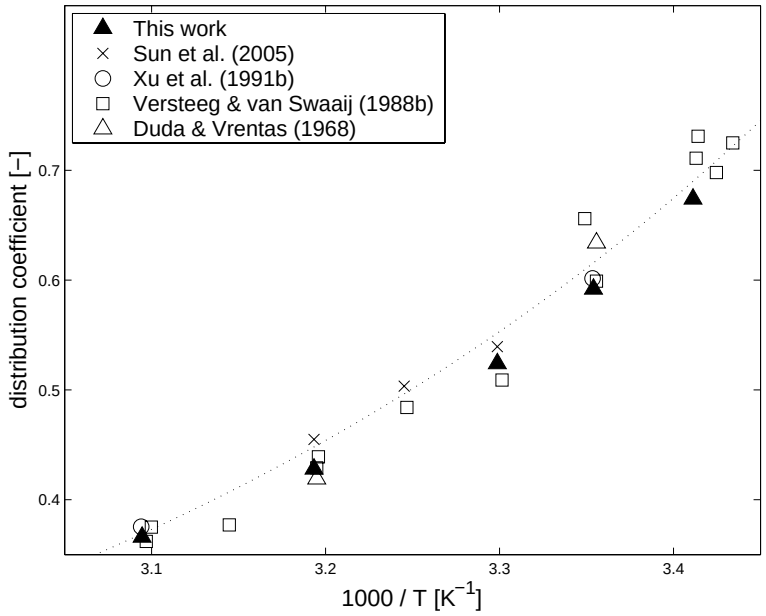

Figure 2.1: The distribution coefficient of N_2O in water as a function of temperature. Dotted line represents the correlation for N_2O solubility in water as proposed by Versteeg and Van Swaaij [1988b].

2.2.3 Surface tension

Surface tension measurements were carried out with a Krüss K9 Tensiometer, using the Wilhelmy plate method. Measurements were performed at temperatures of (293 ± 1) and (313 ± 1) K. The maximum experimental uncertainty caused by these temperature changes amounts to 0.3 mN m^{-1} (for water).

2.3 Results and discussion

2.3.1 Density and viscosity

The measured values of density and viscosity as a function of concentration and temperature are listed in Table 2.2. The experimental uncertainty is estimated at 0.01 % (density) and 1 % (viscosity).

Table 2.2: Densitiy and viscosity of aqueous piperazine solutions.

	C_{PZ} [kmol m^{-3}]	ρ [kg m^{-3}]	μ [mPa s]
T = 293.15 K	0.623	1000.46	1.260
	1.006	1002.49	1.524
	1.490	1005.40	1.865
T = 298.15 K	0.623	999.37	1.105
	1.006	1001.30	1.310
	1.490	1004.11	1.616
	1.686	1005.39	1.803
T = 303.15 K	0.623	997.94	0.980
	1.006	999.79	1.154
	1.490	1002.47	1.402
	1.686	1003.66	1.556
T = 313.15 K	0.623	994.25	0.787
	1.006	996.03	0.922
	1.490	998.49	1.091
	1.686	999.49	1.201
T = 323.15 K	0.623	989.76	0.650
	1.006	991.53	0.747
	1.490	993.86	0.876
	1.686	994.74	0.956

Sun et al. [2005] also reported density and viscosity data for aqueous piperazine solutions at temperatures of 303.15, 308.15 and 313.15 K and PZ concentrations ranging from 0.23 to 0.92 kmol m^{-3}. The work of Cullinane [2005] contains experimental density and viscosity data at temperatures of 298.15 and 313.15 K at a molality range from 0.5 to 1.8 mol piperazine per kg water. A graphical comparison between the three different data sets at 298.15, 303.15 and 313.15 K is shown in Figures 2.2 and 2.3.

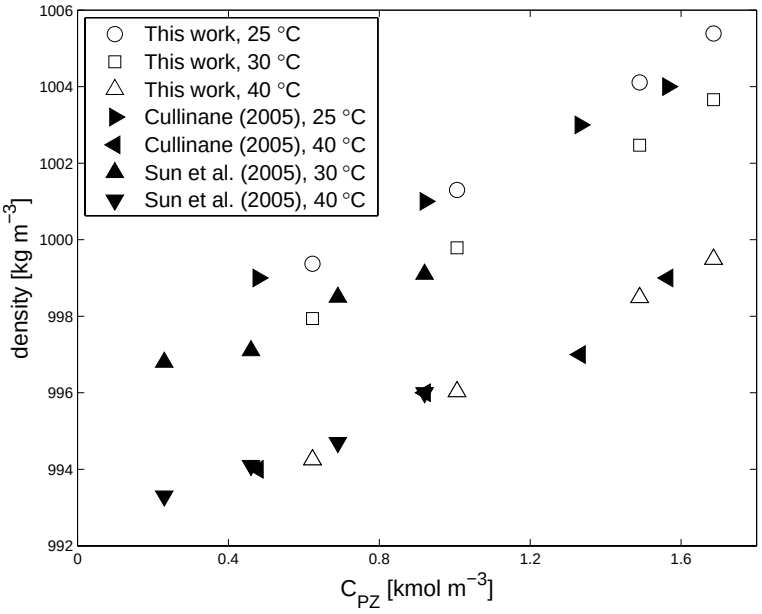

Figure 2.2: . Density of aqueous piperazine solutions as a function of PZ concentration.

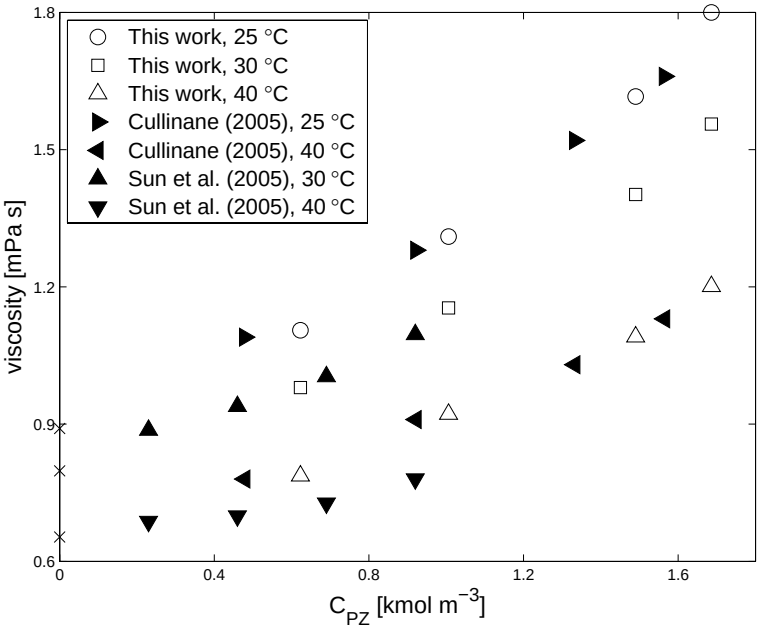

Figure 2.3: . Viscosity of aqueous piperazine solutions as a function of PZ concentration.

Figure 2.2 shows that the presently reported densities are in good agreement with the data by Cullinane [2005], Sun et al. [2005]; the deviation between the three data sets is always smaller than 0.25 %. As for the reported viscosities, however, this is not completely the case, as illustrated in Figure 2.3. The present data are in very good agreement with data reported by Cullinane [2005], but the comparison with the experimental data of Sun et al. [2005] shows, that, while their data at 303.15 K are in good agreement with the present data, their data at 313.15 K are consistently a bit lower than the present data and the data reported by Cullinane [2005].

Pure water viscosity data (represented by $\times$), taken from Lide [1994], have been included in Figure 2.2 to compare the trends in all three data series. And although the comparison is a very simple one, it does give an indication that the data sets presented in this work and in the work of Cullinane [2005] seem to be more consistent with the limiting case of pure water than the experimental viscosities presented by Sun et al. [2005].

2.3.2 N_2O solubility

The solubility of N_2O in aqueous PZ solutions, quantified in dimensionless form by the distribution coefficient m, is listed in Table 2.3. The experimental uncertainty is within 5.0 %. The solubility data at 298.15, 303.15 and 313.15 K are compared to the corresponding data sets presented by Cullinane [2005] and Sun et al. [2005] in Figure 2.4.

Table 2.3: N_2O solubility, as the distribution coefficient, in aqueous piperazine solutions.

C_{PZ} [kmol m^{-3}]	$T = 293.15$ K	$T = 298.15$ K	$T = 303.15$ K	$T = 313.15$ K	$T = 323.15$ K
0.219	0.678	0.590	0.529	0.423	0.354
0.589	0.669	0.588	0.522	0.424	0.358
0.835	0.674	0.591	0.525	0.425	0.355
0.970	0.662	0.584	0.520	0.424	0.358
1.365	0.637	0.565	0.501	0.410	0.350
1.472	0.637	0.564	0.505	0.417	0.355
1.799		0.550	0.492	0.409	0.351

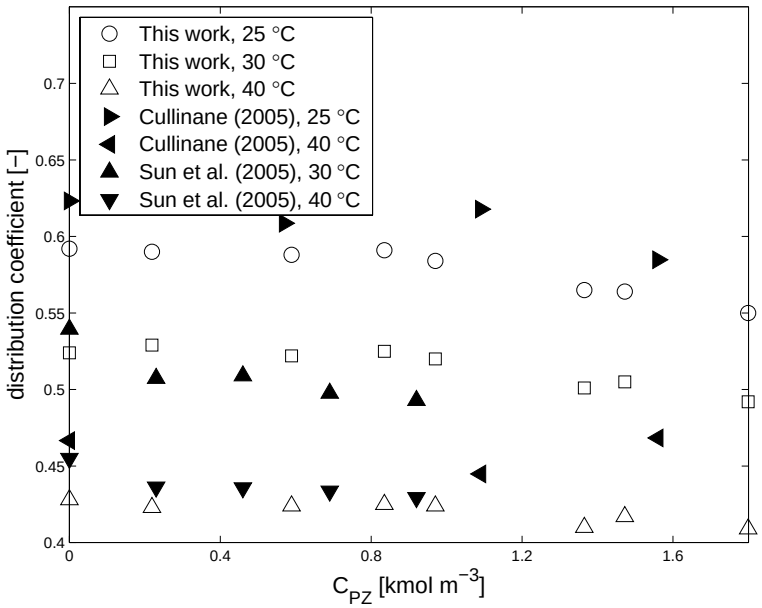

Figure 2.4: Solubility of N_2O, as the distribution coefficient, in aqueous piperazine solutions as a function of PZ concentration.

Figure 2.4 shows that the three data sets are reasonably in line with each other; the maximum deviation in the experimental results is found at a temperature of 313.15 K between the experimental data of Cullinane [2005] on one hand and the present data and the experimental data of Sun et al. [2005] on the other hand. It is noted that an increasing piperazine concentration does have a marginal effect on the N_2O solubility of the solution.

2.3.3 Surface tension

Surface tensions have been measured for three piperazine concentrations and the results are listed in Table 2.4. Each reported value is the average of at least three measurements. Along with the new surface tension data, also literature data on diethanolamine (DEA) and MDEA solutions are listed.

Table 2.4: Surface tension of aqueous piperazine solutions and aqueous diethanolamine and N-methyldiethanolamine solutions.

Amine	C_{amine} [kmol m^{-3}]	w_{amine} [%]	γ [mN m^{-1}]		Source
			$T = 293.15$ K	$T = 313.15$ K	
none	0	0	72.7	69.8	this work
PZ	0.5	4.3	71.7	68.5	this work
PZ	1.0	8.6	70.1	67.8	this work
PZ	1.5	12.9	69.3	67.6	this work
DEA		10	64.14	61.65	Aguila-Hernández et al. [2001]
DEA		10	63.90	61.74	Rinker et al. [1994]
MDEA		10	62.24	58.08	Rinker et al. [1994]

The addition of a small amount of piperazine to water does not have a pronounced effect on the surface tension of the solution at both 293 and 313 K, whereas the addition of more conventional (alkanol)amines such as DEA and MDEA causes a considerable drop in the surface tension.

2.4 Conclusions

This chapter reports experimentally determined densities, viscosities and N_2O solubilities of aqueous piperazine solutions at different concentrations and temperatures, thereby expanding the data set already available in the literature. A comparison with the experimental data reported by Cullinane [2005], Sun et al. [2005] shows a reasonable to good agreement for all results. Also, the surface tension of aqueous piperazine solutions was measured at temperatures of 293 and 313 K, and it was found that the addition of a small amount of piperazine to water does not have such a pronounced effect on the surface tension as observed for conventional (alkanol)amines like DEA and MDEA.

Acknowledgements

C. van Aken, A.H.G. Cents, T. Kleingeld, W. Lengton and H.F.G. Moed are acknowledged for their respective parts in the experimental work.

Chapter 3

Amine Diffusion in Aqueous Piperazine and Aqueous Piperazine - MDEA Solutions

Abstract

The diffusion coefficient of piperazine (PZ) in water has been measured using the Taylor dispersion technique over a temperature range from 293.15 to 368.15 K and piperazine concentrations ranging from 0 to 1.5 kmol m^{-3}. Also, the diffusion coefficients of both N-methyldiethanolamine (MDEA) and PZ have been determined for an aqueous 4.0 kmol m^{-3} MDEA solution blended with 0, 0.5 and 1.0 kmol m^{-3} piperazine at temperatures between 298.15 and 368.15 K. Furthermore, this chapter includes densities and viscosities of aqueous solutions containing both MDEA and piperazine at different concentrations and temperatures. A modified Stokes-Einstein equation was found to be able to estimate the experimental PZ and MDEA diffusivity data from the diffusion coefficient at infinite dilution and the solution's viscosity. The only relation which was able to predict the diffusion coefficient of piperazine at infinite dilution in water with a reasonable accuracy is the method proposed by Othmer and Thakar [1953].

3.1 Introduction

An accurate design of gas-liquid process equipment usually requires accurate knowledge on the mass transfer coefficients and diffusion coefficients. As the mass transfer coefficients are also affected by the diffusion coefficients [Deckwer, 1992], detailed knowledge on the diffusion coefficients are necessary to make the design of this equipment more reliable. They are also essential for a correct and accurate interpretation of many (lab scale) absorption rate experiments, as e.g. the experiments aimed at the determination of the intrinsic kinetics in a gas-liquid process [Danckwerts, 1979, Versteeg and Van Swaaij, 1988a]. In the past, several studies have reported experimental diffusivities of carbon dioxide and various (alkanol)amines in systems relevant for acid gas absorption [Versteeg et al., 1996]. In this contribution, additional data are presented to extend the existing experimental database.

Nowadays a number of different techniques is known for the experimental determination of diffusion coefficients, such as e.g. the diaphragm cell [Stokes, 1960, Brilman et al., 2001], the laminar jet [Unver and Himmelbau, 1964] and the Taylor dispersion method [Baldauf and Knapp, 1983, Matthews and Akgerman, 1988, Snijder et al., 1993]. In the latter method, the diffusion coefficient is obtained from the measured axial dispersion of a solute in a solvent over a long capillary tube. Two advantages of this method are the relatively high rate of data acquisition and the absence of the need to calibrate with a well-known system (as opposed to e.g. the diaphragm cell technique).

In this work, the Taylor dispersion method was used to characterize the diffusion coefficients in a blend of piperazine (PZ) and N-methyldiethanolamine (MDEA) in water, the so-called activated MDEA solvent. This chapter also includes experimental diffusion coefficients of PZ in aqueous PZ solutions at various temperatures and PZ concentrations. Also, the diffusion coefficients of both MDEA and piperazine, respectively, have been determined experimentally for an activated 4.0 kmol m^{-3} MDEA solution at various temperatures and PZ concentrations. Additionally, densities and viscosities of this blend of piperazine and MDEA in aqueous

solution are listed for various compositions and temperatures.

3.2 Experimental

The amine solutions were prepared by dissolving known amounts of piperazine (purity 99 %, Aldrich) and/or MDEA (purity 98 %, Aldrich) in double distilled water. The actual amine concentrations in the prepared solution were measured (at T = 293 K) by means of a volumetric titration with 1.0 N HCl. The experimentally determined piperazine and MDEA concentrations were accurate to within 1.0 % of the concentrations as determined by the weight ratios of the components. The acetone (purity 99 %, Aldrich) and methanol (purity 99 %, Aldrich) solutions in water, used in the validation experiments of the experimental diffusion setup, were prepared in a similar manner. The helium gas (quality 5.0) used in the same setup was supplied by Hoekloos.

3.2.1 Density and viscosity

The density was determined with a commercial density meter (DMA 58, Anton Paar GmbH), in which the temperature could be controlled within ± 0.05 K. The viscosity was measured using an Ubbelohde viscometer having a suitable viscosity range, submerged in a thermostat bath for temperature control (within ± 0.1 K).

3.2.2 Taylor dispersion technique

When a pulse of solute is injected into a solvent showing laminar flow through a capillary tube, the combined action of axial convection and radial molecular diffusion will eventually change the square pulse into a Gaussian curve. By solving the mass balances for such a system, Taylor [1953, 1954], Aris [1956] were able to relate the measured axial dispersion to the diffusion coefficient by:

$$C_m = \frac{N_{inj}}{2\pi R^2 \sqrt{\pi K t}} \exp\left(-\frac{(x-ut)^2}{4Kt}\right) \tag{3.1}$$

$$K = \frac{u^2 R^2}{48D} + D \tag{3.2}$$

where C_m is the measured concentration profile, N_{inj} the excess number of moles injected, x and R are the respective length and radius of the capillary tube, u the fluid velocity, t the time, and D the binary molecular diffusion coefficient. Since the concentration of the solute decreases during the dispersion process, an average value has to be determined. Alizadeh et al. [1980] called this the reference concentration (C_{ref}) which is given by:

$$C_{ref} = C_{solv} + \frac{N_{inj}\left(\frac{5}{16} - \frac{1}{8\sqrt{\pi}}\right)}{\pi R^2\sqrt{2Kt}} \tag{3.3}$$

where C_{solv} is the solvent concentration. More information on the fitting procedure is provided by Snijder et al. [1993].
The experimental setup used is shown schematically in Figure 3.1.

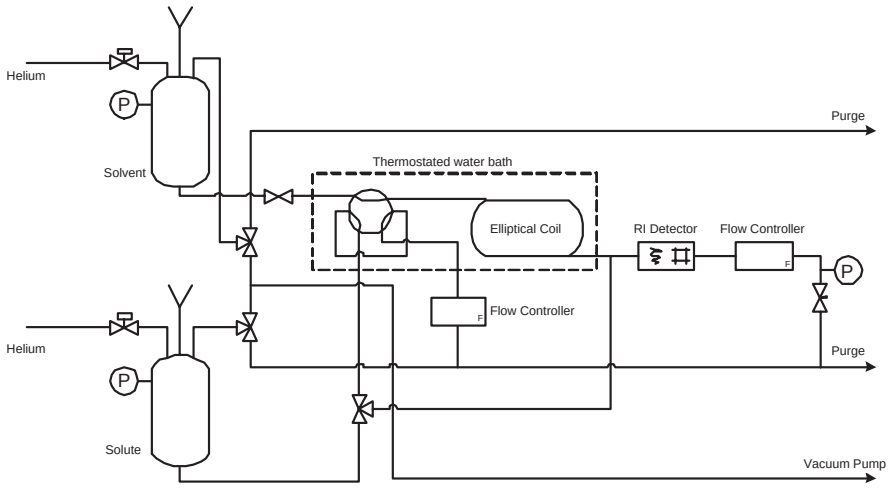

Figure 3.1: Schematic drawing of the Taylor dispersion setup.

Two vessels containing the solute and solvent were kept under a constant 5 bar helium pressure. Introduction of a solute pulse was done by switching a six-way, air actuated, valve back and forth within a few seconds. The capillary tube was elliptically coiled and placed in a water bath for temperature control. The flow was controlled with a mass flow controller (Rosemount Flowmega 5881), located after the refractive index (RI) detector (Varian 350 RI) to obtain a constant pulsation-

free flow throughout the measurement. During measurements at 333 K or higher, a needle valve located behind the RI detector and the flow controller was used to pressurize the coil up to 3 bar in order to avoid bubble formation inside the coil. The influence of the pressure on the diffusion coefficient can be neglected for the pressures applied in the present work [Matthews and Akgerman, 1987]. Prior to each experiment, both the solute and the solvent were degassed by applying vacuum for a short while, and afterwards, the RI detector was calibrated. The setup was connected to a computer, firstly to control the operation of the set-up as e.g. the six-way valve (when injecting a pulse). Secondly, the computer was used to record the RI detector output signal as a function of time, and the subsequent procedure to match the obtained curve to Eqs. 3.1 and 3.1 by adjusting the diffusion coefficient. The dimensions and flow conditions of the setup are given in Table 3.1.

Table 3.1: Details of the experimental setup and operation.

Dimensions		Value	
Length of the coil	L_C	14.92	m
Inner radius of the coil	R	$5.14 \cdot 10^{-4}$	m
Radius of the coil	R_C	0.1	m
Injection volume	V_{inj}	$(2.5 - 4.1) \cdot 10^{-8}$	m^3
Conditions		Value	
Liquid flow speed	u	$(2 - 6) \cdot 10^{-3}$	m s^{-1}
Péclet number	Pe	1500 - 6500	

A disturbance of the laminar fluid flow, secondary flow, can occur due to the coiling of the tube. This can lead to an inaccurately determined molecular diffusion coefficient. In order to avoid this disturbance, the critical $(De)^2Sc$ was determined according to Snijder et al. [1993] for each system. Each experiment was carried out with a $(De)^2Sc$ lower than the critical value.

3.3 Results - density & viscosity

Experimentally determined values of density and viscosity as a function of both amine concentrations and temperature are listed in Tables 3.2, 3.3, 3.4 and 3.5. The experimental error is estimated at 0.01 % (density) and 1 % (viscosity).

The experimental data from Tables 3.2, 3.3, 3.4 and 3.5 for solutions containing no piperazine ($C_{PZ} = 0$) can be compared to the work of Al-Ghawas et al. [1989], who reported densities and viscosities of aqueous MDEA solutions for temperatures ranging from 288.15 to 333.15 K and weight fractions up to 50 percent. A graphical comparison between the data of Al-Ghawas et al. [1989] and the present data on aqueous MDEA solutions (where $C_{PZ} = 0$) at 293.15, 303.15 K and 323.15 K is given in Figures 3.2 and 3.3.

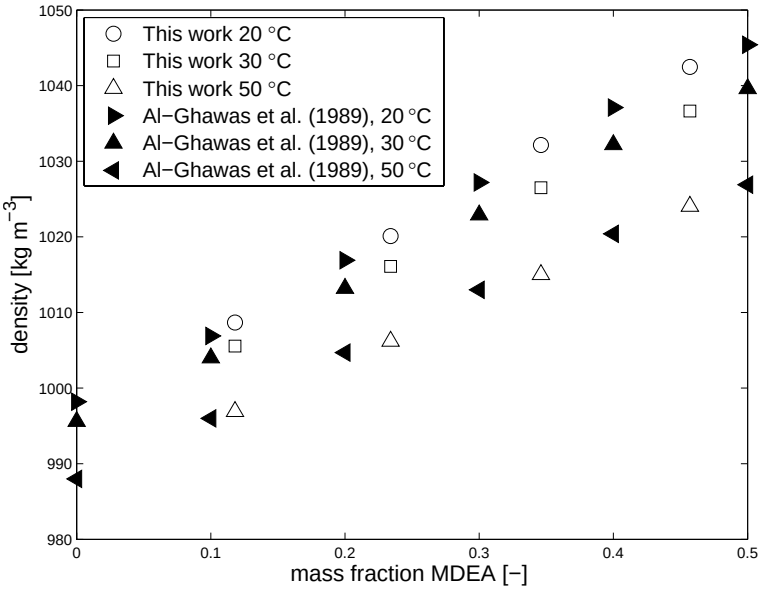

Figure 3.2: Density of aqueous MDEA solutions as a function of MDEA concentration.

Table 3.2: Density and viscosity of aqueous 1.0 kmol m^{-3} MDEA solutions blended with piperazine.

	C_{PZ}, [kmol m^{-3}]	ρ, [kg m^{-3}]	μ, [mPa s]
T = 293.15 K	0	1008.67	1.576
	0.25	1010.12	1.779
	0.5	1011.41	2.003
	0.75	1013.04	2.280
	1	1014.45	2.630
T = 298.15 K	0	1007.14	1.390
	0.25	1008.48	1.534
	0.5	1009.76	1.719
	0.75	1011.29	1.960
	1	1012.61	2.194
T = 303.15 K	0	1005.56	1.224
	0.25	1006.8	1.341
	0.5	1007.88	1.498
	0.75	1009.42	1.680
	1	1010.68	1.866
T = 313.15 K	0	1001.56	0.987
	0.25	1003.41	1.053
	0.5	1003.81	1.164
	0.75	1005.05	1.296
	1	1006.22	1.444
T = 323.15 K	0	996.91	0.793
	0.25	997.60	0.856
	0.5	999.05	0.932
	0.75	1000.24	1.043
	1	1001.25	1.127

Table 3.3: Density and viscosity of aqueous 2.0 kmol m^{-3} MDEA solutions blended with piperazine.

	C_{PZ}, [kmol m^{-3}]	ρ, [kg m^{-3}]	μ, [mPa s]
$T = 293.15$ K	0	1020.1	2.680
	0.25	1021.69	3.082
	0.5	1023.48	3.566
	0.75	1024.98	4.087
	1	1026.53	4.728
$T = 298.15$ K	0	1018.87	2.288
	0.25	1019.68	2.599
	0.5	1021.31	2.992
	0.75	1022.67	3.426
	1	1024.20	3.905
$T = 303.15$ K	0	1016.09	1.971
	0.25	1017.47	2.235
	0.5	1019.05	2.532
	0.75	1020.36	2.901
	1	1021.83	3.265
$T = 313.15$ K	0	1011.33	1.497
	0.25	1012.71	1.675
	0.5	1014.11	1.777
	0.75	1015.21	2.121
	1	1016.31	2.378
$T = 323.15$ K	0	1006.20	1.182
	0.25	1007.42	1.311
	0.5	1008.71	1.474
	0.75	1009.59	1.618
	1	1010.68	1.798

Table 3.4: Density and viscosity of aqueous 3.0 kmol m^{-3} MDEA solutions blended with piperazine.

	C_{PZ}, [kmol m^{-3}]	ρ, [kg m^{-3}]	μ, [mPa s]
T = 293.15 K	0	1032.14	4.786
	0.25	1032.91	5.559
	0.5	1034.37	6.529
	0.75	1035.94	7.966
	1	1037.24	9.1
T = 298.15 K	0	1028.97	3.948
	0.25	1030.42	4.580
	0.5	1031.82	5.329
	0.75	1037.8	6.431
	1	1034.86	7.23
T = 303.15 K	0	1026.49	3.317
	0.25	1027.76	3.900
	0.5	1029.26	4.385
	0.75	1307.50	6.650
	1	1031.96	5.882
T = 313.15 K	0	1020.97	2.415
	0.25	1022.22	2.749
	0.5	1023.46	3.118
	0.75	1025.05	3.645
	1	1025.86	4.043
T = 323.15 K	0	1015.02	1.838
	0.25	1016.11	2.057
	0.5	1017.31	2.311
	0.75	1018.71	2.648
	1	1019.45	2.913

Table 3.5: Density and viscosity of aqueous 4.0 kmol m^{-3} MDEA solutions blended with piperazine.

	C_{PZ}, [kmol m^{-3}]	ρ, [kg m^{-3}]	μ, [mPa s]
T = 293.15 K	0	1042.47	9.553
	0.25	1043.56	10.89
	0.5	1044.73	13.06
	0.75	1046.36	16.25
	1	1047.85	19.65
T = 298.15 K	0	1039.68	7.782
	0.25	1040.58	8.642
	0.5	1041.71	10.15
	0.75	1043.27	12.77
	1	1044.61	15.06
T = 303.15 K	0	1036.64	6.212
	0.25	1038.36	6.991
	0.5	1039.27	8.118
	0.75	1040.64	9.796
	1	1041.92	11.74
T = 313.15 K	0	1030.46	4.292
	0.25	1030.98	4.785
	0.5	1031.89	5.426
	0.75	1033.11	6.460
	1	1034.12	7.558
T = 323.15 K	0	1024.04	3.149
	0.25	1024.21	3.398
	0.5	1025.01	3.843
	0.75	1026.05	4.421
	1	1026.91	5.198

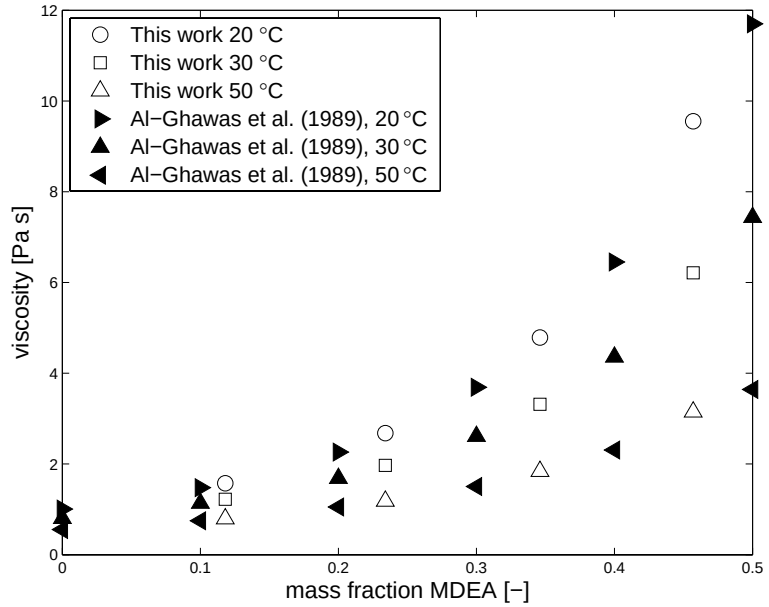

Figure 3.3: Viscosity of aqueous MDEA solutions as a function of MDEA concentration.

Figures 3.2 and 3.3 show that the present density and viscosity data on aqueous MDEA solutions are well in line with the experimental data reported by Al-Ghawas et al. [1989].

3.4 Results - diffusion

3.4.1 Validation of experimental setup and procedure

The diffusion coefficients of the binary systems acetone-water and methanol-water were determined in order to validate the experimental setup. The critical $(De)^2Sc$ number was determined to be about 150 for both systems. The experimentally obtained diffusion coefficients measured at different conditions (composition and temperature) are listed in Tables 3.6, 3.7 and 3.8, and a graphical comparison of the present data with literature data [Rutten, 1992, Lee and Li, 1991, van de Ven-Lucassen et al., 1995, Easteal and Woolf, 1985] is given in Figures 3.4, 3.5 and 3.6. It can be concluded that the newly obtained experimental diffusivity data are very well in line with the experimental data available in the literature.

Table 3.6: Composition dependent diffusion coefficient of acetone in water at 303 K.

Mole fraction acetone	D, $[10^{-9}$ m^2 s$^{-1}]$
0.00	1.39
0.01	1.29
0.10	0.94
0.20	0.77
0.30	0.69
0.70	1.80
0.80	2.19
1.00	5.25

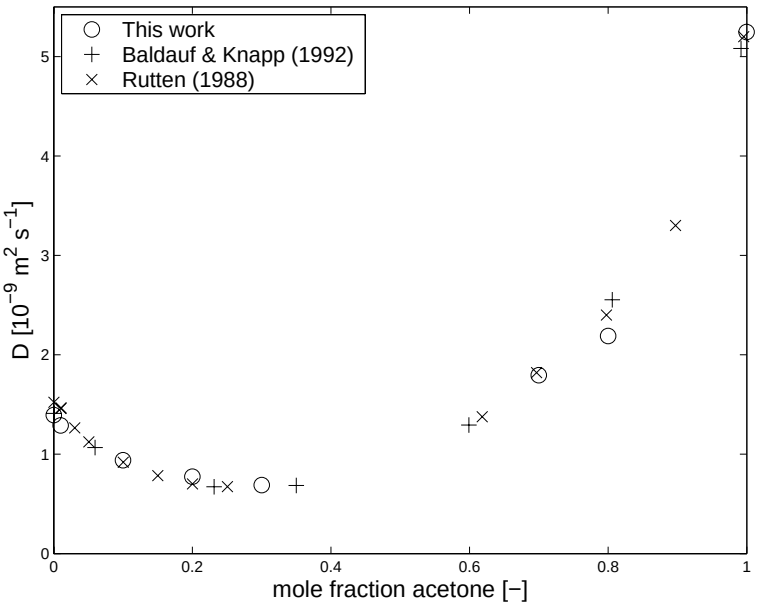

Figure 3.4: Composition dependent diffusion coefficient of acetone in water at 303 K.

Table 3.7: Composition dependent diffusion coefficient of methanol in water at 308 K.

Mole fraction methanol	D, $[10^{-9}$ m^2 s$^{-1}]$
0.00	1.89
0.01	1.81
0.10	1.51
0.20	1.31
0.30	1.26
0.40	1.18
0.50	1.27
0.60	1.36
0.80	1.91
1.00	2.62

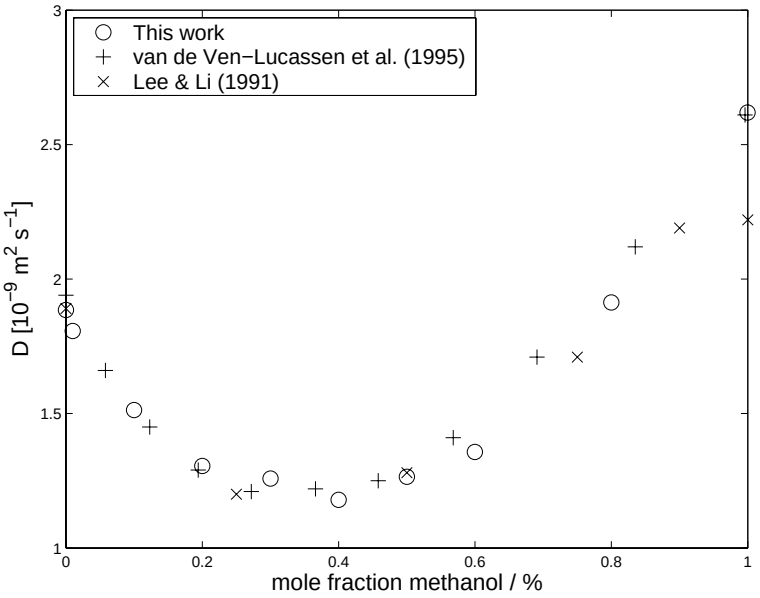

Figure 3.5: Composition dependent diffusion coefficient of methanol in water at 308 K.

Table 3.8: Infinite dilution diffusion coefficient of methanol in water as a function of temperature.

T, [K]	D_0, [10^{-9} m^2 s^{-1}]
298	1.55
313	2.39
333	3.58
353	4.68
363	5.39

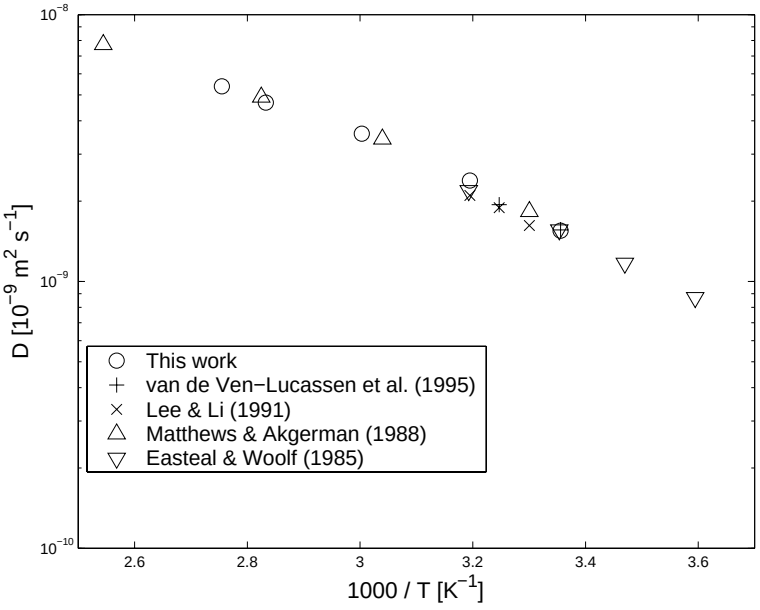

Figure 3.6: Infinite dilution diffusion coefficient of methanol in water as a function of temperature.

3.4.2 Piperazine diffusion in Water

The diffusion coefficient of piperazine in aqueous solution was measured over a concentration range of 0 to 1.4 kmol m^{-3} PZ and temperatures between 293.15 and 368.15 K. The results (averaged over at least three experiments) are listed in Table 3.9. All measurements were carried out with $(De)^2 Sc \leqq 150$.

Table 3.9: Diffusion coefficients in aqueous PZ solutions.

T, [K]	C_{PZ}, [kmol m^{-3}]	D, [10^{-9} m^2 s^{-1}]	T, [K]	C_{PZ}, [kmol m^{-3}]	D, [10^{-9} m^2 s^{-1}]
293.15	$0.8 \cdot 10^{-3}$	0.757	333.15	$1.2 \cdot 10^{-3}$	1.83
	0.284	0.660		0.285	1.66
	0.602	0.617		0.604	1.59
	0.907	0.560		0.913	1.52
	1.46	0.511		1.47	1.41
298.15	$0.8 \cdot 10^{-3}$	0.889	353.15	$1.4 \cdot 10^{-3}$	2.47
	0.285	0.762		0.287	2.36
	0.602	0.714		0.605	2.24
	0.908	0.666		0.915	2.15
	1.46	0.607		1.47	2.01
303.15	$0.9 \cdot 10^{-3}$	1.01	368.15	$1.6 \cdot 10^{-3}$	3.06
	0.285	0.870		0.287	2.89
	0.602	0.799		0.606	2.82
	0.908	0.754		0.917	2.60
	1.46	0.715		1.48	2.59
313.15	$1.0 \cdot 10^{-3}$	1.27			
	0.285	1.11			
	0.603	1.05			
	0.910	0.972			
	1.46	0.948			

As in the work of Snijder et al. [1993], all experimental diffusion coefficients were correlated using one equation accounting for the influence of both temperature and concentration. The resulting relation is given in Eq. 3.4, which was able to

correlate all experimental data with an average deviation of less than 4 % (maximum deviation 9 %).

$$\ln D = -13.672 + \frac{-2160.9}{T} - 19.263 \cdot 10^{-5} C_{PZ} \tag{3.4}$$

Versteeg and Van Swaaij [1988b] suggested a modified Stokes-Einstein equation to estimate the amine diffusion coefficient from the solution's viscosity according to Eq. 3.5. Previously, Snijder et al. [1993] showed in their work that this relation is able to predict the diffusion coefficients of various alkanolamines (MEA, DEA, MDEA and DIPA) in aqueous solution with reasonable accuracy over a wide range of temperatures and concentrations.

$$\frac{D}{D_0} = \left(\frac{\mu_0}{\mu}\right)^{0.6} \tag{3.5}$$

The input parameters to this equation are the viscosity of pure water, m_0, the viscosity of the solution, μ, and the diffusion coefficient at infinite dilution, D_0. Measuring viscosities usually is very straightforward, whereas the experimental determination of D_0 is a more laborious task. In the literature, several correlations have been proposed to estimate the diffusion coefficient at infinite dilution. In the present work, six of these estimation methods were compared and evaluated on their ability to predict the infinitely dilute diffusion coefficient of PZ in water. An important parameter in all methods is the molar volume of piperazine at the normal boiling point, which was estimated using the method of Le Bas [Poling et al., 2001]. This value was compared to the result obtained with an extrapolation relation given by Steele et al. [1997] in their study on the critical properties of piperazine. As both methods yielded a similar value, the value of Le Bas was found reliable enough to use in the diffusion coefficient estimations. The values calculated with the estimation methods were compared to the experimental diffusion coefficients at infinite dilution, taken from Table 3.9 at $C_{PZ} \approx 10^{-3}$ kmol m^{-3}, and the results are listed in Table 3.10 and shown graphically in Figure 3.7.

Both Table 3.10 and Figure 3.7 clearly illustrate that only the prediction method of Othmer & Thakar is able to predict the piperazine diffusion coefficient

Table 3.10: Methods to estimate the diffusion coefficient at infinite dilution in water.

Method	Source	Symbol in Figure 3.7	Average deviation, [%]
Othmer - Thakar	Othmer and Thakar [1953]	○	5.6
Scheibel	Scheibel [1954]	□	12
Wilke - Chang	Wilke [1955]	■	20
Modified W - C[a]	Hayduk and Laudie [1974]	×	12
Hayduk - Laudie	Hayduk and Laudie [1974]	▶	11
Hayduk - Minas	Hayduk and Minhas [1982]	◀	20

[a]Hayduk and Laudie [1974] recommended to adjust the water association parameter in the Wilke-Chang relation from 2.6 to a value of 2.26

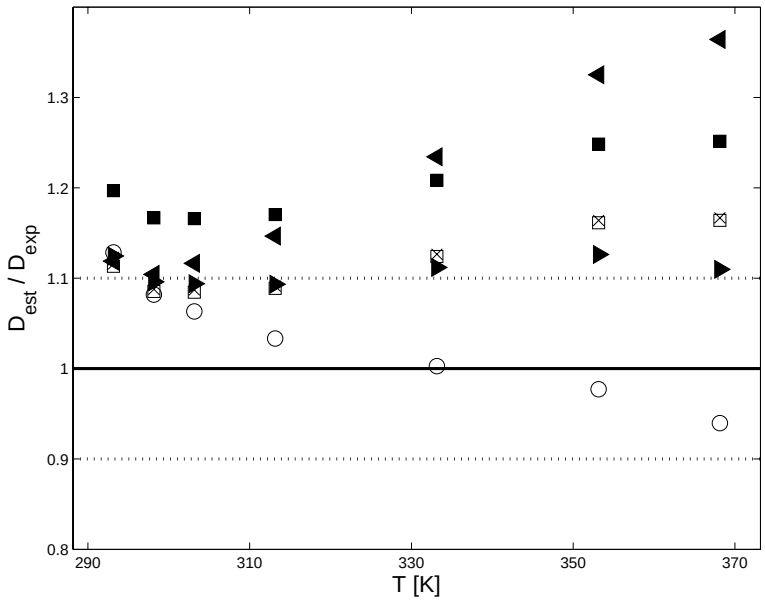

Figure 3.7: Comparison between the experimental infinitely dilute diffusion coefficient and the estimated value according to the estimation methods applied. Symbols are explained in Table 3.10.

at infinite dilution in water within 10 % over the complete temperature range. Also the Hayduk - Laudie equation seems to be a suitable prediction method, although it consistently overpredicts the experimental value with about 10 %. Both the method of Scheibel and the modified Wilke-Chang relation provide satisfactory results

up to a temperature of 313.15 K, but with increasing temperature the agreement between prediction and experiment gradually deteriorates. In the study of Snijder et al. [1993] on the diffusion of MEA, DEA, MDEA and DIPA in aqueous solution, the method of Othmer & Thakar was also found to give the best prediction results (together with the modified Wilke - Chang correlation).

Next, the applicability of the modified Stokes-Einstein relation (Eq. 3.5) was evaluated for the diffusion of piperazine, using the experimental viscosity data reported in Chapter 2 and the experimental diffusion coefficients from Table 3.9. For this purpose, a double logarithmic plot of Eq. 3.5 is shown in Figure 3.8.

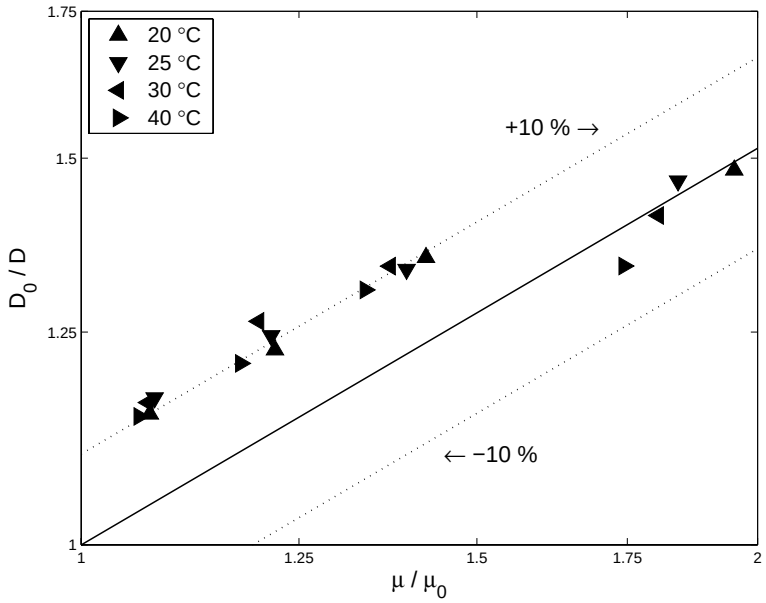

Figure 3.8: Stokes-Einstein plot for the diffusion coefficient of piperazine in aqueous PZ solutions. The solid line represents Eq. 3.5.

Despite the fact there seems to be a small offset between some of the experimental data and the solid line representing Eq. 3.5, it may still be concluded that the modified Stokes-Einstein relation can be used for estimating PZ diffusivities in aqueous piperazine systems (at concentrations $\leqq 1.5$ kmol m^{-3}) satisfactorily, as the deviation is always within about 10 %.

3.4.3 Amine diffusion in PZ - MDEA - H_2O

The diffusion coefficients of both piperazine and MDEA in an aqueous 4.0 kmol m^{-3} MDEA solution activated with 0, 0.5 and 1.0 kmol m^{-3} PZ were measured at temperatures between 298.15 and 368.15 K. In these, in fact, ternary system experiments, the same procedure was followed as in the aqueous piperazine system. In stead of attempting to determine the diffusion coefficients for the ternary system directly, which would require detectors that can measure the concentrations of both solutes independently, the MDEA - PZ - H_2O solution was treated as a pseudo binary system. In other words: To determine the diffusion coefficient of piperazine in this system, the concentration of MDEA was kept constant in both solvent and solute, while the PZ concentration in the solute was slightly increased. Consequently, the change in the RI detection signal is solely caused by a changing piperazine concentration and hence the piperazine diffusion coefficient could be determined using this output RI curve using Eqs. 3.1 and 3.2. The situation with respect to the concentrations was reversed in the experiments in which the MDEA diffusion was to be determined. The results (averaged over at least three experiments) are listed in Table 3.11. All experiments were carried out with $(De)^2 Sc \leqq 47$.

Similarly to the results obtained for the aqueous piperazine system, also the experimentally obtained results listed in Table 10 are compared to predictions made with the modified Stokes-Einstein equation (Eq. 3.5). The MDEA diffusion coefficient at infinite dilution was taken from the work of Snijder et al. [1993]. Due to a lack of viscosity data, this comparison is limited to the conditions listed in Table 3.12.

Table 3.11: Diffusion coefficients in aqueous 4.0 kmol m^{-3} MDEA solutions blended with piperazine.

T, [K]	C_{PZ}, [kmol m^{-3}]	D_{PZ}, [10^{-9} m^2 s^{-1}]	D_{MDEA}, [10^{-9} m^2 s^{-1}]
298.15	10^{-3}	0.252	0.250
	0.5	0.228	0.215
	1.0	0.199	0.182
303.15	10^{-3}	0.303	0.291
	0.5	0.277	0.247
	1.0	0.249	0.213
313.15	10^{-3}	0.434	0.382
	0.5	0.400	0.353
	1.0	0.380	0.301
333.15	10^{-3}	0.736	0.658
	0.5	0.716	0.610
	1.0	0.662	0.538
353.15	10^{-3}	1.14	1.02
	0.5	1.10	0.964
	1.0	1.12	0.886
368.15	10^{-3}	1.48	1.34
	0.5	1.46	1.27
	1.0	1.47	1.16

Table 3.12: Diffusion coefficients in aqueous 4.0 kmol m^{-3} MDEA solutions blended with piperazine.

Case	C_{MDEA}, [kmol m^{-3}]	C_{PZ}, [kmol m^{-3}]	T, [K]	Viscosity - reference
1	4.0	≈ 0	298.15 ; 303.15 ; 313.15	this work
2	4.0	≈ 0	333.15 ; 353.15	Rinker et al. [1994]
3	4.0	0.5	298.15 ; 303.15 ; 313.15	this work
4	4.0	1.0	298.15 ; 303.15 ; 313.15	this work

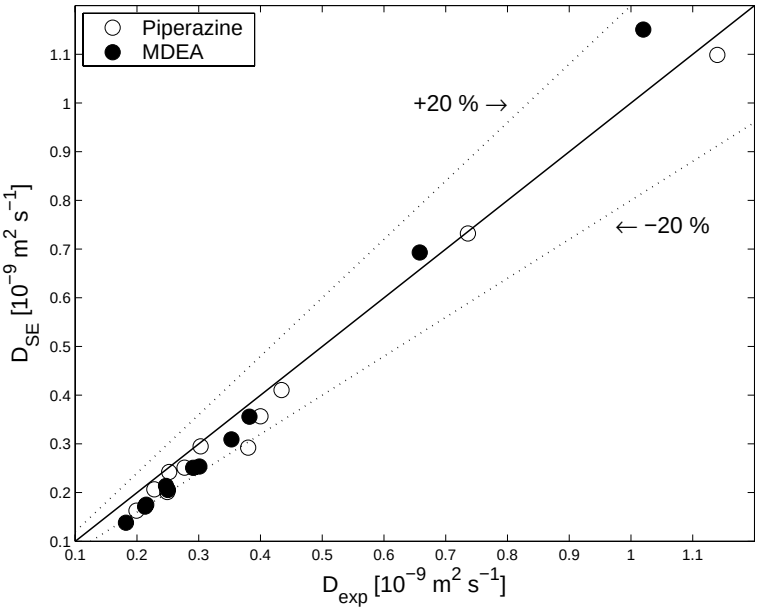

Figure 3.9: Comparison between the experimentally determined diffusion coefficients and the values estimated with the Stokes-Einstein equation.

Figure 3.9 shows that a reasonable agreement exists between the experimentally obtained PZ and MDEA diffusivities for the conditions listed in Table 3.12 and the values obtained using the modified Stokes-Einstein equation. It was found that the experimental diffusion coefficients could be predicted with an average deviation of less than 20 %.

3.5 Conclusions

This chapter reports experimentally determined densities and viscosities of aqueous MDEA solutions blended with piperazine over a wide range of concentrations and temperatures. Results obtained for aqueous MDEA solutions where no piperazine was added were found to be in good agreement with the experimental densities and viscosities reported by Al-Ghawas et al. [1989]. Also, the diffusion coefficient of piperazine in aqueous piperazine solutions was measured at different PZ concentrations and temperatures using the Taylor dispersion technique. It was found that the modified Stokes-Einstein equation, as suggested by Versteeg and Van Swaaij

[1988b] was able to predict the experimental diffusivities with an average deviation of less than 10 %. The method proposed by Othmer and Thakar [1953] gave the best results in estimating the diffusion coefficient of piperazine at infinite dilution in water. Finally, both the diffusivities of MDEA and piperazine were determined for an aqueous 4.0 kmol m^{-3} MDEA solution blended with 0, 0.5 and 1.0 kmol m^{-3} piperazine at temperatures ranging from 298.15 to 338.15 K. Again, the modified Stokes-Einstein equation was found to give a reasonable prediction of the experimental diffusion coefficients.

Acknowledgements

H.F.G. Moed is acknowledged for the construction of the experimental diffusion setup, and C. van Aken, E.S. Hamborg and M. Jadallah are acknowledged for their respective contributions to the experimental work.

Chapter 4

Kinetics of Absorption of Carbon Dioxide in Aqueous Piperazine Solutions

Abstract

In this chapter the absorption of carbon dioxide into aqueous piperazine (PZ) solutions has been studied in a stirred cell, at low to moderate temperatures, piperazine concentrations ranging from 0.6 - 1.5 kmol m^{-3}, and carbon dioxide pressures up to 500 mbar respectively. The obtained experimental results were interpreted using the DeCoursey equation [DeCoursey, 1974] to extract the kinetics of the main reaction, $2PZ + CO_2 \rightarrow PZCOO^- + PZH^+$, which was assumed to be first order in both CO_2 and PZ. The second order kinetic rate constant was found to be 76 m^3 mol^{-1} s^{-1} at a temperature of 298.15 K, with an activation temperature of 4.1 $\cdot 10^3$ K. Also, the absorption rate of CO_2 into partially protonated piperazine solutions was experimentally investigated to identify the kinetics of the reaction $2PZH^+ + CO_2 \rightarrow H^+PZCOO^- + PZH_2^{2+}$. The results were interpreted using the Hogendoorn approach [Hogendoorn et al., 1997], which uses the explicit DeCoursey equation with an infinite enhancement factor which is corrected for reversibility. Also, this reaction was assumed to be first order in both reactants and the second

order rate constant for this reaction was found to be 0.30 ± 0.10 m^3 mol^{-1} s^{-1} at 298.15 K.

4.1 Introduction

Reactive absorption of acid gas components (such as CO_2 and H_2S) from industrial and natural gas streams has been an important part in many industrial processes for decades. The solvents used in these gas treating processes are usually aqueous solutions of alkanolamines [Kohl and Nielsen, 1997]. For particular applications, however, also combinations of solvents are used (e.g. the Shell Sulfolane process). The suitability of an alkanolamine for a certain process is – among others – determined by the characteristics of its kinetics with CO_2. Since the reaction of all alkanolamines with H_2S only involves a proton transfer, its rate can be considered as instantaneous with respect to mass transfer, and thus detailed knowledge of the reaction kinetics of H_2S are of no importance. Recent interest and developments in the bulk removal of CO_2, owing to the Kyoto agreement, involve the addition of an activator (usually a primary or secondary amine) to an aqueous N-methyldiethanolamine (MDEA) solution. The reason for the use of such a blend is related to the relatively high rate of reaction of CO_2 with the activator combined with the advantages of MDEA concerning regeneration and stoicheometric loading capacity, which leads to higher rates of absorption in the absorber column while maintaining a low heat of regeneration in the stripper section.

The use of piperazine (PZ) activated aqueous MDEA solutions was patented by BASF as it proved to be successful when applied in the bulk removal of CO_2 in ammonia plants [Appl et al., 1982]. Since then, several studies have reported on the characteristics and performance of piperazine activated blends:

- PZ activated aqueous MDEA solutions [Bishnoi and Rochelle, 2002a,b, Liu et al., 1999, Xu et al., 1992, 1998, Zhang et al., 2001, 2003]
- PZ activated aqueous AMP solutions [Seo and Hong, 2000, Sun et al., 2005]

- PZ activated aqueous MEA solutions [Dang and Rochelle, 2003]
- PZ activated aqueous K_2CO_3 solutions [Cullinane and Rochelle, 2004, 2005].

Whereas published research on the application of all of the (bulk) amines (such as MDEA, AMP and MEA) is extensive - see e.g. the literature survey on the kinetics between CO_2 and various alkanolamines by Versteeg et al. [1996] - there are only few studies dealing with single aqueous piperazine solutions. Carbon dioxide solubility data have been reported by Bishnoi and Rochelle [2000], Pérez-Salado Kamps et al. [2003] and Aroua and Mohd Salleh [2004], but only two studies on the absorption rate of CO_2 into aqueous piperazine solutions - that can be used to extract kinetic rate data - have been published in literature [Bishnoi and Rochelle, 2000, Sun et al., 2005]. This might seem logical due to the fact that, in industry, piperazine is only used in combination with other (alkanol)amines rather than as a stand-alone solvent, but information on the kinetics of the individual components of a solvent with CO_2 is essential for a better understanding of the mechanism and working principle of the absorption process of CO_2 in blends of alkanolamine solutions. Moreover, in rigorous flux models all these reaction kinetics are required input parameters [Versteeg and Van Swaaij, 1988a]. Once experimentally observed fluxes of CO_2 into aqueous piperazine solutions can be understood and simulated accurately, it is possible to theoretically predict the behavior of blends of piperazine with other (alkanol)amines.

Therefore, this chapter will focus on the experimental absorption of CO_2 into aqueous piperazine solutions, at low to moderate temperatures, different piperazine concentrations and CO_2 partial pressures to obtain more insights in the kinetics of CO_2 with piperazine. Absorption data obtained in the so-called pseudo first-order reaction regime [Danckwerts, 1979] will be used to determine the kinetics of the reaction between CO_2 and PZ in aqueous solution.

4.2 Kinetics

In aqueous environment, piperazine can react with CO_2 to form many different reaction products, as shown by Bishnoi and Rochelle [2000] and Ermatchkov et al. [2002]. In aqueous piperazine solutions, carbon dioxide can react according to reactions (1) to (5):

- Reaction (1), R1:

$$CO_2 + PZ + B \rightleftarrows PZCOO^- + BH^+$$

- Reaction (2), R2:

$$CO_2 + PZCOO^- + B \rightleftarrows PZ\left(COO^-\right)_2 + BH^+$$

- Reaction (3), R3:

$$CO_2 + PZH^+ + B \rightleftarrows H^+PZCOO^- + BH^+$$

- Reaction (4), R4:

$$CO_2 + OH^- \rightleftarrows HCO_3^-$$

- Reaction (5), R5:

$$CO_2 + H_2O \rightleftarrows H_2CO_3$$

where B is any base present in solution (PZ, $PZCOO^-$, PZH^+, H_2O and OH^-).

The aim of this chapter is to identify the most important reaction(s) and the corresponding mechanism(s) and kinetic constant(s). Based on the previous studies by Bishnoi and Rochelle [2000] and Sun et al. [2005], reaction (1) is expected to be the major contributor to the overall observed absorption rate. However, in order to come to the correct kinetic rate (constant) of this reaction, it is important to qualitatively and/or quantitatively determine the (relative) contributions of the other reactions.

The contribution of reaction (5) to the overall rate of absorption into an amine solution can easily be neglected based on the equilibrium constant of this reaction in comparison to the other reactions (see e.g. the piperazine-CO_2 equilibrium studies [Bishnoi and Rochelle, 2000, Pérez-Salado Kamps et al., 2003] mentioned in Section 4.1). Also, the relative contribution of reaction (4) is assumed to be negligible to the overall absorption rate: both the forward rate constant (as e.g. determined by Pohorecki and Moniuk [1988]) and the hydroxide ion concentration in the solution (which can be estimated from the pKa of piperazine and the water hydrolysis equilibrium constant) are much smaller than both the concentration of piperazine and the published values for the kinetic rate constant of reaction (1), respectively - as shown by Sun et al. [2005].

Forward rate constants of reactions (2) and (3) are not available in the literature, but a first estimation for these rate constants can be made using the Brønsted dependency of the reactivity on the pKa [Penny and Ritter, 1983]: This technique has shown that for many alkanolamines, a (linear) relation between the pKa value of an (alkanol)amine and (the logarithm of) the forward rate constant exists. Table 4.1 lists the pKa values as found in the literature for the reactants of reactions (1), (2) and (3).

Table 4.1: Reactants and their pKa values.

Reaction	reactant	pKa (T = 25 °C)	Source
R1	PZ	9.731	Hetzer et al. [1967]
R2	$PZCOO^-$	9.44	Ermatchkov et al. [2002][a]
R3	PZH^+	5.333	Hetzer et al. [1967]

[a]Calculated from equilibrium constant.

If it is assumed that this Brønsted relation is also applicable to piperazine, it seems reasonable to disregard reaction (3), since its forward kinetic rate constant is expected to be a few orders of magnitude smaller than the rate constant for reaction (1), considering the difference in pKa between PZ and PZH^+. The validity of this assumption will be checked experimentally later on.

Assuming the above mentioned Brønsted relation dependence, reaction (2) cannot be neglected beforehand on the basis of a lower pKa with respect to reaction (1), since the difference is marginal. At this point, it is therefore not possible to exactly determine the effect of this reaction on the overall absorption rate. A worst case estimation, however, can be made. Suppose that the forward kinetic rate constants of reactions (1) and (2) are identical in order of magnitude. This seems a reasonable, optimistic estimate comparing their pKa values. In that case, the relative contributions of these reactions are determined by the concentrations of the main reactants PZ and $PZCOO^-$. Kinetic experiments are preferably, also in this chapter, carried out in the so-called pseudo first order regime (see Section 4.3). In this regime, the (interfacial) concentration of (in this case) piperazine is not noticeably decreased due to the reaction with CO_2, and hence the concentration of the reaction product - carbamated piperazine - will be small compared to the remaining piperazine concentration (even close to the gas-liquid interface) and, consequently, the carbamated piperazine can only make a small contribution to the overall absorption rate via reaction (2).

Based on all considerations concerning the various reactions with carbon dioxide in aqueous solutions of piperazine, it seems justified to conclude that the overall absorption rate is, in the kinetic regime where the enhancement factor equals the Ha-number, solely influenced by reaction (1), and therefore determination of the kinetics of reaction (1) will be the main result of the experimental part of this chapter. Also, as noted above, the hypothesis on the rate of reaction (3) is experimentally validated in this chapter.

4.2.1 Reaction mechanism

The kinetics of primary and secondary alkanolamines with CO_2 can be described using the zwitterion mechanism, as originally proposed by Caplow [1968] and later reintroduced by Danckwerts [1979]. It is assumed that this mechanism is also applicable to PZ although it is not an alkanolamine: Piperazine will react with CO_2, the rate being first order both in CO_2 and PZ respectively, under the formation of a

zwitterion, which is consequently deprotonated by any base B present in the liquid, also according to an overall second order (first with respect to PZH^+COO^- and B) reaction rate:

$$PZ + CO_2 \underset{k_{-1}}{\overset{k_2}{\rightleftarrows}} PZH^+COO^- \tag{4.1}$$

$$PZH^+COO^- + B \overset{k_B}{\rightleftarrows} PZCOO^- + BH^+ \tag{4.2}$$

Assuming a quasi steady-state condition for the zwitterion concentration and an irreversible deprotonation step, the kinetic rate equation is given by:

$$R_{CO_2} = \frac{k_2 \left[PZ\right] \left[CO_2\right]}{1 + \frac{k_{-1}}{\sum k_B B}} = \frac{\left[PZ\right] \left[CO_2\right]}{\frac{1}{k_2} + \frac{k_{-1}}{k_2} \frac{1}{\sum k_B B}} \tag{4.3}$$

where $\sum k_B B$ is the contribution of all the bases present in the solution (PZ, $PZCOO^-$, PZH^+, H_2O and OH^-) for the removal of the protons. As e.g. Kumar et al. [2003b] pointed out, there are two asymptotic situations for amines in aqueous solution:

I. In case the deprotonation of the zwitterion is very fast, or $k_{-1} / \sum k_B B \ll 1$, the kinetic equation reduces to simple 2nd order kinetics, as found for primary alkanolamines such as MEA:

$$R_{CO_2} = k_2 \left[CO_2\right] \left[PZ\right] \tag{4.4}$$

II. The reversed situation of case I occurs when $k_{-1} / \sum k_B B \gg 1$. Now the kinetic rate expression reduces to 4.5.

$$R_{CO_2} = k_2 \left[PZ\right] \left[CO_2\right] \left(\frac{\sum k_B B}{k_{-1}} \right) \tag{4.5}$$

Now the reaction order is dependent on the contribution of the individual bases to the deprotonation of the zwitterion. This expression can also account for a shift in reaction order with changing amine concentration, as typically found in the kinetic rate expression of many secondary alkanolamines with CO_2 [Versteeg et al., 1996].

In the case of piperazine, both asymptotic options I and II seem plausible, since on one hand piperazine has a higher pKa value than MEA, which – based on the Brønsted plot technique – results in a high deprotonation rate constant k_B and thus could point towards behaviour type I, whereas on the other hand both its amine groups are in fact secondary amines (like DEA) which would suggest a reactivity according to scenario II.

Both Bishnoi and Rochelle [2000] and Sun et al. [2005] concluded in their studies that aqueous piperazine reacts with CO_2 according to behaviour type I. Bishnoi and Rochelle [2000] drew this conclusion based on absorption rate experiments for piperazine concentrations of 0.2 and 0.6 kmol m^{-3} at approximately 298 K. Sun et al. [2005] based their conclusion on experiments conducted for a concentration range between 0.23 and 0.92 kmol m^{-3} at temperatures of 30, 35 and 40 °C.

The experimental focus of this chapter will include CO_2 absorption rates into aqueous piperazine solutions at three different concentrations (up to 1.5 kmol m^{-3}). Experiments have been carried out at temperatures between 20 and 40 °C to investigate the temperature dependence of the reaction. Also, as already mentioned in the discussion on all occurring reactions, an attempt is made to quantify the reaction rate between CO_2 and the protonated piperazine species. Experimental methods and procedures are explained in Section 4.4.

4.3 Mass transfer

The absorption of a gas A into a reactive liquid is generally described with Eq 4.6:

$$J = \frac{\left(C_{A,G} - \frac{C_{A,L}}{m}\right)}{\frac{1}{k_G} + \frac{1}{mk_L E_A}} \tag{4.6}$$

Simplifications to Eq 4.6 can easily be made, when assuming ideal gas behavior and operating under the following (experimental) conditions:

a fresh and therefore lean liquid (and hence $C_{A,L} = 0$);

a pure gas;

Taking these considerations into account, the absorption of pure CO_2 is given by Eq 4.7:

$$J = k_L E_{CO_2} \frac{m P_{CO_2}}{RT} \tag{4.7}$$

where the (chemical) enhancement factor E_{CO_2} is a function of the Hatta number Ha and the infinite enhancement factor E_{inf}. The Hatta number is defined according to equation 4.8:

$$Ha = \frac{\sqrt{k_{ov} D_{CO_2}}}{k_L} \tag{4.8}$$

where it is assumed that the total reaction rate k_{OV} is completely determined by reaction (1) as discussed in Section 4.2. Under the already mentioned additional assumption that the reaction is first order with respect to carbon dioxide (Section 4.2), this means:

$$k_{ov} = \frac{R^1_{CO_2}}{[CO_2]} \tag{4.9}$$

According to the penetration model [Higbie, 1935], the infinite enhancement factor, E_{inf}, is given by:

$$E_{CO_2,\infty} = \sqrt{\frac{D_{CO_2}}{D_{Am}}} \left(1 + \frac{D_{Am}}{D_{CO_2}} \frac{[Am]\, RT}{\nu_{Am} P_{CO_2} m_{CO_2}} \right) \tag{4.10}$$

It must be noted, however, that Eq 4.10 is only valid for irreversible reactions: For reversible reactions, the infinite enhancement factor decreases for lower values of the equilibrium constant, as shown in Appendix 4.B. However, it will be shown later that the reversibility of the reaction does not play a significant role during the absorption experiments into aqueous piperazine solutions, so the use of Eq 4.10 is justified.

Depending on the absolute value of Ha and the ratio between Ha and E_{inf}, three absorption regimes can be distinguished. For a constant value for the

Hatta number ($Ha > 2$) and with decreasing infinite enhancement factor (for the experiments carried out at constant piperazine concentration this is related to an increasing CO_2 partial pressure), they are:

The pseudo first order regime If the ratio between the Ha number and the infinite enhancement factor is sufficiently large, the following criterion will be obeyed:

$$2 < Ha << E_{\text{inf}} \tag{4.11}$$

Upon satisfaction of Eq 4.11, the reaction of CO_2 with the (alkanol)amine can be considered to take place in the pseudo first order regime and in that case the enhancement factor equals the Ha number. Consequently, Eq 4.7 is changed to:

$$J_{CO_2} = \sqrt{k_{ov} D_{CO_2}} \frac{m_{CO_2} P_{CO_2}}{RT} \tag{4.12}$$

It is obvious from Eq 4.12, that the experimentally observed absorption rate gives direct information on the kinetic rate constant k_{OV}.

The 'intermediate' regime On increasing CO_2 partial pressures (and hence decreasing the value of the infinite enhancement factor), depletion of the amine at the interface starts to occur. In this 'intermediate' regime, it is not possible to derive the kinetic data directly from the CO_2 fluxes and the corresponding enhancement factors. For this 'intermediate' regime, an approximate solution for the enhancement factor as a function of both Ha and E_{inf} is derived by DeCoursey [1974]:

$$E_{DC} = -\frac{Ha^2}{2\left(E_{\text{inf}} - 1\right)} + \sqrt{\frac{Ha^4}{4\left(E_{\text{inf}} - 1\right)^2} + \frac{E_{\text{inf}} Ha^2}{\left(E_{\text{inf}} - 1\right)} + 1} \tag{4.13}$$

Eq. 4.13 was derived for absorption with irreversible second order (1,1) chemical reaction based on Danckwerts' surface renewal theory. Using the 'intermediate' regime to derive the kinetics of reversible reactions basically also requires knowledge about the equilibrium constant of the reaction as this constant influences E_{inf} (see Appendix 4.B). Because of all these mutual interactions,

this region is generally considered to be not attractive to derive the kinetics reliably.

The instantaneous regime The third regime is reached when the infinite enhancement factor becomes significantly smaller than Ha, and now Eq. 4.14 applies:

$$2 < E_{\inf} << Ha \tag{4.14}$$

Here, the reaction is said to be 'instantaneous' with respect to mass transfer, and the rate of absorption is completely limited by diffusion of the reactants and the determination of the kinetics from experimental absorption rate data is not possible. Here, the maximum possible enhancement factor applies and the flux for an irreversible reaction can be described with Eq. 4.15:

$$J_{CO_2} = k_L \left(\sqrt{\frac{D_{CO_2}}{D_{Am}}} + \sqrt{\frac{D_{Am}}{D_{CO_2}} \frac{[Am]\,RT}{\nu_{Am} m P_{CO_2}}} \right) \frac{m P_{CO_2}}{RT} \tag{4.15}$$

Since the kinetics of CO_2 with aqueous piperazine are not known in detail, it is not possible to determine beforehand in which regime absorption experiments are carried out. Therefore - at a constant temperature, liquid stirrer speed and piperazine concentration (and hence a constant Ha number) - a series of absorption experiments should be conducted, with decreasing CO_2 partial pressures, until a linear relationship is found between the experimental CO_2 flux and applied partial pressure - if the assumption concerning a first order dependence of CO_2 in the kinetic expression is indeed correct. According to Eq. 4.12, kinetic rate data can then directly be extracted from the slope.

As mentioned, the reversibility of reaction (1) is not taken into account in the derivation of the mass transfer equations. In this chapter, it is assumed that the reaction can be regarded as irreversible due to the combination of a high value for

Table 4.2: Equilibrium constant values.

T [$^\circ$C]	K_{Eq-1} [a] [molal^{-1}]	pKa$_{PZ}$ [b] [-]	K_{eq} [molal^{-1}]
25	$1.48 \cdot 10^{-5}$	9.731	$8.0 \cdot 10^4$
40	$9.40 \cdot 10^{-6}$	9.367	$2.2 \cdot 10^4$

[a] Taken from Ermatchkov et al. [2002].
[b] Taken from Hetzer et al. [1967].

the equilibrium constant (see Eq. 4.16 and Table 4.2) and the low carbon dioxide loadings present during the experiments.

$$K_{eq} = \frac{[PZCOO^-][PZH^+]}{[CO_2][PZ]^2} = \frac{[PZCOO^-][H_3O^+]}{[CO_2][PZ][H_2O]} \cdot \frac{[PZH^+][H_2O]}{[H_3O^+][PZ]} = K_{Eq-1} \cdot 10^{pKa,PZ} \tag{4.16}$$

Even though, the equilibrium constants listed in Table 4.2 are already fairly large, the influence of reversibility will be studied and discussed to verify the assumption regarding reaction (1) to be irreversible under the experimental conditions in the present work.

4.4 Experimental

The gas-liquid contactor used was a stirred cell reactor operated with a smooth and horizontal gas-liquid interface. The reactor consisted of glass, was thermostatted and it was provided with magnetic stirrers in the gas and liquid phase, which could be controlled independently. Both the reactor and the gas supply vessel were equipped with PT-100 thermocouples and digital pressure transducers and measured signals were recorded in the computer. The pressure transducer connected to the stirred cell was a Druck PMP 4070 (range 0 to 199.99 mbar) and the gas supply vessel was equipped with a PDCR 910 (range 0 - 5 bar), also obtained from Druck. Two different modes of operation were adopted in the absorption experiments: one mode for aqueous piperazine solutions and the other for protonated piperazine in aqueous solution, respectively.

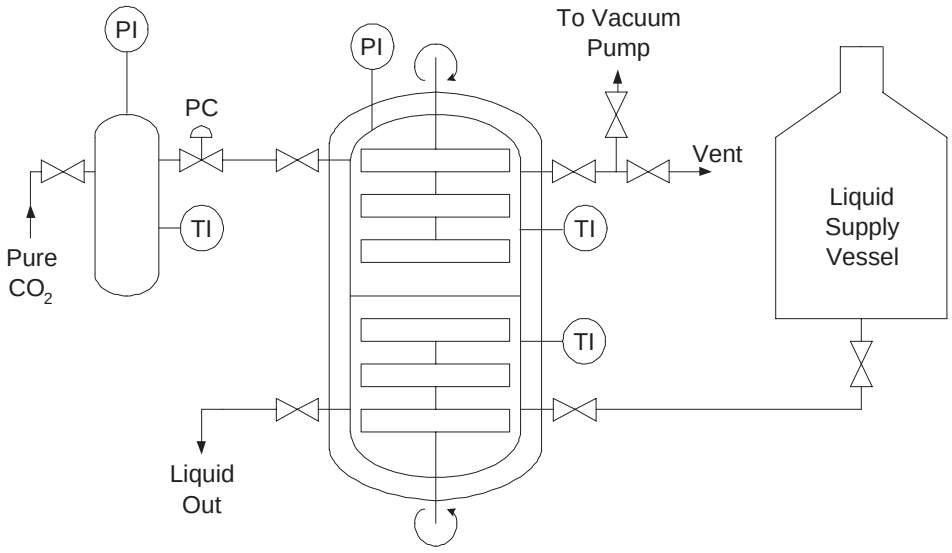

Figure 4.1: Schematic diagram of the experimental setup.

4.4.1 Absorption into aqueous piperazine solutions

During all experiments that aimed at determining the kinetics of reaction (1), the reactor was operated batchwise with respect to the liquid phase and 'semi-continuous' with respect to the gas phase - as experiments were carried out at a constant (CO_2) pressure. This type of operation is preferred over a batchwise type of operation with respect to the gas phase in view of experimental accuracy: for the first reaction, the pseudo first order criteria indicated the requirement of a relatively low CO_2 partial pressure in the reactor. During batchwise operation with respect to the gas phase and the occurrence of a fast reaction, this would directly imply a relatively high pressure decrease (from an already low initial pressure) over a rather short period of time. A 'semi-continuous' operation makes a longer experimental period of time in the desired pseudo first order regime possible, thereby improving the experimental accuracy. To allow for this mode of operation, the reactor was connected to a calibrated gas supply vessel by means of a pressure controller (Brooks Instr., type 5866).

In a typical experiment, a known amount of piperazine (99 % , Aldrich) was dissolved in about 600 mL of water and the solution was transferred to the liquid

supply vessel, after which the liquid was degassed by applying vacuum for a short while. Next, the solution was transferred to the stirred cell, where it was allowed to equilibrate at a desired, set temperature – and the corresponding vapour pressure was recorded. Then, the pressure controller was set to the desired (total) pressure, and subsequently CO_2 (purity 99.995 %, obtained from Hoekloos) was allowed to flow from the gas supply vessel to the reactor. Next, the stirrers in both phases were switched on and the pressure decrease in the gas supply vessel was recorded as a function of time. The CO_2 flux into the liquid was determined according to Eq. 4.17:

$$J_{CO_2} = \frac{dP_{GV}}{dt} \cdot \frac{1}{RT_{GV}A_{GL}} \tag{4.17}$$

The corresponding CO_2 partial pressure in the reactor was calculated by subtracting the lean liquid's vapour pressure, determined explicitly at the beginning of the experiment, from the constant total pressure in the reactor during the experiment. The piperazine concentration was checked afterwards by volumetric titration with 1.0 N HCl.

In a typical series of experiments, the procedure above was repeated at different pressures, until - at a constant piperazine concentration and temperature - a pressure-flux curve was obtained which included the linear pseudo first order regime, as discussed in the previous section. In all experiments, both the liquid volume of and the stirring speed in the liquid phase respectively were kept constant to ensure a constant mass transfer coefficient k_L per concentration and temperature.

The maximum carbon dioxide loadings at the end of an experiment varied between 0.006 mol mol^{-1} and 0.025 mol mol^{-1}, corresponding with PZ conversions of 1.2 and 5 % respectively, depending on the applied CO_2 partial pressure in an experiment. These loadings are more than a decade lower than the loadings used by Bishnoi and Rochelle [2000] in their experimentally determined equilibrium CO_2 pressures. They reported experimental CO_2 equilibrium pressures of 32 and 42 Pa, both at a CO_2 loading of 0.32 and a temperature of 40 $^\circ$C. Since these CO_2 partial pressures already are (at least) a factor 10 lower than the CO_2 pressures applied in

this work, it is justified to assume that the influence of (bulk) reverse reactions can be neglected for the experimental conditions used in the present work.

4.4.2 Absorption into protonated piperazine solutions

When determining the kinetics of CO_2 and protonated piperazine in an aqueous solution (reaction (3)), the setup was operated batchwise with respect to both the liquid and the gas phase. The experimental method therefore differs from the one described in the constant pressure experiments with aqueous piperazine. For these experiments, it was not necessary to follow the (relatively more) complicated procedure as described in the previous section, since the reaction rate of carbon dioxide with PZH^+ is expected to be much slower than its reaction with PZ (as explained in the Theory section), and this second – simpler – method has been found to be well applicable for systems with a low(er) kinetic rate constant. The experimental procedure applied for the determination of the kinetics of CO_2 with PZH^+ was, in fact, similar to the one described by both Blauwhoff et al. [1984] and Kumar et al. [2003b], and will therefore only be briefly summarized here.

In a typical experiment, an equimolar amount of piperazine and hydrochloric acid (Aldrich) was dissolved in about 600 mL of double distilled water. HCl was chosen, since it, being a strong acid, will protonate the most basic groups in solutions irreversibly and thus convert all piperazine molecules to PZH^+. For simplicity reasons, it is assumed that the presence of the chloride ions does not influence the reaction (rate) or the mass transfer process, even though it must be noted that its concentration is identical to the PZH^+ concentration in solution. As the goal of these second set of experiments is only to validate the justification of neglecting reaction (3) with respect to reaction (1), this seems acceptable. The prepared solution was transferred to the liquid supply vessel, where vacuum was applied shortly to remove all inert gases. Then, the solution was transferred to the stirred cell reactor where it was allowed to equilibrate at the desired temperature, after which the vapour pressure was recorded. Next, pure CO_2 was fed into the reactor, the reactor was closed and the stirrers in both phases were switched on. The pressure decrease in

time due to absorption of CO_2 was recorded using a computer.

If the CO_2 partial pressure above the solution is sufficiently low so that the pseudo first order conditions are met, the kinetics of the reaction can be determined using the following equation [Blauwhoff et al., 1984]:

$$\ln\left(P_{CO_2,t}\right) = \ln\left(P_t - P_{vap}\right) = \ln\left(P_0 - P_{vap}\right) - \sqrt{k_{ov} D_{CO_2}} \frac{A_{GL}}{V_G} m_{CO_2} t \qquad (4.18)$$

Typically, a plot of the left-hand side of Eq. 4.18 as function of time will yield a graph as shown in Figure 4.2. If initially the pseudo first order conditions are not satisfied (i.e. mass transfer takes place in the instantaneous absorption regime), the slope will change in time. When the pressure has decreased sufficiently – and the pseudo first order conditions are satisfied – the slope will reach a constant value, from which the kinetic rate constant k_{OV} is to be determined (Eq. 4.18).

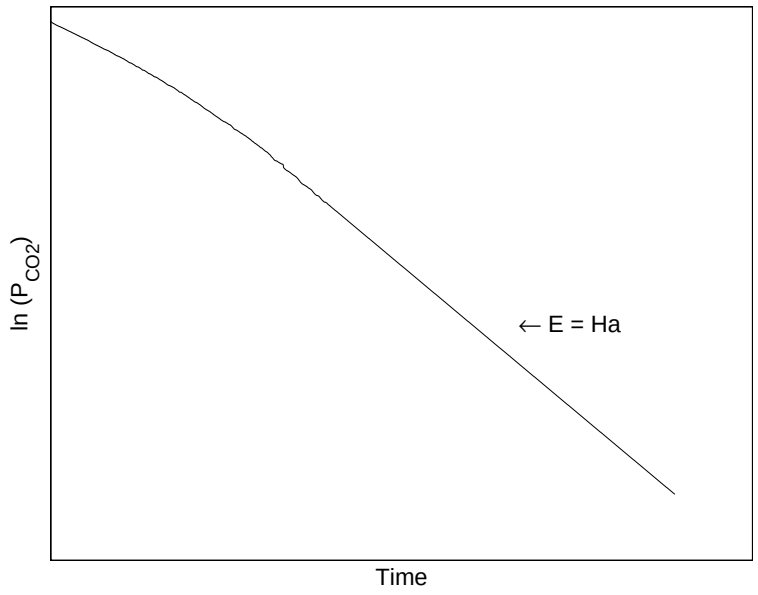

Figure 4.2: Typical result of a batch experiment.

Again, experimental conditions were adjusted to keep the maximum carbon dioxide loading low to minimize the influence of reversibility of the reaction. In all experiments, the loading never exceeded 0.002 mol CO_2 per mol PZH^+.

4.5 Results

4.5.1 Absorption into aqueous piperazine solutions

Experimentally determined fluxes of CO_2 at different partial pressures have been listed in Tables 4.3, 4.5 and 4.4.

Table 4.3: Flux of CO_2 into aqueous solutions of 0.6, 1.0 and 1.5 M PZ at 20 °C.

[PZ] = 0.6 M		[PZ] = 1.0 M		[PZ] = 1.5 M	
P_{CO2} [mbar]	J_{CO2} [mmol m^{-2} s^{-1}]	P_{CO2} [mbar]	J_{CO2} [mmol m^{-2} s^{-1}]	P_{CO2} [mbar]	J_{CO2} [mmol m^{-2} s^{-1}]
2.53	0.632	3.72	1.07	3.95	1.29
3.34	0.79	3.89	1.20	4.64	1.50
3.68	0.91	4.11	1.11	4.92	1.64
4.26	0.98	4.12	1.20	5.88	1.88
4.72	1.11	4.40	1.30	10.5	2.90
5.96	1.32	5.31	1.45	16.1	3.99
8.22	1.69	6.00	1.70	76.4	7.14
10.9	2.02	6.25	1.67	176	8.02
13.1	2.31	7.03	1.88	277	8.46
15.8	2.55	7.90	1.98	477	9.2
36.3	3.55	7.94	1.93		
126	4.64	8.33	1.87		
262	5.16	8.33	2.08		
369	5.39	8.43	2.15		
472	5.63	8.45	2.19		
		10.7	2.47		
		10.9	2.51		
		13.5	3.29		
		16.1	3.35		
		16.1	3.36		

Table is continued on next page

Table 4.3 continued for 1.0 M PZ

[PZ] = 1.0 M					
P_{CO2} [mbar]	J_{CO2} [mmol m^{-2} s^{-1}]	P_{CO2} [mbar]	J_{CO2} [mmol m^{-2} s^{-1}]	P_{CO2} [mbar]	J_{CO2} [mmol m^{-2} s^{-1}]
26.1	4.16	102	6.32	352	7.53
26.2	4.16	172	6.94	402	7.67
36	4.51	252	7.11	406	7.6
36.2	4.68	252	7.16	472	7.79
75.7	6.01	352	7.66		

Table 4.4: Flux of CO_2 into aqueous solutions of 1.0 M PZ at 30 and 40 $^\circ$C.

T = 30 $^\circ$C		T = 40 $^\circ$C			
P_{CO2} [mbar]	J_{CO2} [mmol m^{-2} s^{-1}]	P_{CO2} [mbar]	J_{CO2} [mmol m^{-2} s^{-1}]	P_{CO2} [mbar]	J_{CO2} [mmol m^{-2} s^{-1}]
4.14	1.28	5.31	1.69	42.1	7.27
4.71	1.48	5.32	1.69	60.7	8.99
5.32	1.56	5.60	1.64	101	9.98
6.14	1.88	5.86	2.03	136	11.30
6.56	1.93	6.40	2.08	178	11.10
8.21	2.37	6.55	1.86	179	11.10
9.5	2.63	6.78	2.09	228	12.10
11.9	3.28	7.93	2.30	278	12.30
14.0	3.49	8.29	2.46	338	12.50
31.6	5.93	8.54	2.43	403	12.90
55.1	7.5	10.7	3.1		
156	9.07	12.2	3.53		
233	9.44	16.2	4.53		
308	9.94	20.3	4.99		
433	10.70	25.9	5.82		

Table 4.5: Flux of CO_2 into aqueous solutions of 0.6, 1.0 and 1.5 M PZ at 25 °C.

[PZ] = 0.6 M		[PZ] = 1.0 M		[PZ] = 1.5 M	
P_{CO2} [mbar]	J_{CO2} [mmol m^{-2} s^{-1}]	P_{CO2} [mbar]	J_{CO2} [mmol m^{-2} s^{-1}]	P_{CO2} [mbar]	J_{CO2} [mmol m^{-2} s^{-1}]
3.15	0.77	3.44	1.01	3.77	1.26
3.62	0.96	3.48	0.98	4.34	1.4
3.94	0.875	3.92	1.14	4.84	1.57
4.15	1.02	4.28	1.34	5.25	1.73
4.37	1.03	4.36	1.37	6.22	1.92
4.86	1.15	5.07	1.39	7.27	2.41
5.50	1.29	6.1	1.67	7.94	2.35
6.48	1.39	6.82	1.82	10.4	3.17
6.92	1.55	6.88	2.04	18.5	4.84
7.06	1.63	7.25	2.02	26.7	5.85
8.09	1.98	7.39	2.14	68	8.29
14.2	2.68	10.4	2.61	195	9.81
22.2	3.35	10.6	2.72	345	10.52
27.0	3.71	10.8	2.66	468	10.90
75.8	4.85	19.5	4.00		
128	5.41	19.6	4.13		
128	5.43	28.6	4.82		
243	5.92	143	7.83		
343	6.08	244	8.19		
343	6.13	419	8.79		
415	6.20	463	9.04		
463	6.46				
463	6.53				

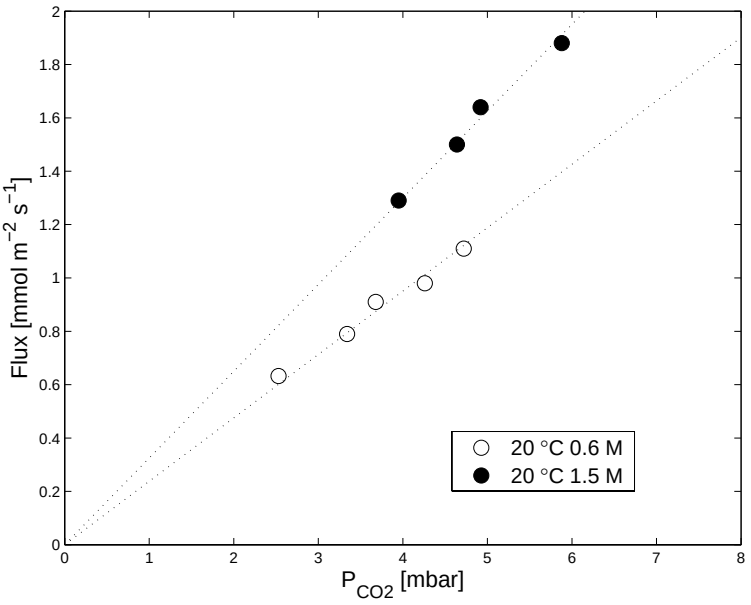

Figure 4.3: Two series of experimentally observed fluxes, apparently measured in the pseudo first order regime.

As pointed out in Section 4.3, only the data taken at sufficiently low CO_2 partial pressures, where a linear relation exists between the experimentally observed flux and the CO_2 partial pressure (as illustrated in Figure 4.3 for two series of measurements) are to be used in the determination of the kinetic rate, as this constant slope might indicate pseudo first order behavior. From the corresponding rates of absorption, the overall pseudo first order rate constant, k_{OV}, of reaction (1) can be calculated according to Eq. 4.12, thereby already assuming that the contributions of reactions (2) and (3) are negligible. It should be noted, that at this point the first order dependence of CO_2 still has not been validated, but - as already mentioned above - the fact that there seems to be a linear relation between flux and CO_2 pressure (if '$E = Ha$') is an indication that the reaction is indeed first order in carbon dioxide.

Further details as to which experimental data have been used in the kinetic rate determination are listed in Table 4.6, along with the required physical properties and calculation results. The listed physical properties are, in fact, the distribution

Table 4.6: Kinetic data for the reaction of CO_2 with piperazine in aqueous solutions.

T [K]	C [kmol m^{-3}]	N^a [-]	slope^b [mmol m^{-2} s^{-1} mbar^{-1}]	$m_{N2O}{}^c$ [-]	$D_{N2O}{}^d$ [$\cdot$ 10^{-9} m^2 s^{-1}]	k_{OV} [$\cdot$ 10^3 s^{-1}]
293.15	0.6	5	0.238	0.669	1.30	29.4
293.15	1.0	7	0.285	0.662	1.12	50.3
293.15	1.5	4	0.325	0.637	0.95	82.8
298.15	0.6	7	0.239	0.590	1.51	33.6
298.15	1.0	11	0.285	0.584	1.31	56.2
298.15	1.5	4	0.327	0.564	1.10	94.0
303.15	1.0	5	0.302	0.493	1.73	68.1
313.15	1.0	5	0.321	0.429	2.15	85.3

[a]Number of experimental data used in determining kinetics, taken from Tables 4.3, 4.5 and 4.4.

[b]Average dJ/dp slope over those N points.

[c]The values for the distribution coefficient were taken from Chapter 2 (20 & 25 °C) and Sun et al. [2005] (30 & 40 °C).

[d]The diffusion coefficients at 30 & 40 °C were taken from Sun et al. [2005]. Diffusion coefficients at 20 & 25 °C were estimated using a modified Stokes-Einstein Eq. as shown in Appendix 4.B.

and diffusion coefficients of N_2O in aqueous PZ solutions, and they were converted to the corresponding CO_2 values using the well-known and widely applied $N_2O : CO_2$ analogy (the reader is referred to Versteeg and Van Swaaij [1988b] for the conversion equations).

Before drawing conclusions from Table 4.6, it needs to be verified if the pseudo first order conditions (Eq. 4.11) have been satisfied in these experiments. A list of governing Hatta numbers and corresponding (irreversible) infinite enhancement factors (according to Eq. 4.10) are listed in Table 4.7. The diffusion coefficient of piperazine – necessary in the calculation of the infinite enhancement factor – was estimated using the diffusion coefficient of MDEA, corrected for the molecular weight by multiplying with a factor 1.38. The diffusion coefficient of MDEA as a function of temperature and concentration was calculated with the experimentally derived equation given by Snijder et al. [1993]:

$$\ln D_{MDEA} = -13.808 - \frac{-2360.7}{T} - 24.727 \cdot 10^{-5}[MDEA] \tag{4.19}$$

Table 4.7: Calculated Ha numbers and corresponding (infinite) enhancement factors.

T [K]	C [kmol m^{-3}]	$k_{L,0}$ [m s^{-1}]	k_{OV} [$\cdot$ 10^3 s^{-1}]	Ha [-]	P_{CO2} [mbar]	D_{PZ} [$\cdot$ 10^{-9} m^2 s^{-1}]	E_{inf}[a] [-]
293.15	0.6	2.02	29.4	320	4.72	0.62	1140
293.15	1.0	1.69	50.3	465	6.00	0.56	1551
293.15	1.5	1.42	82.8	651	5.88	0.51	2553
298.15	0.6	2.23	33.6	331	5.50	0.71	1119
298.15	1.0	1.98	56.2	449	7.39	0.67	1452
298.15	1.5	1.69	94.0	628	5.25	0.61	3928
303.15	1.0	2.31	68.1	486	6.56	0.75	1812
313.15	1.0	2.97	85.3	465	6.40	0.97	2218

[a] same m and D as used in calculations in Table 4.6

Table 4.7 clearly shows that in all cases the Ha number is more than substantially larger than two, and, that the ratio between the infinite enhancement factor and the Hatta number is about a factor four. Pseudo first order behaviour is, however, only really ensured at ratios between E_{inf} and Ha of least a factor 10, so with a factor of 4 it might be necessary not only to interpret the results according to Eq. 4.12 ('pseudo first order regime') but also with help of Eq. 4.13 ('intermediate regime'). The ratio between E_{inf} and Ha could not be increased by further lowering the CO_2 partial pressure, because the error in the determination of the CO_2 partial pressure (which is needed in the interpretation of the experiments) would become unacceptable. This is because the CO_2 partial pressure is indirectly determined by the difference between the actual reactor pressure and the vapour pressure of the fresh solution. At low CO_2 partial pressures, the difference between the actual pressure and the vapour pressure is relatively small as compared to the actual pressure and the relative error in the determination of the CO_2 partial pressure thus increases rapidly below $P_{CO2} \simeq 4$ mbar (400 Pa). When using Eq. 4.13, the kinetics are derived by using the Ha-number as a fitting parameter so that the enhancement factor calculated using Eq. 4.13 matches the experimentally observed enhancement

factor. For this procedure only data that matched the criterium '$E_{inf} > 1.2 \cdot E_{exp}$' were used, therewith excluding data with a low sensitivity towards the kinetics. The accordingly obtained results are listed in Table 4.8.

Table 4.8: Results of the reinterpretation of the experimental data based on the DeCoursey approximation.

T [K]	C [kmol m^{-3}]	N^a [-]	Ha-DC^b [-]	k_{OV}-DC [$\cdot$ 10^3 s^{-1}]	Ha-PFO^c [-]	k_{OV}-PFO [$\cdot$ 10^3 s^{-1}]
293.15	0.6	10	364	38.2	320	29.4
293.15	1.0	25	512	61.2	465	50.3
293.15	1.5	6	740	106.8	651	82.8
298.15	0.6	13	386	45.7	331	33.6
298.15	1.0	17	513	73.3	449	56.2
298.15	1.5	11	708	119.5	628	94.0
303.15	1.0	10	559	90.2	486	68.1
313.15	1.0	18	504	100.4	465	85.3

[a]Number of data points used in the calculation of the average Ha number.
[b]The Hatta number as a result from the data regression.
[c]The Hatta number assuming pseudo first order behavior (Table 4.7).

Table 4.8 shows that the determination of the kinetics using Eq. 4.13 yields a larger overall kinetic rate constant (10 - 30 %), which was to be expected following the conclusions drawn before concerning the pseudo first order conditions. These results obtained from the analysis based on Eq. 4.13 will be used in all following discussions and conclusions.

A graphical representation between all experimentally observed enhancement factors and the calculated enhancement factors based on the DeCoursey approximation - using the kinetics as listed in Table 4.8, and all physical constants as listed in Table 4.6 - is given in Figure 4.4.

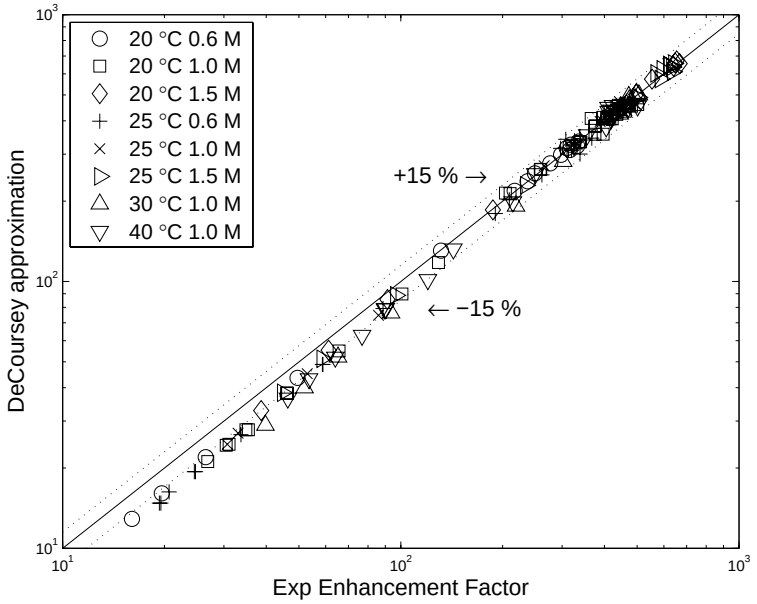

Figure 4.4: Parity plot of experimental enhancement factor and the DeCoursey approximation using the irreversible infinite enhancement factor.

Figure 4.4 shows that for all experimental absorption rates listed in Tables 4.3, 4.5 and 4.4, experimental values and predictions calculated from the DeCoursey equation are in good agreement with each other. Deviations between model and experiment might be attributed to, among others, the estimated diffusion coefficients for both CO_2 and piperazine.

Before elaborating further on the results, first the assumption concerning the (ir)reversibility of the reaction should be validated. It was stated earlier, that reaction (1) could be regarded irreversible based on the relatively high value for the equilibrium constant and the very low CO_2 loadings applied in this work. Therefore, in Table 4.9 the infinite enhancement factor adapted for reversibility according to Secor and Beutler [1967] and modified for the penetration theory as suggested by Hogendoorn et al. [1997] is listed and compared to the irreversible infinite enhancement factor as presented earlier in Table 4.8. The governing equations and definitions as well as a calculation example are given in Appendix 4.B.

Table 4.9: Reversible and irreversible infinite enhancement factors.

T [K]	C [kmol m^{-3}]	P_{CO2} [mbar]	$E_{inf,irrev}$ [a] [-]	$E_{inf,rev}$ [b] [-]	k_{OV}(irrev) [$\cdot 10^3$ s^{-1}]	k_{OV}(rev) [$\cdot 10^3$ s^{-1}]
293.15	0.6	4.72	1140	1031	38.2	40.1
293.15	1.0	6.00	1551	1419	61.2	65.2
293.15	1.5	5.88	2553	2336	106.8	107.5
298.15	0.6	5.50	1119	991	45.7	47.7
298.15	1.0	7.39	1452	1308	73.3	77.6
298.15	1.5	5.25	3298	2918	119.5	122.2
303.15	1.0	6.56	1812	1565	90.2	96.4
313.15	1.0	6.40	2218	1755	100.4	112.5

[a] Same m and D as in Table 4.6

[b] See Appendix 4.B for governing equations and calculation example.

As the difference between both the reversible and irreversible infinite enhancement factors never exceeds 10-20 % , it is fairly safe to state that reversibility only has a marginal influence on the actual kinetics experiments: The maximum deviation in the overall kinetic rate constant between using the irreversible and the reversible infinite enhancement factor is 10 %, observed at 313.15 K. It should be noted here, that the use of this approximation method introduces an error in the obtained overall kinetic rate constant. However, for the conditions applied in this work, the average deviation between the approximated result and the exact numerical solution is always less than 5 % [Hogendoorn et al., 1997].

Now, a closer look is given to the results presented in Table 4.8. The data obtained at different PZ concentrations at 20 and 25 $^\circ$C are to be used to identify the mechanism of the reaction of piperazine with CO_2 . Usually, a log-log plot of the apparent kinetic rate k_{OV} versus the amine concentration is made to investigate which of the asymptotic cases described in Section 4.2 is valid: The reaction order with respect to the amine is given directly by the slope of the graph. A log-log plot of the present data at 20 and 25 $^\circ$C yields a reaction order with respect to

piperazine of about 1.0 - 1.3. However, considering the uncertainty with respect to the CO_2 diffusion coefficient, the reaction order with respect to PZ is assumed to be one at this stage, also based on following considerations:

- Based on the literature on the kinetics between CO_2 and a wide variety of aqueous (alkanol)amines, it seems fair to assume that the reaction order with respect to CO_2 to be one;
- Both previous studies on the kinetics between CO_2 and aqueous PZ have reported a partial reaction order of piperazine of one.

Now, the corresponding k_2 rate constants are calculated from the apparent kinetic rate k_{OV} resulting from the DeCoursey relation (based on an irreversible enhancement factor) as listed in Table 4.8, based on the considerations above, and the resulting values are listed in Table 4.10.

Table 4.10: Second order kinetic rate constants.

T [K]	C [kmol m^{-3}]	k_{OV} [$\cdot$ 10^3 s^{-1}]	k_2 [m^3 kmol^{-1} s^{-1}]
293.15	0.6	38.2	64
293.15	1.0	61.2	61
293.15	1.5	106.8	71
298.15	0.6	45.7	76
298.15	1.0	73.3	73
298.15	1.5	119.5	80
303.15	1.0	90.2	90
313.15	1.0	100.4	100

The obtained k_2 values at 20 and 25 $^\circ$C seem to support the assumption with respect to the reaction order of piperazine, since the value per temperature is more or less constant (within 10 %) over the concentration range studied. Had the assumption been false, a much larger effect of the concentration on the kinetic rate constant k_2 would have been expected. Therefore, an overall second order reaction rate according to Eq. 4.4 (with the corresponding k_2 constants as determined in

Table 4.10) is assumed in all further calculations and discussions.

In summary, this last paragraph has provided three different methods to interpret the experimentally obtained absorption rates, all of which are based on a (more or less) different principle – as pointed out in Table 4.11.

Table 4.11: Methods used to interpret experimental data.

Method	Enhancement factor from		Infinite enhancement factor	
First Order	$E = Ha$	Eq. 4.12	irreversible	Eq. 4.10
DeCoursey relation	$E \propto (Ha, E_{inf})$	Eq. 4.13	irreversible	Eq. 4.10
Hogendoorn approximation	$E \propto (Ha, E_{inf})$	Eq. 4.13	reversible	Eq. 4.32

As already shown in Tables 4.6,4.8 and 4.9, these different interpretation techniques can lead to different kinetic rate constants. A schematic overview of the results is given in Table 4.12, where the forward kinetic rate constants k_2 have been determined assuming first order dependence in piperazine (see Table 4.10).

Table 4.12: Second order kinetic rate constants according to the interpretation methods applied.

T	$k_2{}^a$ [m^3 kmol^{-1} s^{-1}]		
[K]	'PFO'	'DeCoursey'	'Hogendoorn'
293.15	52	65	68
298.15	58	76	80
303.15	68	90	96
313.15	85	100	113

[a]For 20 and 25 $^\circ$C, the average k_2 values over the three concentrations are listed.

The results obtained with the DeCoursey relation (based on an irreversible enhancement factor) are considered to be the most accurate, since on one hand the pseudo first order criteria are probably not fully satisfied (see results listed in Table 4.7). On the other hand, the effect of reversibility on the results is so small that it doesn't outweigh the extra uncertainties that are introduced when applying

Hogendoorn's approach, which requires the equilibrium constant of the reactants as well as the diffusion coefficients of all reaction products.

4.5.2 Kinetics of CO_2 with protonated piperazine

As discussed in Section 4.2, the assumption concerning the supposedly negligible relative contribution of reaction (3) to the overall mass transfer rate needs experimental validation. As information concerning the order of magnitude will do in this respect, experiments have been limited to a temperature of 25 °C and a concentration of about 1.0 kmol m^{-3} PZH^+. Since PZH^+ itself is the strongest base present in solution (as all other bases such as PZ and OH^- have been neutralised by the (excess) HCl), the overall reaction can be described according to Eq. 4.20:

$$CO_2 + 2PZH^+ \rightleftarrows H^+PZCOO^- + PZH_2^{2+} \tag{4.20}$$

As in the reaction of piperazine with CO_2, it also assumed that the formation of the zwitterion is the rate determining step in Eq. 4.20 (reaction (3)), characterized by a second order kinetic rate constant k_2, as the reaction is assumed to react first order in both CO_2 and PZH^+.

$$CO_2 + PZH^+ \overset{k_2}{\rightleftarrows} H^+PZH^+COO^- \tag{4.21}$$

Absorption experiments into these protonated piperazine solutions ($[PZH^+] = 0.99$ kmol m^{-3}) were performed with a batch wise operated gas phase and at initial CO_2 partial pressures of about 40 to 45 mbar. Apparent pseudo first order behavior - a straight slope according to Eq. 4.18 (see Figure 4.2) - was found at pressures below about 15 mbar CO_2. Experiments were carried out at different liquid stirrer speeds to validate the assumption concerning operating in the pseudo first order regime, where the stirrer speed (or the mass transfer coefficient k_L) should not influence the flux. Results of the kinetic experiments are listed in Table 4.13.

Table 4.13: Experimental results on the kinetics of the reaction between CO_2 and PZH^+, applying batchwise operation of the setup.

N [min^{-1}]	k_L [a] [$\cdot 10^{-5}$ m s^{-1}]	$10^6\sqrt{k_{OV} \cdot D}$ [b]	Enhancement factor [c]
48.60	1.20	346	29.0
73.1	1.59	412	25.9
90.4	1.85	481	26.0
106.5	2.07	498	24.1
122.6	2.28	527	23.1

[a] $k_L \propto N^{0.7}$

[b] The slope has been interpreted assuming that '$E = Ha$' was valid

[c] $E = \sqrt{k_{OV} \cdot D}/k_L$

It is obvious from the results that the observed apparent kinetic rate term $k_{OV} \cdot D$ does not reach a constant value with increasing stirrer speed and physical mass transfer coefficient k_L (i.e. decreasing Ha number), which implies that the experiments have not (completely) been carried out in the pseudo first order regime. The (rather large) influence of the k_L on the observed results might be explained by the reversibility of the reaction (between PZH^+ and CO_2), which - depending on the value of the equilibrium constant - can lower the infinite enhancement factor.

This hypothesis was checked by performing some 'semi continuous' experiments at different stirrer speeds and CO_2 partial pressures following the same method as used for aqueous piperazine solutions. Observed experimental fluxes (listed in Table 4.14) were then compared to the fluxes obtained with aqueous piperazine solution at similar conditions (see also Table 4.5).

From Table 4.14, two conclusions can be drawn. Firstly, the enhancement factors observed in the experiments with 14 mbar CO_2 partial pressure are similar to the ones observed in the batch experiments at comparable stirrer speed, which means both experimental methods and results are consistent. Secondly, the experimentally determined CO_2 fluxes into the protonated piperazine solutions are at least one

Table 4.14: Flux of CO_2 into an aqueous solutions of 1.0 M PZH^+ at 25 °C, applying a 'semi-continuous' operation of the setup.

Reactant	N [min^{-1}]	k_L [$\cdot 10^{-5}$ m s^{-1}]	P_{CO2} [mbar]	J_{CO2} [mmol m^{-2} s^{-1}]	Enhancement factor [-]
PZH^+	49.2	1.22	12.9	0.14	28.1
			23.0	0.23	25.0
			34.6	0.30	21.8
	72	1.59	14.1	0.19	26.1
			24.1	0.29	23.3
			34.3	0.37	20.9
	95.8	1.94	14.3	0.22	25.0
			24.3	0.33	22.0
			34.5	0.43	19.9
PZ		1.98	10.8	2.66	
			19.5	4.00	

order of magnitude lower than the absorption rate into the piperazine solutions at similar conditions. Under the previously mentioned assumption of a second order rate determining formation of the zwitterion (see Eq. 4.21) and an equilibrium constant value in the PZH^+ system which is in the same order of magnitude as in the piperazine system, this would imply a considerably lower kinetic rate and hence pseudo first order criteria should be more easily obeyed. As this is obviously not the case, it means that the absorption of CO_2 into protonated piperazine solutions could be influenced by the reversibility of the reaction between carbon dioxide and PZH^+. An indication towards the occurrence of reversibility is the magnitude of the equilibrium constant of the reaction, which - according to the overall reaction given in Eq. 4.20 - is defined as follows:

$$K_{eq} = \frac{[^+HPZCOO^-][PZH_2^{2+}]}{[CO_2][PZH^+]^2} \tag{4.22}$$

Its value can be calculated similarly to Eq. 4.16, using the equilibrium constants as determined by Ermatchkov et al. [2002] and Hetzer et al. [1967], and is found to

be 1.6 molal^{-1}. This value is four orders of magnitude smaller than the equilibrium constant as determined for the reaction between piperazine and CO_2 ($K_{Eq} = 8 \cdot 10^4$ molal^{-1}, see Table 4.1) and therefore it supports the hypothesis with regard to the influence of reversibility.

Now, to interpret the experimental results, a similar approach is followed as for the experimental data for the absorption into aqueous piperazine: The infinite enhancement factor, adjusted to account for reversibility [Hogendoorn et al., 1997, Secor and Beutler, 1967], for the PZH^+ system is calculated, and the 'equilibrium adapted' DeCoursey relation (or the 'Hogendoorn approximation' in Table 4.11) is then applied to calculate the enhancement factor (see Appendix 4.B for all governing equations). The forward kinetic rate constant, k_2 in Eq. 4.21, which is necessary in the determination of the Ha number, is used as the (single) adjustable parameter to match experiment and model. All other necessary parameters were estimated as follows:

- All physicochemical constants were assumed to be identical to the properties listed for the 1.0 M piperazine solution at 298.15 K in Tables 4.6 and 4.7;
- The diffusivity of all piperazine species is assumed to be identical.

The results of this procedure to fit the kinetic rate constant to the experiments are plotted in Figure 4.5.

Figure 4.5 shows that Hogendoorn's approximation method used here is able to describe the experimentally obtained results well, and, since the predicted results were (still) susceptible to (changes in) the guessed value for the forward kinetic rate constant, this constant could indeed be used as an adjustable parameter in the correlation of the experimental results. The fitted second order forward kinetic rate constant was found to have a value of 0.30 ± 0.10 m^3 mol^{-1} s^{-1} at 298.15 K. Although this is merely a global estimation based on an approximation method, it does provide a possibility to quantitatively compare the forward kinetic rate constants of reactions (1) and (3) between CO_2 and piperazine or its protonated

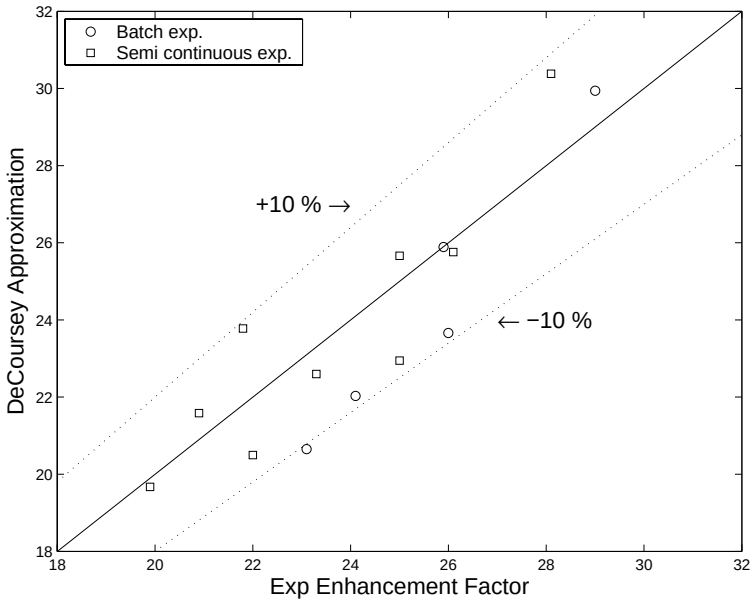

Figure 4.5: Comparison of the experimentally observed enhancement factors in the CO_2 - PZH^+ system with the theoretical prediction based on the Hogendoorn approximation method.

species. The latter was found to be about two orders of magnitude smaller than the former, under the assumption with regard to the rate determining step being the formation of the zwitterion (Eq. 4.21 21), thereby validating the assumption concerning the neglect of reaction (3) in the determination of the reaction rate between piperazine and CO_2 in aqueous environment in - or near - the '$E = Ha$' regime.

4.6 Discussion

It is demonstrated in this chapter - both by the qualitative analysis in Section 4.2 and the quantitative results on the absorption of CO_2 into aqueous solutions of protonated piperazine - that experimental data on the absorption of CO_2 into aqueous piperazine solutions in or near the '$E = Ha$' regime can be interpreted by means of assuming the single presence of the reaction between CO_2 and piperazine. The contribution of reactions of other species present (e.g. OH^- and PZH^+) can correctly

be neglected.

A comparison between the present data, interpreted with the DeCoursey relation (based on an infinite enhancement factor, see Table 4.8 and the kinetic rate data presented by Bishnoi and Rochelle [2000] and Sun et al. [2005] is given in the Arrhenius-plot in Figure 4.6. Due to lack of experimental diffusion coefficient data, and to avoid the comparison being influenced too much by the used estimation method for the diffusion coefficients, it is not the second order kinetic rate constant k_2 that is plotted on the y-axis, but this rate constant multiplied with the diffusion coefficient of CO_2, $k_2 \cdot D_{CO_2}$.

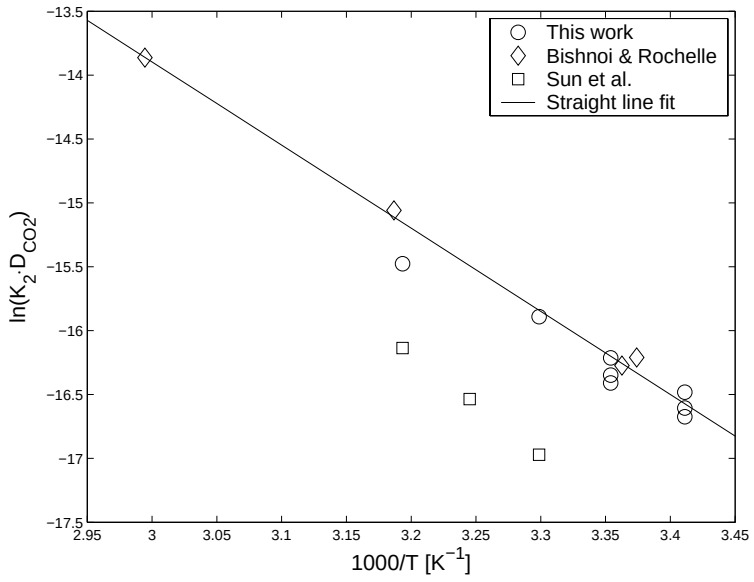

Figure 4.6: The Arrhenius plot of the product $(k_2 \cdot D_{CO2})$ for the reaction of CO_2 with piperazine in aqueous solution. The straight line fit neglects the data of Sun et al. [2005].

Figure 4.6 illustrates that the present data are well in line with the experimental values reported by Bishnoi and Rochelle [2000], and, simultaneously, that there is a distinct deviation between these first two data sets and the kinetic data presented by Sun et al. [2005]. Sun et al. [2005] found much lower values than the data reported in the work of Bishnoi and Rochelle [2000] and the present study.

An explanation could be that the pseudo first order conditions may not have been satisfied in their work: Absorption experiments by Sun et al. [2005] have been carried out at CO_2 partial pressures ranging from 32 to 77.5 mbar, which is a factor 6 to 10 higher than the maximum CO_2 pressures as listed in Table 4.7 (resulting in E_{inf} values that are a factor 6-10 lower than in this work), while the mass transfer coefficient k_L is less than a factor three higher than in the current work, leading to Ha numbers which are less than a factor three lower than in this work. As a result, the ratio between the Ha number and the infinite enhancement factor is a factor 2-3 lower than in this work while they still interpret their experiments as if they were conducted in the pseudo first order regime, which seems not completely justified. Besides this, there appears to be an inconsistency in the work by Sun et al. [2005]: They report the CO_2 diffusion coefficients in aqueous PZ solutions to be smaller than the experimentally determined diffusion coefficients of N_2O, which seems contradictory to the CO_2:N_2O analogy: At the temperatures in their work, the diffusion coefficient of CO_2 should exceed the diffusion coefficient of N_2O. Moreover, the self diffusion coefficient of an amine in its aqueous solution decreases with increasing concentration (due to an increasing liquid viscosity); Sun et al. [2005] report a contradictory behavior.

Bishnoi and Rochelle [2000] performed their absorption experiments in a wetted wall contactor at conditions (a mass transfer coefficient $k_L > 10^{-4}$ m/s and CO_2 partial pressure < 2 mbar) which seem to ensure a pseudo first order behavior. Their experimental results are in good agreement with the present data, with the exception of the data at 313 K. This is partly due to the effect of reversibility of the reaction on our experimental results at this temperature. As the results in Table 4.9 already illustrated, incorporation of reversibility in the determination of the kinetic rate constant shows the highest deviation at T = 313.15 K. Since this data point at 313 K from the present work seems to deviate from the trend set by all other data points from both the present work and the work of Bishnoi and Rochelle [2000], it was decided to omit this data point from the Arrhenius fit. The temperature dependence of the product of the forward second order kinetic rate constant and the

diffusion coefficient is then described by Eq. 4.23.

$$k_{2,PZ-CO_2} \cdot D_{CO_2} = 169.0 \cdot \exp\left(-\frac{6.3 \cdot 10^3}{T}\right) \tag{4.23}$$

Usually, the apparent activation temperature of the diffusion coefficient of CO_2 in aqueous (amine) solutions is in the order of 2.1 K (see e.g. Versteeg et al. [1996]), and hence it seems safe to state that the activation temperature of the reaction amounts to (4.1 ± 0.3) K.

As already mentioned in Section 4.2, the Brønsted plot technique has shown that for various groups of aqueous alkanolamines, there is a (linear) relation between the pKa value of an (alkanol)amine and (the logarithm of) the forward rate constant [Versteeg et al., 1996]. It would be interesting to investigate, whether there also exists a similar relation for amines which resemble piperazine. If this would be the case, such a Brønsted plot can be used for the prediction of the kinetic rate of other amines, and hence it might serve as a tool in designing new activators. Table 4.15 lists the pKa value and corresponding 2^{nd} order kinetic rate constant k_2 for a selection of amines at a temperature of 25 $^\circ$C. The corresponding Brønsted plot is shown in Figure 4.7.

Figure 4.7 indicated that a kind of Brønsted relationship also exists for amines with a ring structure similar to piperazine. Although some of the data plotted in Figure 4.7 are in fact estimates derived via extrapolation from different temperatures, the results seem very promising. According to this plot, the forward kinetic rate constant of a piperazine alike molecule with CO_2 at a temperature of 25 $^\circ$C can be estimated based on the corresponding pKa value according to Eq. 4.24:

$$\ln k_2 = pKa - 6 \tag{4.24}$$

For the carbamated piperazine ($PZCOO^-$), with a pKa of 9.44, this would imply a kinetic rate constant of 31 m^3 mol^{-1} s^{-1} at 25 $^\circ$C. This does not mean that this reaction affects the outcome of the interpretation of the kinetic study in the present work, since the $PZCOO^-$ concentration is negligibly low (always smaller than

Table 4.15: Kinetic rate constants and pKa values at 25 °C for some selected (alkanol)amines.

Amine[a]	pKa[b]	Source	k_2[c]	Source
MEA	9.50	Perrin [1965]	6.0	Versteeg et al. [1996]
DGA	9.47	Littel et al. [1990a]	4.5	Versteeg et al. [1996]
DEA	8.92	Perrin [1965]	1.3	Versteeg et al. [1996]
DIPA	8.88	Kim et al. [1987]	0.1	Versteeg et al. [1996]
MMEA	9.80	Littel et al. [1990a]	7.1	Versteeg et al. [1996]
Piperazine	9.73	Hetzer et al. [1967]	76 / 59	This work,Bishnoi and Rochelle [2000]
Piperazine-H^+	5.33	Hetzer et al. [1967]	0.30	This work
Piperidine	11.12	Perrin [1965]	60.2	Sharma [1965]
Morpholine	8.36	Perrin [1965]	18 / 20.5	Sharma [1965], Alper [1990]
Aminoethyl-PZ	9.48	Perrin [1965]	28.0	Bishnoi [2000]
Hydroxyethyl-PZ	9.38	Castro et al. [1997]	11.0	Bishnoi [2000]
Aniline	4.61	Perrin [1965]	0.051	Sharma [1965]
Benzylamine	9.34	Perrin [1965]	8.51	Sharma [1965]
Cyclohexylamine	10.68	Perrin [1965]	8.2	Sada et al. [1986]

[a]Subdivided into different groups depending on the structure (See also Figure 4.7
[b]Some of the pKa values stem from interpolating the available data at different temperatures
[c]Some k_2 constants were obtained via extrapolation of data taken at different temperatures

0.04 kmol m^{-3}), but under other experimental/industrial conditions, such as high CO_2 partial pressure and loading, this reaction is expected to make a (noticeable) contribution to the absorption rate. Of course, it must be kept in mind that this analysis is based on the use of a Brønsted relation, and, although the first results with this limited group of piperazine based amines indicate that the Brønsted relation is applicable, information on more piperazine related amines (especially in the pKa range of 6 to 8) is needed to investigate this relation more thoroughly.

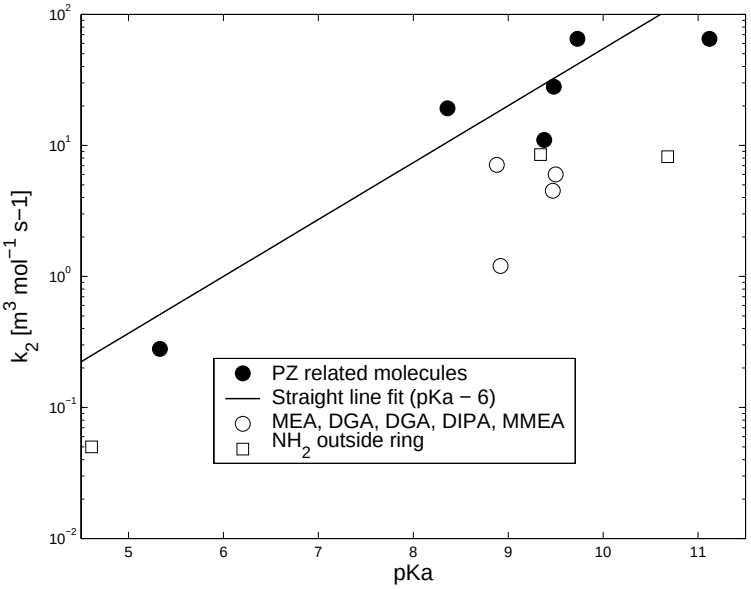

Figure 4.7: Brønsted plot for piperazine and related molecules at 25 °C.

4.7 Conclusions

Aqueous (blends of) amine solutions are frequently used solvents for the removal of acid gas components from industrial gas streams. Particularly the piperazine activated aqueous N-methyldiethanolamine solution has become subject of research since it has proven to be a very promising blend in the bulk removal of carbon dioxide. Although the kinetics of MDEA with carbon dioxide have been studied extensively in the past, only two studies report (mutually strongly deviating) kinetic rate data concerning the reaction between piperazine and CO_2 in aqueous solutions.

In this chapter, a stirred cell setup was used to obtain and report new absorption rate data of CO_2 into aqueous piperazine solutions at different PZ concentrations, CO_2 partial pressures and temperatures. Three different interpretation methods were used to extract the rate constants of the reaction between piperazine and carbon dioxide from the obtained experimental data. First of all the pseudo first order principle, where the enhancement factor equals the Hatta number. Secondly

the DeCoursey relation was used, which gives the enhancement factor as an explicit function of Ha and the (irreversible) infinite enhancement factor and thirdly, the Hogendoorn approximation was applied, which comprises of the DeCoursey relation with an infinite enhancement factor which is corrected for the reversibility of the reaction. As the pseudo first order conditions were probably not fully satisfied and since the effect of reversibility was found to be negligibly small, the DeCoursey equation was considered to be the most suitable method to deduct the kinetic rate constants from the experimental results. The second order kinetic rate constant for the reaction between piperazine and carbon dioxide as obtained with this DeCoursey relation was found to be in good agreement with the kinetic rate data reported by Bishnoi and Rochelle [2000]. The values presented by Sun et al. [2005] are considerably lower, which is probably due to the fact that pseudo first order conditions have not been completely satisfied in their work. The reaction between piperazine and CO_2 in aqueous solutions seems to be an overall second order reaction, which implies instantaneous deprotonation of the zwitterion as typically found for reactions between CO_2 and primary alkanolamines. However, it should be noted, that this finding is partly based on the use of estimated diffusion coefficients, and, therefore, experimental diffusivity data should become available to finally confirm this.

Finally, also the absorption of carbon dioxide into partially protonated piperazine solutions was experimentally investigated. Again, it was found that pseudo first order conditions could not be satisfied, mainly because of the relatively low equilibrium constant for this reaction. The observed experimental enhancement factors were therefore interpreted using the Hogendoorn approximation, hence using an infinite enhancement factor which is corrected for the reversibility of the reaction. The second order kinetic rate constant was found to be approximately 0.30 m^3 mol^{-1} s^{-1}.

Acknowledgements

H.F.G. Moed is acknowledged for the construction of the experimental setup, and T. Kleingeld and C. van Aken are acknowledged for their parts in the experimental work.

4.A Diffusion coefficient of CO_2 used in the determination of kinetic constants

In the determination of the kinetic rate constant from experimental absorption rate results the diffusion coefficient of CO_2 in aqueous piperazine solutions is required. As CO_2 reacts with piperazine, its diffusion coefficient is not independently measurable, and therefore this property was indirectly estimated from the diffusivity of N_2O in aqueous piperazine solutions.

Sun et al. [2005] experimentally determined the N_2O diffusion coefficient in aqueous piperazine solutions at various concentrations for temperatures of 30, 35 and 40 °C. Their data at a piperazine concentration of 0.92 kmol m^{-3} have been used in the interpretation of the kinetic rate experiments at 30 and 40 °C performed in this chapter.

The N_2O diffusivities at temperatures of 20 and 25 °C have been estimated using the modified Stokes-Einstein equation proposed by Versteeg and Van Swaaij [1988b]. Equation 4.25 was found to give satisfactory results in estimating the N_2O diffusivity in various aqueous alkanolamine solutions at different temperatures.

$$(D_{N_2O} \cdot \mu^{0.8})_{PZ\ sol} = \text{constant} = (D_{N_2O} \cdot \eta^{0.8})_{water} \tag{4.25}$$

Viscosities of piperazine solutions at different temperatures and PZ concentrations have been experimentally determined in Chapter 2. Viscosities of water as a function of temperature are listed in Lide [1994], and the diffusion coefficient of N_2O in water

was calculated from the equation presented by Versteeg and Van Swaaij [1988b].

$$D_{N_2O} = 5.07 \cdot 10^{-6} \exp\left(\frac{-2371}{T}\right) \tag{4.26}$$

Details and results of the calculation are listed in Table 4.16.

Table 4.16: Estimation of CO_2 diffusion coefficients.

T [K]	μ_{H2O} [mPa s]	$D_{N2O,H2O}$ [10^{-9} m^2 s^{-1}]	C_{PZ} [kmol m^{-3}]	μ_{PZ-sol} [mPa s]	$D_{estimated}$ [10^{-9} m^2 s^{-1}]
293.15	1.002	1.56	0.6	1.26	1.30
293.15	1.002	1.56	1.0	1.52	1.12
293.15	1.002	1.56	1.5	1.86	0.95
298.15	0.890	1.78	0.6	1.1	1.51
298.15	0.890	1.78	1.0	1.31	1.31
298.15	0.890	1.78	1.5	1.62	1.10

The performance of this rather simple estimation method was tested with the experimental diffusivity data at 30 °C reported by Sun et al. [2005], at a concentration range from 0.23 to 0.92 kmol m^{-3}. A comparison between the experimental results and the values estimated by the modified Stokes-Einstein equation is given in Table 4.17:

Table 4.17: Comparison of Stokes-Einstein relation to experimental diffusivity data.

T [K]	μ_{H2O} [mPa s]	$D_{N2O,H2O}$ [10^{-9} m^2 s^{-1}]	C_{PZ} [kmol m^{-3}]	μ_{PZ-sol}[a] [mPa s]	$D_{estimated}$ [10^{-9} m^2 s^{-1}]	$D_{experimental}$ [10^{-9} m^2 s^{-1}]	Error [%]
303.15	0.798	2.03	0.23	0.887	1.87	1.91	-2.2
303.15	0.798	2.03	0.46	0.939	1.79	1.85	-3.5
303.15	0.798	2.03	0.69	1.004	1.69	1.77	-4.4
303.15	0.798	2.03	0.92	1.096	1.58	1.73	-8.8

[a] Taken from Sun et al. [2005].

Although the modified Stokes-Einstein equation in its current form gives a fair prediction of the experimentally determined diffusion coefficients (the deviation

is $< 10\%$), it should be noted, that the prediction capability seems to deteriorate with increasing piperazine concentration (and hence solution viscosity).

4.B Implementing reversibility in the calculation of the infinite enhancement factor

As already pointed out in Section 4.3, the reversibility of the reaction between CO_2 and piperazine has not been taken into account in the determination of the rate constant, since for the present experiments this reversibility does not influence the infinite enhancement factor or the calculated enhancement factor (by using Eq. 4.13) substantially. In literature, some studies can be found which offer approximate solutions which correct for the reversibility of a reaction system. One of the methods to include reversibility in the expression for the infinite enhancement factor is provided by Secor and Beutler [1967].

Secor and Beutler [1967] derived an equation for the infinite enhancement factor which incorporates the reversibility of a reaction. When the following reaction takes place:

$$\nu_A A + \nu_B B \rightleftarrows \nu_C C + \nu_D D \tag{4.27}$$

The infinite enhancement factor (including reversibility) is defined as follows:

$$E_{A,inf} = 1 + \frac{\nu_A D_C}{\nu_C D_A} \frac{([C]_{int} - [C]_L)}{(m[A]_G - [A]_L)} \tag{4.28}$$

The concentration of C at the interface, C_i, is to be calculated using equations 4.29, 4.30 and 4.31:

$$[B]_{int} = [B]_L + \frac{\nu_B D_C}{\nu_C D_B} ([C]_L - [C]_{int}) \tag{4.29}$$

$$[D]_{int} = [D]_L - \frac{\nu_D D_C}{\nu_C D_D} ([C]_L - [C]_{int}) \tag{4.30}$$

$$K = \frac{[C]_{int}^{\nu_C} [D]_{int}^{\nu_D}}{(m_A[A]_G)^{\nu_A} [B]_{int}^{\nu_B}} \tag{4.31}$$

It is, however, not possible to directly compare the infinite enhancement calculated with Eq. 4.28 to the infinite enhancement used in this chapter (Eq. 4.10), since the latter is based on the penetration theory whereas Eq. 4.28 stems from the film theory. To comply to the penetration theory also, this equation 4.28 was adapted similarly to the method described by Hogendoorn et al. [1997]. The reversible infinite enhancement factor is then given by Eq. 4.32:

$$E_{A,inf} = 1 + \left(\frac{D_C}{D_A}\right)^{0.5} \frac{\nu_A \left([C]_{int} - [C]_L\right)}{\nu_C \left(m[A]_G - [A]_L\right)} \tag{4.32}$$

The overall reaction to be checked for the influence of reversibility is the following reaction between piperazine and carbon dioxide:

$$CO_2 + 2PZ \rightleftarrows PZCOO^- + PZH^+ \tag{4.33}$$

The following assumptions have been made in the calculation of the enhancement factors according to Eq. 4.32:

- Diffusion coefficient of all piperazine species is equal;
- The system behaves ideally;
- No other reactions take place besides reaction (1) between piperazine and CO_2 to form carbamated and protonated piperazine.

The conditions applying to the example to be studied are listed in Table 4.18.

Equations 4.29, 4.30 and 4.31 can be used to calculate the corresponding concentrations at the gas liquid interface necessary for the reversible infinite enhancement factor (Eq. 4.32). Results are listed in Table 4.19. Now, both the infinite enhancement factors can be calculated and the results are shown in Table 4.20.

The results in this calculation example show that the difference between the irreversible and reversible infinite enhancement factor is about 10 % in the case of the kinetic rate experiments in 600 mol m^{-3} at 25 $^\circ$C. Similarly, also the reversible infinite enhancement factors have been calculated for the other kinetic data series, and the resulting values have been listed in Table 4.9 in Section 4.5.

Table 4.18: Conditions and properties of the calculation example for the reversible infinite enhancement factor.

Property			Source
Temperature	298.15	K	Table 4.7
Initial piperazine concentration	600	mol m^{-3}	Table 4.7
CO_2 partial pressure	5.50	mbar	Table 4.7
Equilibrium constant	$8.0 \cdot 10^4$	$molal^{-1}$	Table 4.2
Distribution coefficient	0.802	[-]	Table 4.6
Diffusion coefficient of CO_2	$1.51 \cdot 10^{-9}$	m^2 s^{-1}	Appendix 4.A
Diffusion coefficient of PZ	$0.71 \cdot 10^{-9}$	m^2 s^{-1}	Eq. 4.19

Table 4.19: Interfacial concentrations calculated according to Eq. 4.29, 4.30 and 4.31.

$[PZ]_{int}$	68.6	mol m^{-3}
$[CO_2]_{int}$	0.18	mol m^{-3}
$[PZCOO^-]_{int}$	265.7	mol m^{-3}
$[PZH^+]_{int}$	265.7	mol m^{-3}

Table 4.20: Calculation results for the infinite enhancement factor.

Type	Equation Nr	Value
irreversible	4.10	1119
reversible	4.32	991

Chapter 5

New Type of Stirred Cell Contactor

Abstract

A new mode of operation for the conventional stirred cell is proposed to allow for absorption experiments at substantially lower partial pressures as required for fast, pseudo first order kinetic rate, absorption experiments like e.g. the reaction between piperazine and CO_2. Hereto, a second cell is added to the conventional setup, which contains a solution identical to the one in the 'reactor cell' and hence it serves as a reference for the vapor pressure. Consequently, in case a pure, reactive gas is used, the pressure difference between the two cells is, in fact, the partial pressure of the gas phase reactant in the reactor cell. The new mode of operation was experimentally validated with the well-documented CO_2 - OH^- reaction (in aqueous NaOH solutions) at 25 and 40 $^\circ$C. The obtained forward second order kinetic rate constants, deduced from the experimental data taken at low partial pressures (down to 1.5 mbar), were found to be in good agreement with the values reported literature.

5.1 Introduction

The absorption of a gaseous component into a reactive liquid is an important part in several processes in chemical industry, such as e.g. the removal of acid gases with aqueous (alkanol)amine solutions. An accurate design and operation of these and other absorption processes requires detailed knowledge on (among other things) the intrinsic kinetics of the reaction between the gaseous component and the liquid phase reactant - as already pointed out in the previous chapter. In the literature, several laboratory scale gas liquid model contactors have been proposed to determine the kinetics of industrially relevant gas liquid reactions, such as:

- The laminar jet (e.g. Nijsing et al. [1959], Pohorecki and Moniuk [1988])
- The wetted wall (e.g. Bishnoi and Rochelle [2000])
- The wetted sphere (e.g. Al-Ghawas et al. [1989])
- The stirred cell (see below)

All these contactors have their own advantages and disadvantages with respect to e.g. liquid side mass transfer coefficient, liquid use and ease of operation. Throughout this work, the stirred cell contactor has been used (see e.g. Chapter 4), as it offers specific advantages related to the liquid use, a well-known gas-liquid contact area, ease of operation and, in the past, it has proven to be a reliable method to determine the kinetics in gas-liquid systems [Blauwhoff et al., 1984, Versteeg and Van Swaaij, 1988a, Littel et al., 1990b, Brilman et al., 1997, Kumar et al., 2003b]. One disadvantage of the stirred cell is the relatively low liquid side mass transfer coefficient, k_L, which complicates its applicability in the determination of (extremely) fast gas-liquid reactions. This is explained in the discussion below.

Considering the following reaction, describing the physical absorption of a gaseous component A into a liquid phase and the subsequent irreversible reaction with the liquid phase reactant B:

$$A_G \rightarrow A_L \qquad A_L + 2B_L \rightarrow C + D \tag{5.1}$$

with the reaction rate given by:

$$R_A = -k_2 C_A C_B \tag{5.2}$$

The absorption rate of component A can be described with Eq. 5.3, if the absorption takes place in the pseudo first order (PFO) regime:

$$J_A = \sqrt{k_2 C_B D_A} \frac{m_A P_{A,\text{int}}}{RT} \tag{5.3}$$

Operation in the PFO regime requires that the following criterion is satisfied, with respect to the Ha number and the infinite enhancement factor E_{inf}:

$$2 < Ha \ll E_{\text{inf}} \tag{5.4}$$

where Ha and E_{inf} (definition according to the penetration model for an irreversible reaction) are defined as follows:

$$Ha = \frac{\sqrt{k_2 C_B D_A}}{k_L} \tag{5.5}$$

$$E_{\text{inf}} = \sqrt{\frac{D_A}{D_B}} \left(1 + \frac{D_B C_B RT}{\nu_B D_A m_A P_{A,\text{int}}} \right) \tag{5.6}$$

As a rule of thumb, it can be assumed that Eq. 5.4 is obeyed if the infinite enhancement factor is at least a factor 10 higher than the ruling Ha number:

$$E_{\text{inf}} \geqslant 10 \cdot Ha \tag{5.7}$$

Criterion 5.7 (together with Eqs. 5.5 and 5.6) basically states that, at constant k_L, a higher infinite enhancement factor is required if a faster reaction is to be investigated in the PFO regime: An increasing kinetic rate constant implies an increasing Ha number, which - according to Eq. 5.7 - requires an increasing infinite enhancement factor, which - according to its definition - can only obtained by substantially lowering the governing (interfacial) CO_2 partial pressure.

This is illustrated in the following calculations, where the CO_2 partial pressure, required for PFO conditions, is calculated as a function of kinetic rate constant k_2. These calculations have been made for a stirred cell, with a liquid side mass transfer coefficient k_L of $2 \cdot 10^{-5}$ m s^{-1} as typically found for e.g. CO_2 absorption in aqueous solutions. All other necessary properties used in the calculations have been listed in Table 5.1, and the results are shown graphically in Figure 5.1.

Table 5.1: Constants and values used in the calculation example.

Property	value
C_B	1000 mol m-3
D_A	$1.9 \cdot 10^{-9}$ m^2 s^{-1}
D_B	$0.95 \cdot 10^{-9}$ m^2 s^{-1}
mA	0.75
T	298 K
ν_A	2
P_{H2O}^{vapor} (T = 298 K)	31.4 mbar

Figure 5.1 clearly illustrates the statement made earlier, that an increasing kinetic rate constant requires a decreasing partial pressure in order to remain in the PFO regime in the stirred cell, down to approximately 2-3 mbar CO_2 for a reaction rate comparable to piperazine (k_2 about 75 m^3 $kmol^{-1}$ s^{-1} - see Chapter 4). As a comparison, a similar curve was calculated for the laminar jet or the wetted wall column with a typical liquid side mass transfer coefficient in the order of magnitude of 10^{-4} m/s (in the case of CO_2 absorption in aqueous solutions), which is also illustrated in Figure 5.1.

The stirred cell setup can be operated in two ways to meet the requirement of a low partial pressure:

- Continuous mode of operation: In this mode of operation, carbon dioxide is mixed with an inert gas, usually nitrogen, prior to entering the reactor. The amount of CO_2 in the outlet gas stream is then continuously analyzed using

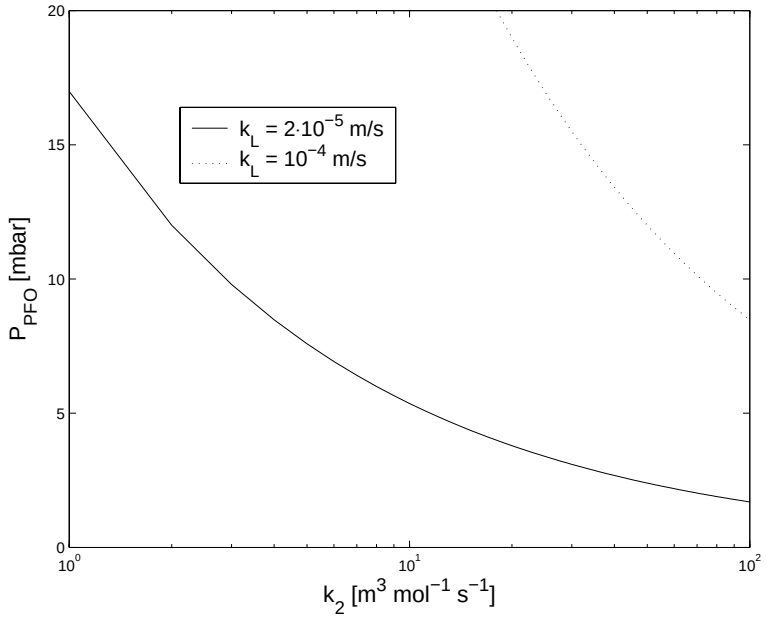

Figure 5.1: The maximum pressure at which PFO behavior is guaranteed ($E_{inf} = 10 \cdot Ha$) as a function of the kinetic rate constant k_2.

e.g. an IR detector, which allows for an accurate determination of the CO_2 partial pressure. Drawbacks of this mode of operation are that it requires extra equipment (presaturators) and calibrations (MFCs). Also, there is a risk of mass transfer resistance in the gas phase, and a non-uniform CO_2 partial pressure in the reactor (i.e. only the outgoing concentration is known and the local partial pressures at different positions in the reactor have to be estimated using information about the residence time distribution of the gas phase in the reactor). If a differential mode of operation is chosen (i.e. a very small difference between inlet and outlet CO_2 concentration), then the risk of increasing experimental errors arises, because the absorption rate is determined from the (small) difference in CO_2 percentage between inlet and outlet, and the total gas flow. Although possible, this method has its problems and limitations with respect to the determination of the kinetics of fast reactions.

- Semi-batch mode of operation: In this mode of operation, pure carbon dioxide

is fed from a calibrated gas supply vessel to the reactor by a (e.g. pressure) controller which is to keep the total pressure in the reactor constant. The local CO_2 partial pressure is determined by the difference between the vapor pressure of the lean solution (recorded prior to an experiment) and the total pressure during an experiment (assuming that CO_2 is the only gas present apart from the vapor of the solution). The absorption rate is determined from the dynamic pressure decrease in the (calibrated) carbon dioxide supply vessel.

The latter method is applied in this work (see Chapter 4) because of the relative ease of operation and the accuracy in the measurement of both flux and CO_2 partial pressure. The uncertainty in the latter quantity, however, increases with decreasing partial pressure and/or increasing temperature (or vapor pressure) - see Eq. 5.8:

$$P_{CO2} = P_{total} - P_{vap} \tag{5.8}$$

Equation 5.8 shows that the CO_2 partial pressure is, in fact, calculated as the difference of two numbers, which poses no problems at relatively high partial pressures. However, at very low partial pressures and/or relatively high vapor pressures, the CO_2 partial pressure is the (small) difference of two large numbers - which can introduce a reasonable uncertainty in this quantity if the vapor pressure is not accurately known. This uncertainty prevented performing extensive kinetic rate experiments in aqueous piperazine at CO_2 partial pressures below 3 mbar with the stirred cell setup used in Chapter 4 - whereas criterion 5.4 would require partial pressures of this magnitude to obey the conditions for the PFO regime.

In this chapter, a new mode of operation for the stirred cell is proposed, which is to circumvent this uncertainty in actual CO_2 partial pressure and allows for low P_{CO2} absorption rate experiments. The method is explained in detail in Section 5.2, and the experimental validation is described in Section 5.3.

5.2 Experimental setup

In order to make the traditional semi-batch mode of operation of the stirred cell setup, as described in the previous chapter, suitable for low (CO_2) partial pressure absorption rate experiments, a more accurate way should be applied to determine the actual (CO_2) partial pressure in the reactor during the experiment. In the method used in Chapter 4 (see Eq. 5.8), the partial pressure was calculated as the difference between the total pressure during the experiment and the lean solution's vapor pressure, recorded prior to the experiment. This introduces an increasing uncertainty in partial pressure with a decreasing ratio between partial and total pressure.

To bypass this problem, a second stirred cell was added to the setup, which is to contain the same solution as the other, reactor stirred cell. During an absorption experiment, the second cell is closed off, while CO_2 is fed to the reactor cell. As both cells contain the same liquid at the same temperature, the second cell serves as a reference cell with respect to the solution's vapor pressure, and hence the actual CO_2 partial pressure in the reactor cell is equal to the differential pressure between the two stirred cells, according to Eq. 5.9:

$$P_{CO_2,R} = (P_{vap,R} + P_{CO_2,R}) - P_{vap,Ref} = \Delta P_{R-Ref} \tag{5.9}$$

A schematic drawing of the modified stirred cell setup is shown in Figure 6.1.

The reactor and the reference cell were made of glass and provided with magnetic stirrers in both the liquid and the gas phase, which could be controlled independently. Both cells were equipped with PT-100 thermocouples in both the liquid and the gas phase and Heise model DXD pressure transducers (range 0 - 1.4 bar) and measured signals were recorded in a computer. Both cells were completely submerged in a waterbath thermostatted by a Julaba ED temperature control unit. This way it was ensured that both cells are subjected to exactly the same temperature. The reactor, always operated with a smooth gas-liquid interface, was connected to a calibrated gas supply vessel by means of a mass flow controller (type

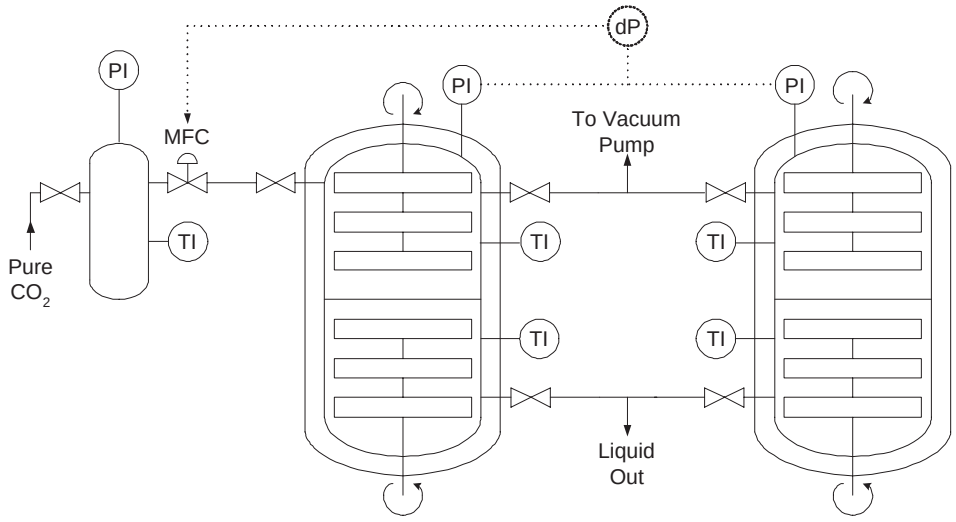

Figure 5.2: Schematic drawing of the experimental setup.

5850S, Brooks Instr.). The mass flow controller was operated automatically via the computer, where a Labview control routine was implemented to keep the actual differential pressure equal to the pre-defined set point. The gas supply vessel was also equipped with both a pressure transducer (Heise model DXD, range 0 - 10 bar) and a PT-100 thermocouple, both of which were recorded in a computer.

The choice for using two pressure transducers rather than one differential pressure transducer was based on practical considerations: The experimental window of operation was increased, without compromising the overall accuracy of the (differential) pressure measurement. Further development and optimization of the setup will include the implementation of a differential pressure transducer, which does not limit the window of operation.

In a typical experiment, an equal amount of solution was transferred to both the reactor and the reference cell, after which the liquid was degassed by applying vacuum for a short while. Next, both the reactor and the reference cell were closed, and the solution in both cells was allowed to equilibrate at the temperature set in the heat pump. Then, the CO_2 partial pressure (or the differential pressure between

the cells) was set to the desired value and the MFC was allowed to flow CO_2 into the reactor. Next, the stirrers in both the liquid and the gas phase were switched on and the pressure decrease in the gas supply vessel was recorded as a function of time. The absorption rate could then determined according to Eq. 5.10:

$$J_A = \frac{dP_{GV}}{dt} \frac{V_{GV}}{RT_{GV} A_{GL}} \tag{5.10}$$

The actual concentration of the reacting liquid phase component was determined by standard volumetric titration with 1.0 N HCl solution.

5.3 Validation of the new setup

Before the new experimental setup and procedure can be regarded as suitable for determining the kinetics of fast, unknown gas-liquid reactions, they have to be validated using a well-known reactive system. In this chapter, the kinetics of carbon dioxide in an aqueous solution of NaOH was chosen as test system. The rate determining step in this system is the reaction between CO_2 and the hydroxide ion, as given in Eq. 5.11 below:

$$CO_2 + OH^- \xrightarrow{k_2} HCO_3^- \tag{5.11}$$

This reaction is suitable for the verification of the experimental setup and procedure for two obvious reasons:

- The system has been well documented in the literature [Pinsent et al., 1951, Nijsing et al., 1959, Barrett, 1966, Pohorecki and Moniuk, 1988, Kucka et al., 2002, Haubrock et al., 2006];
- The second order kinetic rate constant of the reaction is in the order of magnitude of 10 m^3 $kmol^{-1}$ s^{-1} (at ambient temperatures) and is therewith in the same order of magnitude as expected for CO_2 with fast reacting amines like MEA and piperazine - and hence it can be qualified as a fast reaction;
- The reaction can be considered to be irreversible at typical PFO conditions.

The forward kinetic rate constant, k_2, of the reaction between CO_2 and OH^-, given above, was measured in an aqueous solution of 1.0 kmol m^{-3} NaOH (Aldrich, purity 97 %) at 298.15 and 313.15 K.

5.3.1 Experimental results

The absorption rates of CO_2 into an aqueous 1.0 kmol m^{-3} NaOH solution were measured as a function of CO_2 partial pressure and the experimentally obtained results have been listed in Table 5.2, and are shown graphically in Figures 5.3 and 5.4. The experimental error in the values in Table 5.2 are 0.1 mbar in the listed CO_2 partial pressures and estimated to be less than 2 % (by propagation of error) in the obtained absorption rates. The reproducibility of the experiments at (very) low CO_2 partial pressures amounts to 5 % at 25 $^\circ$C up to 10 % at 40 $^\circ$C.

Figures 5.3 and 5.4 show that, for both temperatures, initially a linear relation exists between the experimental absorption rate and the CO_2 partial pressure. Also included in the plots are the (calculated) ratios between the infinite enhancement factor E_{inf} and the Hatta number as an indication as to where criterion 5.7 has been satisfied. It is clear from these E_{inf}:Ha ratios, that the pseudo first order criteria were obeyed at the conditions used to determine the PFO slope in the graphs (see also Table 5.3). Therefore, the kinetic rate constants k_2 can be determined from the initial slopes of the graph (see also Sections 4.3 and 4.5.1). Further details concerning the calculation of the required physical properties are given below, and the final results of the kinetic rate constant calculations have been listed in Table 5.3. Details on the obtained Hatta numbers and the OH^- diffusion coefficient necessary in the calculation of E_{inf} - used in the ratio plotted in Figures 5.3 and 5.4 - are listed in Table 5.4.

Table 5.2: Flux of CO_2 into an aqueous 1.0 kmol m^{-3} solution at 298.15 and 313.15 K.

$T = 298.15$ K		$T = 313.15$ K	
P_{CO2} [mbar]	Flux [10^{-3} mol m^{-2} s^{-1}]	P_{CO2} [mbar]	Flux [10^{-3} mol m^{-2} s^{-1}]
1.48	0.166	1.91	0.245
1.92	0.218	1.92	0.265
1.92	0.209	2.01	0.277
2.31	0.239	2.04	0.292
2.48	0.243	2.30	0.359
2.91	0.292	2.33	0.329
3.88	0.421	3.00	0.374
4.57	0.446	3.39	0.428
4.57	0.490	3.89	0.490
4.75	0.462	3.98	0.482
4.82	0.520	4.89	0.599
6.86	0.644	4.96	0.664
6.89	0.639	10.00	1.124
9.82	0.886	10.40	1.203
10.21	0.916	13.53	1.530
10.83	0.891	13.76	1.515
12.83	1.159	13.91	1.510
13.29	1.169	14.74	1.684
16.26	1.382		
19.83	1.624		
19.85	1.575		

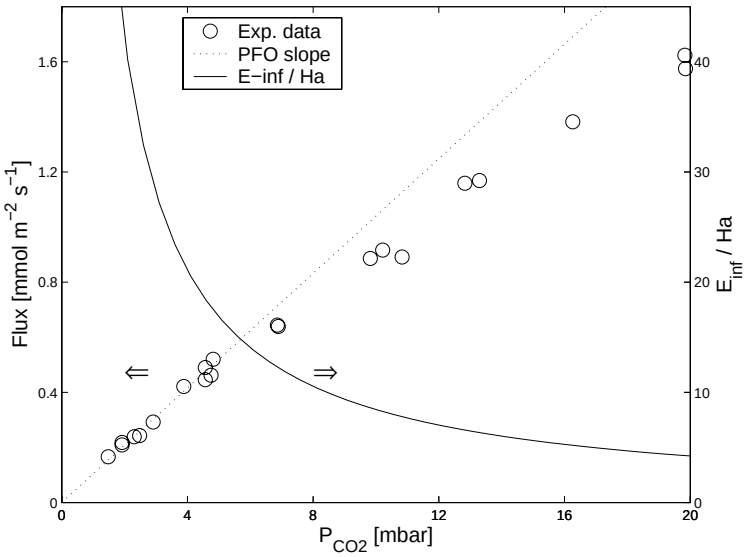

Figure 5.3: The experimentally observed flux as a function of CO_2 partial pressure at 25 ° C.

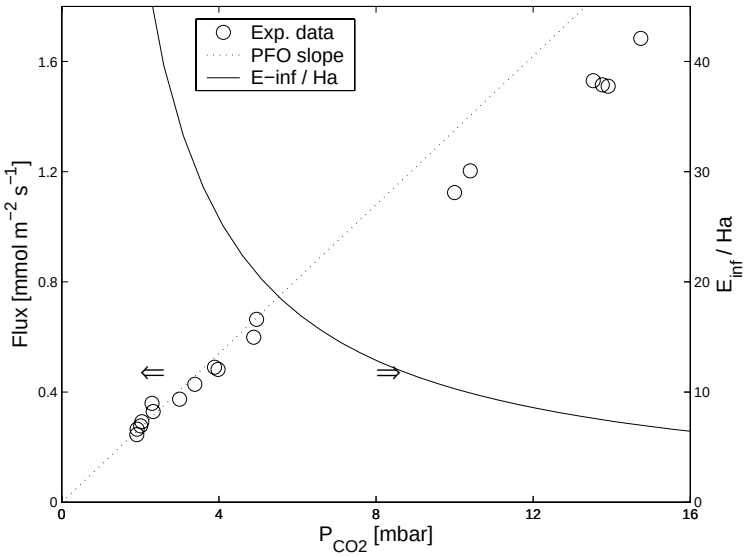

Figure 5.4: The experimentally observed flux as a function of CO_2 partial pressure at 40 ° C.

Table 5.3: Kinetic data for the reaction of CO_2 with NaOH in aqueous solutions.

T [K]	Conc [kmol m^{-3}]	N	slope[a] [mmol m^{-2} s^{-1} mbar^{-1}]	m_{CO2}	D_{CO2} [10^{-9} m^2 s^{-1}]	k_2 [m^3 kmol^{-1} s^{-1}]
298.15	1.0	11	0.104 ± 0.006[b]	0.607	1.62	11.0 ± 1.5
313.15	1.0	10	0.135 ± 0.009	0.467	2.27	25.0 ± 3.0

[a]Slope of the curve shown in Figures 5.3 and 5.4
[b]Standard deviation in slope

Table 5.4: Data used in the calculation of the E_{inf}:Ha ratio in Figures 5.3 and 5.4.

T [K]	k_L [10^{-9} m s^{-1}]	Ha	D_{OH}[a] [10^{-9} m^2 s^{-1}]
298.15	1.35	313	2.71
313.15	2.15	350	3.79

[a]The diffusion coefficients of OH^- were estimated to be a factor 1.67 larger than D_{CO2}, following the work of Nijsing et al. [1959].

The distribution coefficient m, needed in the calculation of the kinetic rate constant, was corrected for the NaOH concentration using the correction from Barrett [1966]:

$$\log \frac{m}{m_w} = -(h_+ + h_- + h_g) \cdot I \tag{5.12}$$

where I is the ionic strength of the solution and the values of h_+, h_- and h_g were taken from Barrett [1966] and listed in Table 5.5. The distribution coefficient of CO_2 in pure water was taken from the correlation proposed by Versteeg and Van Swaaij [1988b].

The diffusion coefficient of CO_2 in aqueous NaOH was calculated from the solution's viscosity, μ, according to the modified Stokes-Einstein equation proposed by Nijsing et al. [1959]:

$$\frac{D}{D_w} = \left(\frac{\mu}{\mu_w}\right)^{-0.85} \tag{5.13}$$

The CO_2 diffusion coefficient in water was calculated using the correlation proposed by Versteeg and Van Swaaij [1988b], the viscosity of the NaOH solution at 25 °C was taken from Sipos et al. [2001], while the viscosity at 40 °C was taken from Hitchcock and McIlhenny [1935].

Table 5.5: Contributions in Eq. 5.12, taken from Barrett [1966].

Parameter	species	value [m^3 / kmol]
h_+	Na^+	0.091
h_-	OH^-	0.066
h_g ($T = 25$ °C)	CO_2	-0.019
h_g ($T = 40$ °C)	CO_2	-0.026

5.3.2 Comparison with literature

The presently obtained kinetic rate constants (Table 5.3) are compared to those reported in the literature in Table 5.6.

Table 5.6: Reported forward kinetic rate constants k_2 (in m^3 kmol^{-1} s^{-1}) for an aqueous 1.0 kmol m^{-3} NaOH solution.

Source	Contactor type	k_2 ($T = 25$ °C)	k_2 ($T = 40$ °C)
Pohorecki and Moniuk [1988]	laminar jet	12.9	31.1
Kucka et al. [2002]	stirred cell	9.2	26.5
Haubrock et al. [2006]	stirred cell	14.0	-
Present work	double stirred cell	11.0	25.0

From the results listed in Table 5.6, it may be concluded that the present kinetic rate constants are in good agreement with the values reported in the literature. The presently obtained value at 25 °C is somewhat lower than the constants reported by Pohorecki and Moniuk [1988] and Haubrock et al. [2006], while it exceeds the kinetic constant reported by Kucka et al. [2002]. At 40 °C, the present value is essentially equal to the rate constant reported by Kucka et al. [2002], and about 20 % lower than the value reported by Pohorecki and Moniuk [1988]. Taking

the E_{inf}:Ha ratios in Figures 5.3 and 5.3 into account, it can be concluded that PFO conditions were obeyed in this work.

5.4 Conclusions

In this chapter, a new mode of operation for the conventional stirred cell gas-liquid contactor is proposed that theoretically allows for absorption experiments at (very) low (CO_2) partial pressures, required for the experimental determination of fast gas-liquid reactions (in the pseudo first order regime).

Hereto, a second stirred cell is added to the conventional stirred cell experimental setup (see e.g. Chapter 4). This second cell is filled with a solution identical to the one in the 'reactor cell' and hence it can serve as a reference for the vapor pressure in this reactor cell. Consequently, in case only one reactive gas is present in the reactor cell, the pressure difference between the two cells is, in fact, the partial pressure of the gas phase reactant in the reactor cell.

This new mode of operation was experimentally validated with the well-documented CO_2 - OH^- reaction (in aqueous NaOH solutions) at 25 and 40 $^\circ$C. It was shown that absorption experiments could be carried out at low CO_2 partial pressures (down to 1.5 mbar), while maintaining the reproducibility and the accuracy in the measurements. The forward second order kinetic rate constants, deduced from the experimental data taken at very low partial pressures, were found to be in good agreement with the values reported literature. More extensive experiments at different conditions (e.g. applying higher NaOH concentrations and/or the - faster absorbing - KOH salt) are recommended for a more thorough validation of the new setup.

In addition to the absorption rate experiments, the main focus of this chapter, it should be noted that the currently proposed configuration of the stirred cell setup may also be suitable for obtaining vapor-liquid equilibrium data (see Chapters

7 and 8) at low (CO_2) partial pressures (down to 1.0 mbar).

Acknowledgements

The author would like to thank H.F.G. Moed for the construction of the experimental setup, B. Knaken is acknowledged for the technical assistance, and N. Aldenkamp is acknowledged for his part in the experimental work.

Chapter 6

Absorption of Carbon Dioxide into Aqueous Solutions of MDEA and Piperazine

Abstract

In this chapter, experimental data are presented on the rate of absorption of CO_2 into aqueous solutions containing a mixture of piperazine and MDEA, the so-called activated MDEA solvent. The absorption experiments are carried out in a stirred cell contactor, operated with a flat gas-liquid interface. Carbon dioxide fluxes have been determined in aqueous solutions containing 4.0 kmol m^{-3} MDEA, activated with either 0.5 or 1.0 kmol m^{-3} PZ (resulting in a total amine concentration of 4.5 or 5.0 kmol m^{-3}), at various carbon dioxide loadings and partial pressures and at 298 K. A mass transfer model, based on the kinetics of the individual components PZ and MDEA with CO_2, was used to predict the experimentally observed absorption rates without the need for any additional fit parameters. The theoretical absorption model was able to describe the experimental results with reasonable accuracy at low carbon dioxide loadings. Experimental data at higher loadings, however, were increasingly underpredicted by the model. This is likely due to the non-ideality of the liquid phase, which was not taken into account in the calculation of the

equilibrium composition.

6.1 Introduction

The removal of carbon dioxide from gas streams has been an important process in industry for many years due to a number of different reasons, such as e.g. corrosion, catalyst poisoning as well as pipeline capacity issues. Also, the recent ratification of the Kyoto protocol has led to increasing investments in research and development in the field of carbon dioxide capture. Usually, the selective or bulk removal of CO_2 is achieved by absorption in (aqueous) solvents containing (blends of) (alkanol)amines, the composition depending on the process requirements [Kohl and Nielsen, 1997]. One very attractive solvent seems a blend of piperazine (PZ) and N-methyldiethanolamine (MDEA) in water (the so-called 'activated' MDEA solvent [Appl et al., 1982]. The principle of such a blend of a tertiary amine and a primary or secondary amine is based on the combination of the specific advantageous properties of the individual components: The rate of absorption in the absorber column is enhanced via the high rate of reaction of piperazine with CO_2, while a low heat of regeneration in the stripper section is maintained, stemming from the relatively low heat of reaction of MDEA with CO_2.

An accurate design of both the absorption and the desorption column requires detailed information on the thermodynamics of the system on one hand, and mass transfer characteristics and the liquid phase reaction rates involving CO_2 on the other hand. In spite of the recent growth of interest on these PZ activated MDEA solvents, there is only a limited set of experimental data available in the literature on the rate of absorption of CO_2 into these blends.

Xu et al. [1992] used a disk column to determine experimental absorption rates of pure carbon dioxide into aqueous MDEA solutions (1.75 - 4.28 kmol m^{-3}) containing relatively small amounts of piperazine ($\leqq$ 0.021 kmol m^{-3}, and hence below 1 %) at near atmospheric pressure. Bishnoi and Rochelle [2002a] reported

experimental absorption rates in a wetted-wall column. They performed absorption experiments into solutions typically containing 4.0 kmol m^{-3} MDEA and 0.6 kmol m^{-3} PZ, at different temperatures, CO_2 liquid loadings and partial pressures.

In this chapter, new experimental data are presented on the rate of absorption of CO_2 into aqueous solutions containing both piperazine and MDEA. The absorption experiments have been carried out in a stirred cell contactor, operated with a flat gas-liquid interface. Carbon dioxide fluxes have been determined in 4.0 kmol m^{-3} MDEA solutions activated with either 0.5 or 1.0 kmol m^{-3} PZ (resulting in a total amine concentration of 4.5 or 5.0 kmol m^{-3}), at various carbon dioxide loadings and partial pressures. Although the experimental conditions are not fully comparable to the ones in industrial applications, the setup is very well suited for the present purpose; to obtain better insights in the basic working principle of mixed amine solutions. The new experimental data will be compared to predictions made with a rigorous mass transfer model. Depending on the agreement between experiment and model, conclusions will be presented concerning the mechanism of absorption.

6.2 Reactions and mass transfer model

6.2.1 Reactions

During the absorption of carbon dioxide into aqueous solutions containing piperazine and MDEA, several reactions take place. These reactions can be divided into two groups, namely those with finite reaction rates and the reactions that can be assumed to be at equilibrium. The former group include the reactions of the various bases present in solution with CO_2:
There is the reaction between CO_2 and the tertiary amine MDEA, which takes place according to a base catalyzed hydration reaction:

$$CO_2 + MDEA + H_2O \overset{k_{MDEA}}{\longleftrightarrow} MDEAH^+ + HCO_3^- \tag{6.1}$$

Carbon dioxide can react with the hydroxide ions present in the solution:

$$CO_2 + OH^- \overset{k_{OH}}{\longleftrightarrow} HCO_3^- \tag{6.2}$$

Also, piperazine reacts with CO_2 to form a carbamate, according to the following overall kinetic equation [Bishnoi and Rochelle, 2000]:

$$CO_2 + 2PZ \overset{k_{PZ}}{\longleftrightarrow} PZCOO^- + PZH^+ \tag{6.3}$$

Furthermore, the PZ carbamate ion and even the protonated piperazine species are able to react with CO_2 (see e.g. Bishnoi and Rochelle [2000], Ermatchkov et al. [2002] and Chapter 4:

$$CO_2 + PZCOO^- + B \longleftrightarrow PZ(COO^-)_2 + BH^+ \tag{6.4}$$

$$CO_2 + PZH^+ + B \longleftrightarrow H^+PZCOO^- + BH^+ \tag{6.5}$$

where B can be any base present in solution (such as e.g. MDEA, PZ and OH^-).

The second group of reactions consists of the equilibrium reactions involving only a proton transfer, and can therefore be considered to be instantaneously fast:

$$MDEA + H_3O^+ \longleftrightarrow MDEAH^+ + H_2O \tag{6.6}$$

$$OH^- + H_3O^+ \longleftrightarrow 2H_2O \tag{6.7}$$

$$CO_3^{2-} + H_3O^+ \longleftrightarrow HCO_3^- + H_2O \tag{6.8}$$

$$PZ + H_3O^+ \longleftrightarrow PZH^+ + H_2O \tag{6.9}$$

$$PZCOO^- + H_3O^+ \longleftrightarrow H^+PZCOO^- + H_2O \tag{6.10}$$

$$PZH^+ + H_3O^+ \longleftrightarrow PZH_2^{2+} + H_2O \tag{6.11}$$

In this chapter all species listed in the reactions above were taken into account, with the exception of diprotonated and dicarbamated piperazine as well as protonated PZ carbamate. Consequently, the reactions involving these components (Eqs. 6.4, 6.5, 6.10 and 6.11) were not included in the numerical mass transfer model used in this chapter.

6.2.2 Partial differential equations

The mass transfer model describing the complete process of diffusion and reaction consists of partial differential equations formulated according to Eq. 6.12 for each individual component i present in the model:

$$\frac{dC_i}{dt} = D_i \frac{d^2C_i}{dx^2} + \sum \nu_i R_i \tag{6.12}$$

in which R_i is any reaction in which species i takes place, multiplied with the corresponding stoichiometric factor ν_i. Both finite and instantaneous reactions are numerically treated as reversible reactions with finite rate, in which the reverse reaction rate constant is calculated using the equilibrium constant of the corresponding reaction. The presence of multiple equilibrium constants within one rate equation is caused by the fact that the actual reaction rate is the product of several more elementary reactions. All required equilibrium constants appearing in the rate equations are to be defined later on in this section.

The kinetic rate equations of the finite reactions (Eqs. 6.1 - 6.3) are then given by Eqs. 6.13 - 6.15.

$$R_1 = k_{MDEA}\left(C_{MDEA}C_{CO_2} - \frac{K_{MDEA}C_{H_2O}}{K_{HCO3}K_{H2O}}C_{MDEAH^+}C_{HCO_3^-}\right) \tag{6.13}$$

$$R_2 = k_{OH}\left(C_{OH^-}C_{CO_2} - \frac{C_{HCO_3^-}}{K_{HCO3}}\right) \tag{6.14}$$

$$R_3 = k_{PZ}\left(C_{PZ}C_{CO_2} - \frac{K_{PZCOO}K_{PZ}}{K_{HCO3}K_{H2O}C_{PZ}}C_{PZH^+}C_{PZCOO^-}\right) \tag{6.15}$$

The equilibrium reactions are described in a similar manner, but with an extremely large kinetic rate constant k_{inf} as illustrated below for reaction Eq. 6.6:

$$R_6 = k_{\text{inf}}\left(C_{MDEA}C_{H_3O^+} - K_{EQ}C_{MDEAH^+}C_{H_2O}\right) \tag{6.16}$$

By defining all reactions in this manner, it is automatically assumed that at equilibrium, the total net reaction rate is zero, as the backward reaction rate is then equal to the forward reaction rate:

$$R_x = 0 = R_{\rightarrow} - R_{\leftarrow} \tag{6.17}$$

The total set of equations above build a system of 11 non-linear PDEs, which - together with well-defined boundary and initial conditions - is to be solved for all 11 components.

6.2.3 Boundary and initial conditions

At the gas-liquid interface ($x = 0$), the fluxes of the non-volatile components are set equal to zero, which implies the following set of boundary conditions:
At $x = 0$, $t > 0$:

$$\frac{dC_i}{dx} = 0 \tag{6.18}$$

As for carbon dioxide, the volatile species in the system, the boundary condition defined in Eq. 6.19 applies, as the experiments in this chapter were carried out using pure CO_2.
At $x = 0$, $t > 0$:

$$C_{CO_2} = \frac{m_{CO_2} P_{CO_2}}{RT} \tag{6.19}$$

At the liquid bulk ($x = \infty$), the concentrations of all species are set equal to the equilibrium bulk composition. The same applies for the initial condition:
At $x = \infty$, $t > 0$:

$$C_i = C_{EQ} \tag{6.20}$$

At $t = 0$, $0 \leqq x \leqq \infty$:

$$C_i = C_{eq} \tag{6.21}$$

6.2.4 Bulk concentrations

The liquid bulk composition at any given loading, amine concentration and temperature is calculated from the MDEA, the PZ and the water/hydrogen balance (Eq 6.22 - 6.24), the carbon dioxide balance (Eq. 6.25) and the electro-neutrality condition (Eq. 6.26) combined with the remaining six independent chemical equilibria present in the model.

$$C_{MDEA} + C_{MDEAH^+} = C_{MDEA,0} \tag{6.22}$$

$$C_{PZ} + C_{PZH^+} + C_{PZCOO^-} = C_{PZ,0} \tag{6.23}$$

$$C_{H_2O} + C_{H_3O^+} + C_{OH^-} + C_{HCO_3^-} + C_{PZH^+} + C_{MDEAH^+} = C_{H_2O,0} \tag{6.24}$$

$$\alpha_{CO_2}\left(C_{PZ} + C_{PZH^+} + C_{PZCOO^-} + C_{MDEA} + C_{MDEAH^+}\right) = C_{CO_2} + C_{HCO_3^-} + C_{CO_3^{2-}} + C_{PZCOO^-} \tag{6.25}$$

$$C_{PZH^+} + C_{MDEAH^+} + C_{H_3O^+} = C_{OH^-} + C_{HCO_3^-} + 2C_{CO_3^{2-}} + C_{PZCOO^-} \tag{6.26}$$

$$K_{H_2O} = \frac{C_{OH^-} C_{H_3O^+}}{C_{H_2O} C_{H_2O}} \tag{6.27}$$

$$K_{HCO_3^-} = \frac{C_{HCO_3^-}}{C_{OH^-} C_{CO_2}} \tag{6.28}$$

$$K_{CO_3^{2-}} = \frac{C_{OH^-} C_{HCO_3^-}}{C_{CO_3^{2-}} C_{H_2O}} \tag{6.29}$$

$$K_{PZCOO^-} = \frac{C_{PZ} C_{HCO_3^-}}{C_{PZCOO^-} C_{H_2O}} \tag{6.30}$$

$$K_{PZ} = \frac{C_{PZ} C_{H_3O^+}}{C_{PZH^+} C_{H_2O}} \tag{6.31}$$

$$K_{MDEA} = \frac{C_{MDEA} C_{H_3O^+}}{C_{MDEAH^+} C_{H_2O}} \tag{6.32}$$

This results in a system of 11 equations to be solved for the 11 unknown concentrations of the species present in the bulk of the liquid. It should be noted that in this chapter the system's non-ideality has not been taken into account in the calculation of the liquid bulk (equilibrium) speciation.

6.2.5 Numerical treatment and flux calculation

The system of partial differential equations as defined above in Eqs. 6.12 - 6.32 was solved numerically using the discretization schemes and numerical methods originally suggested by Versteeg et al. [1989]. The numerical model was essentially identical to the one used by Littel et al. [1991] in the modelling of simultaneous absorption of H_2S and CO_2 in mixed amine solutions. Therefore, for further information on the numerical treatment, the reader is referred to Versteeg et al. [1989] and Littel et al. [1991].

The CO_2 flux was calculated according to Eq. 6.33 below:

$$J_{CO_2} = \frac{1}{\tau} \sum_{N} \left. \frac{\partial C_{CO_2}(t)}{\partial x} \right|_{x=0} \Delta t \qquad \text{with} \qquad \tau = \frac{4\pi D_{CO_2}}{k_L^2} \tag{6.33}$$

The numerical model was extensively validated using various analytical approximation methods [Versteeg et al., 1989] before it was applied in a study on absorption rates into mixed amine solutions [Versteeg et al., 1990, e.g.]. Therefore, the numerical model itself can be regarded reliable and suitable for this study.

6.2.6 Constants and physical properties

The simulation model requires several physical properties as well as kinetic and equilibrium constants, all of which have been listed in Table 6.1 for the two experimental series to be studied in this chapter.

Table 6.1: Conditions, properties and constants used in the numerical model.

		Series 1	Series 2		Source[a]
General conditions					
MDEA concentration	C_{MDEA}	4.0		kmol m^{-3}	
PZ concentration	C_{PZ}	0.5	1.0	kmol m^{-3}	
Temperature	T	298.15		K	
Mass transfer coeff.	k_L	0.45	0.36	$\cdot 10^{-5}$ m s^{-1}	A
Physical properties					
Distribution coeff. CO_2	m	0.62	0.61		A
Viscosity	μ	10.2	15.1	mPa s	Chapter 3
Diffusion coeff. CO_2	D_{CO2}	0.48	0.39	$\cdot 10^{-9}$ m^2 s^{-1}	B
Diffusion coeff. MDEA	D_{MDEA}	0.215	0.182	$\cdot 10^{-9}$ m^2 s^{-1}	Chapter 3
Diffusion coeff. PZ	D_{PZ}	0.228	0.199	$\cdot 10^{-9}$ m^2 s^{-1}	Chapter 3
Diffusion coeff. ions	D_{ION}	0.22	0.19	$\cdot 10^{-9}$ m^2 s^{-1}	B

Table is continued on next page

[a] A and B refer to the remarks summed up below the table.

Table 6.1 continued

		Series 1	Series 2		Source
Equilibrium constants					
Water dissociation	K_{H_2O}	$3.3 \cdot 10^{-9}$			P&R[a]
Bicarbonate formation	$K_{HCO_3^-}$	$4.4 \cdot 10^{4}$		$m^3\ mol^{-1}$	P&R
Carbonate formation	$K_{CO_3^{2-}}$	$3.9 \cdot 10^{-6}$			P&R
MDEA protonation	K_{MDEA}	$5.1 \cdot 10^{-11}$			P-S K.[b]
PZ protonation	K_{PZ}	$3.3 \cdot 10^{-12}$			Hetzer et al. [1967]
Carbamate hydrolysis	K_{PZCOO^-}	$5.5 \cdot 10^{-4}$			Ermatchkov et al. [2002]
Kinetic rate constants					
CO_2 + MDEA	k_{MDEA}	$5.3 \cdot 10^{-3}$		$m^3\ kmol^{-1}\ s^{-1}$	Littel et al. [1990b]
CO_2 + OH^-	k_{OH}	8.4		$m^3\ kmol^{-1}\ s^{-1}$	Pinsent et al. [1951]
CO_2 + PZ	k_{PZ}	76		$m^3\ kmol^{-1}\ s^{-1}$	Chapter 4
Equilibrium reactions	k_{inf}	10^{15}		$m^3\ kmol^{-1}\ s^{-1}$	

[a] P&R denotes Posey and Rochelle [1997].
[b] P-S K. denotes Pérez-Salado Kamps and Maurer [1996].

A. The liquid side mass transfer coefficient and the distribution coefficient
Both these properties have been determined indirectly with the use of N_2O as model component in the experiments. The CO_2:N_2O analogy has been applied to convert the obtained experimental data to the listed (carbon dioxide) values.

B. The diffusion coefficients of carbon dioxide and ions
Pacheco [1998] presented a modified Stokes-Einstein equation to estimate the diffusivity of N_2O in (alkanol)amine solutions as a function of temperature and viscosity:

$$D_{N2O} = 5.33 \cdot 10^{-12} \frac{T}{\mu^{0.545}} \tag{6.34}$$

The solution viscosities were taken from Chapter 3, and the resulting N_2O diffusion coefficients were converted to the corresponding CO_2 diffusivities using the CO_2:N_2O analogy.
All ion diffusion coefficients were assumed equal and calculated as the concentration

based average of the diffusion coefficients of molecular MDEA and piperazine, which were taken from Chapter 3.

6.3 Experimental

In the absorption experiments, a stirred cell reactor operated with a smooth and horizontal gas-liquid interface was used. The reactor consisted of glass, was thermostatted and it was provided with magnetic stirrers in the gas and liquid phase, which could be controlled independently. The reactor was connected to a calibrated gas supply vessel via a Brooks type 5866 pressure controller. Both the reactor and the gas supply vessel were equipped with PT-100 thermocouples and digital pressure transducers and measured signals were recorded in the computer. Two pressure transducers were connected to the stirred cell, namely a Druck DPI 260 (range 0 to 199.99 mbar) and a Druck DPI 267 for the experiments conducted at higher pressures. The gas supply vessel was equipped with a PDCR 910 (range 0 - 5 bar), also obtained from Druck.

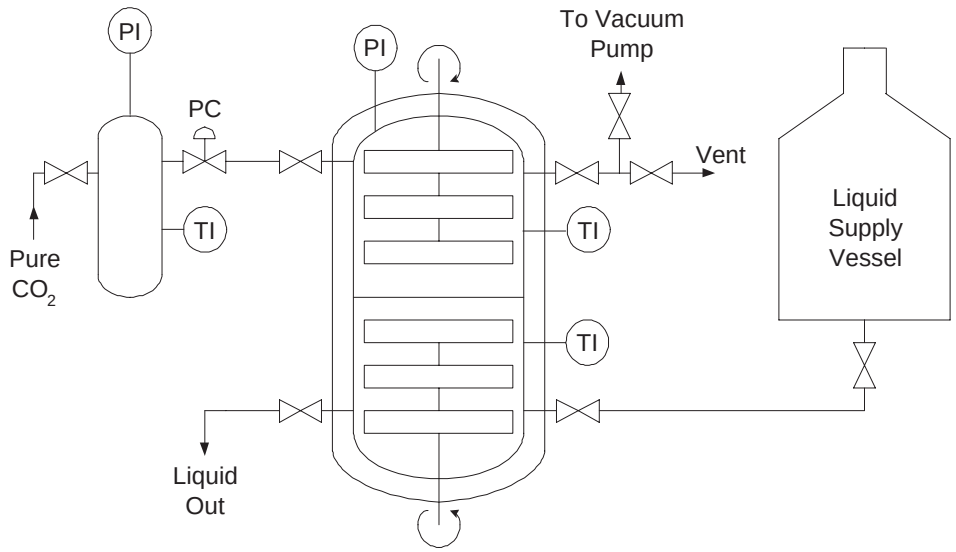

Figure 6.1: Schematic diagram of the experimental setup.

In a typical experiment, sufficient amounts of MDEA (99 %, Aldrich) and piperazine (99 %, Aldrich) were dissolved in water to obtain the desired concen-

tration of both amines. Next, a desired amount of solution (typically about 0.7 L) was charged into the reactor, where it was degassed by applying vacuum for a short while. After the vapor-liquid equilibrium was established, the solution's vapor pressure was noted down. Now, pure carbon dioxide was added from the gas vessel to preload the solution to the intended level. The actual CO_2 content of the solution was calculated according to Eq. 6.35 from the difference in the gas vessel pressure before and after the preloading:

$$\alpha_{CO_2} = \frac{1}{V_L \left(C_{MDEA} + C_{PZ}\right)} \frac{\Delta P_{GV} V_{GV}}{R T_{GV}} \tag{6.35}$$

After the preloading procedure, the solution was allowed to stir overnight to ensure equilibrium was obtained. Next, the pressure controller was set to the desired set point and, consecutively, the valve between the gas supply vessel and the stirred cell reactor was opened, and the absorption rate was determined from the pressure decrease in the gas supply vessel in time, according to Eq. 6.36:

$$J_{CO_2} \cdot A_{GL} = \frac{V_{GV}}{R T_{GV}} \frac{dP_{GV}}{dt} \tag{6.36}$$

The actual absorption rate measurement took about five minutes, after which the valve between reactor and gas supply vessel was closed and then the liquid was allowed to equilibrate for about 30-45 minutes. Next, a new run could be started with a higher CO_2 partial pressure. Introductory experiments showed that this equilibration time between the different experimental runs was sufficiently large. In the present study, absorption experiments were carried out with solutions containing 4.0 kmol m^{-3} MDEA activated with either 0.5 or 1.0 kmol m^{-3} piperazine at 298 K and a constant liquid stirrer speed. Carbon dioxide liquid loadings were varied between about 0.05 and 0.4 mole CO_2 per mole of total amine and the absorption rates were determined at CO_2 partial pressures of 20, 50, 70, 100, 250 and 400 mbar.

6.4 Results

In Tables 6.2 and 6.3 the experimental data obtained in the stirred cell setup are listed as a function of carbon dioxide liquid loading and partial pressure. The

experimental errors are estimated to be 4 % in loading, 2 % in flux and ranging from 0.2 to 2 mbar in partial pressure respectively, all by propagation of error. As can be seen from the experimental data listed in the tables, the reproducibility in the measurements is within 5 %.

Table 6.2: Experimental absorption rates into a 4.0 M MDEA / 0.5 M PZ aqueous solution.

A. Carbon Dioxide Partial Pressure ≈ 20 mbar		
CO_2 loading [mol mol^{-1}]	P_{CO2} [mbar]	Flux [$\cdot 10^{-3}$ mol m^{-2} s^{-1}]
0.039	19.5	0.693
0.039	19.9	0.707
0.041	20.1	0.682
0.100	19.6	0.426
0.100	19.6	0.379
0.100	19.9	0.396
0.150	19.9	0.221
0.151	19.6	0.218
0.190	20.1	0.046
B. Carbon Dioxide Partial Pressure ≈ 50 mbar		
CO_2 loading [mol mol^{-1}]	P_{CO2} [mbar]	Flux [$\cdot 10^{-3}$ mol m^{-2} s^{-1}]
0.040	50.2	1.05
0.040	49.9	1.04
0.041	50.5	1.01
0.100	49.9	0.705
0.100	49.9	0.707
0.100	50.1	0.719
0.150	50.1	0.472
0.151	50.0	0.489

Table is continued on next page

Table 6.2 continued

CO_2 loading [mol mol^{-1}]	P_{CO2} [mbar]	Flux [$\cdot 10^{-3}$ mol m^{-2} s^{-1}]
0.190	50.3	0.333
0.203	49.5	0.293
0.210	49.6	0.265
0.300	50.7	0.031
0.300	49.9	0.030
C. Carbon Dioxide Partial Pressure ≈ 70 mbar		
CO_2 loading [mol mol^{-1}]	P_{CO2} [mbar]	Flux [$\cdot 10^{-3}$ mol m^{-2} s^{-1}]
0.191	70.4	0.429
0.340	70.1	0.053
0.345	69.8	0.053
D. Carbon Dioxide Partial Pressure ≈ 100 mbar		
CO_2 loading [mol mol^{-1}]	P_{CO2} [mbar]	Flux [$\cdot 10^{-3}$ mol m^{-2} s^{-1}]
0.041	100	1.30
0.041	100	1.26
0.042	101	1.26
0.101	100	0.918
0.101	100	0.943
0.151	100	0.719
0.152	100	0.720
0.191	100	0.546
0.204	100	0.509
0.300	101	0.264
0.301	100	0.259
0.336	100	0.165
0.341	100	0.126
0.345	100	0.141

Table is continued on next page

Table 6.2 continued

E. Carbon Dioxide Partial Pressure ≈ 250 mbar		
CO_2 loading [mol mol^{-1}]	P_{CO2} [mbar]	Flux [$\cdot 10^{-3}$ mol m^{-2} s^{-1}]
0.041	254.0	1.58
0.042	253.9	1.57
0.044	254.3	1.57
0.102	253.9	1.17
0.102	253.9	1.20
0.102	253.8	1.19
0.152	254.1	1.09
0.192	254.2	0.886
0.205	253.6	0.852
0.301	255.0	0.601
0.302	253.7	0.633
0.336	252.7	0.527
0.341	253.6	0.503
0.345	253.6	0.508
F. Carbon Dioxide Partial Pressure ≈ 400 mbar		
CO_2 loading [mol mol^{-1}]	P_{CO2} [mbar]	Flux [$\cdot 10^{-3}$ mol m^{-2} s^{-1}]
0.044	404	1.76
0.044	404	1.76
0.046	404	1.73
0.104	404	1.40
0.105	404	1.48
0.105	404	1.46
0.154	404	1.24
0.155	404	1.20
0.194	404	1.06
0.207	404	1.03
0.304	405	0.804

Table is continued on next page

Table 6.2 continued

CO_2 loading [mol mol^{-1}]	P_{CO2} [mbar]	Flux [$\cdot 10^{-3}$ mol m^{-2} s^{-1}]
0.305	404	0.847
0.338	404	0.691
0.342	404	0.758
0.347	404	0.725

Table 6.3: Experimental absorption rates into a 4.0 M MDEA / 1.0 M PZ aqueous solution.

A. Carbon Dioxide Partial Pressure ≈ 20 mbar		
CO_2 loading [mol mol^{-1}]	P_{CO2} [mbar]	Flux [$\cdot 10^{-3}$ mol m^{-2} s^{-1}]
0.050	20.9	0.941
0.100	20.8	0.694
0.166	20.8	0.404
0.206	20.9	0.261
0.238	21.0	0.161
B. Carbon Dioxide Partial Pressure ≈ 50 mbar		
CO_2 loading [mol mol^{-1}]	P_{CO2} [mbar]	Flux [$\cdot 10^{-3}$ mol m^{-2} s^{-1}]
0.051	51.2	1.35
0.101	51.1	1.08
0.166	51.0	0.765
0.206	51.1	0.552
0.238	51.3	0.476
0.326	51.3	0.183

Table is continued on next page

Table 6.3 continued

C. Carbon Dioxide Partial Pressure ≈ 70 mbar		
CO_2 loading [mol mol^{-1}]	P_{CO2} [mbar]	Flux [$\cdot 10^{-3}$ mol m^{-2} s^{-1}]
0.052	71.3	1.49
0.167	71.2	0.871
0.239	71.4	0.578
0.326	71.5	0.281
D. Carbon Dioxide Partial Pressure ≈ 100 mbar		
CO_2 loading [mol mol^{-1}]	P_{CO2} [mbar]	Flux [$\cdot 10^{-3}$ mol m^{-2} s^{-1}]
0.052	101	1.56
0.101	101	1.36
0.167	101	0.999
0.207	101	0.822
0.239	101	0.722
0.326	101	0.405
E. Carbon Dioxide Partial Pressure ≈ 250 mbar		
CO_2 loading [mol mol^{-1}]	P_{CO2} [mbar]	Flux [$\cdot 10^{-3}$ mol m^{-2} s^{-1}]
0.053	255.2	1.90
0.101	255.1	1.59
0.168	255.0	1.33
0.207	255.1	1.11
0.239	255.3	0.997

Table is continued on next page

Table 6.3 continued

F. Carbon Dioxide Partial Pressure ≈ 400 mbar		
CO_2 loading [mol mol^{-1}]	P_{CO2} [mbar]	Flux [$\cdot 10^{-3}$ mol m^{-2} s^{-1}]
0.056	405	2.16
0.104	405	1.76
0.170	405	1.47
0.209	405	1.31
0.241	405	1.17
0.328	405	0.909

A graphical comparison between the experimental data listed in Tables 6.2 and 6.3, and absorption rates predicted by the numerical model is given in Figures 6.2 and 6.3.[1]

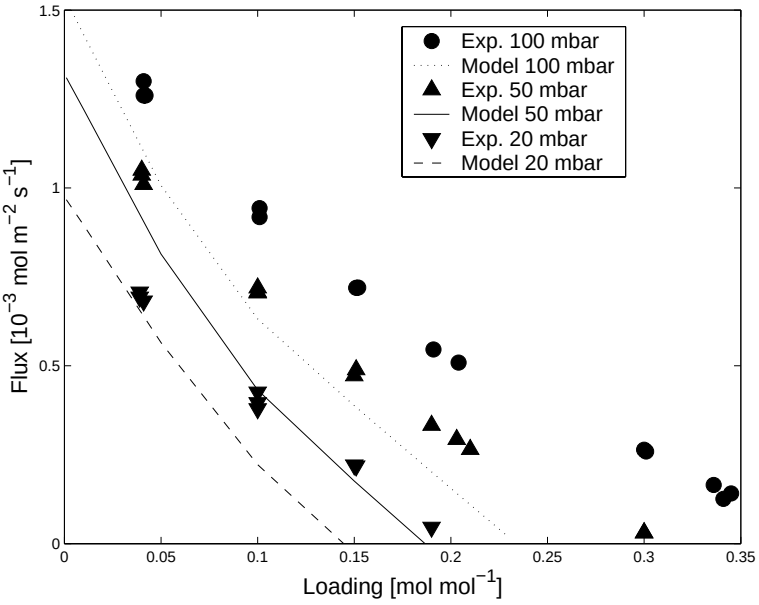

Figure 6.2: Flux prediction and experiment for 4.0 M MDEA / 0.5 M PZ at 298.15 K.

[1]Similar curves were observed for the absorption rates at CO_2 partial pressures of 70, 250 and 400 mbar.

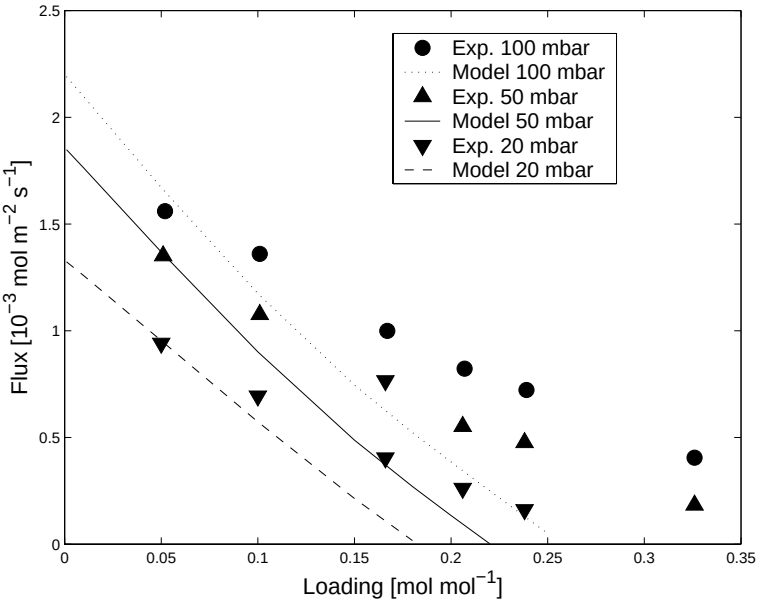

Figure 6.3: Flux prediction and experiment for 4.0 M MDEA / 1.0 M PZ at 298.15 K.

From Figures 6.2 and 6.3, three basic trends can be observed:

- At very low loadings, a very good agreement exists between model and experiment. This is illustrated with Figure 6.4, which represents a parity plot between experimental and model predicted flux at low loading ($\leqq$ 0.06 mol mol^{-1}).

- The numerical model is able to predict the influence of loading on the experimentally obtained fluxes reasonably;

- With increasing CO_2 loading, the model starts to increasingly underpredict the experimentally determined absorption rates. The parity plot shown in Figure 6.5 illustrates this for the absorption data for two carbon dioxide partial pressures in the 4.0 kmol m^{-3} MDEA / 0.5 kmol m^{-3} piperazine solution.

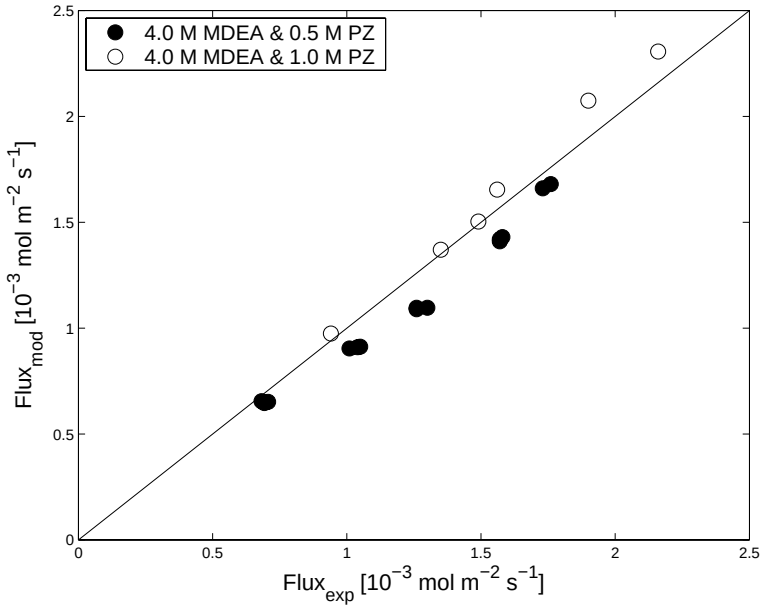

Figure 6.4: Parity plot of experimental and model predicted flux at low CO_2 loading ($\leqq$ 0.06 mol mol^{-1}).

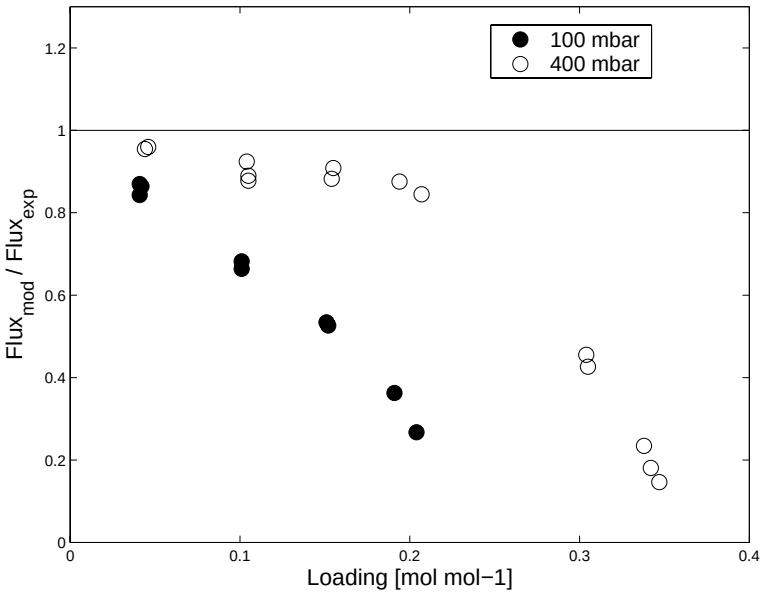

Figure 6.5: Parity plot of experimental and model predicted flux as a function of CO_2 loading for 4.0 M MDEA and 0.5 M PZ.

The explanations for these trends are:

- At very low loadings the speciation of the liquid phase composition is usually well-known and hence also the concentrations of the reactive species and the 'driving force' for mass transfer. At higher loadings, the speciation becomes less defined and basically it is impossible to calculate the concentrations of the reactive species and the CO_2 equilibrium concentration;

- Also, the model in its present form does not account for liquid phase non-ideality in the calculation of the liquid bulk composition. A thermodynamically sound model should be able to provide a more realistic liquid bulk speciation and hence more reliable initial and bulk-side boundary conditions;

- Moreover, as was shown by Haubrock et al. [2005], activity-based rate constants must be used for ionic liquids rather than concentration based data: The presently used amine solutions gradually change from an essentially non-ionic solvent to an ionic liquid at higher loading.

- The effect of loading on the physical properties, such as e.g. the distribution coefficient and the diffusion coefficients, are not known and in the simulations it is assumed that these properties remain constant, and identical to the value at zero loading.

- Finally, the reactivity of the second amine group of piperazine has not been taken into account in the model and it is likely to assume that both the reaction to form dicarbamate and the equilibrium between PZ carbamate and its protonated species play an increasingly important role with increasing loading - at least in the loading range studied in this chapter.

6.5 Conclusions

In this chapter, a stirred cell reactor was used to obtain more, additional, experimental data on the the rate of absorption of carbon dioxide into (partially) loaded

aqueous 4.0 kmol m^{-3} MDEA solutions activated with 0.5 and 1.0 kmol m^{-3} piperazine at 298.15 K. The experimentally observed absorption rates were compared to predictions made with a rigorous mass transfer model, which was based on the kinetics of the individual components PZ and MDEA with CO_2.

It was found, that the theoretical absorption model was able to describe the experimental results satisfactorily at low carbon dioxide loadings. Versteeg et al. [1990] also studied absorption rates into mixtures of alkanolamines at very low loadings and they reported similar results. The experimental data taken at higher CO_2 loadings, however, were increasingly underpredicted by the model. Possible causes are the non-ideality of the system which has not been taken into account in the calculation of the equilibrium composition, changes in physical properties with increasing loading, and the reactivity of the second amine group of piperazine which had not been taken into account in the numerical model.

Future work should therefore include the extension of the numerical model to account for the reactions involving the second amine group of piperazine to form protonated carbamate and dicarbamate. Further improvements in the model involve the incorporation of liquid phase non-ideality in the calculation of the equilibrium composition in the bulk: A thermodynamically sound equilibrium model should provide a more reliable liquid phase speciation than the one used in the present model, thus also resulting in a more accurate determination of the driving force for /CO absorption. The thermodynamics of aqueous solutions containing piperazine and/or MDEA will therefore be the focus of the next chapters.

Acknowledgements

The author would like to acknowledge H.F.G. Moed and B.C.A. van der Veer for their respective parts in the experimental work and E.P. van Elk for the numerical model.

Chapter 7

Solubility of Carbon Dioxide in Aqueous Piperazine Solutions

Abstract

In this chapter, new experimental data are presented on the solubility of carbon dioxide in aqueous piperazine solutions, for concentrations of 0.2 and 0.6 molar piperazine and temperatures of 25, 40 and 70 $^{\circ}$C. The present data, and other data available in literature, were correlated using a model based on the electrolyte equation of state (EoS), as originally proposed by Fürst and Renon [1993]. The final model derived, containing only seven adjustable (ionic) parameters, was able to describe the available experimental data (>150 data points for total and/or CO_2 partial pressure) with an average deviation of 16 %.

7.1 Introduction

The selective or bulk removal of carbon dioxide from process gas streams is an important step in many industrial processes, for a number of possible reasons. In the presence of water, CO_2 - being an acid gas - can cause corrosion to process equipment. Secondly, it reduces the heating value of a natural gas stream and wastes valuable pipeline capacity. In LNG (liquefied natural gas) plants, it should be removed to prevent freezing in the low-temperature chillers, whereas it would poison the catalyst in the manufacture of ammonia. Finally, CO_2 - being a greenhouse gas - is also held responsible for the recent climate changes. One technology used in the removal of carbon dioxide is the absorption - desorption process, in which (solutions of) alkanolamines are frequently used as solvents [Kohl and Nielsen, 1997]. Depending on the process requirements, different types and combinations of (alkanolamine based) solvents can be used.

Nowadays, the addition of an accelerator, or more specifically piperazine (PZ), to aqueous N-methyldiethanolamine (MDEA) solutions has found widespread application in the removal and absorption of carbon dioxide from process gases. The success of such a blend of a primary or secondary amine with a tertiary amine is based on the relatively high rate of reaction of CO_2 with the former combined with the low heat of reaction of CO_2 with the latter, which leads to higher rates of absorption in the absorber column and lower heats of regeneration in the stripper section. Crucial for an optimal design and operation of absorber and stripper is detailed knowledge on mass transfer and kinetics on one hand and thermodynamic equilibrium on the other hand.

The objective of this chapter is firstly to present experimental data on CO_2 equilibrium solubility in aqueous PZ solutions, which are complementary to data already available in the literature [Bishnoi and Rochelle, 2000, Pérez-Salado Kamps et al., 2003, Aroua and Mohd Salleh, 2004]. More experimental data than currently available in literature are necessary, because these published data sets are restricted to low-concentration low-pressure data on one hand and high-concentration high-

pressure on the other hand. Secondly, a thermodynamic model is described in this chapter to correlate all (reliable) experimental data.

In the literature, many thermodynamic models have been presented to describe the solubilities of acid gases like CO_2 and H_2S in (blends of) amine solutions. The applied models can be subdivided into three different approaches:

- The empirical approach as introduced by Kent and Eisenberg [1976];
- The application of an excess Gibbs energy model ('the γ-ϕ-approach'), which forms the basis for e.g. the electrolyte NRTL (Non-Random Two Liquid) model [e.g. Austgen et al., 1989] and the Clegg-Pitzer equation [e.g. Li and Mather, 1994];
- The use of an equation of state (EoS) model, which is a fairly new development, finding application in recent publications [Fürst and Planche, 1997, Kuranov et al., 1997, Vallée et al., 1999, Chunxi and Fürst, 2000, Solbraa, 2002]. Only few papers using an EoS approach have been published so far, all but one applying the electrolyte equation of state as originally proposed by citetfur93. Kuranov et al. [1997] applied the hole theory in their EoS, but they correlated a limited set of experimental data.

In this chapter, also the electrolyte EoS approach is applied, mostly based on the following considerations:

- Identical equations for gas and liquid phase;
- Relative straightforward fitting procedures of binary/ionic parameters;
- Pressure effects are taken into account;
- Possibility to extend the model to include hydrocarbons.

It must be noted, however, that some of the above-mentioned considerations also can be applicable to other models.

Recent publications have focussed on correlating CO_2 (and H_2S) solubility and partial pressure for aqueous MDEA solutions [Chunxi and Fürst, 2000, Solbraa, 2002] and DEA [Vallée et al., 1999] with results comparable to the NRTL model. Before being able to describe also the (quaternary) system MDEA - PZ - H_2O - CO_2, all (reactive) ternary subsystems need to be correlated. Therefore, this chapter will focus on the reactive subsystem PZ - H_2O - CO_2, presenting new data on the CO_2 solubility in aqueous piperazine solutions and correlating both these and other published experimental data sets with the electrolyte EoS.

7.2 Experimental

7.2.1 Experiments with diluted CO_2 using a continuous gas feed

The experimental setup and procedure are similar to those as used by Kumar et al. [2003a] and will therefore be described only briefly here. A schematic drawing of the setup is shown in Figure 7.1. For the experiments with diluted gas streams, the operation with respect to the liquid was always batch wise, while the mode with respect to gas phase was continuous. The heart of the setup consisted of a thermostatted reactor of approximately 1.6 L in volume, which was equipped with a high intensity gas-inducing impeller in the liquid phase and a propeller type impeller in the gas phase. Also, the reactor was provided with a digital pressure transducer and a thermocouple. During continuous operation with respect to the gas phase, the inlet gas flows of both N_2 and CO_2 were controlled using mass flow controllers (Brooks Instr., type 5850). Prior to entering the reactor, the desired gas flows of N_2 and CO_2 were pre-saturated with an amine solution identical to the one in the reactor and water respectively. After pre-saturation, the gas flows were mixed and fed to the bottom of the reactor using a sintered stainless steel sparger. The outlet gas flow of the reactor was continuously analyzed for CO_2 content using an IR-analyzer, type UNOR 610.

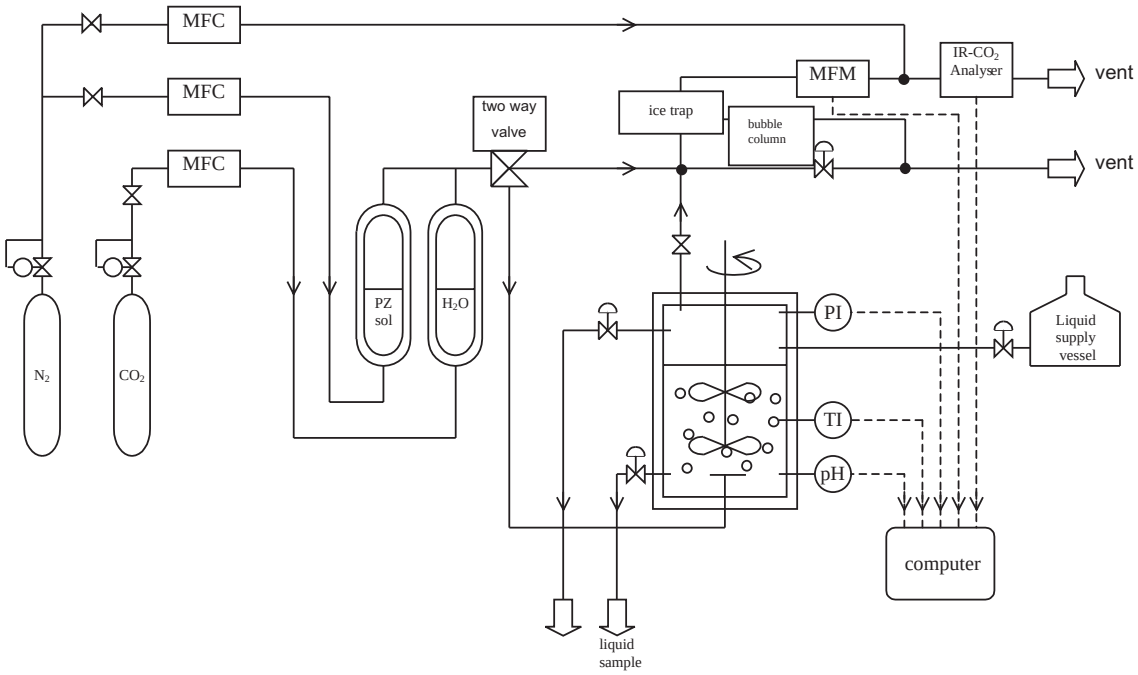

Figure 7.1: Schematic drawing of the 'continuous' setup.

In a typical experiment, a known amount of piperazine (purity 99 %, Aldrich) was dissolved in about 500 mL of water and the mass flow controllers were adjusted to obtain the desired feed flow and composition. Next, the gas was passed through the reactor and at the attainment of equilibrium (i.e. the gas inlet composition equals the outlet composition), the gas phase CO_2 content was recorded and subsequently a sample was drawn from the liquid phase. From this liquid sample both the amount of piperazine (standard potentiometric titration with 0.1 N HCl) and the total CO_2 content (desorption/titration procedure as described by Blauwhoff et al. [1984]) in the mixture were determined.

7.2.2 Experiments with pure CO_2 using the batch mode in the gas phase

Experimental data for CO_2 partial pressures exceeding 25 kPa were obtained in a second setup, which mainly consisted of a thermostatted vigorously stirred reactor

(ca. 2 L) connected to a calibrated gas vessel (see Figure 7.2). Both reactor and gas supply vessel were equipped with a temperature and pressure indicator. Also, a vacuum pump was connected to the reactor, to remove all inert gases from the setup and dissolved gases from the amine solutions prior to an experiment.

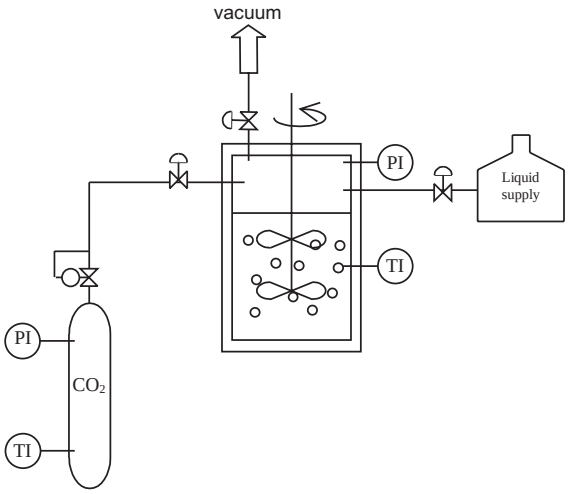

Figure 7.2: Schematic drawing of the 'batch' setup.

In a typical experiment, a known amount of piperazine solution (prepared in the same way as described in the previous section) was transferred to the reactor vessel, after which the liquid was degassed by applying vacuum for a short while. Next, the solution was allowed to equilibrate at the desired temperature and consecutively the (vapor) pressure was recorded. Then, the gas supply vessel was filled with pure carbon dioxide and the initial pressure in this vessel was measured. Next, the stirrer was switched on and a sufficient amount of CO_2 was fed from the gas supply vessel to the reactor. The gas supply to the reactor was closed and the contents of the reactor was allowed to reach equilibrium - which was reached when the reactor pressure remained constant. The actual CO_2 partial pressure could be calculated from this final (equilibrium) reactor pressure corrected for the vapor pressure of the lean solution, thereby assuming that the solution vapor pressure is not influenced by the CO_2 loading. The difference between initial and final pressure in the gas vessel was used to calculate the corresponding CO_2 loading of the solution. In some experiments, the loading was also analyzed with the technique used for the

continuous setup experiments. The actual piperazine concentration in the solutions was determined afterwards using a standard potentiometric titration with 0.1 N HCl.

Experiments have been carried out for two piperazine concentrations (0.2 and 0.6 kmol m^{-3}) at temperatures of 298, 313 and 343 K.

7.3 Theoretical background

7.3.1 Chemical equilibrium

As the process is chemical absorption of carbon dioxide, several chemical equilibria have to be taken into account in the modelling, considering both acid-base as well as (di)carbamate formation/hydrolysis reactions:

Water dissociation: $2H_2O \overset{K_I}{\leftrightarrows} OH^- + H_3O^+$

Bicarbonate formation: $2H_2O + CO_2 \overset{K_{II}}{\leftrightarrows} HCO_3^- + H_3O^+$

Carbonate formation: $H_2O + HCO_3^- \overset{K_{IIb}}{\leftrightarrows} CO_3^{2-} + H_3O^+$

Piperazine protonation: $H_2O + PZH^+ \overset{K_{III}}{\leftrightarrows} PZ + H_3O^+$

Piperazine diprotonation: $H_2O + PZH_2^{2+} \overset{K_{IIIb}}{\leftrightarrows} PZH^+ + H_3O^+$

Hydrolysis of piperazine mono-carbamate: $PZ + HCO_3^- \overset{K_{IV}}{\leftrightarrows} H_2O + PZCOO^-$

Hydrolysis of piperazine di-carbamate: $PZCOO^- + HCO_3^- \overset{K_V}{\leftrightarrows} H_2O + PZ(COO^-)_2$

Monocarbamate protonation: $H_2O +^+ HPZCOO^- \overset{K_V I}{\leftrightarrows} PZCOO^- + H_3O^+$

All equilibria involving carbamated piperazine species (K_{IV}, K_V and K_{VI}) have been identified and quantified by Bishnoi and Rochelle [2000] and Ermatchkov et al. [2002]. The equilibrium constants of the latter have been used in the present work (see Table 7.1), since they have been measured over a larger temperature interval. In order to reduce the number of species in the model, three assumptions have been made:

- The first one concerns the concentration of the carbonate ion, which is assumed to be negligible, considering the pH range of interest and the equilibrium constant for this reaction (see also Table 7.1). The same assumption was made by e.g. Chunxi and Fürst [2000], Solbraa [2002] in their modelling of the CO_2 solubility in aqueous MDEA.

- Secondly, it is common to neglect the mole fractions of both OH^- and H_3O^+ in the modelling of acid gas equilibria in e.g. MDEA solutions [Chunxi and Fürst, 2000, Solbraa, 2002] and, partially, this has also been assumed in the present work. This assumption can be justified by the fact that on the one hand amines like piperazine are weak bases, whereas on the other hand acid gases like CO_2 are weak acids in water. In the current model, only the H_3O^+ fraction has been neglected. Since PZ is a stronger base than MDEA, the OH^- fraction could play a minor role (only at low carbon dioxide loading). The neglecting of H_3O^+ ions has been validated in initial model simulations; its fraction never exceeded the value 10^{-7}.

- The third simplification involves the neglecting of diprotonated piperazine (PZH_2^{2+}). This assumption is based on the second pKa of piperazine, which is e.g. 5.3 at 298 K and therefore too low to be of relevance in the current model and the pH range of interest [Bishnoi and Rochelle, 2000].

With these assumptions, the model is reduced to a system of nine species [namely H_2O, OH^-, CO_2, HCO_3^-, PZ, PZH^+, $PZCOO^-$, $PZ(COO^-)_2$ and $^+HPZCOO^-$], to be solved with five independent equilibrium constants, the total mass balance, total piperazine and carbon dioxide balances and the electroneutrality condition.

Table 7.1: Coefficients for the chemical equilibrium constants used in the model.

	C_0	C_1	C_2	C_3	$K_{T=313K}$	T, [$^\circ$C]	Source
K_I	132.899	-13445.9	-22.4773	0	$9.3{\cdot}10^{-18}$	0 - 225	P&R[a]
K_{II}	231.465	-12092.1	-36.7816	0	$9.0{\cdot}10^{-9}$	0 - 225	P&R
K_{IIb}	216.049	-12431.7	-35.4819	0	$1.1{\cdot}10^{-12}$	0 - 225	P&R
K_{III}	18.135	3814.4	0	-0.015096	$1.3{\cdot}10^{11}$	0 - 50	Hetzer et al. [1967]
K_{IIIb}	14.134	2192.3	0	-0.017396	$6.5{\cdot}10^{6}$	0 - 50	Hetzer et al. [1967]
K_{IV}	-4.6185	3616.1	0	0	$1.0{\cdot}10^{3}$	0 - 60	Erm[b]
K_V	0.36150	1322.3	0	0	98.1	0 - 60	Erm
K_{VI}	14.042	3493.1	0	0	$8.8{\cdot}10^{10}$	0 - 60	Erm

[a] P&R denotes Posey and Rochelle [1997].
[b] Erm denotes Ermatchkov et al. [2002].

All chemical equilibrium constants in this work are defined in the mole fraction scale with as reference state infinite dilution in water for all species except water. Mathematically, all constants are then defined as follows:

$$K_{eq} = \prod (\gamma_i x_i)^{\nu_i} \tag{7.1}$$

with ν_i the stoichiometric constant as defined by the reactions described earlier. The following temperature dependence is adopted for all constants:

$$\ln K_{eq} = C_0 + \frac{C_1}{T} + C_2 \cdot \ln(T) + C_3 \cdot T \tag{7.2}$$

Values and sources for coefficients C_0 - C_3 are listed in Table 7.1.
The present EoS model derives each component's activity coefficient (γ_i in Eq. 7.1) from its fugacity coefficient φ_i, in accordance with its reference state. For water (reference state the pure component) this implies:

$$\gamma_{H_2O} = \frac{\varphi_{H_2O}(P, T, x_{H_2O})}{\varphi^{pure}_{H_2O}(P, T)} \tag{7.3}$$

For all other species, with reference state infinite dilution in water, Eq. 7.4 applies:

$$\gamma_i = \frac{\varphi_i(P, T, x_i)}{\varphi_i(P, T, x_i \to 0)} \tag{7.4}$$

Equilibrium between liquid and vapor phase is attained by obeying the equal fugacity condition, as defined by Eq. 7.5:

$$x_1\varphi_i^L P = f_i^L \equiv f_i^V = y_1\varphi_i^V P \tag{7.5}$$

The fugacity coefficient can be deduced from the residual Helmholtz energy, as shown by Eq. 7.6:

$$RT\ln\varphi_i = \left[\frac{\partial}{\partial n_i}A^R(T,V,n)\right]_{T,P,n_{i\neq j}} - RT\ln Z \tag{7.6}$$

All the individual terms of the applied Helmholtz function, A^R, accounting for the system's non-ideality will be discussed in the next section.

7.3.2 Electrolyte equation of state

As stated in the introduction, the presently developed model is based on the electrolyte equation of state, as proposed by Fürst and Renon [1993]. The general equation defines the Helmholtz energy as a sum of four contributions:

$$\left(\frac{A-A^{IG}}{RT}\right) = \left(\frac{A^R}{RT}\right) = \left(\frac{A^R}{RT}\right)_{RF} + \left(\frac{A^R}{RT}\right)_{SR1} + \left(\frac{A^R}{RT}\right)_{SR2} + \left(\frac{A^R}{RT}\right)_{LR} \tag{7.7}$$

The first two terms take into account the energy stemming from repulsive forces (RF) and (attraction) short range interactions (SR1). The first two terms are implemented by means of the Redlich-Kwong-Soave (RKS) equation of state, expressed as:

$$P = \frac{RT}{V-b_{mix}} - \frac{A_{mix}^{SR}}{V\left(V+b_{mix}\right)} \tag{7.8}$$

where the presence of ions is included in the mixture covolume b_{mix}:

$$b_{mix} = \sum_m x_m b_m + \sum_{ion} x_{ion} b_{ion} \qquad b_m = \frac{2^{1/3}-1}{3}\frac{RT_C}{P_C} \tag{7.9}$$

The mixture attraction parameter $A^{SR}{}_{mix}$ is calculated using the Huron-Vidal mixing rule [Huron and Vidal, 1979]:

$$\begin{aligned} A^{SR}_{mix} &= b_{mix}\left(\sum_m\left(\frac{x_m A^{SR}_m}{b_m}\right)-\frac{G^E_\infty}{\ln 2}\right)\\ \frac{G^E_\infty}{RT} &= \sum_m x_m \frac{\sum_n \tau_{nm} b_n x_n \exp\left(-\alpha_{nm}\tau_{nm}\right)}{\sum_m b_{n'} x_{n'} \exp\left(-\alpha_{n'm}\tau_{n'm}\right)}\\ \tau_{nm} &= \frac{g_{nm}-g_{mm}}{RT}\\ g_{nm}-g_{mm} &= \left(g^{'}_{nm}-g^{'}_{mm}\right)+\left(g^{"}_{nm}-g^{"}_{mm}\right)T = \Delta g^{'}_{nm}+\Delta g^{"}_{nm}T \end{aligned} \tag{7.10}$$

with pure components attraction parameters stemming from the expression proposed by Schwartzentruber and Renon [1989]:

$$\begin{aligned} A^{SR}_m &= \frac{1}{9(2^{1/3}-1)}\frac{\left(RT_C\right)^2}{P_C}\alpha\left(T_R\right)\\ \alpha\left(T_R\right) &= \left[1+m\left(\omega\right)\left(1-T_R^{1/2}\right)-p_1\left(1-T_R\right)\left(1+p_2T_R+p_3T_R^2\right)\right]^2\\ m\left(\omega\right) &= 0.48508+1.55191\omega-0.1561\omega^2 \end{aligned} \tag{7.11}$$

The Helmholtz energy arising from interactions between molecules and ions and between cations and anions (SR2) is included in the third term, which can be regarded as the solvation contribution:

$$\left(\frac{A^R}{RT}\right)_{SR2} = \sum_k\sum_l \frac{x_k x_l W_{kl}}{V\left(1-\varepsilon_3\right)} \tag{7.12}$$

where at least one of k and l is an ion, and ε_3 denotes the packing factor:

$$\varepsilon_3 = \frac{N_A\pi}{6}\sum_k \frac{x_k\sigma_k^3}{V} \tag{7.13}$$

where the summation is over all species present in the solvent.

The long range ionic forces (LR) are represented by a simplified Mean Spherical Approximation (MSA) term, as proposed by Ball et al. [1985]:

$$\left(\frac{A^R}{RT}\right)_{LR} = -\frac{\alpha_{LR}^2}{4\pi}\sum_{ion}\frac{x_i Z_{ion}^2\Gamma}{1+\Gamma\sigma_{ion}}+\frac{\Gamma^3 V}{3\pi N_A} \tag{7.14}$$

with the shielding parameter Γ, the parameter a_{LR} and the system's dielectric constant D defined as follows:

$$\begin{aligned} 4\Gamma^2 &= \alpha_{LR}^2 \sum_{ion} \frac{x_{ion}}{V} \left(\frac{Z_{ion}}{1+\sigma_{ion}\Gamma} \right) \\ \alpha_{LR}^2 &= \frac{e^2 N_A}{\varepsilon_0 DRT} \\ D &= 1 + (D_S - 1) \frac{1-\varepsilon_3^{"}}{1-\frac{\varepsilon_3^{"}}{2}} \\ D_S &= \frac{\sum_m x_m D_m}{\sum_m x_m} \end{aligned} \tag{7.15}$$

where $\varepsilon_3^{"}$ is calculated similarly to ε_3, but now the summation is over ionic species only. The influence of ions on the dielectric constant is incorporated by Pottel's expression [Pottel, 1973].

The build-up of the Helmholtz free energy, described in Eqs. 7.7 through 7.15, is illustrated schematically in Figure 7.3 in order to provide an overview of all parameters and properties needed in the EoS model and their relations.

Analysis of the different kinds of parameters needed for model calculations shows, that a distinction should be made between component properties and constants on one hand and (interaction) parameters related to the thermodynamic model applied on other hand.

The first group contains physical properties and/or constants that can be measured independently, such as critical temperatures and pressures and molecular and ionic diameters. Values for some of these properties, however, are not presently available in open literature. Therefore, in some cases, an approximation method is necessary. A list of all needed properties, their availability in literature and the location of the value used in the present work is given in Table 7.2 (molecular properties) and Table 7.3 (ionic properties).

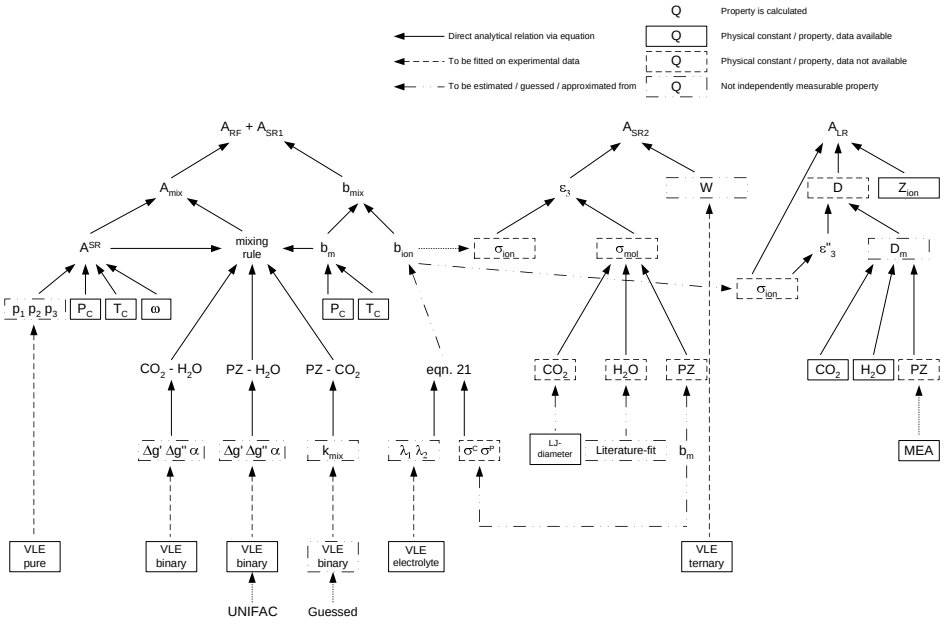

Figure 7.3: Schematic overview of thermodynamic model applied.

Table 7.2: List of physical properties and constants of molecular components.

Molecular property[a]		CO_2	H_2O	PZ	Location
Critical constants	T_C, P_C, ω	yes	yes	yes	Table 7.5
Molecular diameter	σ_m	no	no	no	Table 7.5
Dielectric constant	D	yes	yes	no	Table 7.5

[a]Availability of value of specific property in open literature is listed.

Table 7.3: List of physical properties and constants of ionic species.

Ionic property		Available?	Location
Charge	Z	yes	
Solvated diameter	σ^C, σ^P	no	Table 7.7
Ionic diameter	σ_{ion}	no	Eq. 7.22

The second series consists of parameters that are not independently measurable; they are a consequence of the thermodynamic relations present in the model. These parameters - with the exception of the binary parameter k_{mix} describing the binary interaction between CO_2 and PZ, which is guessed - have been determined by means of fitting the model to (pseudo-) experimental data. A list of these parameters is given in Table 7.4.

Table 7.4: List of parameters fitted in the present work.

System type	Component(s)	Parameter(s)	Exp.data [a]	Approx.	Location
Pure	CO_2	p_1, p_2, p_3	yes	-	Table 7.5
	H_2O	p_1, p_2, p_3	yes	-	Table 7.5
	PZ	p_1, p_2, p_3	yes	-	Table 7.5
Binary	CO_2 - H_2O	$2 \cdot \Delta g^{'}$, $2 \cdot \Delta g^{"}$, α	yes	-	Table 7.6
	H_2O - PZ	$2 \cdot \Delta g^{'}$, $2 \cdot \Delta g^{"}$, α	no	UNIFAC	Table 7.6
	CO_2 - PZ	k_{mix}	no	Guessed	Table 7.6
Electrolyte	H_2O - halide salts	λ_1, λ_2	yes	-	Inline text
Ternary	H_2O - PZ - CO_2	$7 \cdot W_{kl}$	yes	-	Table 7.11

[a] Availability of experimental data necessary for obtaining specific parameter(s).

In the following sections, all individual properties and (fit) parameters (and their sources and/or approximation methods used) will be described in more detail.

Pure component parameters

As can be seen from Eqs. 7.11 and 7.15, several pure component parameters and properties (e.g. with respect to the attraction parameter A^{SR} or the dielectric constant D_m) need to be known before the model can be used. The first step involves the determination of the polar parameters p_1, p_2 and p_3, which are present in Schwartzentruber's expression for the pure component attraction parameter A^{SR} (Eq. 7.11). They were obtained by fitting them to experimental vapor pressures of pure components using the following minimization function:

$$F = \min \sum_{exp} \left| \frac{P^{exp} - P^{mod}}{P^{exp}} \right| \tag{7.16}$$

Results of this fitting procedure are listed in Table 7.5, along with each component's critical constants.

Further, the calculation of the mixture dielectric constant requires the knowledge of the dielectric constants for the pure components (see Eq. 7.15). In accordance with literature, these constants were assumed to have the following temperature dependence:

$$D_m = d_0 + \frac{d_1}{T} + d_2 T + d_3 T^2 + d_4 T^3 \tag{7.17}$$

The values for water and carbon dioxide were derived by Chunxi and Fürst [2000], from experimental data of Akhadov [1981], and Lide [1994]. As in the work of Bishnoi and Rochelle [2002b], the dielectric constant of piperazine was assumed to be the same as for MEA. This is allowed since the sensitivity of the model for this constant is very low, which is a consequence of the relatively small fraction of molecular piperazine present in the mixtures: calculated equilibrium pressures (P_{CO_2}) changed at maximum 1.5 % when decreasing the dielectric constant by a factor 4. Constants d_0 - d_4 for MEA were taken from Lide [1994]. All coefficients needed to calculate D_m are listed in Table 7.5.

Finally, each species' molecular diameter, σ_m, is required in the determination of the packing factor. For water and carbon dioxide, these diameters are taken from the literature - the former was estimated by Ball et al. [1985] and for the latter the Lennard-Jones diameter as given by Poling et al. [2001] was used. For piperazine, the diameter was estimated using its covolume [e.g. Chunxi and Fürst, 2000, Solbraa, 2002]:

$$\sigma_{PZ} = \sigma_{H_2O} \left(\frac{b_{PZ}}{b_{H_2O}} \right)^{1/3} \tag{7.18}$$

Values and sources are listed in Table 7.5.

Binary interaction parameters

As the mixture contains polar components, in this work the Huron-Vidal mixing rule was implemented to calculate the mixture attraction parameter A^{SR}_{mix} (see Eq.

Table 7.5: All Pure component parameters and their sources.

	H_2O	PZ	CO_2
T_C, [K]	647.3	661	304.2
P_C, [bar]	220.9	58.0	73.8
ω, [-]	0.344	0.31	0.225
Source	Poling et al. [2001]	Steele et al. [1997]	Poling et al. [2001]
p_1	0.074168	-0.19842	0.054244
p_2	-0.94308	-2.857	-1.2603
p_3	-0.70403	2.0373	-0.031337
Source [a]	Lide [1994]	Steele et al. [1997]	Simmrock et al. [1986]
		Heilen et al. [1994]	
d_0	-19.29	148.9	0.79062
d_1	$2.98 \cdot 10^{4}$	0	0
d_2	-0.0196	-0.62491	0.010639
d_3	$1.31 \cdot 10^{-4}$	$0.771 \cdot 10^{-3}$	$-2.851 \cdot 10^{-5}$
d_4	$-3.11 \cdot 10^{-7}$	0	0
Source	Chunxi and Fürst [2000]	Lide [1994]	Lide [1994]
σ_m, [10^{-10} m]	2.52	3.96	3.94
Source	Ball et al. [1985]	Eq. 7.18	Poling et al. [2001]

[a] The references contain the VLE data used in the regression of parameters p_1, p_2 and p_3.

7.10). Per binary pair, this mixing rule includes one non-randomness parameter (α_{nm}) and two interaction coefficient terms (τ_{nm} and τ_{mn}) which are temperature dependent (see Eq. 7.10), which results in a total of five parameters to be derived per binary pair, namely $\Delta g'_{nm}$ and $\Delta g''_{nm}$, $\Delta g'_{mn}$ and $\Delta g''_{mn}$, and α. For H_2O - CO_2 these parameters can be derived from experimental CO_2 gas solubility data in water at various temperatures and pressures, thereby applying the following objective function:

$$F = \min \sum_{exp} \left| \frac{P^{exp}_{CO_2} - P^{mod}_{CO_2}}{P^{exp}_{CO_2}} \right| \tag{7.19}$$

Unfortunately, there are no (useful) binary (VLE) data for systems with PZ available in literature. One possibility is to fit the parameters describing both PZ - H_2O and PZ - CO_2 mixtures on the total (reactive) system, but - considering this involves 10 (extra) fit parameters - this could lead to erroneous results. Therefore, in order to reduce the number of fit parameters as well as the risk of erroneous fitting, another approach was adopted in this work:

- Firstly, the interaction parameters describing the binary system PZ - H_2O have been fitted to pseudo data, which have been acquired using the Dortmund modified UNIFAC package present in Aspen Plus 11.1. Using the same goal function as for CO_2 - H_2O, the results as given in Table 7.6 were obtained.

- Secondly, similar to the work of Solbraa [2002], the following correlations were used to describe the interaction between CO_2 and the presently used amine (in this chapter piperazine):

$$\begin{aligned} &\alpha, g'_{mn}, g'_{nm} = 0 \\ &g_{mm} = -\frac{A_m^{SR}}{b_m} \\ &g_{nm} = -2\frac{\sqrt{b_n b_m}}{b_n + b_m}\left(g_{nn} \cdot g_{mm}\right)^{1/2}\left(1 - k_{mix}\right) \end{aligned} \tag{7.20}$$

  With these parameters, the Huron-Vidal mixing rule is reduced to the classical Van der Waals mixing rule, thereby reducing the number of adjustable parameters to one for the binary pair CO_2 - PZ (namely k_{mix}).

Following this procedure, the number of adjustable parameters for both binary systems with PZ (H_2O - PZ and CO_2 - PZ) was reduced from ten to six.

All binary interaction coefficients used in the present model are listed in Table 7.6.

Ionic interaction parameters

Basically, there are three types of ionic parameters in the model, namely the ionic diameter σ_{ion}, the ionic covolume b_{ion} and the ionic interaction parameters W_{kl}. In

Table 7.6: Binary interaction coefficients used in the model.

System	$\Delta g'_{nm}$ [kJ mol^{-1}]	$\Delta g''_{nm}$ [kJ mol^{-1} K^{-1}]	$\Delta g'_{mn}$ [kJ mol^{-1}]	$\Delta g''_{mn}$ [kJ mol^{-1} K^{-1}]	α [-]	Source
H_2O - CO_2	-17.76	-27.84	46.89	1.05	0.035	Houghton[ab]
H_2O - PZ	-9.04	31.69	-15.87	53.49	0.361	UNIFAC
PZ - CO_2	$k_{mix} = 0.2$				0	Guessed [c]

[a]Houghton refers to Houghton et al. [1957].

[b]The reference contains the experimental data on CO_2 solubility in H_2O used in the regression.

[c]The value for k_{mix} is an arbitrary one. This is allowed since the model is not sensitive to this parameter.

order to reduce the number of unknown parameters, the following assumptions have been made:

1. The ionic covolume b_{ion} and the ionic diameter σ_{ion} can be calculated using Eqs. 7.21 and 7.22 [Fürst and Renon, 1993, Zuo and Fürst, 1997]:

$$\begin{aligned} b_c &= \lambda_1 \left(\sigma_c^S\right)^3 + \lambda_2 \\ b_a &= \lambda_1 \left(\sigma_a^P\right)^3 + \lambda_2 \end{aligned} \tag{7.21}$$

$$\sigma_{ion} = \sqrt[3]{\frac{6 b_{ion}}{N_A \pi}} \tag{7.22}$$

The advantage of using Eqs. 7.21 and 7.22 is the immediate reduction in the number of unknown parameters from two (covolume and radius) to only one, namely the Stokes' or Pauling solvated diameter (σ^S and σ^P) . The other 'new' parameters - λ_1 and λ_2 - are to be obtained by fitting VLE data of strong electrolytes (in the relevant solvent).

Solvated diameters of typical ions - such as OH^- (3.52 Å) and HCO_3^- (3.36 Å) - can be found in literature. If this is not the case - such as for e.g. $PZCOO^-$ - there are two alternatives:

- using these parameters as adjustable (fit) parameters;

- making an educated guess, based on their molecular structures and the structure and diameter of the 'parent molecule'.

The latter procedure has been followed in this work; diameters of all piperazine-related species have been estimated in a similar manner as Vallée et al. [1999] applied to estimate diameters of DEA-related species. The estimated solvated diameters have been listed in Table 7.7:

Table 7.7: Estimated solvated diameters for piperazine related species.

Species	PZ	$PZCOO^-$	$PZ(COO^-)_2$	$^+HPZCOO^-$	PZH^+
Solv. diameter, [Å]	3.96	5.5	7.0	5.4	3.9

The solvent dependent parameters λ_1 and λ_2 have been obtained by fitting the experimental osmotic data of Robinson and Stokes [1959] on 28 strong electrolytes (halide salts) in water, which is the solvent in the PZ - H_2O - CO_2 systems, applying the following objective function:

$$F = \min \sum_{exp} \left| \frac{\Phi^{exp} - \Phi^{mod}}{\Phi^{exp}} \right| \tag{7.23}$$

where Φ denotes the osmotic coefficient. Their values were found to be $11.27 \cdot 10^{-7}$ m^3 mol^{-1} $Å^{-3}$ and $5.42 \cdot 10^{-5}$ m^3 mol^{-1} respectively.

2. As in previous work on the application of the electrolyte EoS [e.g. Fürst and Renon, 1993], it seems reasonable to only take into account the interactions between cations and molecules (W_{cm}) and cations and anions (W_{ca}). Other interactions were ignored because of the charge repulsion effect (anion-anion and cation-cation interaction), or due to the generally lower solvation of anions as compared to cations (anion-molecule interaction).

3. For the application in treating processes, the value of the OH^- mole fraction is $< 10^{-6}$, which makes the influence of the interaction between OH^- and PZH^+ on the model negligible.

In total, this leaves the following seven (ionic) variables to be fitted to experimental data sets:

cation-molecule interactions W_{cm}	PZH^+ with H_2O , PZ and CO_2
cation-anion/zwitterion interactions W_{ca}	PZH^+ with $PZCOO^-$, $PZ(COO^-)_2$, HCO_3^- and $^+HPZCOO^-$

At this point, the ionic interaction coefficients W_{cm} and W_{ca} were the only unknown variables left in the set of equations needed to calculate CO_2 partial pressures with the EoS model. In the present work, they were assumed to be temperature independent in order to limit the number of fit parameters. Generally, however, this assumption only holds for a limited temperature interval, as shown by Zuo and Fürst [1997].

In conclusion, a total number of seven ionic interaction coefficients W_{kl} remains, that cannot be determined independently. Therefore, these parameters had to be fitted on the available VLE data - the results of which will be described in Section 7.4.2.

7.4 Results

7.4.1 Experimental results

All experimentally obtained data on CO_2 solubility with their corresponding partial pressure are listed in Tables 7.8 and 7.9 and are graphically represented in Figures 7.4, 7.5 and 7.6.
The experimental error in this work is estimated (based on propagation of error) at 4 % (in loading) and 5 % (in CO_2 partial pressure) respectively.
When comparing the present data to those three sets already available in literature, it can be concluded that:

- The solubility data in 0.6 kmol m^{-3} aqueous PZ solutions (Table 7.8) are in good agreement with the data presented by Bishnoi and Rochelle [2000], which is clearly illustrated in Figure 7.4.

Table 7.8: Experimental VLE data of CO_2 in 0.6 M PZ solution.

T = 25 °C		T = 40 °C		T = 70 °C	
loading	P_{CO2}	loading	P_{CO2}	loading	P_{CO2}
[mol CO_2 / mol PZ]	[kPa]	[mol CO_2 / mol PZ]	[kPa]	[mol CO_2 / mol PZ]	[kPa]
0.7	0.31	0.64	0.37	0.36	0.27
0.75	0.41	0.73	0.82	0.5	0.67
0.81	0.72	0.76	1.62	0.54	1.72
0.88	1.53	0.78	3.27	0.62	3.19
0.89	2.95	0.83	4.09	0.62	3.86
0.97	5.36	0.87	5.99	0.71	4.53
0.98	7.38	0.91	10.08	0.68	5.34
0.98	10.92	0.94	10.41	0.71	7.31
1.02	26.87	0.99	26.52	0.76	10.41
1.03	66.98	0.98	39.61	0.88	38.01
1.06	103.93	1.03	92.81	0.92	82.07
1.08	111.37	1.03	104.7	0.96	94.1

Table 7.9: Experimental VLE data of CO_2 in 0.2 M PZ solution.

T = 25 °C		T = 40 °C		T = 70 °C	
loading	P_{CO2}	loading	P_{CO2}	loading	P_{CO2}
[mol CO_2 / mol PZ]	[kPa]	[mol CO_2 / mol PZ]	[kPa]	[mol CO_2 / mol PZ]	[kPa]
0.81	0.45	0.63	0.38	0.47	0.51
0.84	0.64	0.76	0.88	0.59	1.18
0.89	1.00	0.88	2.63	0.7	2.57
0.92	1.70	0.98	10.11	0.78	5.03
0.94	2.94	1.07	68.51	0.97	45.3
0.99	5.38	1.14	101.71	1.03	80.5
0.98	8.5			1.03	87.8
1.02	10.67				
1.23	107.23				

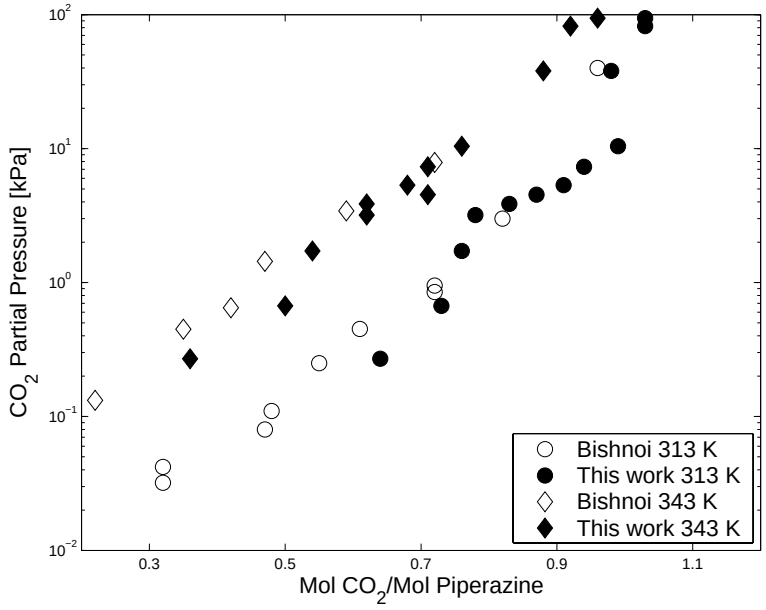

Figure 7.4: Comparison of the 0.6 M PZ data of Bishnoi and Rochelle [2000] at 313 K and 343 K with the present data.

- Aroua and Mohd Salleh [2004] published CO_2 solubility data at lower piperazine concentrations - varying between 0.1 and 1.0 kmol m^{-3} - at temperatures ranging from 20 to 50 $^{\circ}$C. Because they also performed experiments with solutions containing both 0.2 and 0.6 kmol m^{-3} at a temperature of 40 $^{\circ}$C , their results are easily comparable to the current data sets but also to some data by Bishnoi and Rochelle [2000].

  This comparison is shown graphically in Figures 7.5 and 7.6, from which it can be observed that there is a substantial (more or less constant) discrepancy between the data by Aroua and Mohd Salleh [2004] and the other data in the plots. The large, but consistent, deviation between the Aroua's VLE data on one hand and the current data and Bishnoi's data on the other hand, seems to point out that it is useless to fit the ionic interaction parameters W_{kl} on all three experimental data sets simultaneously as this would result in model predictions that would deviate substantially from all three experimental data sets. As the data of Bishnoi's study seem to be consistent with the

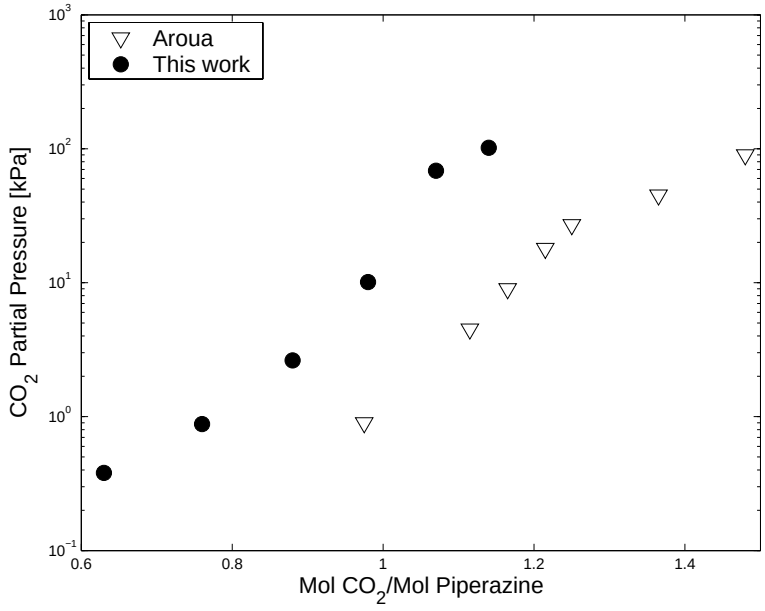

Figure 7.5: Comparison of 0.2 M PZ data of Aroua and Mohd Salleh [2004] at 313 K with the present data.

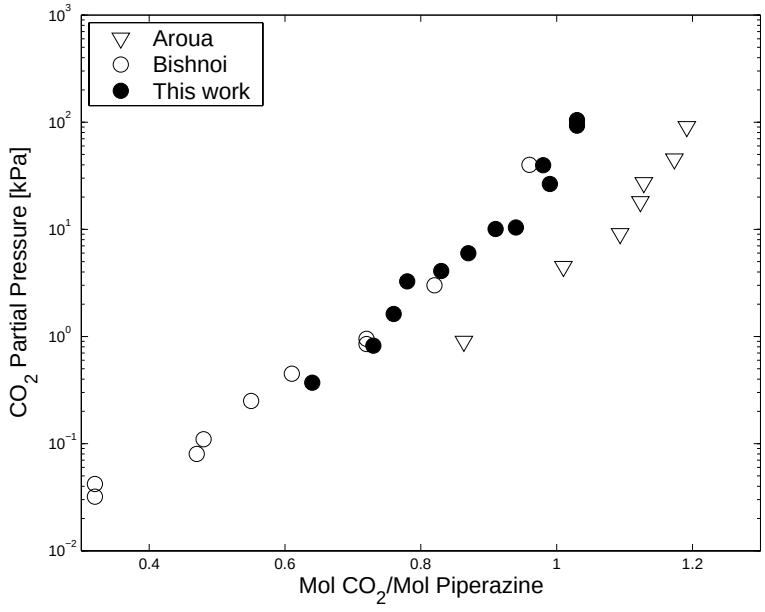

Figure 7.6: Comparison of 0.6 M PZ data of Aroua and Mohd Salleh [2004] at 313 K with the present data and data by Bishnoi and Rochelle [2000].

Table 7.10: Results of consistency check of the present data at two different CO_2 loadings.

C_{PZ}	CO_2 loading - 1 [mol CO_2 / mol PZ]	P_{CO2} [kPa]	CO_2 loading - 2 [mol CO_2 / mol PZ]	P_{CO2} [$\cdot 10^2$ kPa]	Source
0.2 M	0.76	0.88	1.07	0.69	this work
0.6 M	0.76	1.76	1.03	0.93 - 1.05	this work
2.0 mol kg^{-1}	0.73	≈ 6	1.02	≈ 1.6	P-S K [a]

[a] Pérez-Salado Kamps et al. [2003] list total pressure data in their paper. The values in the table are estimated by subtracting the water vapor pressure, which is 73.8 mbar at 313.15 K, from the total pressure values of 133 mbar and 1.71 bar respectively.

experimental data from this study, these data sets are thought to be more reliable and, therefore, only the data of Bishnoi and Rochelle [2000] and the experimental data as obtained in this study were used in the modelling part of this chapter.

- A thorough consistency check of the current data with the data by Pérez-Salado Kamps et al. [2003] is not possible, since they performed experiments in 2.0 and 4.0 molal PZ solutions. A rough consistency check, however, is possible: At fixed loading and temperature, the CO_2 partial pressure should increase with increasing piperazine concentration [Chunxi and Fürst, 2000]. In Table 7.10, experimental equilibrium pressures for three different concentrations are compared at similar loadings at a temperature of 313 K.

  As shown in Table 7.10, the simple consistency check with the data by Pérez-Salado Kamps et al. [2003] holds. However, some low pressure data in 2.0 molal solutions are required for a more sound comparison.

7.4.2 Modelling results

As mentioned before, the data presented by Aroua and Mohd Salleh [2004] were excluded from the database used in the fitting procedure. The database was further screened for unreliable data (series) using the two following generally found trends in acid gas VLE diagrams [Chunxi and Fürst, 2000]:

- At a fixed loading and temperature, the CO_2 partial pressure will increase with increasing amine concentration;
- At a fixed loading and amine concentration, the CO_2 partial pressure will increase with increasing temperature.

In addition, initial model simulations were performed to further screen and reduce the database: When an individual experimental result and the preliminary model calculation deviated more than a factor of two, that particular data point was excluded from the database to prevent it from dominating the fit. This was the case for some data measured in the 1.0 loading range where a steep slope exists between '$logP$' and 'loading'. The final database consisted of 153 experimental data points (out of 170) to be used in the determination of the seven model variables W_{kl}.

In order to maintain consistency throughout all individual fitting procedure steps, the goal function F to be minimized in the final data regression was also chosen as follows:

$$F = \sum_{\text{exp}} \left| \frac{P^{\text{exp}} - P^{\text{mod}}}{P^{\text{exp}}} \right| \tag{7.24}$$

where the P either denotes the CO_2 partial pressure (Bishnoi and Rochelle [2000], this work) or the total system pressure [Pérez-Salado Kamps et al., 2003]. The obtained values for these adjustable parameters are listed in Table 7.11 and further results of the data fit and modelling are listed in Table 7.12 and shown graphically in Figures 7.7 through 7.10.

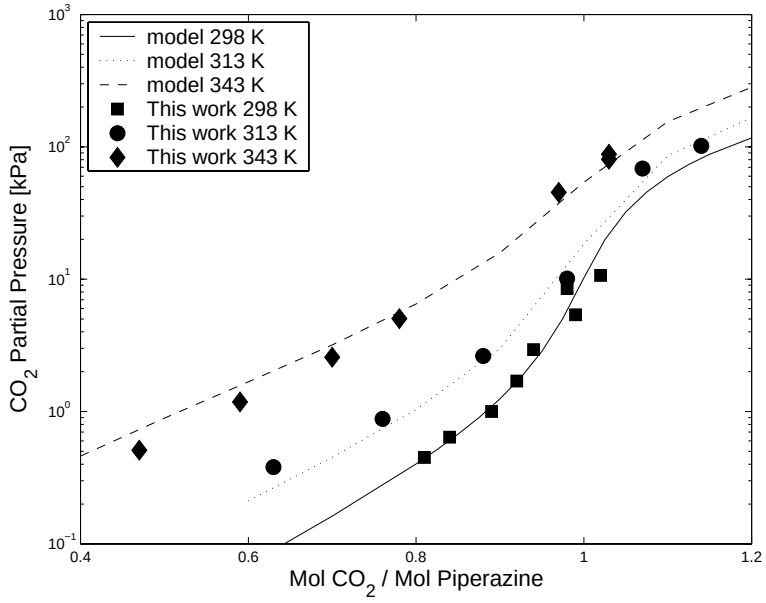

Figure 7.7: Representation of CO_2 solubility at various temperatures in the case of 0.2 M PZ solution.

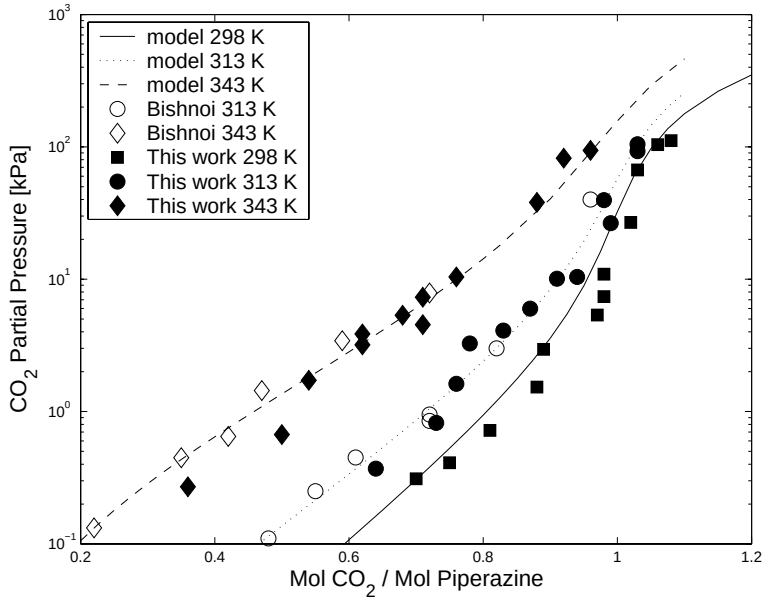

Figure 7.8: Representation of CO_2 solubility at various temperatures in the case of 0.6 M PZ solution.

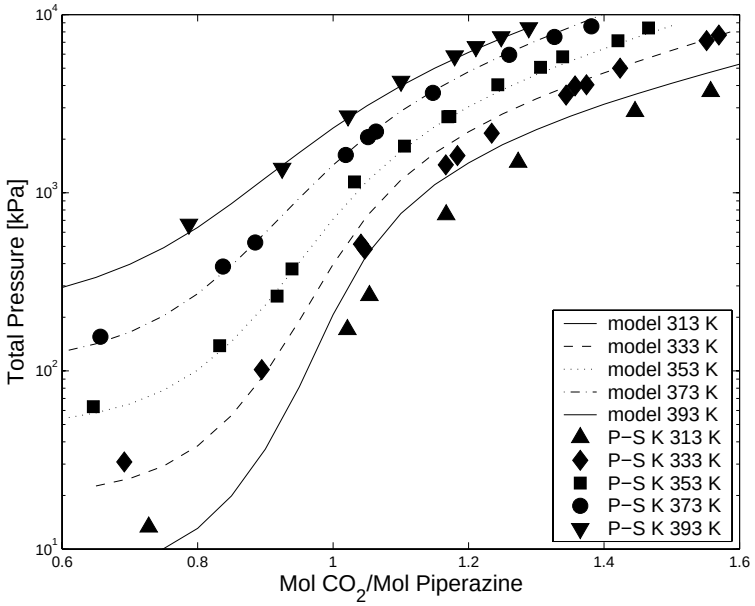

Figure 7.9: Representation of CO_2 solubility at various temperatures in the case of 2.0 molal PZ solution. P-S K denotes Pérez-Salado Kamps et al. [2003].

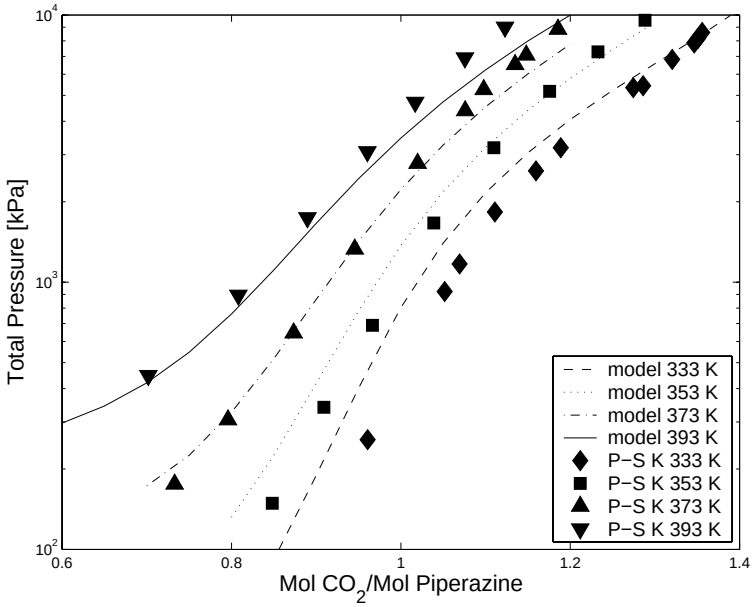

Figure 7.10: Representation of CO_2 solubility at various temperatures in the case of 4.0 molal PZ solution. P-S K denotes Pérez-Salado Kamps et al. [2003].

Table 7.11: The ionic interaction coefficients W_{kl} found in the regression of the experimental database.

W_{kl}	$[\cdot 10^{-3}$ m^3 mol$^{-1}]$
PZH^+ - H_2O	0.169
PZH^+ - PZ	0.437
PZH^+ - CO_2	0.074
PZH^+ - $^+HPZCOO^-$	0.234
PZH^+ - HCO_3^-	-0.023
PZH^+ - $PZCOO^-$	-0.024
PZH^+ - $PZ(COO^-)_2$	-0.202

Table 7.12: Experimental database used in the data fit and the resulting deviations with the model.

Source	[PZ]	Temperatures [K]	Loading range [mol CO_2 / mol PZ]	N [a]	AAD [b] [%]
This work	0.2 M	298, 313, 343	0.47 - 1.23	21	16.4
	0.6 M	298, 313, 343	0.36 - 1.08	30	19.9
B&R[a]	0.6 M	313, 343	0.16 - 1.64	17	16.4
P-S K.[b]	2.0 m	313, 333, 353, 373, 393	0.54 - 1.64	48	12.4
	4.0 m	333, 353, 373, 393	0.50 - 1.36	37	15.6
Total				153	15.7

[a] N = Number of data points used in the fitting procedure.
[b] AAD = Average Absolute Deviation.
[a] B&R denotes Bishnoi and Rochelle [2000].
[b] P-S K. denotes Pérez-Salado Kamps et al. [2003].

As can be seen from Table 7.12, the average deviation between experimental and model pressure amounts to ca. 16 %, which is good considering the experimental scatter on one hand and the various assumptions and simplifications made on the other hand.

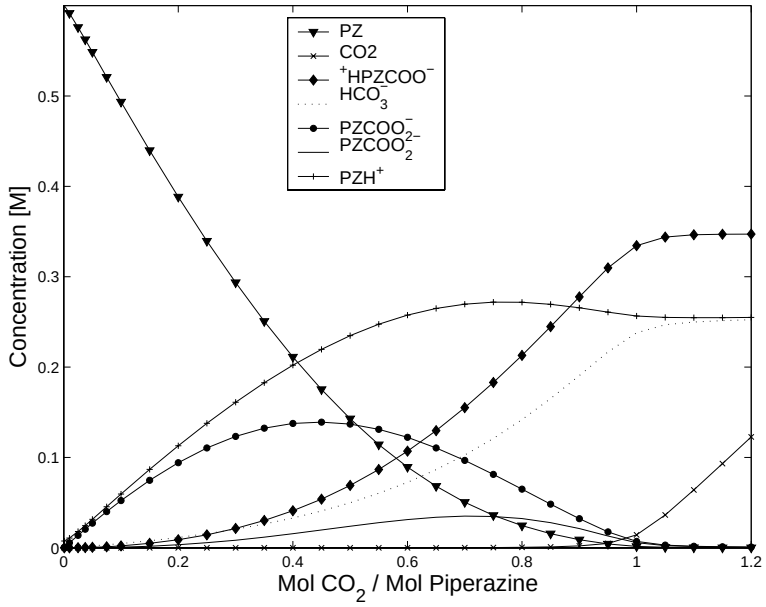

Figure 7.11: Predicted speciation of a 0.6 M PZ solution at 40 °C. It must be noted that the points are not experimental data but results obtained by simulations, added for clarity.

Pérez-Salado Kamps et al. [2003] used the Pitzer model to correlate their own CO_2 solubility in aqueous piperazine solutions. They report an average deviation of 4 % between model and experiment. When applying their model to the data of Bishnoi and Rochelle [2000], a mean deviation of 22 % between experiments and prediction is found. However, in their model, nine ionic interactions are present - all temperature dependent - giving a total of 18 adjustable variables.

Besides the previously described 'pressure - loading curves', the presently developed VLE model is also useful to predict speciation in loaded amine solutions. Information on the species distribution is indispensable when trying to predict acid gas absorption rates into (partially) loaded solutions, since rigorous mass transfer models require the (exact) bulk composition of the liquid phase [Versteeg and Van Swaaij, 1988a]. Figure 7.11 shows a typical speciation plot of the PZ - H_2O - CO_2 system at 313 K.

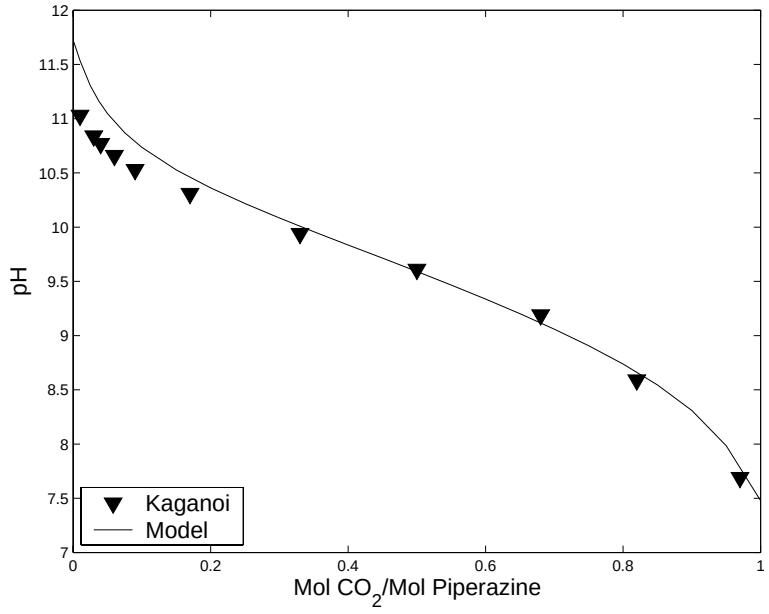

Figure 7.12: Comparison between experimental and predicted pH of 0.6 M PZ solution loaded with CO_2.

As one can see from Figure 7.11, the contribution of the piperazine dicarbamate is never dominant, indicating that the theoretical chemical loading of 2 moles CO_2 per mol piperazine is never reached. At lower CO_2 loadings, both piperazine carbamate and protonated carbamate are present in the solutions. On increasing loading (≥ 0.5), however, the former is gradually converted to the latter, which can easily be explained by the accompanying decrease in pH of the solution. Similar speciation results were also reported by Bishnoi and Rochelle [2000] and Pérez-Salado Kamps et al. [2003].

The ability to predict speciation implies that the current model can also predict certain physical properties such as pH and (ionic) conductivity. Kaganoi [1997] measured both pH and conductivity in loaded 0.6 M aqueous piperazine solutions. Those experimental data were extracted from the graphical representations in the paper by Bishnoi and Rochelle [2000] and compared to predictions of the model presented in this chapter. As the model does not include the H_3O^+ ion, pH values have been deduced from the OH^- ions present in the model. Results are shown in

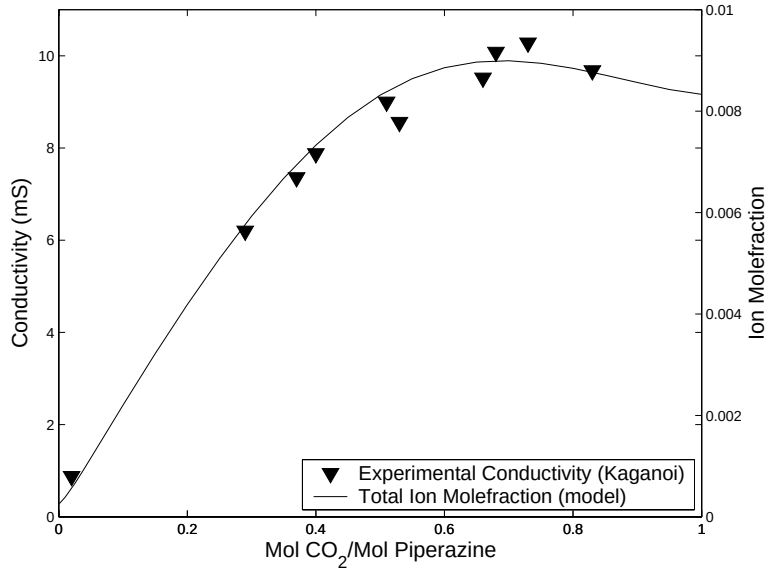

Figure 7.13: Measured and predicted ionic conductivity in a 0.6 M PZ solution loaded with CO_2.

Figures 7.12 and 7.13 below.

Both Figure 7.12 and 7.13 show that the presently developed model is able to predict both pH and ionic conductivity reasonably well. Only at low loadings, there seems to be a (consistent) discrepancy between the predicted and measured pH. This might be caused by the binary parameters describing the piperazine-water interaction: Chang et al. [1993] state that especially at low loadings, representation of of acid gas solubility is sensitive to the binary amine-water interaction coefficients.

7.5 Conclusions

Removal of acid gases is usually achieved by absorption in solvents consisting of aqueous amine solutions. One very promising solvent is a blend of piperazine (PZ) and N-methyldiethanolamine (MDEA) solution in water (the so-called 'activated' MDEA solvent). Detailed design of absorption-desorption units using this amine blend requires a thermodynamically sound composition model, not only to calculate

equilibrium partial pressures over a (partially) loaded solution, but also to predict component speciation in the liquid bulk. This chapter adds new experimental data on the ternary subsystem PZ - H_2O - CO_2 at different concentrations and temperatures.

The electrolyte equation of state (EoS), as originally proposed by Fürst and Renon [1993], has been used to correlate these and other available experimental data on the same system. The final model contains a total of seven ionic parameters to be adjusted to an experimental database of 153 data points. The model was found to be able to predict CO_2 pressures with an average deviation of about 16 % from experimental data.

Even though modelling results are satisfactory, some aspects of the currently presented EoS model can be further improved. Binary parameters on the piperazine - water system have been estimated using the UNIFAC method since no experimental data are available. No difficulties have been encountered in the present situation, since it is known that the amine - H_2O interaction parameters in acid gas models are only important in the low loading range [Chang et al., 1993]. As the current experimental database does not contain any data in the low loading range, the use of the UNIFAC method for the determination of the binary interactions of PZ with water seems acceptable. However, to get more precise values for these interaction coefficients, it is obvious that new, additional experimental data are needed. The results of this chapter makes the extension of the EoS model towards the quaternary system water - MDEA - piperazine - carbon dioxide possible.

Acknowledgements

H.F.G. Moed is acknowledged for the construction of both experimental setups, and H.B.S. Dijkstra is acknowledged for his contributions to the experimental work.

Chapter 8

Solubility of Carbon Dioxide in Aqueous Blends of Piperazine and MDEA

Abstract

In this chapter, new experimental equilibrium data are reported on the solublity of carbon dioxide into aqueous solutions of N-methyldiethanolamine (MDEA) and piperazine (PZ) over a wide range of conditions. These data not only include CO_2 solubilities and their corresponding partial pressures, pH and conductivities, but also a limited number of liquid speciation data obtained using NMR spectroscopy. The present data, and other data reported in the literature, were correlated with the electrolyte equation of state, as originally introduced by Fürst and Renon [1993]. The final model was able to describe the thermodynamics of the quaternary CO_2 - PZ - MDEA - H_2O reasonably well over a wide range of experimental conditions.

8.1 Introduction

The technology of adding small amounts of an accelerator to an aqueous solution of a tertiary (alkanol)amine has found widespread application in the selective or bulk removal of carbon dioxide from process gas streams. The principle behind the use of these solvents is based on the relatively high rate of reaction of carbon dioxide with the accelerator, usually a primary or secondary amine, and the low heat of reaction of CO_2 with the tertiary amine. This leads to higher absorption rates in the absorber section, while maintaining a low heat of regeneration of the solvent in the desorber column. One commonly used solvent nowadays is a piperazine (PZ) activated aqueous solution of N-methyldiethanolamine (MDEA). Indispensable for a good understanding of the behavior of these amine solutions in the absorption-desorption process is a detailed knowledge on the thermodynamics of the solvent. On one hand, the CO_2 equilibrium partial pressure over a loaded amine solution determines the operating window in absorber and stripper, while, on the other hand, a thermodynamic model provides information on the speciation of the solvent, which - among other things - determines (local) driving forces, reactions rates and hence rates of absorption. And although a piperazine activated aqueous MDEA solution is a commonly used solvent these days, only few studies on the thermodynamics of this system have been reported in the literature.

Xu et al. [1998] investigated the effect of the addition of piperazine on the equilibrium partial pressure and liquid loading of carbon dioxide in aqueous MDEA solutions. They reported CO_2 liquid loadings and corresponding partial pressures over solutions containing 4.28 kmol m^{-3} MDEA and PZ concentrations up to 0.515 kmol m^{-3}. Liu et al. [1999], from the same research group as Xu et al. [1998], determined experimental CO_2 solubilities over a wide range of conditions. They varied both the piperazine and the MDEA concentrations, as well as the temperature in their experiments. Moreover, they describe their data using two modelling approaches: a thermodynamic model that incorporates an extended Debye-Hückel expression, and a simple Kent-Eisenberg approach. Neither of the models derived, however, include any of the carbamated piperazine species [$PZCOO^-$, $^+HPZCOO^-$

and $PZ(COO^-)_2$].

Bishnoi and Rochelle [2002b] reported experimental carbon dioxide solubilities in a 4.0 M MDEA aqueous solution activated with 0.6 M PZ at temperatures of 313 and 343 K and partial pressures up to approximately 7.5 kPa. In addition to the solubility data, they also measured the speciation of the liquid for one MDEA - PZ solution loaded with CO_2 using NMR spectroscopy. They applied the electrolyte NRTL model to describe their solubility data and NMR (speciation) data. The obtained model was able to predict the experimental data of Xu et al. [1998] and Liu et al. [1999] reasonably well.

Pérez-Salado Kamps et al. [2003] studied the experimental solubility of CO_2 in aqueous solutions of 2 molal MDEA and 2 molal PZ at a temperature of 353 K, and at total pressures ranging from 0.18 to 6.4 MPa. Also, a thermodynamic model, based on Pitzer's equation, was developed and model predictions were compared to the experimental data available at that time. It was found that the model was not able to accurately describe the experimental data taken at CO_2 partial pressures below 100 kPa. It should be noted, however, that no additional (fit) parameters were present in the model to account for the interactions between PZ- and MDEA-species, such as e.g. between $PZCOO^-$ and $MDEAH^+$.

Si Ali and Aroua [2004] studied the effect of piperazine on the equilibrium CO_2 liquid loading in an aqueous MDEA solution experimentally. Hereto, they determined the CO_2 loading - at constant temperature and CO2 partial pressure - in aqueous MDEA solutions (at concentrations of 2.0, 1.98, 1.90 and 1.80 kmol m^{-3}) with respectively 0, 0.01, 0.05 and 0.1 kmol m^{-3} PZ (hence keeping the total 'amine-groups' concentration constant in all experiments). They concluded that the addition of PZ increased the solubility of CO_2 in the low partial pressure region when compared to 'pure' MDEA solutions.

This chapter will focus on the thermodynamics of the equilibrium solubility

of CO_2 in aqueous solutions containing both PZ and MDEA. Firstly, new experimental CO_2 solubility data will be presented to extend the existing experimental database on this system. These new data not only include equilibrium pressure data, but also corresponding information on the liquid pH and conductivity of the loaded solvent. Also, a limited number of experimental speciation data will be presented that have been obtained using NMR spectroscopy. Secondly, in this chapter a thermodynamic model is developed to correlate the experimental data currently available in the literature. The thermodynamic model used is based on the electrolyte equation of state (EoS), as originally introduced by Fürst and Renon [1993]. This approach has been used to successfully describe CO_2 and/or H_2S solubilities in aqueous systems containing MDEA, MEA or DEA, and in Chapter 7, it was also proven to be suitable for describing the solubility of carbon dioxide in aqueous piperazine solutions.

8.2 Experimental

As mentioned in Section 8.1, this chapter includes experimental VLE data, which provide information on the solubility and corresponding partial pressure of CO_2 in aqueous MDEA/PZ solutions, as well as a limited number of liquid speciation data obtained with NMR spectroscopy for these solutions. The experimental methods and procedures that have been used to obtain these data will be described in this section.

8.2.1 Vapor-liquid-equilibrium experiments

The experimental set-up used in this work was essentially the same as the 'continuous setup' used in Chapter 7, and will therefore not be described in detail. However, some modifications were made to make the setup suitable for the determination of pH and conductivity for the experiments in this chapter.

- Firstly, the reactor was connected to a calibrated gas vessel, which was equipped with both a digital pressure transducer and a thermocouple. The presence

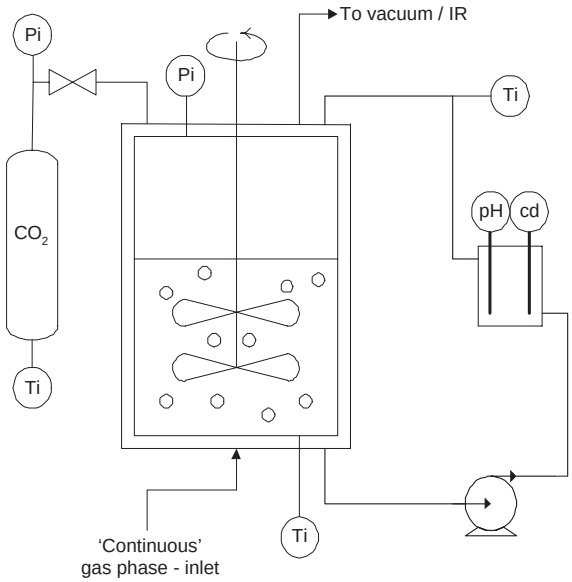

Figure 8.1: Schematic drawing of the reactor part in the experimental setup.

of the gas vessel made it possible to supply a certain amount of pure CO_2 to the solution in the reactor.

- Secondly, a sampling loop (total volume ca 200 mL) was attached to the reactor for measuring the liquid's pH and conductivity during an experiment. In the sampling loop, a small liquid pump was installed and operated in such a way that the average residence time inside the loop was well below 60 seconds. Insulation was applied to the entire sampling loop to avoid heat loss, and, to be able to verify this, also the 'returning' liquid temperature was measured with a thermocouple. The actual measuring electrodes themselves were placed straight-up inside a small glass vessel within the loop. The liquid's pH was determined with a Mettler DG 111-SC pH electrode, which was calibrated using standard buffer solutions with known pH. A Radiometer CDC 104 (nominal cell constant 1.0 cm^{-1}) type electrode connected to an analogous conductivity meter type CDM 2d was used to measure the conductivity of the solution.

A schematic drawing of the modifications made to the setup is shown in Figure 8.1. For a detailed picture of the setup, the reader is referred to Chapter 7.

In a typical experiment, a known amount of both piperazine (99 %, Aldrich) and MDEA (99 %, Aldrich) were dissolved in water and transferred to the reactor. Here, the solution was degassed by applying vacuum for a short while, and subsequently allowed to equilibrate at the desired temperature, after which the (vapor) pressure was recorded. Simultaneously, the gas supply vessel was filled with pure CO_2 and the initial pressure in this vessel was noted. Now, the stirrer in the reactor was switched on and a desired amount of carbon dioxide was fed from the gas supply vessel to the reactor. Then, the gas supply vessel was closed and the contents of the reactor was allowed to reach equilibrium, which was achieved, usually within about 30 minutes, when the reactor temperature and pressure as well as the pH and conductivity measured in the sampling loop remained constant. The total amount of carbon dioxide fed to the reactor was then determined by the initial and end pressure in the gas supply vessel, according to Eq. 8.1:

$$n_{CO_2} = \frac{V^{GV} \Delta P^{GV}}{RT^{GV}} \tag{8.1}$$

The use of the ideal gas law in Eq. 8.1 is allowed, as the maximum pressure in the gas supply vessel never exceeded 4 bar. The corresponding liquid loading at a certain CO_2 partial pressure is then determined by Eq. 8.2:

$$\alpha_{CO_2} = \frac{1}{V_{liq}^{R}\left([MDEA] + [PZ]\right)} \cdot \left(n_{CO_2} - \frac{P_{CO_2}^{R} V_{gas}^{R}}{RT^{R}} \right) \tag{8.2}$$

The method that was used to determine the corresponding partial pressure depended on whether the setup was operated in a batch-wise or continuous mode of operation during the experiment.

8.2.2 Procedure 'continuous experiments'

In experiments where the equilibrium partial pressure of CO_2 was expected to lie below about 10 kPa, the setup was operated in a continuous mode with respect to the gas phase. During these experiments, a gas flow consisting of N_2 and CO_2 was - after presaturation by an amine solution and water respectively - sent to the reactor, and the CO_2 concentration in the outgoing gas stream was measured

using an IR analyzer, type UNOR 610. The composition of the inlet gas stream was adjustable and controlled by two calibrated mass flow controllers. Now, upon attainment of equilibrium in the reactor, initially a small sweep stream of pure N_2 gas was passed through the reactor, and the CO_2 content of the outgoing gas stream was measured. The sweep stream was sufficiently small - and hence the gas phase residence time sufficiently large - to ensure that the outgoing gas concentration was at near-equilibrium. Next, the MFC controlling the carbon dioxide gas flow was set to such a value, that the composition of the inlet flow would match the measured outlet composition. This 'trial & error' procedure of adjusting the carbon dioxide MFC (and hence inlet composition) to the detected CO_2 content in the outlet, was repeated until the IR analyzer did give a stable signal. At this point, usually attained within about 20 - 30 minutes, the inlet gas composition (set by the MFCs) matched the outlet composition, which in turn determines the equilibrium composition of the gas in this experiment.

8.2.3 Procedure 'batch experiments'

In experiments where the equilibrium partial pressure of CO_2 exceeded 10 kPa, the reactor was operated batch-wise with respect to the gas phase. Now, the CO_2 partial pressure was directly calculated from the total equilibrium pressure in the reactor corrected for the lean solution vapor pressure. Hereby, it was assumed that the vapor pressure was not influenced by the amount of CO_2 present in the solution.

8.2.4 Validation

The experimental setup and procedures were validated by measuring the carbon dioxide solubility in an aqueous solution of 2.0 kmol m^{-3} MDEA at 313 K, a system for which results are extensively reported in the literature. Results are listed in Table 8.1 and compared to literature sources in Figure 8.2.

Figure 8.2 shows that the new experimental data are well in line with solubility data reported in the literature and therefore the results obtained with the

Table 8.1: Solubility results in 2.0 kmol m^{-3} aqueous MDEA at 313 K.

CO_2 loading [mol CO_2 mol^{-1} amine]	P_{CO2} [kPa]	Gas phase mode of operation
0.122	1.25	continuous
0.213	3.24	continuous
0.294	5.97	continuous
0.361	8.5	batch
0.382	9.2	batch
0.478	15.4	batch
0.610	30.0	batch
0.627	32.4	batch
0.807	93.6	batch
0.810	91.6	batch

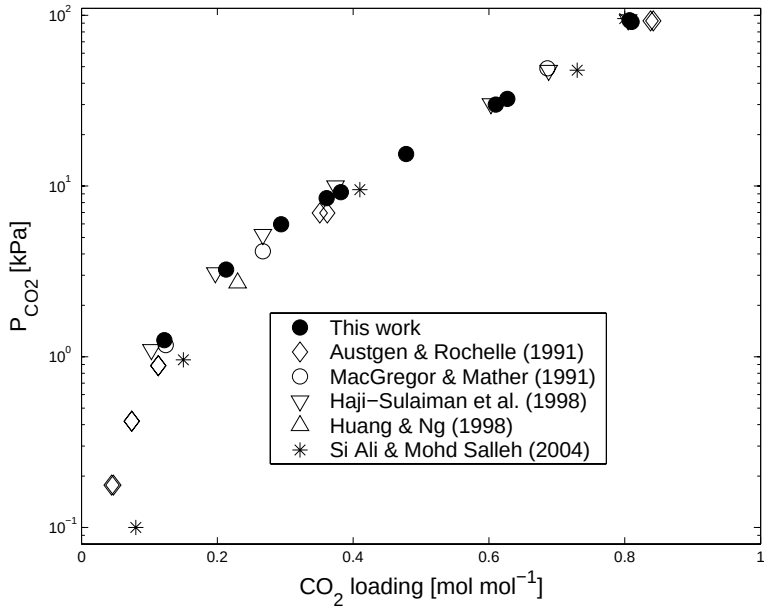

Figure 8.2: CO_2 solubilities in 2.0 kmol m^{-3} aqueous MDEA solution at 313 K.

current experimental setup and using the experimental procedures can be considered to be reliable.

8.2.5 NMR spectroscopy experiments

Carbon dioxide partial pressure data are generally the kind of equilibrium solubility data used in the regression of (thermodynamic) parameters present in acid gas equilibria modelling. However, the ability of a model to describe or predict equilibrium pressures, does not automatically imply that it can also correctly predict the liquid phase speciation - which in turn is a vital input in the rate-based rigorous modelling of both the absorption and desorption column. The model predicted speciation can, partly and indirectly, be validated with the use of experimental pH and conductivity data, if available, as these data provide information on the activity of the H3O+ (and the OH-) ion and on the total ion concentration present in solution. Even more specific information on the liquid phase composition of a loaded (alkanol)amine solution can be obtained using NMR spectroscopy, as illustrated in the work of Bishnoi and Rochelle [2000, 2002b], Ermatchkov et al. [2002], Poplsteinova Jakobsen et al. [2005]. To obtain more information on the liquid phase speciation as a function of carbon dioxide loading, also in this chapter the liquid phase composition of an aqueous 4.0 kmol m^{-3} MDEA, 1.0 kmol m^{-3} PZ has been determined using NMR measurements at 298.15 K. The experimental procedure regarding the NMR spectroscopy and required details are described below.

The amine solution was prepared by dissolving known amounts of piperazine (purity 99 %, Aldrich) and MDEA (purity 99 %, Aldrich) in water and deuterium oxide (purity 99 %, Aldrich). The final solution contained about 10 volume % D_2O to ensure a good 'lock signal' in the NMR apparatus.

Subsequently, about 0.8 mL of the solution was injected with a syringe into a Wilmad 528-PV-7 NMR tube. The NMR tube was connected to a calibrated gas supply vessel equipped with a Heise 3710 pressure transducer. A desired amount of carbon dioxide (quality 4.0, Hoekloos) was added from the gas supply vessel to the NMR tube, and the resulting CO2 loading was calculated from the pressure difference in the gas supply vessel, using Eqs. 8.1 and 8.2. In the loading calculation, it was assumed that the amount of CO_2 present in the gas phase was negligible com-

pared to the amount absorbed by the liquid. Next, the sample tubes were allowed to equilibrate in a softly shaken thermostatted bath for at least a week, after which the NMR spectra were taken.

The liquid phase composition was determined using ^{1}H, ^{13}C, H-H and C-H NMR spectroscopy on a Bruker AvanceII 600 MHz spectrometer, equipped with a TXI (^{1}H, H-H and C-H experiments) or BBO (^{13}C experiments and C-H experiments) probe. The 2D data were used to identify the individual peaks in the ^{1}H and ^{13}C spectra, whereas the ^{1}H NMR results were used for a more quantitative analysis of the different reaction products. As it is not possible with the presently applied method to distinguish between a base and its protonated counterpart (e.g. MDEA and $MDEAH^{+}$) or the ratio of the two, without an extensive calibration procedure (see e.g. Poplsteinova Jakobsen et al. [2005]), only the following three (piperazine) groups could be quantified:

- piperazine, protonated piperazine and diprotonated piperazine
- piperazine monocarbamate, and its protonated counterpart
- piperazine dicarbamate

The ratio between total MDEA and total PZ was used as an internal reference to check the consistency of the measurements.

8.3 Electrolyte equation of state modelling

8.3.1 General

The thermodynamic model applied in this work is the electrolyte equation of state (EoS), as originally introduced by Fürst and Renon [1993], in which the system's non-ideality is calculated from (the sum of) four different contributions to the (reduced) free Helmholtz energy of the system (see Eq. 8.3):

$$\left(\frac{A-A^{IG}}{RT}\right)=\left(\frac{A^{R}}{RT}\right)=\left(\frac{A^{R}}{RT}\right)_{RF}+\left(\frac{A^{R}}{RT}\right)_{SR1}+\left(\frac{A^{R}}{RT}\right)_{SR2}+\left(\frac{A^{R}}{RT}\right)_{LR} \quad (8.3)$$

The first two terms in Eq. 8.3 describe the molecular interactions (repulsive forces, RF, and short range interactions, SR1) in the system. Interactions between molecular and ionic species as well as ion-ion interactions are included in the second short range term (SR2). The fourth contribution to the reduced Helmholtz energy stems from the long range ionic forces (LR). All governing equations describing these individual contributions are listed in detail in Chapter 7, and will therefore not be given here.

The total model, which will be used to describe the quaternary H_2O - CO_2 - PZ - MDEA system, requires - besides various physical and/or thermodynamic constants - several sets of pure, binary or ternary (fit) parameters which need to be determined on beforehand on the corresponding subsystems. A schematic overview of the model structure is given in Figure 8.3.

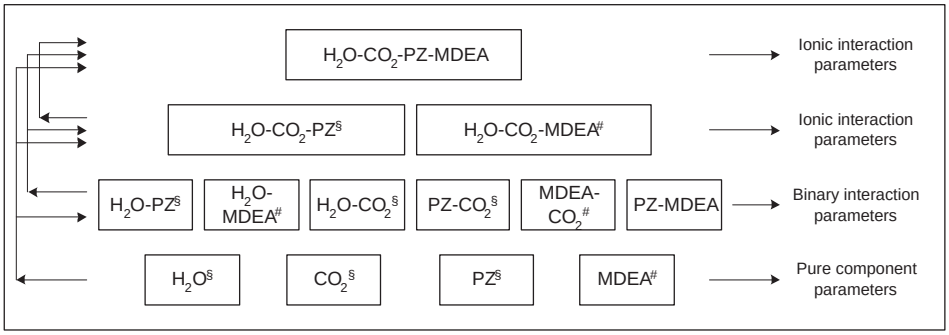

Figure 8.3: Schematic overview of the model structure.

In Chapter 7, the electrolyte EoS model was used to successfully describe the CO_2 solubility in aqueous piperazine solutions. From Figure 8.3, it can be concluded that many parameters necessary for the present, quaternary system, model, are also parts of the previously developed model for the ternary system PZ - CO_2 - H_2O. For information on the (method of) determination and/or estimation of these sets of parameters (marked with § in Figure 8.3) and their respective values, the reader is therefore referred to Chapter 7. The parameters of the ternary subsystem PZ - CO_2 - H_2O are used 'as is' in the quaternary system.

The second ternary subsystem MDEA - CO_2 - H_2O has been more frequently studied. From the experimental literature data available, the required EoS parameters will be derived. This is discussed in the next section.

8.3.2 Thermodynamics of the ternary MDEA - CO_2 - H_2O system

Before the model can be used to describe the quaternary system, also the (reactive) ternary system with MDEA needs to be correlated according to the EoS approach, since the majority of the remaining, unknown, parameters in the total model (marked with # in Figure 8.3) are a part of this second ternary system, consisting of MDEA, carbon dioxide and water.

Initially, the various pure component and binary interaction parameters were determined in a similar manner as in the previous chapter for PZ - CO_2 - H_2O: The polar parameters p_1, p_2, p_3 of MDEA were fitted to the experimental pure vapor pressure data of Noll et al. [1998], while both freezing point depression data [Chang et al., 1993] and VLE data [Voutsas et al., 2004, Xu et al., 1991b] were used to regress the interaction parameters in the MDEA - water system. Following the work of Solbraa [2002], the interaction between MDEA and CO_2 had to be described with a single k_{mix} parameter, since no experimental data are available on this system. All resulting (pure and binary) fit parameters and the experimental data sources have been listed in Table 8.2, along with the various physical and critical constants. All other, remaining parameters needed in the MDEA - CO_2 - H_2O modelling, such as e.g. the pure water parameters and the H_2O - CO_2 interaction parameters, can be found in Chapter 7.

The chemical equilibria considered in this subsystem are:

Water dissociation: $$2H_2O \overset{K_I}{\leftrightarrows} OH^- + H_3O^+$$

Table 8.2: Parameters used in the modelling of the MDEA - CO_2 - H_2O equilibrium.

Single component parameters		Binary systems	
MDEA		H_2O - MDEA	
P_C, [bar]	38.8	$\Delta g'_{12}$, [kJ mol-1]	26.26
T_C, [K]	677.8	$\Delta g''_{12}$ [J mol-1 K-1]	-91.5
Acentric factor	1.242	$\Delta g'_{21}$ [kJ mol-1]	-13.52
Source	C&F[a]	$\Delta g''_{21}$, [J mol-1 K-1]	50.5
p_1	0.5244	$\alpha_{12} = \alpha_{21}$	0.27
p_2	-1.1529	Source	Chang et al. [1993]
p_3	0		Voutsas et al. [2004]
Source	Noll et al. [1998]		Xu et al. [1991b]
Molecular diameter	4.50	MDEA - CO_2	
Source[b]	C&F	Interaction parameter k_{mix}	0.2
	Solbraa [2002]	Source	Solbraa [2002]
d_0[c]	8.16	Ionic $MDEAH^+$ parameter	
d_1	$8.9 \cdot 10^3$	Ionic diameter	4.50
Source	C&F	Source	C&F, Solbraa [2002]

[a] C&F denotes Chunxi and Fürst [2000].
[b] All sources deduce the molecular diameter from the amine covolume.
[c] The temperature dependence of the dielectric constant of MDEA is given in Eq. 7.17.

Bicarbonate formation: $$2H_2O + CO_2 \overset{K_{II}}{\leftrightarrows} HCO_3^- + H_3O^+$$

MDEA protonation: $$H_2O + MDEAH^+ \overset{K_{III}}{\leftrightarrows} MDEA + H_3O^+$$

All chemical equilibrium constants in this work are defined in the mole fraction scale with as reference state infinite dilution in water for all species except water, their temperature dependence is given by Eq. 8.4 and the corresponding coefficients C_0 - C_2 are listed in Table 8.3.

$$\ln K = C_0 + \frac{C_1}{T} + C_2 \ln T \tag{8.4}$$

Table 8.3: Coefficients for the chemical equilibrium constants used in the model.

	C_0	C_1	C_2	$K_{(T=313K)}$	T, [$^\circ$C]	Source
K_I	132.899	-13445.9	-22.4773	$9.3 \cdot 10^{-18}$	0 - 225	Posey and Rochelle [1997]
K_{II}	231.465	-12092.1	-36.7816	$9.0 \cdot 10^{-9}$	0 - 225	Posey and Rochelle [1997]
K_{III}	-83.490	-819.7	10.9756	$1.8 \cdot 10^{-12}$	5 - 95	P-S K.[a]

[a]P-S K denotes Pérez-Salado Kamps and Maurer [1996].

With respect to the implementation of the ternary MDEA system in the quaternary model, the following simplifications and assumptions have been made:

- The concentration of H_3O^+ in the solution is marginally small for typical operating conditions and can therefore be neglected, which is a generally accepted assumption considering the basic environment of aqueous alkanolamine - acid gas solutions.

- Also the presence of carbonate ions is neglected, based on the pH range of interest and the equilibrium constant for this reaction. The same simplification was adopted in previous equilibrium studies [Chunxi and Fürst, 2000, Solbraa, 2002].

- Only interactions between cations and anions, and cations and molecular species were included in the model, all other ionic interactions were neglected - as in previous publications on the electrolyte EoS modelling.

- The ionic interaction between $MDEAH^+$ and the hydroxide ion OH^- has been set to zero, as preliminary simulation runs showed that the influence of this parameter on the model outcome was negligibly small for typical operating conditions.

In the literature, many different experimental data series on the solubility of CO_2 in aqueous MDEA solutions have been reported, which could be used in the regression of the (four) remaining ionic interaction parameters for the ternary MDEA - CO_2 - H_2O system (see Table 8.4). In this work, the experimental database

as suggested by Huttenhuis et al. [2005] was used to fit the ionic interaction parameters. Huttenhuis et al. [2005] critically reviewed the different available experimental data series, and they proposed a database which includes (internally and mutually consistent) solubility data over a wide range of temperature, MDEA concentration and CO_2 loading. The objective function for minimization was the same as used throughout the entire study:

$$F = \min \sum_{exp} \left| \frac{P^{exp} - P^{mod}}{P^{exp}} \right| \tag{8.5}$$

The model correlation results are listed in Table 8.4, while the values for the ionic interaction parameters resulting from the regression are listed in Table 8.5. A graphical comparison between experimental and model predicted values is given in Figure 8.4.

Table 8.4: Experimental MDEA - H_2O - CO_2 database and modelling results.

Reference	MDEA [wt. %]	Temperatures [K]	CO_2 loading [mol mol^{-1}]	N	AAD [%]
Lemoine et al. [2000]	23.6	298	0.02 - 0.26	13	19.9
Austgen and Rochelle [1991]	23.4	313	0.006 - 0.65	14	23.8
Kuranov et al. [1997]	19.2	313	0.79 - 1.23	9	17.7
	18.8	313,333,373,413	0.18 - 1.25	32	
	32.1	313,333,373,393,413	0.11 - 1.16	40	
Rho et al. [1997]	20.5	323,348,373	0.026 - 0.848	32	33.6
	50	323,348,373	0.0087 - 0.385	26	
P-S K.[a]	32.0	313	0.85 - 1.24	5	29.5
	48.8	313, 353,393	0.32 - 0.56	23	
Huang and Ng [1998]	23	313,343,373,393	0.00334 - 1.34	29	33.6
	50	313,343,373,393	0.00119 - 1.16	37	
Rogers et al. [1998]	23	313,323	0.000591 - 0.1177	20	27.8

[a] P-S K. denotes Pérez-Salado Kamps et al. [2001].

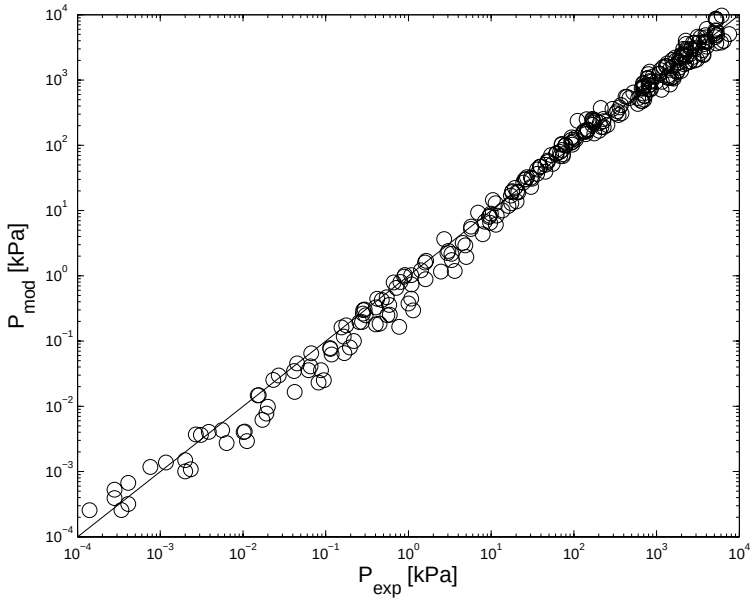

Figure 8.4: Comparison between experimental and model predicted values for the MDEA - CO_2 - H_2O system.

Table 8.5: Ionic interaction parameters for the MDEA - CO_2 - H_2O system.

W_{kl}	[m^3 $kmol^{-1}$]
$MDEAH^+$ - H_2O	0.1189
$MDEAH^+$ - MDEA	0.0756
$MDEAH^+$ - CO_2	-0.0705
$MDEAH^+$ - HCO_3^-	-0.1473

The results presented in Table 8.4 and Figure 8.4 show that the model is well able to describe experimental (carbon dioxide partial and total system) pressures as a function of the liquid loading for aqueous MDEA solutions. However, this ability alone is not a reliable hallmark for the quality of a thermodynamic model, as it does not tell whether the liquid phase speciation is correct. A thermodynamic model to be used in gas treating processes should not only be able to predict the CO_2 pressure versus loading curve, but also the speciation of the liquid as a function of loading. This is because the speciation is required in the determination of the actual

driving force for CO_2 absorption, and thus required for the rigorous mass transfer modelling used in the design and operation of industrial absorbers. The ability of the present model to predict the speciation of the ternary subsystem MDEA - CO_2 - H_2O has been validated with a limited number of available experimental speciation data as reported by Poplsteinova Jakobsen et al. [2005], who used NMR to determine the liquid composition of loaded aqueous MDEA solutions at 20 and 40 °C. A comparison between the model predictions and the experimental data is given in Figures 8.5 and 8.6. From these speciation plots, it can be concluded that the model predicted speciation is well in line with the experimentally reported liquid composition. The model, however, does seem to overpredict the molecular CO_2 fraction in the liquid.

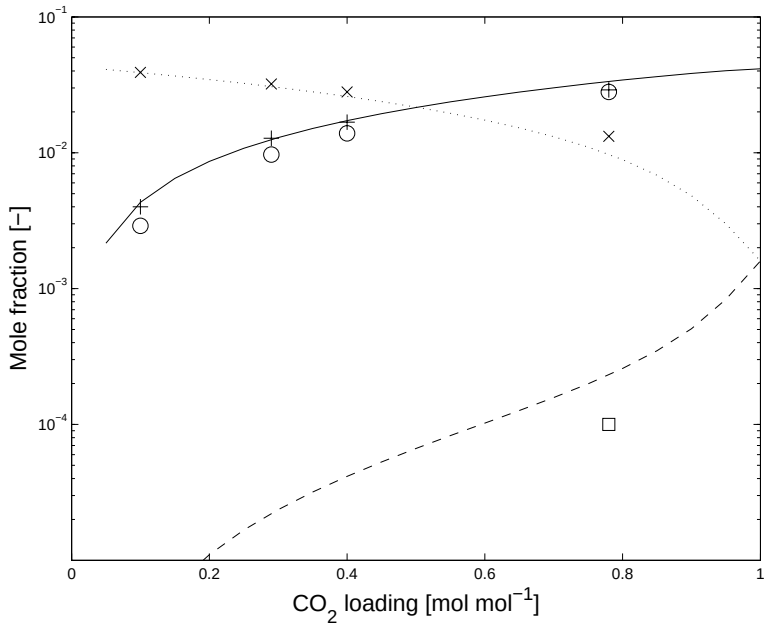

Figure 8.5: Model predicted and experimentally determined speciation of an aqueous 23 wt. % MDEA solution at 20 °C. Legend below.

Legend:	experiment	model
MDEA	×	dotted line
$MDEAH^+$	+	solid line
HCO_3^-	○	solid line
CO_2	□	dashed line

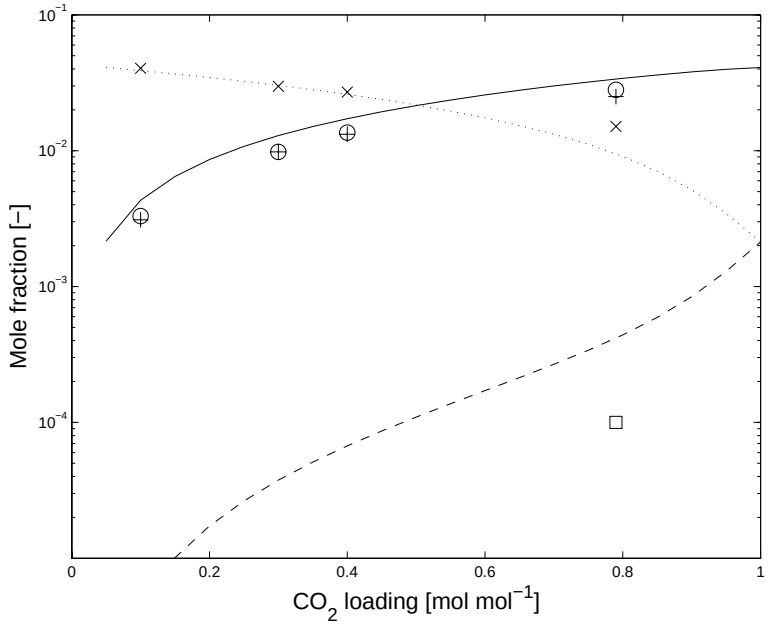

Figure 8.6: Model predicted and experimentally determined speciation of an aqueous 23 wt. % MDEA solution at 40 °C. Legend below Figure 8.6.

Additionally, the model has been tested using two other experimentally determined physical properties, namely the pH of a solution and the physical solubility of CO_2. Posey [1996] measured the pH of an aqueous 50 wt. % MDEA solution as a function of carbon dioxide loading, and his results are compared to the model prediction in Figure 8.7. Judging from this figure, it can be concluded that the model is able to predict the trend in pH fairly well, despite a seemingly constant offset between experimental value and model prediction. The second property investigated is the physical solubility of CO_2 - or its Henry coefficient - in aqueous MDEA. As this property cannot be measured directly, it is usually obtained via the experimental solubility of N_2O corrected for CO_2 using the widely accepted CO_2:N_2O analogy. A comparison between 'experiment' (i.e. derived from the N_2O solubility data as reported by e.g. Versteeg and Van Swaaij [1988b] and Kierzkowska-Pawlak and Zarzycki [2002]) and model prediction (obtained via the pseudo physical MDEA - H_2O - CO_2 system when all reactions are switched off) is shown in Figure 8.8, from which it's obvious that the model is not able to qualitatively nor quantitatively predict

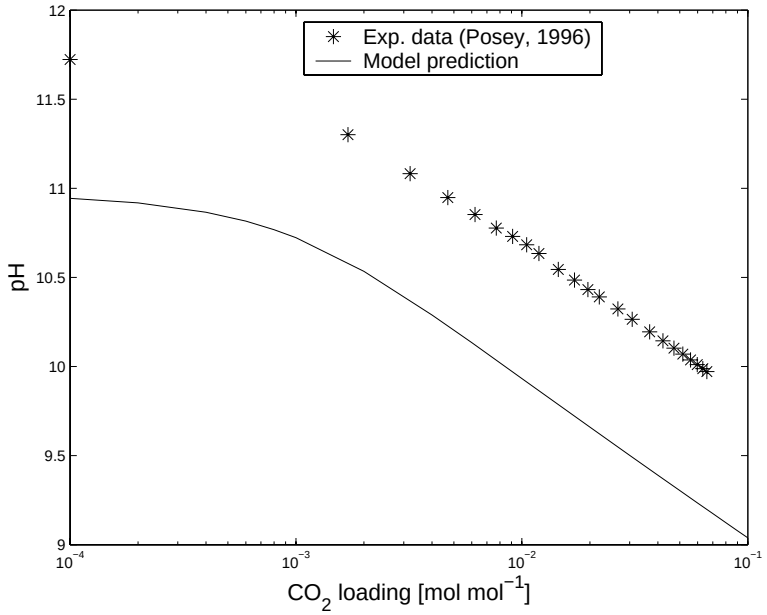

Figure 8.7: Model predicted and experimental pH for an aqueous 50 wt. % MDEA solution at ≈ 22.5 $^{\circ}$C.

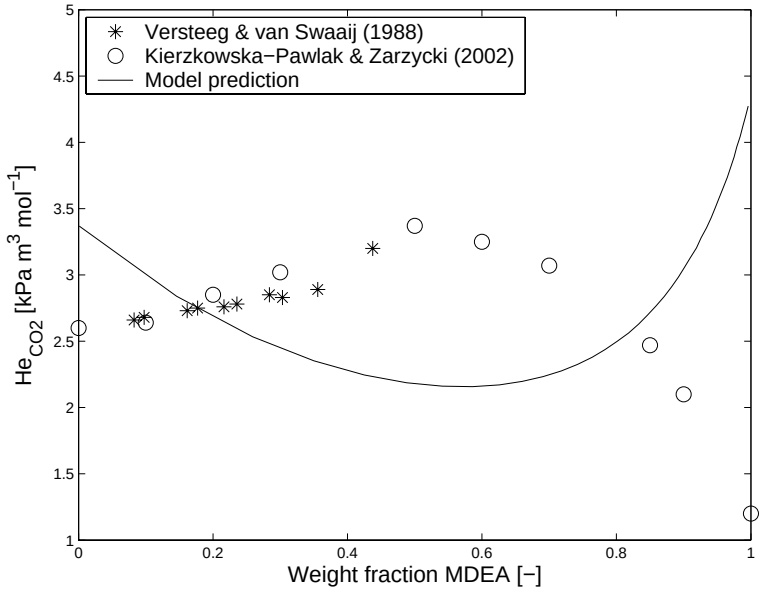

Figure 8.8: Comparison between model prediction and experimental He coefficient data in aqueous MDEA solutions.

the physical solubility of carbon dioxide in aqueous MDEA solutions. However, the absolute deviation between model and experiment is not too dramatic in the region of interest in this study (i.e. less than 50 weight % MDEA).

8.3.3 Discussion

Based on the results obtained so far, the electrolyte EoS model has proven to be suitable for describing both ternary (reactive) subsystems from which the MDEA - PZ - CO_2 - H_2O system is 'constructed'. Chapter 7 already showed that the model was able to successfully describe CO_2 solubilities in aqueous piperazine solutions, and moreover, the model was found to predict experimentally observed pH and conductivity data well. It was shown in this chapter that also experimental (carbon dioxide partial and/or total) pressures over loaded MDEA solutions are correlated well by the electrolyte EoS. Furthermore, the model predicted speciation was found to be well in line with experimental liquid composition data. Also, the model was found to predict the pH of a loaded MDEA solution fairly well (at least the dependence of the pH with loading), but it fails when the physical solubility of CO_2 in aqueous MDEA is concerned[1] . When considering the results concerning the speciation, pH and physical solubility of CO_2, it should be kept in mind that the interaction parameters as now used in the model have been regressed using the available experimental pressure vs. loading data only.

When the two subsystems (second level from the top in Figure 8.3) are combined to form the final quaternary model, basically two new (series of) interaction parameters are introduced:

- Firstly, the (binary) molecular interaction between MDEA and piperazine needs to be identified.
- Secondly, five additional, mutual ionic interaction parameters are needed in the model. This group of parameters includes on one hand the interaction

[1]When making this statement it is implicitly assumed that the application of the CO_2:N_2O analogy is valid and can be used to estimate the 'experimental' physical CO_2 solubility.

between $MDEAH^+$ and (neutral and negatively charged) piperazine-species, and, on the other hand, the interaction between PZH^+ and MDEA.

All these parameters are to be regressed over experimental solubility data in aqueous solutions containing both MDEA and piperazine. The results will be discussed in Section 8.5.

8.4 Experimental results

8.4.1 Equilibrium partial pressure results

All experimentally obtained solubilities of carbon dioxide in aqueous solutions of MDEA and PZ are listed in Tables 8.6 to 8.10, along with the corresponding partial pressures, pH and conductivity data.[2]

[2]For the lowest CO_2 loading data points, the corresponding partial pressure has not been listed: At these loadings, the CO_2 partial pressure was (expected to be) too low to be accurately determined with the IR detector.

Table 8.6: Results 4.0 M MDEA and 0.6 M PZ at 313 K.

Loading [mol mol^{-1}]	P_{CO2} [kPa]	pH [-]	Cond. [mS]	Loading [mol mol^{-1}]	P_{CO2} [kPa]	pH [-]	Cond. [mS]
0.062		9.99	1.70	0.327	12.6	9.07	6.50
0.123	0.72	9.61	2.90	0.339	12.8	9.02	6.90
0.126	0.90			0.426	25.3	8.88	8.20
0.178	2.07	9.38	4.00	0.498	39.0	8.78	9.50
0.189	2.70	9.35	3.80	0.504	39.0	8.76	9.40
0.232	4.36	9.24	5.30	0.568	58.4	8.65	10.45
0.250	5.24	9.21	4.70	0.578	60.4	8.65	10.5
0.283	7.00	9.14	6.20	0.621	78.5	8.65	11.0
0.284	7.33	9.14	5.60	0.632	80.0	8.58	11.1
0.310	9.38	9.09	6.25	0.638	89.7	8.62	11.3
0.312	8.65	9.07	6.90				

Table 8.7: Results 2.8 M MDEA and 0.7 M PZ at 303 K.

Loading [mol mol^{-1}]	P_{CO2} [kPa]	pH [-]	Cond. [mS]	Loading [mol mol^{-1}]	P_{CO2} [kPa]	pH [-]	Cond. [mS]
0.042		10.38	1.80	0.518	9.4	9.10	12.0
0.838		10.16	2.50	0.523	10.7	9.52	12.1
0.124		9.89	3.55	0.573	15.2	8.92	12.6
0.169		9.76	4.20	0.664	25.7	8.81	15.2
0.208	0.51	9.58	5.40	0.681	36.1	9.16	16.0
0.252	0.96	9.49	6.00	0.689	32.1	9.17	15.9
0.303	1.75	9.33	7.50	0.708	38.9	8.65	16.0
0.348	2.61	9.28	8.25	0.758	56.4	8.52	17.0
0.399	4.16	9.13	9.50	0.790	73.7	8.43	17.9
0.435	5.23	9.10	9.90	0.784	70.4	8.91	18.0
0.468	6.80	8.99	11.0	0.818	93.8	8.34	18.2
0.513	8.65	8.95	11.6	0.815	96.9	8.81	18.5
0.537	10.2	8.86	12.3	0.837	100.1	8.31	19.7

Table 8.8: Results 2.8 M MDEA and 0.7 M PZ at 323 K.

Loading [mol mol^{-1}]	P_{CO2} [kPa]	pH [-]	Cond. [mS]	Loading [mol mol^{-1}]	P_{CO2} [kPa]	pH [-]	Cond. [mS]
0.0633		10.00	3.80	0.418	19.7	9.01	15.8
0.127	0.68	9.66	6.25	0.483	32.8	8.91	18.6
0.155	1.05	9.52	7.00	0.541	45.8	8.77	19.8
0.190	2.00	9.52	8.30	0.584	60.3	8.72	21.8
0.233	3.19	9.30	9.60	0.610	69.5	8.65	22.0
0.255	4.68	9.33	10.4	0.636	84.0	8.62	23.2
0.310	6.99	9.15	12.1	0.657	94.5	8.55	23.4
0.323	8.37	9.15	12.5				

Table 8.9: Results 0.5 M MDEA and 1.5 M PZ at 298 K.

Loading [mol mol^{-1}]	P_{CO2} [kPa]	pH [-]	Cond. [mS]	Loading [mol mol^{-1}]	P_{CO2} [kPa]	pH [-]	Cond. [mS]
0.112		11.28	4.50	0.843	10.6	8.35	13.6
0.177		11.12	5.90	0.906	26.8	8.02	14.5
0.278		10.80	8.50	0.909	29.1	7.98	15.0
0.328		10.67	9.10	0.943	53.7	7.75	15.1
0.436		10.32	10.9	0.965	81.1	7.58	15.45
0.502	0.25	10.12	11.5	0.967	80.1	7.58	15.5
0.640	1.02	9.68	12.9	0.978	102	7.47	15.75
0.675	1.55	9.57	12.8	0.984	110	7.44	15.9
0.807	7.15	9.02	13.9				
0.826	9.02	8.98	14.0				

Table 8.10: Results 0.5 M MDEA and 1.5 M PZ at 313 K.

Loading [mol mol^{-1}]	P_{CO2} [kPa]	pH [-]	Cond. [mS]	Loading [mol mol^{-1}]	P_{CO2} [kPa]	pH [-]	Cond. [mS]
				0.731	8.1	8.60	19.5
0.0948		10.30	6.20	0.749	9.7	8.55	19.6
0.184		10.04	9.25	0.817	20.1	8.29	20.3
0.281		9.76	12.4	0.865	36.9	8.05	21.0
0.369		9.54	14.1	0.870	38.8	8.07	21.0
0.4645	0.45	9.24	17.0	0.900	59.2	7.91	21.4
0.555	1.38	8.97	18.0	0.906	64.1	7.86	21.5
0.649	3.76	8.65	19.6	0.921	79.8	7.79	21.8
0.740	9.24	8.34	20.0	0.923	80.8	7.75	21.5
0.843		7.96	21.0	0.934	96.0	7.88	22.0
				0.936	98.8	7.70	21.9

The experimental error in this work is estimated at 4 % in loading, by propagation of error. Depending on the type of experiment, the error in CO_2 partial pressure can amount to max. 10 % in the continuous gas phase experiments and to 5 % when the gas phase was batch-wise operated, respectively. The experimentally determined pH data are estimated to be accurate within 0.1 pH point, while the error in the reported conductivities ranges from 0.05 mS (for conductivities $\leqq$ 5 mS) up to 0.25 mS for higher conductivities.

Additional to the VLE data listed in Tables 8.6 to 8.10, also the pH of the lean solutions were determined. For accuracy reasons, these measurements were performed in a separate setup, described by Hamborg et al. [2006], using a pH glass electrode (Metrohm, type 6.0258.010) with a resolution of 0.1 mV and 0.1 K. The results are listed in Table 8.11.

Table 8.11: Experimental pH data of the lean aqueous PZ/MDEA solutions.

C_{MDEA} = 4.0 kmol m^{-3} C_{PZ} = 0.6 kmol m^{-3}		C_{MDEA} = 2.8 kmol m^{-3} C_{PZ} = 0.7 kmol m^{-3}		C_{MDEA} = 0.5 kmol m^{-3} C_{PZ} = 1.5 kmol m^{-3}	
T, [K]	pH	T, [K]	pH	T, [K]	pH
24.9	12.09	24.9	12.04	24.9	12.18
29.8	11.96	29.9	11.92	29.9	12.04
40.1	11.71	40.1	11.67	40.1	11.77
50	11.45	50.1	11.42	50.2	11.51

Parts of the data series in Tables 8.6, 8.7 and 8.8 can be compared to data from literature as these data points were measured at similar concentrations and temperatures.

The data listed in Table 8.6 are graphically compared to the equilibrium data reported by Bishnoi and Rochelle [2002b] in Figure 8.9, and it is obvious from this figure, that both data series agree very well. Moreover, at low loadings a double logarithmic plot shows a linear relation between the CO_2 partial pressure and the equilibrium loading, which proves that also the data from the present study are

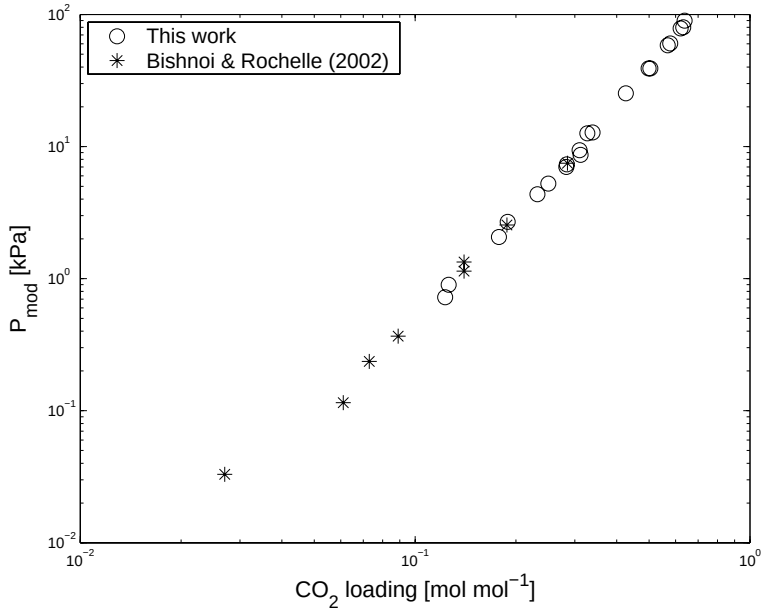

Figure 8.9: Solubility of CO_2 into aqueous solution of 4.0 kmol m^{-3} MDEA and 0.6 kmol m^{-3} PZ at 313 K.

internally consistent (see e.g. Chunxi and Fürst [2000]).

The (graphical) comparison - shown in Figures 8.10 and 8.11 - between the experimental CO_2 solubilities in aqueous solutions containing 2.8 kmol m^{-3} MDEA and 0.7 kmol m^{-3} piperazine as listed in Tables 8.7 and 8.8 and the data reported by Liu et al. [1999], shows the following trends:

- The present experimental data are found to be internally consistent;
- The new data at 50 °C are well in line with the data reported by Liu et al. [1999];
- At 30 °C the agreement between both sets of equilibrium data is less satisfactory.Unfortunately, no explanation could be given for this observation.

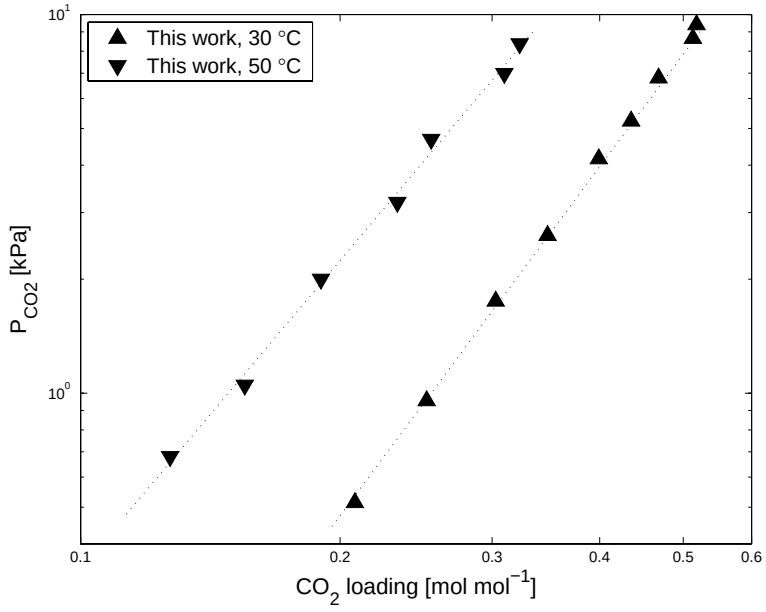

Figure 8.10: Solubility of CO_2 into aqueous solution of 2.8 kmol m^{-3} MDEA and 0.7 kmol m^{-3} PZ at low CO_2 loadings.

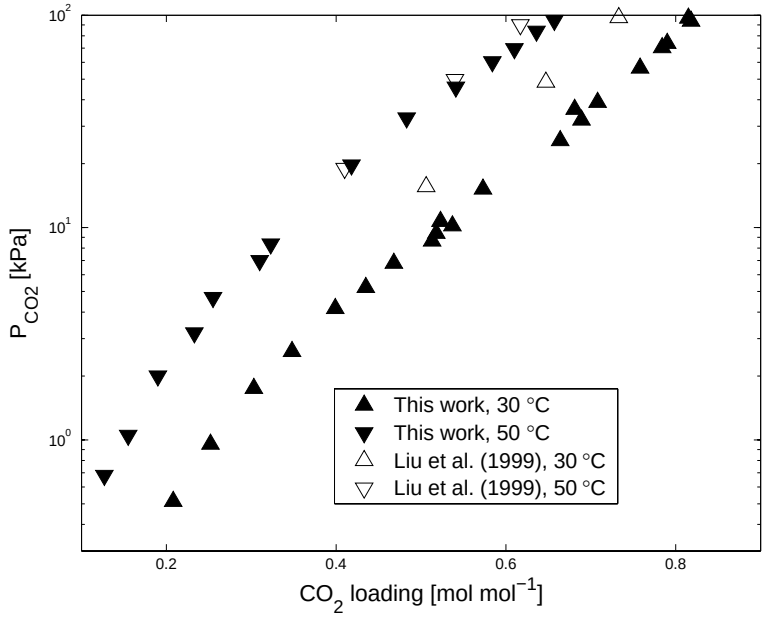

Figure 8.11: Solubility of CO_2 into aqueous solution of 2.8 kmol m^{-3} MDEA and 0.7 kmol m^{-3} PZ.

8.4.2 NMR speciation results

The NMR spectroscopy data taken in 4.0 kmol m^{-3} aqueous MDEA activated with 1.0 kmol m^{-3} piperazine at 298.15 K were analyzed for the concentration of the different piperazine reaction product ratios as explained in the experimental section. The results are listed in Table 8.12.

Table 8.12: Liquid phase speciation of a 4.0 M MDEA, 1.0 M PZ at 298.15 K as determined by NMR.

Sample /run[b]	CO_2 loading [mol mol^{-1}]	PZ : MDEA[a]	$C_{PZ} + C_{PZH^+}$ [kmol m^{-3}]	$C_{PZCOO^-} + C_{+PZCOO^-}$ [kmol m^{-3}]	$C_{PZ(COO^-)_2}$ [kmol m^{-3}]
2	0.070	0.24	0.67	0.30	0.029
3a	0.100	0.24	0.58	0.37	0.055
3b	0.100	0.24	0.57	0.37	0.056
4a	0.053	0.24	0.77	0.22	0.013
4b	0.053	0.24	0.76	0.23	0.014
5	0.108	0.24	0.51	0.41	0.079
6[c]	0.210	0.24	0.52	0.4	0.078

[a]Ratio between total PZ species and total MDEA species
[b]Runs a and b are duplicate experiments taken with the same sample.
[c]Sample 6 was prepared by adding extra carbon dioxide to sample 5.

8.5 Modelling results and discussion

As pointed out earlier in this chapter, the final thermodynamic model still contains a total of six, at this point unknown, parameters. These latter parameters describe the mutual ionic interaction between piperazine and MDEA species. It is clear that these cannot be determined from any other (reactive) subsystem. Secondly, also the binary interaction between PZ and MDEA remains unknown, since in literature no (useful) experimental VLE data on this subsystem are available. Overall, a total of six adjustable parameters will be regressed over a selection of experimental pressure data reported on the aqueous CO_2 - PZ - MDEA system.

As already mentioned in Section 8.1, several experimental VLE data series are available in the literature. These data series were divided into three categories with respect to the regression of the remaining adjustable parameters:

1. A regression set : This selection of experimental data will be used in the actual regression of the adjustable parameters;

2. An extrapolation set : The VLE data in this set will be compared to model predictions obtained using the model and the adjustable parameters as obtained in the regression with the regression set;

3. Non-reliable experimental data : These data will not be used in the regression nor the extrapolation part of the simulation.

Figure 8.2 on the solubility of CO_2 in aqueous 2.0 kmol m^{-3} MDEA illustrates that the equilibrium partial pressures reported by Si Ali and Aroua [2004] are considerably lower than the other literature sources, especially at lower carbon dioxide loadings, and hence their data might be prone to experimental error. As this also raises questions concerning the reliability of their solubility data in aqueous MDEA/PZ solutions, the data of Si Ali and Aroua [2004] were classified as aforementioned category 3 data: .
A detailed description of both the regression set (category 1) and the extrapolation set (category 2) data is given below.

The experimental database used in the regression (category 1) contained the experimental data series reported by Bishnoi and Rochelle [2002b], Liu et al. [1999], Pérez-Salado Kamps et al. [2003], thereby including solubility data taken at a wide range of experimental conditions (see Table 8.13). The following remarks should be made regarding the final regression:

- The data series reported by Liu et al. [1999] on solubilities in solutions containing 4.77 M MDEA and 0.53 M PZ were excluded from the regression, as the MDEA concentration exceeded the maximum concentration (4.3 M) taken

into consideration in the MDEA ternary subsystem which has been discussed in Section 8.3.2. These particular data, however, have been added to the extrapolation data set (category 2);

- Also, preliminary model optimization runs were conducted and data points for which the difference between experimentally determined and model predicted (CO_2 partial and/or total) pressure was more than a factor two, were also eliminated from the database;

- These preliminary model optimization runs also indicated that the model showed little to no sensitivity to the (adjustable) parameters describing the interaction between $MDEAH^+$ and $PZCOO^-$ and the interaction between PZH^+ and MDEA. Therefore, these parameters were set to an arbitrary value of 10-20 m^3 $kmol^{-1}$ (see also Table 8.14). It should be noted, that the negligible sensitivity of the model towards these parameters might just be a 'local' effect and this might thus change when the values of the other four interaction parameters are changed considerably;

- Finally, during the preliminary runs it was observed that model calculations for low loading data showed a large sensitivity towards the binary parameter k_{mix} describing the interaction between piperazine and MDEA. The effect of the regressed ionic parameters was more pronounced at moderate to high carbon dioxide loading cases.

The final experimental database used in the regression of the parameters is specified in detail in Table 8.13. Results of the model optimization are listed both in Table 8.14 (regressed parameter values) and Table 8.13 (average deviations between experiment and model) and a parity plot between experimental value and model description is given in Figure 8.12.

From Table 8.13 and Figure 8.12, it can be concluded that the present model is able to correlate experimental total and CO_2 partial pressure data within an average absolute deviation of about 20 % over all the experimental conditions included in the experimental database in Table 8.13.

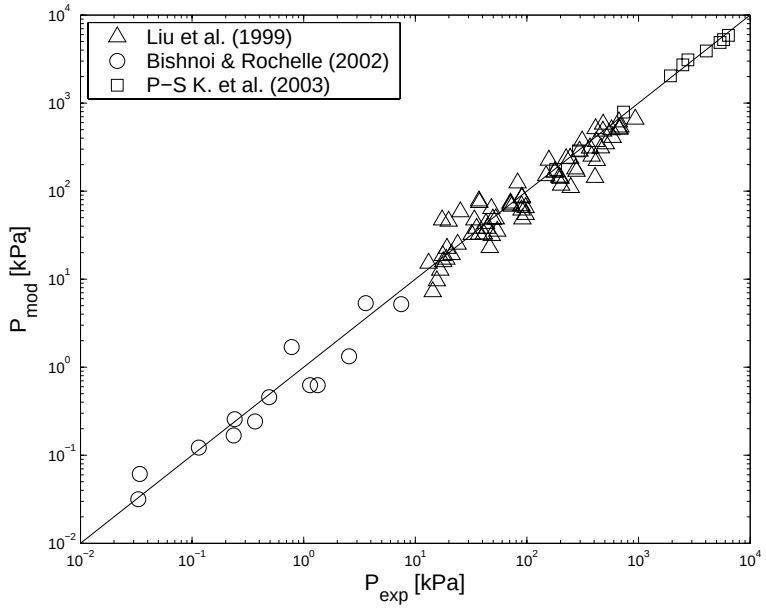

Figure 8.12: Results of model regression on selected experimental database.

Table 8.13: Experimental database used in regression of quaternary (ionic) interaction parameters.

	C_{MDEA} [kmol m^{-3}]	C_{PZ} [kmol m^{-3}]	Temperatures [K]	Loading range [mol mol^{-1}]	N/n^a	AAD [%]
B&R[b]	4.0	0.6	313	0.027 - 0.285	8/8	31.2
	4.0	0.6	343	0.014 - 0.093	3/5	20.6
Liu et al. [1999]	1.35	0.35	323 ; 343	0.349 - 0.955	10/10	14.3
	1.53	0.17	323 ; 343	0.387 - 0.980	10/10	15.1
	2.8	0.7	303;323;343;363	0.147 - 0.842	16/20	24.2
	3.15	0.35	303;323;343;363	0.198 - 0.880	17/20	23.5
	3.75	1.55	323 ; 343	0.247 - 0.746	10/10	25.4
P-S K.[c]	2.0 molal	2.0 molal	353	0.64 - 1.13	10/10	6.8
Total					84/93	20.4

[a]Experimental data points used / Total reported experimental data points

[b]B&R denotes Bishnoi and Rochelle [2002b].

[c]P-S K. denotes Pérez-Salado Kamps et al. [2003].

Table 8.14: Resulting values of the regressed interaction parameters.

Parameter-type	Species	Final value[a]
k_{mix}	MDEA - PZ	-0.426
W	$MDEAH^+$ - PZ	0.600 $\cdot 10^{-3}$ m^3 mol^{-1}
W	$MDEAH^+$ - $^+HPZCOO^-$	0.095 $\cdot 10^{-3}$ m^3 mol^{-1}
W	$MDEAH^+$ - $PZCOO^-$	10-20 $\cdot 10^{-6}$ m^3 mol^{-1}
W	$MDEAH^+$ - $PZ(COO^-)_2$	-0.424 $\cdot 10^{-3}$ m^3 mol^{-1}
W	PZH^+ - MDEA	10-20 $\cdot 10^{-6}$ m^3 mol^{-1}

[a]The ionic interaction parameters between $MDEAH^+$ and $PZCOO^-$, and PZH^+ and MDEA were not regressed, as discussed earlier.

Next, the model's extrapolation qualities were explored using the experimental data series that were not used in the parameter regression: These data not only include the experimental VLE data measured in the present study, but also the experimental solubilities reported by Xu et al. [1998] and the one series from the experimental data of Liu et al. [1999] which was left out of regression set. A comparison between the experimentally obtained and model predicted values is given graphically in Figure 8.13.

Table 8.15: Experimental solubility data that were not used in the regression.

	C_{MDEA} [kmol m^{-3}]	C_{PZ} [kmol m^{-3}]	Temperatures [K]	Loading range [mol mol^{-1}]	N	AAD [%]
Xu et al. [1998]	4.28	0.103;0.257;0.515	343	0.052 - 0.29	11	27.0
Liu et al. [1999]	4.77	0.53	323, 343	0.193 - 0.760	10	16.7
This work	4.0	0.6	313	0.123 - 0.638	20	26.2
	2.8	0.7	303, 323	0.127 - 0.837	36	24.9
	0.5	1.5	298, 313	0.465 - 0.984	28	33.3

From the results shown in Figure 8.13 and Table 8.15, the following can be concluded with respect to the different data sets:

- Model predicted CO_2 partial pressures are in good agreement with the experimental data reported by Xu et al. [1998];

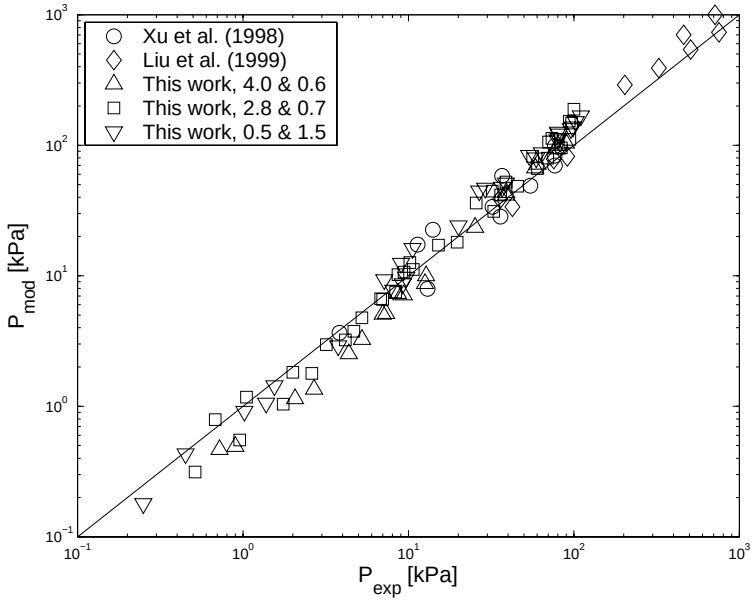

Figure 8.13: Comparison between model predicted and experimentally determined CO_2 partial pressures.

- The model is well able to predict the experimental solubility data of Liu et al. [1999] in aqueous 4.77 M MDEA / 0.53 M PZ solutions, which were left out of the parameter regression;
- All three presently reported new experimental data series are predicted reasonably well by the model. The agreement between model prediction and the experimental CO_2 partial pressures above an aqueous 0.5 M MDEA / 1.5 M PZ solution is slightly worse than for the other two data series presented in this chapter.

Other experimental data to validate the model are (direct and/or indirect) speciation data, such as pH, conductivity and NMR data. Figures 8.14 and 8.15 show a comparison between model predicted pH and conductivity (as the total ion mole fraction present in the liquid) in an aqueous 4.0 M MDEA / 0.6 M PZ solution at 313 K, and the presently obtained experimental data listed in Table 8.6.

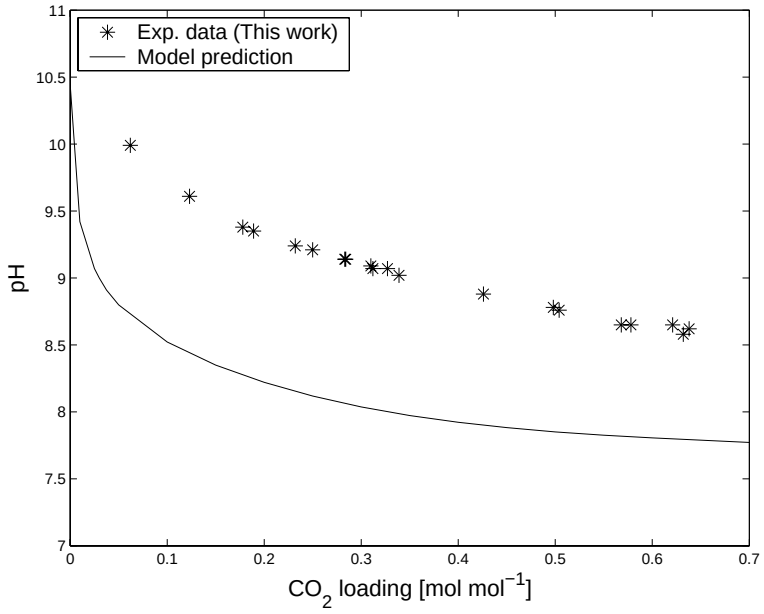

Figure 8.14: Model predicted and experimental pH for an aqueous 4.0 M MDEA / 0.6 M PZ solution at 313 K.

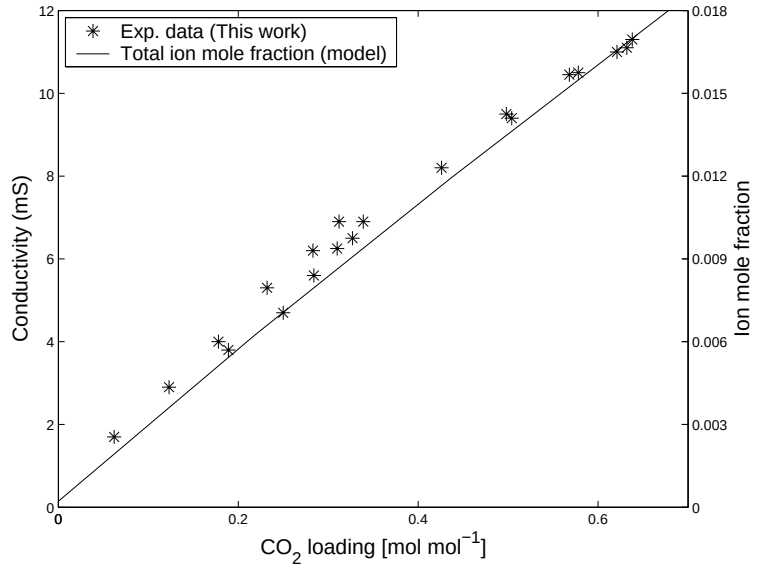

Figure 8.15: Model predicted and experimental conductivity for an aqueous 4.0 M MDEA / 0.6 M PZ solution at 313 K.

Figure 8.14 illustrates - as in the case for the aqueous MDEA solution shown earlier (Figure 8.7) - that, although the model is able to describe the experimentally observed trend in pH with increasing loading, it cannot predict the absolute pH values accurately. Figure 8.15 shows that the total ion mole fractions predicted by the model are well in line with the experimentally observed trend in conductivity. Similar plots and trends are found when comparing model predictions to the other experimental pH and conductivity data listed in Tables 8.7, 8.8, 8.9 and 8.10.

The experimentally determined pH data of lean solutions, listed in Table 8.11, serve as the basis of a second comparison between model prediction and experimental value. In Table 8.16, these experimental data - as well as the experimental pH of a 50 wt. % MDEA solution - are compared to predictions made with the EoS model. Table 8.16 also contains the pH as calculated when assuming the solution behaves ideally (i.e. $\gamma = 1$). Again, the comparison shows that an offset exists between experimental and model predicted pH value.

A comparison between the model predicted liquid phase composition and the available experimental NMR speciation data is given in Table 8.17 [Bishnoi and Rochelle, 2002b] and Figure 8.16 (present data, see also Table 8.12). The generally observed trend as seen in Figure 8.16 seems logical - at least for loadings up to about 0.12:

- With increasing loading, the relative amount of (protonated) piperazine decreases;
- With increasing loading, the relative amount of (protonated) piperazine carbamate increases;
- With increasing loading, the relative amount of $PZ(COO^-)_2$ increases.

However, the speciation at a loading of 0.21 seems to deviate from the aforementioned trend. The speciation seems nearly identical to that at a loading of 0.108, but at this moment no explanation can be presented for this observation.

Table 8.16: Model predicted and experimental pH values of lean solutions.

Solution	T, [$^\circ$ C]	pH_{exp}	pH_{ideal}	pH_{EoS} [a]	pH_{EoS} [b]
50 wt. % MDEA[c]	23.3	11.72	11.77	10.93	10.95
C_{MDEA} = 4.0 kmol m^{-3},	25.0	12.09	11.98	10.88	10.90
C_{PZ} = 0.6 kmol m^{-3}	30.0	11.96	11.84	10.72	10.74
	40.0	11.71	11.58	10.43	10.46
	50.0	11.45	11.34	10.18	10.21
C_{MDEA} = 2.8 kmol m^{-3},	25.0	12.04	11.94	10.96	10.98
C_{PZ} = 0.7 kmol m^{-3}	30.0	11.92	11.80	10.81	10.83
	40.0	11.67	11.53	10.53	10.56
	50.0	11.42	11.29	10.29	10.31
C_{MDEA} = 0.5 kmol m^{-3},	25.0	12.18	12.00	11.62	11.62
C_{PZ} = 1.5 kmol m^{-3}	30.0	12.04	11.86	11.46	11.46
	40.0	11.77	11.59	11.16	11.16
	50.0	11.51	11.34	10.89	10.89

[a] Calculated at a CO_2 loading of 10^{-4} mol mol^{-1}

[b] Calculated at a CO_2 loading of 10^{-5} mol mol^{-1}

[c] Taken from Posey [1996], CO_2 loading = 10^{-4} mol mol^{-1}

Table 8.17: Experimental and model predicted speciation in 3.0 M MDEA / 1.0 M PZ solution with a CO2 loading of 0.52 mol mol^{-1} at 298 K.

Piperazine species	Fraction of total piperazine	
	Experiment[a]	Model
PZ + PZH^+	0.13	0.05
$PZCOO^-$ + $^+HPZCOO^-$	0.57	0.26
$PZ(COO^-)_2$	0.36	0.69

[a] calculated from ratios given by Bishnoi and Rochelle [2002b].

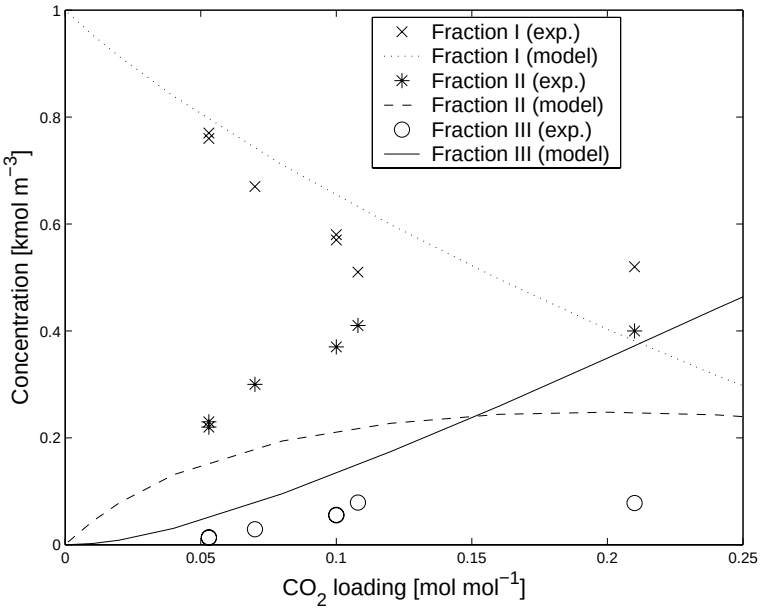

Figure 8.16: Experimental and model predicted speciation of a 4.0 M MDEA / 1.0 M PZ solution loaded with CO_2 at 298.15 K. Fraction I denotes PZ + PZH^+, Fraction II denotes $PZCOO^-$ + $^+HPZCOO^-$, Fraction III denotes $PZ(COO^-)_2$.

Figure 8.16 shows that the model seems to predict the experimentally observed trends in speciation data qualitatively well over the range studied. Both Figure 8.16 and Table 8.17 illustrate that the model e.g. tends to overpredict the amount of dicarbamated piperazine, whereas the fraction of the monocarbamate species is underpredicted.

Based on the results obtained in both the prediction of the VLE data (Table 8.13, Figure 8.12) and the speciation study (Table 8.17, Figure 8.16), it should be concluded that although the model is generally well suited to predict VLE data, the model in its current form seems not to be able to describe the speciation in the quaternary system PZ - MDEA - CO_2 - H_2O satisfactorily over all experimental conditions studied.

However, based on the results obtained so far, the electrolyte EoS model does show very promising results. Firstly, it should be stressed that in the EoS

approach, it is possible to build a multiple component system from smaller, 'lower level' systems - as e.g. illustrated in Figure 8.3 on page 167 - without the need for adjusting parameters when going from one level to a higher level. The direct consequence (and a major advantage) is that the amount of adjustable parameters per (sub)system is limited. Secondly, it should be noted that various additional improvements can be made to the model in its current state to the determination of the required interaction parameters - especially in some of the lower level subsystems, where educated guesses were necessary to determine several interaction parameters.

The first improvements can be made with regard to the binary interaction parameters involving MDEA, PZ and H_2O which are to be regressed on experimental VLE data on the respective physical systems. And, while few experimental data have been reported on the MDEA - H_2O system, no (useful) data are available on the system PZ - H_2O and MDEA - PZ. At present, the required binary interaction between piperazine and water has been estimated using pseudo data generated with the UNIFAC method (7), while the MDEA - PZ interaction has been included using a single mixing parameter, which was regressed together with the quaternary ionic interaction parameters. It is known in the literature, that acid gas solubility models exhibit a high sensitivity towards the amine - water interaction, especially at low loadings (see e.g. Chang et al. [1993]. Based on the modelling results obtained in this chapter it can be said that the same conclusion holds for the interaction between piperazine and MDEA. The same can be concluded from the modelling work done by Bishnoi and Rochelle [2002b], who reported that a precise fit of their (low loading) solubility data could only be obtained, when the binary PZ - MDEA interaction parameters present in their electrolyte NRTL model were regressed. This implies, that experimental VLE data on these systems are vital for a more accurate determination of the corresponding interaction parameters.

Secondly, the molecular interaction between the amines and carbon dioxide should be described in a different, more realistic manner. At present, this interaction is estimated using only one simple mixing parameter per amine to reduce the

overall number of adjustable parameters, but Figure 6b on the Henry coefficient of carbon dioxide in aqueous MDEA solutions clearly illustrates that this simple approach seems to introduce an error to the modelling results. One solution could be to fit these amine - CO_2 interactions to experimental N_2O solubility data in aqueous amine solutions, corrected by means of the CO_2:N_2O analogy. A more accurate set of binary interaction parameters, to be obtained following the suggestions above - would immediately reduce the relative uncertainty with respect to the current values of the ionic interaction parameters.

Thirdly, in the EoS studies carried out so far and including this one, the VLE data of tertiary and quaternary systems have been taken as the single (and only) source for the regression of interaction parameters. Based on the results seen in this chapter, it is suggested to also include other types of experimental data in the optimization of the interaction parameters, such as NMR speciation data, conductivity data and pH data: The relative uncertainty in the use of the presently derived interaction parameters (as listed in Table 8.14) is illustrated with the VLE data in 0.5 M MDEA / 1.5 M PZ solutions, for which model predictions were slightly worse than for the other predicted data series (Table 8.15 and Figure 8.13). This might, for example, partly be due to an error in the ionic PZH^+ - MDEA parameter, which could play a more pronounced role in solutions with an excess of piperazine. The inclusion of other data than the conventional VLE data in the regression of interaction parameters should be done at the lowest possible level (see Figure 8.3), so that the basis of the determination of the interaction parameters to be used in higher order systems becomes much more solid and thus reduce the uncertainty in these parameters considerably. Problem in this might be the formulation of a good target function for minimization, in which an appropriate weight is attributed to the various experimental results (i.e. VLE data, speciation data, pH, conductivity).

All these efforts will help to make that the electrolyte EoS model cannot only satisfactorily describe and predict VLE data, but also correctly predict speciation data. This way it will become a very powerful tool in rate based (rigorous) modelling

of industrial absorber and desorber columns.

8.6 Conclusions

The bulk removal of carbon dioxide from process gas streams is, in industry, usually carried out via an absorber - desorber combination. One promising solvent used in this process step is the piperazine (PZ) activated aqueous N-methyldiethanolamine (MDEA) solution, since it combines the benefits of both PZ (high rate of reaction with CO_2) and MDEA (a low heat of reaction with —COO). An accurate design and modelling of the absorption - desorption process requires detailed knowledge concerning the thermodynamics of these absorbent systems, not only to calculate carbon dioxide partial pressures at specific experimental conditions, but also to predict the liquid phase composition, which is an essential input in rate based column models. In this chapter, new experimental CO_2 solubility data in aqueous solutions containing both MDEA and PZ are reported, which not only list the carbon dioxide partial pressure at a certain CO_2 liquid loading, but also the corresponding conductivity and pH of the solution. In addition to these data, NMR spectroscopy has been applied to obtain experimental data on the liquid phase speciation of an aqueous MDEA - PZ solution, partially loaded with carbon dioxide.

Simultaneously, the electrolyte equation of state (EoS) model, which was used in the previous chapter to successfully describe the thermodynamics of the piperazine - water - carbon dioxide system, was extended to include MDEA. Prior to the extension, the ternary subsystem MDEA - H_2O - CO_2 needed to be described in order to obtain information concerning the interaction parameters unique to this system. It was found, that the electrolyte EoS model was able to describe the available VLE data reasonably well, and moreover, also the model predicted liquid phase speciation was well in line with the experimental composition data reported by Poplsteinova Jakobsen et al. [2005]. The thermodynamic model, however, failed to accurately describe the physical solubility of CO_2 in aqueous MDEA solutions.

On application of the total model to the quaternary PZ - MDEA - CO_2 - H_2O system, it was observed that a total of four adjustable parameters needed to be regressed on experimental solubility data. The final model derived was found to correlate a wide selection of experimental solubility data well, and furthermore the model was able to predict the new VLE data as obtained in this study. The model calculated liquid phase composition, however, did not match the limited available experimental (NMR) data, and therefore it should be concluded that the model in its current state is still not optimally suited for application in rigorous mass transfer models.

Nevertheless, the electrolyte EoS model has shown very promising results, which is remarkable when considering the relatively high uncertainty in the current binary parameters describing the binary systems involving piperazine and/or MDEA (such as PZ - H_2O and PZ - MDEA but also MDEA - CO_2). Hence, more experimental VLE data on these physical subsystems are essential for a further development and refinement of the electrolyte equation of state. Moreover, the need for additional liquid phase speciation data should be stressed, as the strength of a thermodynamic model is, in the end, truly determined by its ability to predict speciation in a reliable and realistic manner.

Acknowledgements

The author wishes to acknowledge H.F.G. Moed for the construction of the experimental setups, and C. van Aken, E.S. Hamborg, A.R. Hansmeier and T. Kolkman for their respective contributions to the experimental work. Furthermore, A.H. Velders is acknowledged for the NMR spectroscopy experiments.

Nomenclature

A	Helmholtz energy	[J]
A_{GL}	gas liquid interface	[m^2]
A^{SR}	attraction parameter	[J mol^{-1}]
b	covolume	[m^3 mol^{-1}]
C	concentration	[kmol m^{-3}]
C_0, C_1, C_2, C_3	coefficients in the calculation of K_{eq} (Eqs. 7.2 and 8.4)	
d_0, d_1, d_2, d_3, d_4	coefficients in the calculation of D (Eq. 7.17)	
d_{pore}	pore diameter	[m]
D	dielectric constant	[-]
D	diffusion coefficient	[m^2 s^{-1}]
D_0	diffusion coefficient at infinite dilution	[m^2 s^{-1}]
De	Dean number, $Re/\omega^{0.5}$	[-]
e	electron charge, 1.60219 $\cdot 10^{-19}$	[C]
E	enhancement factor	[-]
E_{inf}	infinite enhancement factor	[-]
f	fugacity	[Pa]
$g^{'}$, $g^{"}$	interaction parameter in mixing rule	[J m^{-3}], [J m^{-3}]
G^E_∞	excess Gibbs energy at infinite pressure	[J mol^{-1} K^{-1}]
h_+, h_-, h_g	coefficients in Eq. 5.12	[m^3 $kmol^{-1}$]
Ha	Hatta number	[-]
I	ionic strength	[kmol m^{-3}]
J	flux	[mol m^{-2} s^{-1}]
k_2, k_{-1}, k_A	kinetic rate constants	[m^3 $kmol^{-1}$ s^{-1}] or [s^{-1}]
k_{OV}	overall kinetic rate	[s^{-1}]

K	Taylor-Aris dispersion coefficient	[m^2 s^{-1}]
K, K_{eq}	equilibrium constant	
k_G	gas side mass transfer coefficient	[m s^{-1}]
k_L	liquid side mass transfer coefficient	[m s^{-1}]
L_C	length of the coil in Taylor dispersion setup	[m]
m	distribution coefficient	[-]
m	molality	[mol kg^{-1} water]
M	molarity	[kmol m^{-3}]
n	number of moles	[mol]
N	excess number of moles	[mol]
N	stirrer speed	[min^{-1}]
N	number of experiments, steps, etc	[-]
N_A	Avogadro's number, 6.02205 $\cdot 10^{23}$	[mol^{-1}]
P	(partial) pressure	[kPa] or [mbar]
P_0	initial pressure	[kPa]
p_1, p_2, p_3	polarity parameters	[-]
Pe	Péclet number, $2uR/D$	[-]
R	universal gas constant, 8.3144	[J mol^{-1} K^{-1}]
R	radius of the tube in Taylor dispersion setup	[m]
R_C	radius of the coil in Taylor dispersion setup	[m]
R_x	reaction x	[kmol m^{-3} s^{-1}]
$R_{\rightarrow}$, $R_{\leftarrow}$	forward resp. backward reaction	[kmol m^{-3} s^{-1}]
Re	Reynolds number, $2\rho uR/\mu$	[-]
Sc	Schmidt number, $\mu/\rho D$	[-]
t	time	[s]
T	temperature	[K] or [$^\circ$C]
u	fluid velocity	[m s^{-1}]
V	(molar) volume	[m^3]
w	weight fraction	[-] or [%]
W	electrolyte interaction parameter	[m^3 mol^{-1}]
x	axial coordinate	[m]
x	(liquid) mole fraction	[-]

y	vapor mole fraction	[-]
Z	charge	[-]
Z	compressibility factor	[-]

Greek

α	binary nonrandomness parameter	[-]
α	correction factor for attraction parameter A^{SR}	[-]
α	loading	[mol mol^{-1}]
$\alpha_L R^2$	defined in Eq. 7.15	[m^{-1}]
γ	activity coefficient	[-]
γ	surface tension	[N m^{-1}]
Γ	shielding parameter	[m^{-1}]
θ	contact angle	[$^\circ$]
ε_0	vacuum permittivity, 8.85419 $\cdot 10^{-12}$	[C^2 J^{-1} m^{-1}]
ε_3, $\varepsilon_3^{"}$	packing factor	[-]
λ_1, λ_2	ionic parameter in electrolyte EoS	[-]
μ	viscosity	[mPa s]
μ_0	viscosity of water	[mPa s]
ν	stoichiometric coefficient	[-]
ρ	density	[kg m^{-3}]
σ	ionic/molecular diameter	[m]
σ^C, σ^P	solvated diameter	[$\mathring{A}$]
τ	mixing rule parameter	[-]
τ	penetration time	[s]
φ	fugacity coefficient	[-]
Φ	osmotic coefficient	[-]
ω	acentric factor	[-]
ω	radius ratio, R_C/R	[-]

Subscript and superscript

a	anion
c	cation
C	critical
DC	DeCoursey
eq	equilibrium
exp	experimental
G, gas	gas phase
GV	gas supply vessel
inj	injected
int	interface
ion	ions, ionic
$irrev$	irreversible
L, liq	liquid phase
LR	long range
LY	Laplace-Young
mix	mixture
$pure$	pure component
R	reactor
R	reduced, residual
ref	reference
rev	reversible
RF	repulsive forces
S	solvent
SE	Stokes-Einstein
$solv$	solvent
SR	short range
t	time
V	vapor phase
vap	vapor
w	water

Bibliography

J. Aguila-Hernández, A. Trejo, and J. Gracia-Fadrique. Surface tension of aqueous solutions of alkanolamines: Single amines, blended amines and systems with nonionic surfactants. *Fluid Phase Eq.*, 185:165–175, 2001.

Y.Y. Akhadov. *Dielectric properties of binary solutions.* Oxford: Pergamon Press, 1981.

H.A. Al-Ghawas, D.P. Hagewiesche, G. Ruiz-Ibanez, and O.C. Sandall. Physicochemical properties important for carbon dioxide absorption in aqueous methyldiethanolamine. *J. Chem. Eng. Data*, 34:385–391, 1989.

A. Alizadeh, C. A. Nieto de Castro, and W. A. Wakeham. The theory of the Taylor dispersion technique for liquid diffusivity measurements. *Int. J. Thermophys.*, 1: 243–283, 1980.

E. Alper. Kinetics of reactions of carbon dioxide with diclycolamine and morpholine. *Chem. Eng. J.*, 44:107–111, 1990.

M. Appl, U. Wagner, H.J. Henrici, K. Kuessnet, F. Volkamer, and N. Ernst-Neust. Removal of CO_2 and/or H_2S and/or COS from gases containing these constituents. *US Patent Nr 4336233*, 1982.

R. Aris. On the dispersion of a solute in a fluid flowing through a tube. *Proc. Roy. Soc. Lond. A*, 235:67–77, 1956.

M.K. Aroua and R. Mohd Salleh. Solubility of CO_2 in aqueous piperazine and its

modelling using the Kent-Eisenberg approach. *Chem. Eng. Technol.*, 27:65–70, 2004.

D.M. Austgen and G.T. Rochelle. Model of vapor-liquid equilibria for aqueous acid gas-alkanolamine systems - 2. Representation of H_2S and CO_2 solubility in aqueous mixtures of MDEA with MEA or DEA. *Ind. Eng. Chem. Res.*, 30:543–555, 1991.

D.M. Austgen, G.T. Rochelle, X. Peng, and C.-C. Chen. Model of vapor-liquid equilibria for aqueous acid gas-alkanolamine systems using the electrolyte - NRTL equation. *Ind. Eng. Chem. Res.*, 28:1060–1073, 1989.

W. Baldauf and H. Knapp. Experimental determination of diffusion coefficients, viscosities, densities and refractive indexes of 11 binary liquid systems. *Ber. Buns. Ges. Phys. Chem.*, 87:304–309, 1983.

F.X. Ball, H. Planche, W. Fürst, and Renon H. Representation of deviation from idealitiy in concentrated aqueous solutions of electrolytes using a mean spherical approximation molecular model. *A.I.Ch.E. J.*, 31:1233–1240, 1985.

P.V.L. Barrett. *Gas absorption on a sieve plate*. PhD thesis, University of Cambridge, 1966.

S. Bishnoi. *Carbon dioxide absorption and solution equilibrium in piperazine activated methyldiethanolamine*. PhD thesis, University of Texas, 2000.

S. Bishnoi and G.T. Rochelle. Absorption of carbon dioxide into aqueous piperazine: Reaction kinetics, mass transfer and solubility. *Chem. Eng. Sci.*, 55:5531–5543, 2000.

S. Bishnoi and G.T. Rochelle. Absorption of carbon dioxide in aqueous piperazine / methyldiethanolamine. *A.I.Ch.E. J.*, 48:2788–2799, 2002a.

S. Bishnoi and G.T. Rochelle. Thermodynamics of piperazine / methyldiethanolamine / water / carbon dioxide. *Ind. Eng. Chem. Res.*, 41:604–612, 2002b.

P.M.M. Blauwhoff, G.F. Versteeg, and W.P.M. Van Swaaij. A study on the reaction between CO_2 and alkanolamines in aqueous solutions. *Chem. Eng. Sci.*, 39:207–255, 1984.

D.W.F. Brilman, W.P.M. Van Swaaij, and G.F. Versteeg. On the absorption of isobutene and trans-2-butene in sulfuric acid solutions. *Ind. Eng. Chem. Res.*, 36: 4638–4650, 1997.

D.W.F. Brilman, W.P.M. Van Swaaij, and G.F. Versteeg. Diffusion coefficient and solubility of isobutene and trans-2-butene in aqueous sulfuric acid solutions. *J. Chem. Eng. Data*, 46:1130–1135, 2001.

M. Caplow. Kinetics of carbamate formation and breakdown. *J. Am. Chem. Soc.*, 90:6795–6803, 1968.

J.K. Carson, K.N. Marsh, and A.E. Mather. Enthalpy of solution of carbon dioxide in (water + monoethanolamine, or diethanolamine, or N-methyldiethanolamine) and (water + monoethanolamine + n-methyldiethanolamine at t = 298.15 K. *J. Chem. Therm.*, 32:1285–1296, 2000.

E.A. Castro, J.G. Santos, J. Téllez, and M.I. Umaña. Structure-reactivity correlations in the aminolysis and pyridinolysis of bis(phenyl) and bis(4-nitrophenyl) thionocarbonates. *J. Org. Chem.*, 62:6568–6574, 1997.

H.-T. Chang, M. Posey, and G.T. Rochelle. Thermodynamics of alkanolamine-water solutions from freezing point measurement. *Ind. Eng. Chem. Res.*, 32:2324–2335, 1993.

L. Chunxi and W. Fürst. Representation of CO_2 and H_2S solubility in aqueous MDEA solutions using an electrolyte equation of state. *Chem. Eng. Sci.*, 55: 2975–2988, 2000.

J.T. Cullinane and G.T. Rochelle. Carbon dioxide absorption with aqueous potassium carbonate promoted by piperazine. *Chem. Eng. Sci.*, 59:3619–3630, 2004.

J.T. Cullinane and G.T. Rochelle. Thermodynamics of aqueous potassium carbonate, piperazine, and carbon dioxide. *Fluid Phase Eq.*, 227:197–213, 2005.

T.J. Cullinane. *Thermodynamics and kinetics of aqueous piperazine with potassium carbonate for carbon dioxide absorption.* PhD thesis, University of Texas, 2005.

P.V. Danckwerts. The reacion of CO_2 with ethanolamines. *Chem. Eng. Sci.*, 34: 443–446, 1979.

H.Y. Dang and G.T. Rochelle. CO_2 absorption rate and solubility in monoethanolamine / piperazine / water. *Sep. Sci. Tech.*, 38:337–357, 2003.

W.-D. Deckwer, editor. *Bubble column reactors.* Chicester: John Wiley & Sons, 1992.

W.J. DeCoursey. Absorption with chemical reaction: Development of a new relation for the Danckwerts model. *Chem. Eng. Sci.*, 29:1867–1872, 1974.

J.F. Duda and J.C. Vrentas. Laminar liquid jet diffusion studies. *A.I.Ch.E. J.*, 14: 286–294, 1968.

A.J. Easteal and L.A. Woolf. Pressure and temperature dependence of tracer diffusion coefficients of methanol, ethanol, acetonitrile, and formamide in water. *J. Phys. Chem.*, 89:1066–1069, 1985.

V. Ermatchkov, Á. Pérez-Salado Kamps, and G. Maurer. Chemical equilibrium constants for the formation of carbamates in (carbon dioxide + piperazine + water) from ^{1}H - NMR - spectroscopy. *J. Chem. Therm.*, 35:1277–1289, 2002.

W. Fürst and H. Planche. Modélisation de la thermodynamique de lextraction des gaz acides par les amines. *Entropie*, 202/203:31–35, 1997.

W. Fürst and H. Renon. Representation of excess properties of electrolyte solutions using a new equation of state. *A.I.Ch.E. J.*, 39:335–343, 1993.

E.S Hamborg, J.P.M Niederer, and G.F. Versteeg. Determination of dissociation constants of CO_2 absorbents between 293 K 353 K using electromotive force

measurements. *Proc. 8th Int. Conf. on Greenhouse Gas Control Technologies (GHGT-8) in Trondheim, Norway*, 2006.

J. Haubrock, J.A. Hogendoorn, and G.F. Versteeg. The applicability of activities in kinetic expressions: A more fundamental approach to represent the kinetics of the system CO_2-OH^- in terms of activities. *IJCRE*, 3, 2005.

J. Haubrock, J.A. Hogendoorn, and G.F. Versteeg. The applicability of activities in kinetic expressions: A more fundamental approach to represent the kinetics of the system CO_2-OH^--salt in terms of activities. *Proc. 17th Int. Congress of Chemical and Process Engineering (CHISA-2006) in Prague, Czech Republic*, 2006.

W. Hayduk and H. Laudie. Prediction of diffusion coefficients for nonelectrolytes in dilute aqueous solutions. *A.I.Ch.E. J.*, 20:611–615, 1974.

W. Hayduk and B.S. Minhas. Correlations for prediction of molecular diffusivities in liquids. *Can. J. Chem. Eng.*, 60:295–298, 1982.

G. Heilen, H.J. Mercker, D. Frank, R.A. Reck, and R. Jäckh. *Ullmann's encyclopedia of industrial chemistry*, volume A2. Weinheim: VCH, 5th edition, 1994.

H.B. Hetzer, R.A. Robinson, and R.G. Bates. Dissociation constants of piperazinium ion and related thermodynamic quantities from 0 to 50 °C. *J. Phys. Chem.*, 72: 2081–2086, 1967.

R. Higbie. The rate of absorption of a pure gas into a still liquid during short periods of exposure. *Trans. Am. Inst. Chem. Engrs.*, 31:365, 1935.

L.B. Hitchcock and J.S. McIlhenny. Viscosity and density of pure alkaline solutions and their mixtures. *Ind. Eng. Chem.*, 27:461–466, 1935.

J.A. Hogendoorn, R.D. Vas Bhat, J.A.M. Kuipers, W.P.M. van Swaaij, and G.F. Versteeg. Approximation for the enhancement factor applicable to reversible reactions of finite rate in chemically loaded solutions. *Chem. Eng. Sci.*, 52:4547–4559, 1997.

G. Houghton, A.M. McLean, and P.D. Ritchie. Compressibility, fugacity and water solubility of carbon dioxide. *Chem. Eng. Sci.*, 6:132–137, 1957.

S.H. Huang and H.J. Ng. Solubility of H_2S and CO_2 in alkanolamines. *GPA Res. Rep.*, 155:8, 1998.

M.-J. Huron and J. Vidal. New mixing rules in simple equations of state for representing vapour-liquid equilibria of strongly non-ideal mixtures. *Fluid Phase Eq.*, 3:255–271, 1979.

P.J.G. Huttenhuis, N.J. Agrawal, J.A. Hogendoorn, and G.F. Versteeg. Experimental determination of H_2S and CO_2 solubility data in aqueous amine solutions and a comparison with an electrolyte equation of state. *Proc. 7^{th} World Congress of Chemical Engineering in Glasgow, United Kingdom*, 2005.

M.H. Jenab, M.A. Abdi, S.H. Najibi, W.V. Vahidi, and N.S. Matin. Solubility of carbon dioxide in aqueous mixtures of N-methyldiethanolamine + piperazine + sulfolane. *J. Chem. Eng. Data*, 50:583–586, 2005.

S. Kaganoi. Carbon dioxide absorption in methyldiethanolamine with piperazine or diethanolamine. Master's thesis, University of Texas, 1997.

R.L. Kent and B. Eisenberg. Better data for amine treating. *Hydroc. Proc.*, 55:87, 1976.

H. Kierzkowska-Pawlak and R. Zarzycki. Solubility of carbon dioxide and nitrous oxide in water + methyldiethanolamine and ethanol + methyldiethanolamine solutions. *J. Chem. Eng. Data*, 47:1506–1509, 2002.

J.-H. Kim, C. Dobrogowska, and L.G. Hepler. Thermodynamics of ionization of aqueous alkanolamines. *Can. J. Chem.*, 65:1726–1728, 1987.

A.L. Kohl and R.B. Nielsen. *Gas purification.* Houston: Gulf Publishing Company, 5th edition, 1997.

L. Kucka, E.Y. Kenig, and A. Górak. Kinetics of the gas-liquid reaction between carbon dioxide and hydroxide ions. *Ind. Eng. Chem. Res.*, 41:5952–5957, 2002.

P.S. Kumar, J.A. Hogendoorn, P.H.M Feron, and G.F. Versteeg. New absorption liquids for the removal of CO_2 from dilute gas streams using membrane contactors. *Chem. Eng. Sci.*, 57:1639–1651, 2002.

P.S. Kumar, J.A. Hogendoorn, S.J. Timmer, P.H.M Feron, and G.F. Versteeg. Equilibrium solubility of CO_2 in aqueous potassium taurate solutions: Part 2. Experimental VLE data and model. *Ind. Eng. Chem. Res.*, 42:2841–2852, 2003a.

P.S. Kumar, J.A. Hogendoorn, S.J. Timmer, P.H.M Feron, and G.F. Versteeg. Kinetics of the reaction of CO_2 with aqueous potassium salt of taurine and glycine. *A.I.Ch.E. J.*, 49:203–213, 2003b.

G. Kuranov, N. Rumpf, G. Maurer, and N. Smirnova. VLE modelling for aqueous systems containing methyldiethanolamine, carbon dioxide and hydrogen sulfide. *Fluid Phase Eq.*, 136:147–162, 1997.

S.S. Laddha, J.M. Diaz, and P.V. Danckwerts. The N_2O analogy; the solubilities of CO_2 and N_2O in aqueous solutions of organic Compounds. *Chem. Eng. Sci.*, 36: 228–229, 1981.

Y.E. Lee and F.Y. Li. Binary diffusion coefficients of the methanol/water system in the temperature range 30-40 $^\circ$ C. *J. Chem. Eng. Data*, 36:240–243, 1991.

B. Lemoine, Y.-G. Li, R. Cadours, C. Bouallou, and D. Richon. Partial vapor pressure of CO_2 and H_2S over aqueous methyldiethanolamine solutions. *Fluid Phase Eq.*, 172:261–277, 2000.

Y.-G. Li and A.E. Mather. Correlation and prediction of the solubility of carbon dioxide in a mixed alkanolamine solution. *Ind. Eng. Chem. Res.*, 33:2006–2015, 1994.

D.R. Lide, editor. *Handbook of chemistry and physics*. CRC Press, 75th edition, 1994.

R.J. Littel, M. Bos, and G.J. Knoop. Dissociation constants of some alkanolamines at 293, 303, 318, and 333 K. *J. Chem. Eng. Data*, 35:276–277, 1990a.

R.J. Littel, B. Filmber, G.F. Versteeg, and W.P.M. Van Swaaij. Modelling of simultaneous absorption of H_2S and CO_2 in alkanolamine solutions: The influence of parallel and consecutive reversible reactions and the coupled diffusion of ionic species. *Chem. Eng. Sci.*, 46:2303–2313, 1991.

R.J. Littel, W.P.M. van Swaaij, and G.F. Versteeg. The kinetics of carbon dioxide with tertiary amines in aqueous solutions. *A.I.Ch.E. J.*, 36:1633–1640, 1990b.

H.-B. Liu, C.-F. Zhang, and G.-W. Xu. A study on equilibrium solubility for carbon dioxide in methyldiethanolamine-piperazine-water solution. *Ind. Eng. Chem. Res.*, 38:4032–4036, 1999.

M.A. Matthews and A. Akgerman. High-temperature diffusion of hydrogen, carbon monoxide, and carbon dioxide in liquid n-heptane, n-dodecane, and n-hexadecane. *J. Chem. Eng. Data*, 32:319–322, 1987.

M.A. Matthews and A. Akgerman. Infinite dilution diffusion coefficients of methanol and 2-propanol in water. *J. Chem. Eng. Data*, 33:122–123, 1988.

R.A.T.O Nijsing, R.H. Hendriksz, and H. Kramers. Absorption of co_2 in jets and falling films of electrolyte solutions, with and without chemical reaction. *Chem. Eng. Sci.*, 10:88–104, 1959.

O. Noll, A. Valtz, D. Richon, T. Getachew-Sawaya, I. Mokbel, and J. Jose. Vapor pressures and liquid densities of N-methylethanolamine, diethanolamine, and N-methyldiethanolamine. *Int. Elec. J. Phys. Chem. Data*, 4:105–119, 1998.

D.F. Othmer and M.S. Thakar. Correlating diffusion coefficients in liquids. *Ind. Eng. Chem.*, 45:583–589, 1953.

M.A. Pacheco. *Mass transfer, kinetics and rate-based modelling of reactive absorption.* PhD thesis, University of Texas, 1998.

D.E. Penny and T.J. Ritter. Kinetic study of the reaction between carbon dioxide and primary amines. *J. Chem. Soc. Far. Trans. 1*, 79:2103–2109, 1983.

Á. Pérez-Salado Kamps, A. Balaban, M. Jödecke, G. Kuranov, N.A. Smirnova, and G. Maurer. Solubility of single gases carbon dioxide and hydrogen sulfide in aqueous solutions of N-mehtyldiethanolamine at temperatures from 313 to 393 K and pressures up to 7.6 Mpa: New experimental data and model extension. *Ind. Eng. Chem. Res.*, 40:696–706, 2001.

Á. Pérez-Salado Kamps and G. Maurer. Dissociation constant of N-methyldiethanolamine in aqueous solution at temperatures from 278 K to 368 K. *J. Chem. Eng. Data*, 41:1505–1513, 1996.

Á. Pérez-Salado Kamps, J. Xia, and G. Maurer. Solubility of CO_2 in (H_2O + piperazine) and in (H_2O + MDEA + piperazine). *A.I.Ch.E. J.*, 49:2662–2670, 2003.

D.D. Perrin. *Dissociation constants of organic bases in aqueous solutions.* London: Butterworths, 1965.

B.R.W. Pinsent, L. Pearson, and F.J.W. Roughton. The kinetics of combination of carbon dioxide with water and hydroxide ions. *Trans. Far. Soc.*, 47:263–269, 1951.

R. Pohorecki and W. Moniuk. Kinetics of reaction between carbon dioxide and hydroxyl ions in aqueous electrolyte solutions. *Chem. Eng. Sci.*, 43:1677–1684, 1988.

B.E. Poling, J.M. Prausnitz, and J.P. OConnell, editors. *The properties of gases and liquids.* Boston: McGraw-Hill COmpanies, Inc., 5th edition, 2001.

J. Poplsteinova Jakobsen, J. Krane, and H.F. Svendsen. Liquid-phase composition determination in CO_2-H_2O-alkanolamine systems: An NMR study. *Ind. Eng. Chem. Res.*, 44:9894 –9903, 2005.

M.L. Posey. *Thermodynamic model for acid gas loaded aqueous alkanolamine solutions.* PhD thesis, University of Texas, 1996.

M.L. Posey and G.T. Rochelle. A thermodynamic model of methyldiethanolamine-CO_2-H_2S-water. *Ind. Eng. Chem. Res.*, 36:3944–3953, 1997.

R. Pottel. *Water, a comprehensive treatise, vol. 3.* New York: Plenum Press, 1973.

S.W. Rho, K.P. Yoo, J.S. Lee, S.C. Nam, J.E. Son, and B.M. Min. Solubility of CO_2 in aqueous methyldiethanolamine solutions. *J. Chem. Eng. Data*, 42:1161–1164, 1997.

E.B. Rinker, D.W. Oelschlager, A.T. Colussi, K.R. Henry, and O.C. Sandall. Viscosity, density, and surface tension of binary mixtures of water and N-methyldiethanolamine and water and diethanolamine and tertiary mixtures of these amines with water over the temperature range 20-100 $^\circ$ C. *J. Chem. Eng. Data*, 39:392–395, 1994.

R.A. Robinson and R.H. Stokes. *Electrolyte solutions : The measurement and interpretation of conductance, chemical potential and diffusion in solutions of simple electrolytes.* London: Butterworths scientific publications, 1959.

W.J. Rogers, J.A. Bullin, and R.R. Davidson. FTIR measurements of acid gas-methyldiethanolamine systems. *A.I.Ch.E. J.*, 44:2423–2430, 1998.

P.W.M. Rutten. *Diffusion in liquids.* PhD thesis, Delft University of Technology, 1992.

E. Sada, H. Kumazawa, and M.A. Butt. Solubilities of gases in aqueous solutions of amine. *J. Chem. Eng. Data*, 22:277–278, 1977.

E. Sada, H. Kumazawa, and M.A. Butt. Solubility and diffusivity of gases in aqueous solutions of amines. *J. Chem. Eng. Data*, 23:161–163, 1978.

E. Sada, H. Kumazawa, Y. Osawa, M. Matsuura, and Z.Q. Han. Reaction kinetics of carbon dioxide with amines in non-aqueous solvents. *Chem. Eng. J.*, 33:87–95, 1986.

G.B. Scheibel. Liquid diffusivities. *Ind. Eng. Chem.*, 46:2007–2008, 1954.

J. Schwartzentruber and H. Renon. Development of a new cubic equation of state for phase equilibrium calculations. *Fluid Phase Eq.*, 52:127–134, 1989.

R.M. Secor and J.A. Beutler. Penetration theory for diffusion accompanied by a reversible chemical reaction with generalized kinetics. *A.I.Ch.E. J.*, 13:365–373, 1967.

D.J. Seo and W.H. Hong. Effect of piperazine on the kinetics of carbon dioxide with aqueous solutions of 2-amino-2-methyl-1-propanol and piperazine. *Chem. Eng. Sci.*, 60:503–516, 2000.

M.M. Sharma. Kinetics of reactions of carbonyl sulfide and carbon dioxide with amines and catalysis by brønsted bases of the hydrolysis of COS. *Trans. Far. Soc.*, 61:681–687, 1965.

B. Si Ali and M.K. Aroua. Effect of piperazine on CO_2 loading in aqueous solutions of MDEA at low pressure. *Int. J. Thermophys.*, 25:1863–1870, 2004.

K.H. Simmrock, R. Janowsky, and A. Ohnsorge. *Critical data of pure substances - chemistry data series, Vol. 2 Part 1.* Frankfurt am Main: DECHEMA, 1986.

P. Sipos, A. Stanley, S. Bevis, G. Hefter, and P.M. May. Viscosities and densities of concentrated aqueous NaOH/$NaAl(OH)_4$ mixtures at 25 °C. *J. Chem. Eng. Data*, 46:657–661, 2001.

E.D. Snijder, M.J.M. te Riele, G.F. Versteeg, and W.P.M. van Swaaij. Diffusion coefficients of several aqueous alkanolamine solutions. *J. Chem. Eng. Data*, 38: 475–480, 1993.

E. Solbraa. *Equilibrium and non-equilibrium thermodynamics of natural gas processing.* PhD thesis, Norwegian University of Science and Technology, 2002.

W.V. Steele, R.D. Chirico, S.E. Knipmeyer, A. Nguyen, and N.K. Smith. Thermodynamic properties and ideal-gas enthalpies of formation for dicyclohexyl sulfide, diethylenetriamine, di-n-octyl sulfide, dimethyl carbonate,

piperazine, hexachloroprop-1-ene, tetrakis(dimethylamino)ethylene, n,n-bis-(2-hydroxyethyl)ethylenediamine, and 1,2,4-triazolo[1,5-a]pyrimidine. *J. Chem. Eng. Data*, 42:1037–1052, 1997.

R.H. Stokes. An improved diaphragm-cell for diffusion studies and some tests of the method. *J. Am. Chem. Soc.*, 72:763–767, 1960.

W.-C. Sun, C.-B. Yong, and M.-H. Li. Kinetics of the absorption of carbon dioxide into mixed aqueous solutions of 2-amino-2-methyl-1-propanol and piperazine. *Chem. Eng. Sci.*, 60:503–516, 2005.

G. Taylor. Dispersion of soluble matter in solvent flowing slowly through a tube. *Proc. Roy. Soc. Lond. A*, 219:186–203, 1953.

G. Taylor. Conditions under which dispersion of a solute in a stream of solvent can be used to measure molecular diffusion. *Proc. Roy. Soc. Lond. A*, 225:473–477, 1954.

A.A. Unver and D.M. Himmelbau. Diffusion coefficients of CO_2, C_2H_4, C_3H_6, C_4H_8 in water from 6 $^\circ$C to 65 $^\circ$C. *J. Chem. Eng. Data*, 9:428–431, 1964.

G. Vallée, P. Mougin, S. Jullian, and W. Fürst. Representation of CO_2 and H_2S absorption by aqueous solutions of diethanolamine using an electrolyte equation of state. *Ind. Eng. Chem. Res.*, 38:3473–3480, 1999.

I.M.J.J. van de Ven-Lucassen, Kieviet F.G., and Kerkhof J.A.M. Fast and convenient implementation of the Taylor dispersion method. *J. Chem. Eng. Data*, 40:407–411, 1995.

G.F. Versteeg, J.A.M. Kuipers, F.P.H. van Beckum, and W.P.M. Van Swaaij. Mass transfer with complex reversible chemical reactions I. Single reversible chemical reaction. *Chem. Eng. Sci.*, 44:2295–2310, 1989.

G.F. Versteeg, J.A.M. Kuipers, F.P.H. van Beckum, and W.P.M. Van Swaaij. Mass transfer with complex reversible chemical reactions II. Parallel reversible chemical reactions. *Chem. Eng. Sci.*, 45:183–197, 1990.

G.F. Versteeg, L.A.J. Van Dijck, and W.P.M. Van Swaaij. On the kinetics between CO_2 and alkanolamines both in aqueous and non-aqueous solutions. An overview. *Chem. Eng. Comm.*, 144:113–158, 1996.

G.F. Versteeg and W.P.M. Van Swaaij. On the kinetics between CO_2 and alkanolamines both in aqueous and non-aqueous solutions I. Primary and secondary amines. *Chem. Eng. Sci.*, 43:573–585, 1988a.

G.F. Versteeg and W.P.M. Van Swaaij. Solubility and diffusivity of acid gases (CO_2 and N_2O in aqueous alkanolamine solutions. *J. Chem. Eng. Data*, 33:29–34, 1988b.

E. Voutsas, A. Vrachnos, and K. Magoulasm. Measurements and thermodynamic modeling of the phase equilibrium of aqueous N-methyldiethanolamine solutions. *Fluid Phase Eq.*, 224:193–197, 2004.

P. Wilke, C.R.; Chang. Correlation of diffusion coefficients in dilute solutions. *A.I.Ch.E. J.*, 1:264–270, 1955.

G.-W. Xu, C.-F. Zhang, A.-J. Qin, W.-H. Gao, and H.-B. Liu. Gas-liquid equilibrium in a CO_2-MDEA-H_2O system and the effect of piperazine on it. *Ind. Eng. Chem. Res.*, 37:1473–1477, 1998.

G.-W. Xu, C.-F. Zhang, A.-J. Qin, and Y.-W. Wang. Kinetics study on absorption of carbon dioxide into solutions of activated methyldiethanolamine. *Ind. Eng. Chem. Res.*, 31:921–927, 1992.

S. Xu, F.D. Otto, and A.E. Mather. Physical properties of aqueous AMP solutions. *J. Chem. Eng. Data*, 36:71–75, 1991a.

S. Xu, S. Qing, Z. Zhen, C. Zhang, and J.J. Carrol. Vapor pressure measurements of aqueous N-methyldiethanolamine solutions. *Fluid Phase Eq.*, 67:197–201, 1991b.

X. Zhang, J. Wang, C.-F. Zhang, Y.-H. Yang, and J.-J. Xu. Absorption rate into a MDEA aqueous solution blended with piperazine under a high CO_2 partial pressure. *Ind. Eng. Chem. Res.*, 42:118–122, 2003.

X. Zhang, C.-F. Zhang, S.-J. Qin, and Z.-S. Zheng. A kinetics study on the absorption of carbon dioxide into a mixed aqueous solution of methyldiethanolamine and piperazine. *Ind. Eng. Chem. Res.*, 40:3785–3791, 2001.

Y.X. Zuo and W. Fürst. Prediction of vapor pressure for nonaqueous electrolyte solutions using an electrolyte equation of state. *Fluid Phase Eq.*, 138:87–104, 1997.

List of Publications

P.W.J.Derks, H.B.S. Dijkstra, J.A. Hogendoorn and G.F. Versteeg (2005). Solubility of carbon dioxide in aqueous piperazine solutions, *AIChE Journal*, vol. 51(8), pp. 2311-2327

P.W.J. Derks, J.A. Hogendoorn and G.F. Versteeg (2005). Solubility of N_2O in, and density, viscosity, and surface tension of aqueous piperazine solutions, *Journal of Chemical and Engineering Data*, vol. 50(6), pp. 1947-1950

P.W.J. Derks, T. Kleingeld, C. van Aken, J.A. Hogendoorn and G.F. Versteeg (2006). Kinetics of absorption of carbon dioxide in aqueous piperazine solutions, *Chemical Engineering Science*, vol. 61(20), pp. 6837-6854

Presentations

P.W.J. Derks, J.A. Hogendoorn and G.F. Versteeg (2006). Solubility of carbon dioxide in aqueous blends of piperazine and N-methyldiethanolamine, In *Proceedings of the 8th International Conference on Greenhouse Gas Control Technologies (GHGT-8)*, Trondheim, Norway, 19 - 22 June 2006 (poster presentation)

P.W.J. Derks, J.A. Hogendoorn and G.F. Versteeg (2006). Absorption of carbon dioxide into aqueous solutions of MDEA and piperazine, In *Proceedings of the 17th International Congress of Chemical Engineering (CHISA 2006)*, Prague, Czech Republic, 27 - 31 August 2006 (keynote lecture)

Levensloop

Peter Derks werd op 31 december 1976 geboren in Helmond. Hij groeide op in het pittoreske Noordbrabantse dorp Bakel, alwaar hij de basisschool St. Willibrordus bezocht. Middelbaar onderwijs genoot hij aan het St.-Willibord gymnasium in Deurne, waarvan hij in juni 1995 het VWO diploma in ontvangst mocht nemen.

In augustus 1995 begon hij aan de opleiding Chemische Technologie aan de Universiteit Twente. In het kader van deze opleiding liep hij in het najaar van 2000 stage bij Basell Polyolefins te Wesseling, Duitsland. In de zomer van 2002 studeerde hij af bij de vakgroep Ontwikkeling en Ontwerp van Industriële Processen op een afstudeerscriptie getiteld: "Supercritical fluids in heterogeneous catalysis". In september van hetzelfde jaar werd het behaalde ingenieursdiploma in ontvangst genomen.

Direct na afloop van zijn studie begon hij in september 2002 bij de vakgroep Ontwikkeling en Ontwerp van Industriële Processen om als assistent in opleiding een promotieonderzoek te verrichten naar de absorptie van kooldioxide in piperazine geactiveerd MDEA. De resultaten van het onderzoek staan beschreven in dit proefschrift.

Per 1 september 2006 is Peter als senior process engineer in dienst getreden bij de Procede Group BV te Enschede.

Dankwoord

Met het dankwoord ben ik aangekomen bij het laatste, maar waarschijnlijk wel het meest gelezen, deel van mijn proefschrift. Het tot stand komen van dit boekje was nooit gelukt zonder de hulp van een hoop mensen, die ik hier wil bedanken.

Allereerst gaat mijn dank uit naar mijn assistent promotor en mentor Kees Hogendoorn. Zijn wetenschappelijke input, talrijke ideeën en suggesties tijdens mijn onderzoek, maar ook zijn kritische kijk op behaalde resultaten hebben enorm bijgedragen aan dit proefschrift, en daarnaast is ook de vriendschappelijke band die we de afgelopen jaren hebben opgebouwd me enorm veel waard. Vervolgens wil ik mijn promotor Geert Versteeg bedanken voor de kans om te promoveren en het in mij gestelde vertrouwen. Het moge duidelijk zijn dat ik veel geprofiteerd heb van je jarenlange ervaring op het gebied van reactorkunde en acid gas treating. Ook de wekelijkse babbels over onze cluppies waren altijd leuk, met uitzondering dan van het lopende seizoen... John Niederer wil ik bedanken voor zijn enthousiasme, interesse en hulp gedurende de tijd dat ie deel uitmaakte van onze vakgroep. In dit rijtje hoort eigenlijk ook mijn afstudeerbegeleider Wim Brilman thuis, die het 'heilige vuur' bij mij heeft aangewakkerd ondanks mijn aanvankelijke scepsis ten aanzien van een promotie onderzoek. Wim bedankt!

Het werkt motiverend als je weet dat je onderzoek met belangstelling wordt gevolgd vanuit de industrie, en derhalve wil ik Frank Geuzebroek van Shell bedanken voor de getoonde interesse in mijn werk. In een later stadium is mijn onderzoek ook deel uit gaan maken van het CATO project, wat er zeker toe heeft bijgedragen dat

ik ook meer naar de andere aspecten van CO_2 capture ben gaan kijken. Daarnaast wil ik de betrokkenheid van CATO (veelal in de persoon van Erik Lysen) bij de 'CO_2 promovendi' binnen OOIP gedurende de 'moeilijke tijden' niet onbenoemd laten.

Een belangrijk onderdeel van dit proefschrift zijn de experimentele data die erin gepresenteerd worden. Deze resultaten had ik nooit kunnen behalen zonder de hulp van een groot aantal mensen.

Ten eerste zijn er natuurlijk de technici die de opstellingen bouwen, aan de praat krijgen en trouble-shooten. Bij deze een woord van dank aan Benno Knaken (toch op 1 - dankzij het alfabet), Gerrit Schorfhaar, Henk Jan Moed, Robert Meijer, Robert Brouwer en Wim Leppink. In het bijzonder wil ik Henk Jan bedanken, die verantwoordelijk is geweest voor het realiseren van mijn meetopstellingen.

Verder ben ik een hoop dank verschuldigd aan de studenten die met mijn opstellingen gewerkt hebben. Dit heeft niet alleen een hele sloot nauwkeurige meetdata opgeleverd, maar veelal ook inzichten in de (on)mogelijkheden van sommige ideeën. Antje Hansmeier, Bart van der Veer, Coen van Aken, Hans Dijkstra, Hendrik Roelvink, Nick Aldenkamp, Robert Jan Zwiers, Timo Kleingeld en Tom Kolkman: Hartstikke bedankt! Hierbij zal ik zeker mijn collega Espen Hamborg niet over het hoofd zien, die volledig belangeloos tijd heeft vrijgemaakt om voor mij metingen te doen. Mange takk!

Ook wil ik Wim Lengton en Adri Hovestad bedanken voor hun tips en hulp bij de analysevraagstukken binnen mijn onderzoek. Ook een woord van dank aan Aldrik Velders van SMCT: de NMR-data nemen een belangrijke plaats in binnen het hele VLE gedeelte. Ook Edwin van Elk krijgt bij deze een bedankje voor zijn hulp bij het numerieke fluxmodel.

Zonder de benodigde onderdelen geen opstelling, zonder chemicaliën geen oplossing, en zonder gassen viel er niks te absorberen. Aan alledrie had ik geen

gebrek en dat is te danken aan de dames en heren van de inkoopafdeling (Benny Hövels, Henk Bruinsma, Ineke Klinkenberg, Nelly Voss, Roy Schnörr en Wim Platvoet) en aan Karin Schildkamp, op wie ik volledig kon vertrouwen voor een goede, snelle afhandeling van mijn bestelde chemicaliën en gassen. Ook alle andere ondersteunende diensten en afdelingen binnen CT/TNW wil ik bij deze bedanken. Ook andere UT-mensen die ik hier wellicht vergeten ben te nomen, wil ik bij deze alsnog bedanken.

De afgelopen jaren op het Vlugterlab waren niet helemaal 'all work & no play'. Ik heb enorm veel mensen leren kennen, zowel tijdens mijn afstuderen als tijdens mijn promotie bij OOIP en ik moet zeggen: Het waren (alles bij elkaar) zes fantastische jaren. De talloze borrels, Doedelzakbezoekjes, kaartavondjes, stapavondjes, voetbalpotjes en de zeilweekenden zal ik nooit vergeten. Bij deze wil ik dan ook iedereen van het Vlugterlab bedanken voor deze mooie tijd!

Iedereen afzonderlijk te noemen zou mijn boekje een halve kilo zwaarder maken, maar een paar mensen moet ik er toch even uitlichten.

Allereerst is er Smitje: na een slordige 17 jaar samen in Deurne en Enschede op 'school' te hebben gezeten, zitten we nu weliswaar bij verschillende bedrijven, maar nog steeds binnen dezelfde gang. Dat 'ASD mechanisme' moet je me toch nog eens uitleggen! Dan is er mijn Duitse Herr Kollege Jens, de laatste jaren mijn trouwe koffie- en lunchmaat, en een zeer goede BBQ-gastheer. Ik kijk nu al uit naar de skivakanties bij jou in Zwitserland(?) ! En ook Cents, tegen wil en dank mijn vaste klaverjasmaat, mag ik niet vergeten. Toine, wat zal ik zeggen, de vrijdagen waren toch altijd een verhaal apart. Ook bedankt dat je op wilt treden als paranimf.

Natuurlijk gaat mijn dank ook uit naar mijn vrienden in Bakel, niet alleen voor de 'Brabantse nachten' maar ook voor het feit dat ik altijd op jullie zal kunnen rekenen. Uiteraard noem ik hier ook het thuisfront: mijn ouders, mijn broer(tje) en zijn vriendin, en Harry & Flappie. Jullie hebben me altijd gesteund en stonden

altijd voor me klaar, en daarvoor ben ik jullie ontzettend dankbaar. Daarnaast ben ik blij dat (onze) Marcel ook op wil treden als paranimf.

Last but not least, I wish to thank my girl Kátia: Obrigado miss PC!

Houdoe en bedankt iedereen!!

Peter, 30 november 2006